Sigma receptor ligands

Rybczynska, Anna A.

Sigma Receptor Ligands:

Novel Applications in Cancer Imaging and Treatment

Anna A. Rybczynska

The author gratefully acknowledges the financial support of:

Graduate School for Drug Exploration

University of Groningen

University Medical Center Groningen

Bitmap Brothers

Amgen

Ina Veenstra-Rademaker Foundation

Von Gahlen Netherland B.V.

Cover design: Robert Łotocki (www.bitmap-brothers.pl)

Printed by: CPI Wöhrmann Print Service, Zutphen

ISBN: 978-90-367-5309-8 (hardcopy)
978-90-367-5310-4 (electronic version)

rijksuniversiteit
groningen

Sigma Receptor Ligands:

Novel Applications in Cancer Imaging and Treatment

Proefschrift

ter verkrijging van het doctoraat in de
Medische Wetenschappen
aan de Rijksuniversiteit Groningen
op gezag van de
Rector Magnificus, dr. E. Sterken,
in het openbaar te verdedigen op
woensdag 29 februari 2012
om 12.45 uur

door

Anna Agnieszka Rybczynska

geboren op 20 april 1982
te Bielsko-Biala, Poland

Promotores:	Prof. Dr. R.A.J.O. Dierckx Prof. Dr. P.H. Elsinga
Copromotor:	Dr. A. van Waarde
Beoordelingscommissie:	Prof. Dr. K. Ishiwata Prof. Dr. C. van de Wiele Prof. Dr. A.G.J. van der Zee

ISBN: 978-90-367-5309-8 (hardcopy)
978-90-367-5310-4 (electronic version)

EXPERIENCE

On the open sea I've been fishing -
Finding my own water sliver;
To catch a great fish I've been running,
I've met once in a mountain river.

Paranimfen:	Dawid J. Rybczyński Paul de Bruyn

Table of contents

Chapter 1

Scope and overview of the thesis

Cancer is a disease of modern civilization and the second leading cause of human deaths [1,2]. This is mainly due to the aging population and the current lifestyle [3]. Specifically, GLOBCAN 2008 estimated that 7.6 million people died from cancer worldwide in 2008 accounting for a 11% risk of dying from cancer before the 75-year of age [2,4]. With these numbers in mind, the prospect of curing cancer might seem daunting. However, specific knowledge of the molecular hallmarks of cancer has already enabled us to develop better tools for prevention, detection and treatment. Here, I will first provide a brief overview of these hallmarks of cancer, followed by the current available treatment and diagnostic options. This overview will hopefully help to localize the research presented in the further chapters of this thesis in the current trends in oncology.

Hallmarks of cancer

Cancer is a complex disease due to its heterogeneous origins. For example, almost every cell type can generate a cancer cell and all these cancers manifest themselves with varying symptoms. This process of tumorigenesis includes four development phases shared by all cancers, namely initiation, promotion, progression, and conversion [5] (Fig. 1).

In all these phases of development, cancer cells acquire many adaptations to avoid elimination by the body's defense mechanisms and to acquire a selective advantage over neighboring cells [6]. Among the most characteristic cancer adaptations are self-sufficiency in providing growth signals, insensitivity to growth inhibition, evasion of apoptosis (programmed cell death), sustained angiogenesis (vascularization), tissue invasion and metastasis, and the potential for unlimited self-replication [5,6] (Fig. 1). Acquisition of selective advantages is usually the result of genome instability that enables cancers to stratify mutations in genes controlling the aforementioned processes [7,8]. As a result of these mutations, the balance between tumor suppressor genes and oncogenes is disturbed.

For instance, self-sufficiency in providing growth signals and insensitivity to growth-inhibitory signals can result from active Harvey rat sarcoma viral oncogene homolog (H-Ras) or loss of the suppressor retinoblastoma protein (Rb), which induces uncontrolled division of cancer cells and, ultimately, cancer promotion and progression [5,7].

Furthermore, evasion of apoptosis, during which apoptotic mechanisms become impaired, may be exemplified by the mutation in the tumor suppressor gene p53 [9]. The p53 mutation is found in more than 50% of cancers, where it contributes to resistance of cancer to apoptosis-inducing treatment [5]. Another example for increased pro-survival signaling and impaired apoptosis is upregulation of the PI3K-Akt pathway. A proto-

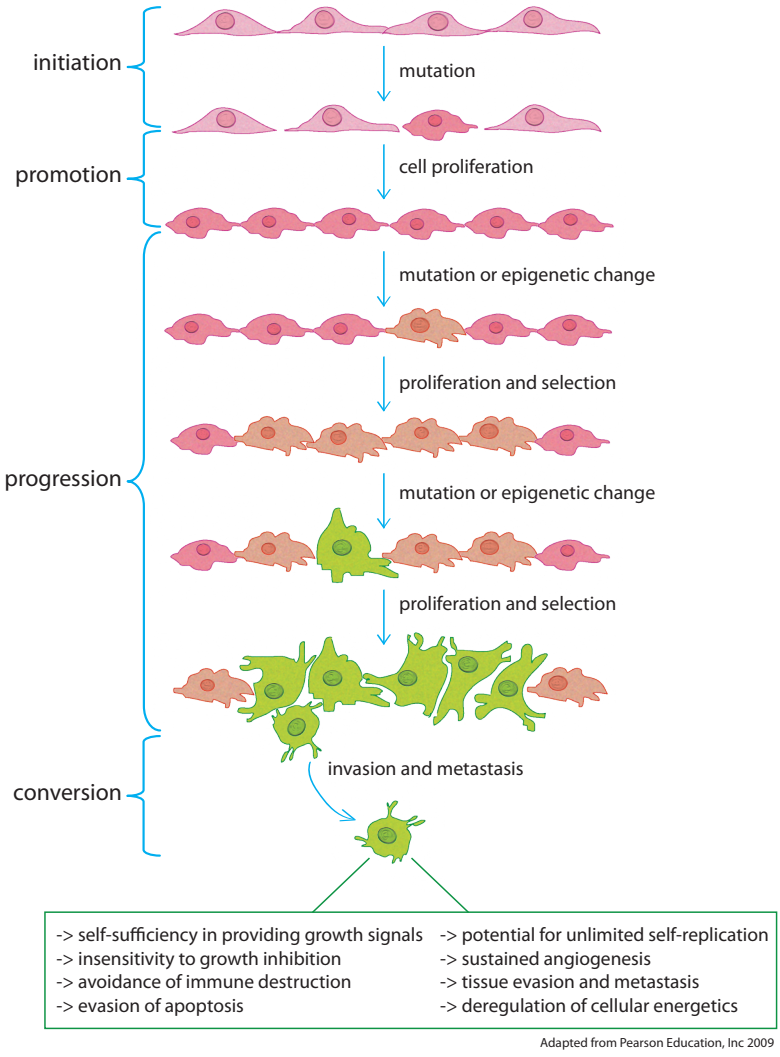

Fig. 1. Phases of cancer development. Tumorigenesis is initiated by multifactor mutations in cell. Disease is promoted if the mutation-burdened cell escapes body's defense mechanisms, starts to proliferate abnormally and possesses genomic flexibility allowing further mutations and/or epigenetic changes. During tumor progression several adaptation, proliferation and selection cycles take place. This process of acquiring more invasive and resistant phenotype increases tumor survival. Finally, highly motile cancer cells will move from the primary tumor and hatch to distant locations in the body, beginning an advanced stage of the disease.

oncogenic phosphatidylinositol-3-kinase (PI3K) is a key cellular signaling coordinator of processes such as cell growth, proliferation, differentiation, motility, survival and intracellular trafficking [7,10]. Cancer cells with mutation of the PIK3CA oncogene or mutation/deletion of the PtdIns(3,4,5)P3 phosphatase (PTEN) tumor suppressor gene have hyperactive signaling downstream of PI3K, allowing cancerous transformation [11]. Probably the best known downstream effector from PI3K is Akt kinase [12]. In its active phosphorylated form, Akt kinase stimulates the aerobic glycolysis, regulates cell cycle and facilitates pro-survival mechanisms in cancer. Therefore, cells which develop resistance to apoptosis (via p53, PI3K-Akt or other pathways) will have a selective advantage compared to their neighbors based on their ability to survive e.g. hypoxic environment and acidosis [7]. Surviving hypoxia means stabilization of hypoxia inducible factor 1-alpha (HIF1α) and, possibly consequently, increased glucose metabolism. Increased glucose metabolism through increased aerobic glycolysis and decreased reliance on mitochondrial oxidative phosphorylation is a biochemical hallmark of cancer cells and, as mentioned below, an important characteristic for cancer diagnosis [13]. The propensity of the cancerous tissue to have different energy metabolism than the non-cancerous tissue was discovered by Otto Warburg, a Nobel Prize winner in 1931 [14]. Interestingly, increased glucose metabolism and decreased perfusion results in acidosis of cancer environment [7]. Due to these processes, cells with superior invasive behavior are selected.

Angiogenesis, a process of vasculature formation, is necessary to constantly supply a growing tumor with necessary oxygen and nutrients and to remove metabolic byproducts. For example, in cells which survive hypoxia, HIF1α may contribute to formation of tumor microvasculature by increasing transcription of several angiogenic genes such as vascular endothelial growth factor (VEGF), platelet-derived growth factor (PDGF) and nitric oxide synthase (NOS) [15].

Immortalization of tumor cells with their acquired adaptations must be completed in order to allow limitless replication, circumvent senescence and continue the progression step. The immortalization of cancer cells can be achieved or potentiated by for example increased expression/activity of telomerase enzyme and decreased p53 suppressor function [16].

Limitations, such as space for division and access to nutrients, are bypassed by cancer cells able to invade adjacent tissues and metastasize to distant sites in the body. Dissemination of cancer cells from the primary tumor requires cessation of cell-cell contacts and increased cell motility. These contacts can be reshaped by the activity of extracellular proteases on cell contact proteins such as cadherins, cell adhesion molecules (CAMs) and integrins [5]. Cell motility is achieved by formation of various plasma membrane structures, such as invadopodia and pseudopodia, which require actin cytoskeleton remodeling by a variety of specialized proteins [17].

Cancer treatment

Surgery: In 1862, an American antiques collector and dealer, Edwin Smith, purchased an old scroll of papyrus detailing one of the first recorded descriptions of surgery performed in 3000 BC [18], (for overview see Fig. 2). This and other scrolls confirm early attempts at tumor identification and treatment in ancient Egypt, then still considered as an incurable disease. Since then, developments in surgery have made it the foundation of treatment methods for early diagnosed non-hematological cancers [19]. However, invasion of cancer into the host tissue or, in advanced carcinoma, multiple metastases to distant sites are limiting factors in surgical intervention.

Radiation therapy: In 1899, Marie Curie-Skłodowska and her husband Pierre Curie discovered that certain elements such as radium or polonium emit harmful energy, termed as radioactivity [20,21]. After further development and refinement, radiation therapy was introduced as a cancer treatment modality in the 1920s [22]. Radiation

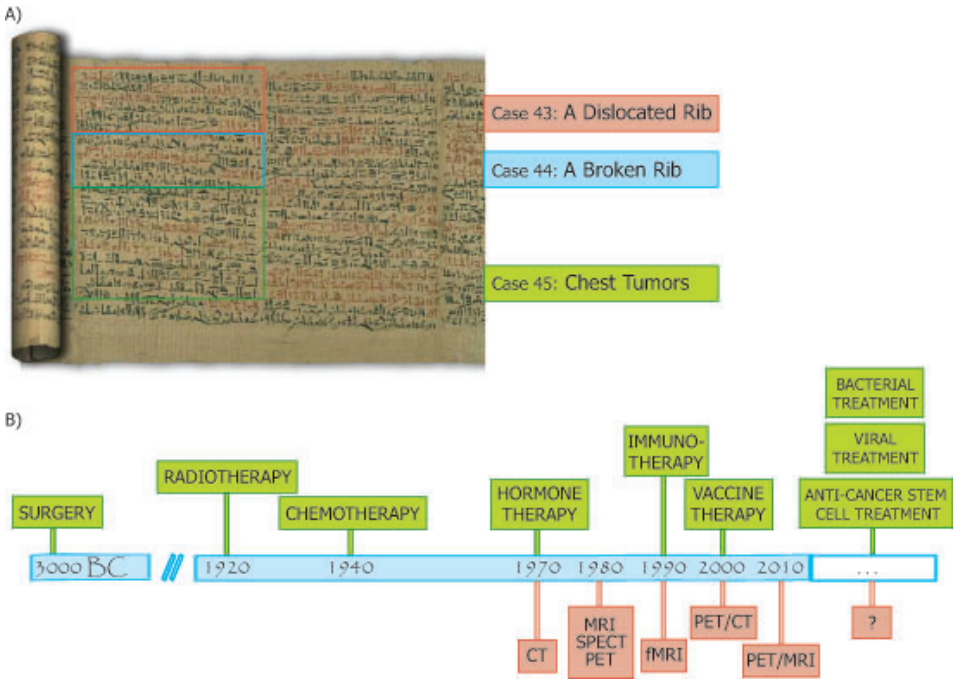

Fig. 2. Development of cancer treatment modalities: A) Smith's Surgical Papyrus (provided by Dr. George Thoma at the US National Library of Medicine); B) a historical timeline of cancer treatment and imaging method development.

therapy works by damaging cellular DNA, and in this way prevents cells from growing and dividing. Therefore, rapidly dividing cells, like cancer cells or bone marrow cells, are more vulnerable to radiation therapy than cells which divide more slowly. However, some cancers are less susceptible to this treatment and radiation can inflict irreversible damage to healthy tissues and organs.

Chemotherapy: In the 1940s, the first cancer chemotherapy with nitrogen mustards and folic acid antagonistic drugs was performed [22-24]. Thereafter, many different chemotherapeutics were discovered and introduced into clinical use (e.g. doxorubicin, cisplatin, paclitaxel and vincristine). Various chemotherapeutic regimes such as dose-intense treatment, sequential therapy, adjuvant therapy and combination therapy were subsequently designed to increase cancer cell death and overcome cancer resistance. Unfortunately, chemotherapy kills all rapidly dividing cells and cells which are unable to successfully repair the damage and, therefore, it lacks cancer specificity.

Hormonal therapy: In the 1970s, attention was focused on the development of more personalized anti-cancer therapy. The first attempt at hormonal therapy was a treatment of hormone receptor-positive cancer cells with tamoxifen [25]. The main cancers treated with hormonal therapy today are prostate and breast cancer [26,27].

Targeted therapy: The first available targeted therapy dates from the late 1990s [28]. Targeted therapy is based on targeting a specific deregulated protein in cancer cells. Targeted therapy is still a very active area of research which includes e.g. monoclonal antibody therapy (e.g. rituximab and trastuzumab/Herceptin, FDA approval in 1997 and 1998, respectively), small-molecule therapy (e.g. imatinib/Glivec, FDA approval in 2001), immunotherapy (e.g. autologous immune enhancement therapy used in Japan since 1990, or human leukocyte interferon-α, FDA approval in 2009), anti-angiogenic therapy (bevacizumab/Avastin, first FDA approval in 2004), vaccine therapy (Sipuleucel-T, FDA approval in 2010), etc. Furthermore, novel targeted modalities are being designed such as anaerobic bacteria that may be applied in the future in combination with other treatments [22]. These bacteria could actively remove the poorly oxygenated part of the tumor and become inactive upon contact with well perfused tumor parts, whereas the other anti-cancer agent(s) could be active in the oxygenized part of the tumor.

In summary, cancer cells introduce many changes to their phenotype to gain advantage over their neighbors. Although these new characteristics allow cancer to survive in difficult circumstances, cancer cells also become greatly reliant on such features for their survival. Therefore, detailed information on specific cancer characteristics in individual patients is essential in order to select or design an effective, unique anti-cancer treatment and compose the best drug combinations for cumulative or enhanced elimination of cancer cells.

Imaging cancer

Unfortunately, treatment of cancer is usually not curative because its effectiveness strongly depends on early diagnosis, precise localization of primary and metastatic lesions, and a well designed therapy regime. Therefore, early detection and characterization of cancer are essential for increasing patient survival. Cancer diagnosis can be performed by either invasive or non-invasive methods. The invasive approaches include techniques such as biopsy or surgery followed by pathological examination. They are limited to local tumor characterization (the metaphorical "tip of the iceberg") and cannot provide a view of total cancer burden e.g. all metastatic lesions. The non-invasive approaches include (i) screening for cancer markers in blood (which does not provide any data on anatomic or functional cancer characteristics), (ii) imaging techniques such

A)

Positron-emitting isotopes	Half-life	β+ fraction	Max. energy (MeV)	Mean range (mm)	Daughter isotope
^{18}F	109.8 min	0.97	0.63	0.3	^{18}O
^{11}C	20.4 min	0.99	0.96	0.4	^{11}B
^{13}N	9.97 min	1.00	1.20	0.7	^{13}C
^{15}O	2.04 min	1.00	1.74	1.1	^{15}N
^{68}Ga	68.3 min	0.88	1.83	1.2	^{68}Zn
^{89}Zr	78.4 h	0.23	0.90	1.1	^{89}Y

B)

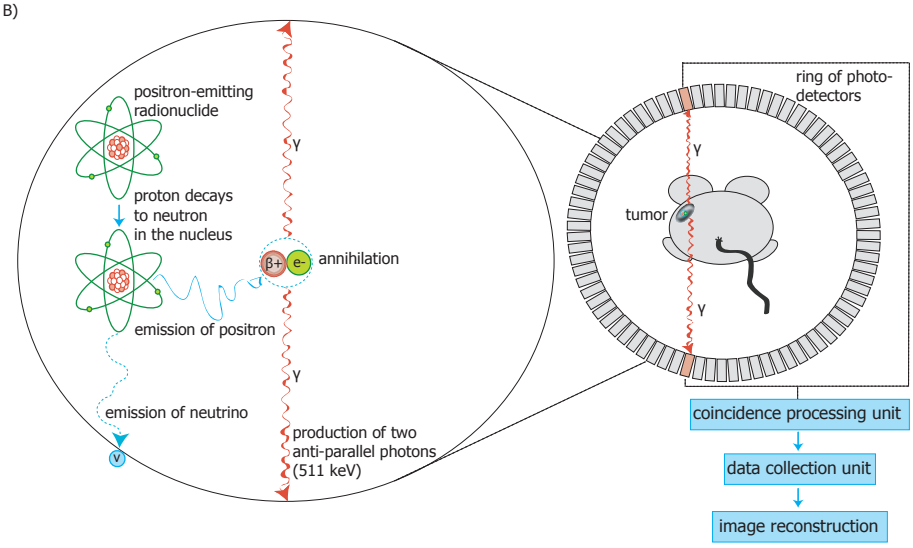

Fig. 3. Positron emission tomography: A) the most common positron-emitting isotopes in PET; B) a scheme depicting principles of PET: the left and right panel shows accordingly a physical principle and a practical methodology.

as sonography, CT (computed tomography) or MRI (magnetic resonance imaging) which show only anatomical changes, (iii) molecular imaging techniques like SPECT (single-photon emission computed tomography) and PET (positron emission tomography), which show biological changes [29,30]. PET is an attractive and powerful tool in oncology because it allows studying functions of intact cancer cells in their own environment in the intact living subject.

PET is a highly-sensitive nuclear medicine technique which uses radioactive isotopes with positron decay (Fig. 3). Positrons are particles with the same mass as an electron but a positive rather than a negative charge. They are short-lived and their annihilation results in two 511 keV gamma photons which can be detected by a dedicated camera. PET can be employed to image many biological functions (e.g. flow, molecule expression, enzymatic activity or transport) either in the whole body or in a target organ (Fig. 3B) [31]. The concept of radionuclide-based indicators for disease monitoring originates from a Hungarian scientist, George von Hevesy, nowadays considered as the father of nuclear medicine and awarded with a Nobel Prize in Chemistry in 1943. ^{18}F, ^{11}C, ^{13}N and ^{15}O are the isotopes commonly used in PET (Fig. 3A). During PET imaging, radioactively labeled molecules are injected in very low mass amounts into a subject's body to detect and quantify molecular processes in one temporal and three spatial domains. The resulting time-activity curves, pharmacokinetic data and images enable localization and staging of cancer, make prognosis or evaluation of treatment outcome possible, and therefore facilitate diagnosis and management of patients [30,32]. Furthermore, radioactive tracers may be used for studying the behavior of biomolecules not only *in vitro* but also *in vivo*. PET technology creates a direct link between basic sciences (biology, chemistry and physics) and research and treatment of patients (medicine).

Although the PET scan was already available in the late 1970s, the widespread use of this technique in oncology did not occur earlier than the 1990s when whole-body FDG scans became a clinical possibility. PET was acknowledged as an important tool in oncology with the burst of targeted therapies for cancer at the end of this decade. PET imaging has to continuously adapt in order to accommodate the more personalized treatment of cancer. This is exemplified by creation of small-animal imaging PET, microPET, which accelerates development of novel PET tracers in diverse animal models [33] (Fig. 3). Further progress was brought by the fusion of functional PET imaging with anatomic imaging modalities such as CT (available from 2000s) and MRI (introduced in 2010 by Siemens, in 2011 by Philips) which can provide a description of lesions "with surgical and pathological precision" [34] (Fig. 2).

The most common PET tracer in oncology, accounting for 90% of all oncologic scans, is ^{18}F-fluorodeoxyglucose (^{18}F-FDG). ^{18}F-FDG is, however, a more universal tracer which monitors glucose metabolism in every cell without a great discrimination between

Table 1. Examples of PET tracers used in oncology

Oncologic PET tracer	General target	Biochemical process
^{18}F-fluorodeoxyglucose (FDG)	glucose transporters (GLUTs) & hexokinases (HKs)	→ cellular energetics ~ 90% scans
^{18}F-fluoro-L-thymidine (FLT)	thymidine kinase-1 (TK-1)	→ proliferation
^{18}F-5-fluorouracil (5-FU)	thymidylate synthase	→ proliferation
^{11}C-methionine (MET)	aminoacid transporters	→ aminoacid transport
^{18}F-fluoroethyltyrosine (FET)	aminoacid transporters	→ aminoacid transport
^{11}C/^{18}F-choline analogues	choline kinases	→ phospholipid metabolism
^{18}F-annexin A5	exposure of phosphatidylserine	→ apoptosis/cell death
^{18}F-fluoroestradiol (FES)	estrogen receptor (ERs)	→ endocrine metabolic activity
^{18}F-L-dihydroxyphenylalanine (DOPA)	large aminoacid transporter (LAT), aminoacid decarboxylase (AADC), monoamine oxidase (MAO)	→ endocrine metabolic activity
^{18}F/^{64}Ga-octreotide analogues	somatostatin recepotr 2 (SST2Rs)	→ endocrine metabolic activity
^{18}F-fluorinated androgen analogues	androgen receptors (ARs)	→ endocrine metabolic activity
^{18}F-fluoromisonidazole (FMISO)	intracellular reductases	→ hypoxia
^{89}Zr-cetuximab	epidermal growth factor receptor (EGFR, Her1)	→ evasion & metastases
^{89}Zr-trastuzumab	human epidermal growth factor receptor 2 (Her2/neu)	→ proliferation, survival, differentiation
^{89}Zr-bevacizumab	vascular endothelial growth factor A (VEGF-A)	→ angiogenesis

cancerous and non-cancerous or malignant and non-malignant tissue [35]. Because there is more application for individualized imaging, new tracers for new targets are currently being designed [30]. Current tracers for oncology, which have been developed or are under development, monitor not only metabolism, but also features such as angiogenesis, hypoxia, apoptosis, gene expression, and tumor protein markers (Table 1).

Aim of the thesis

The general purpose of this thesis is to describe the progress made in development of sigma ligands as a novel modality for cancer treatment and imaging.

Overview of chapters

Sigma receptors are a class of proteins found to be highly expressed in tissues such as brain and tumor. There are two confirmed sigma receptor subtypes, sigma-1 and sigma-2. Many artificial sigma receptor agonists and antagonists are available for studying functions of sigma receptors in the body. Activation or deactivation of signaling pathways downstream sigma-1 or sigma-2 receptors was shown to have an effect on cell proliferation and survival. Cancerous cells are significantly more susceptible than non-cancerous cells to a negative regulation (growth inhibition or cell death after application of sigma ligands). Therefore, sigma receptors are emerging diagnostic and therapeutic targets in oncology. Current developments of sigma receptor research in the field of oncology are described in **Chapter 2** (a published review article). This chapter includes

descriptions of the putative endogenous sigma receptor ligands and a literature survey of the proliferation-related expression of sigma receptors in cancerous and non-cancerous tissues. Subsequently, the chapter focuses on the tumoricidal effects of sigma ligands, in particular inhibition of proliferation, activation of death processes and involvement of the sigma-1 and sigma-2 receptor subtypes. Finally, an overview and comparison of radioactively labeled sigma ligands for PET and SPECT imaging is presented.

The following thesis is divided into two experimental sections: an initial one concerning imaging and a second one concerning treatment of cancer.

The first section describes application of the sigma-1 ligand, ^{11}C-labeled 1-(3,4-dimethoxyphenethyl)-4-(3-phenylpropyl)piperazine (^{11}C-SA4503), for tumor imaging in experimental animals using microPET. Uptake of tracers may be affected by many factors such as blood flow, peripheral metabolism or competition by endogenous ligands [36]. Particularly the uptake of ligands binding to a saturable site, in contrast to radiolabeled substrates for transporter or enzyme proteins, can be very sensitive to endogenous ligand competition. Although the endogenous ligand for sigma receptors has not been identified with certainty, steroid hormones may bind to these sites. We therefore examined the *in vitro* and *in vivo* competition between ^{11}C-SA4503 and steroid hormones for binding to sigma-1 receptors in tumor cells (**Chapter 3**). Modification (both an increase and a decrease) of the levels of endogenous progesterone had a significant impact on binding of the tracer to glioma cells. Thus, progesterone and ^{11}C-SA4503 compete for occupancy of a limited number of sigma-1 receptors in tumors. This phenomenon may account for variability in the tumor uptake of sigma-ligands during PET studies of patients. Based on the results of our *in vitro* experiments, tracer uptake may also be affected by the levels of other sex hormones (e.g. testosterone) and their metabolites.

A high physiologic uptake of sigma ligands in the central nervous system (because of a high expression of sigma-1 receptors in the brain) could limit the use of such tracers for PET imaging of brain and intracranial tumors [37]. Therefore, we examined if ^{11}C-SA4503 can detect pituitary adenoma, a spontaneously developing intracranial hormone-secreting tumor in aged rats (prevalence 41-66% in Wistar Hannover rats of Taconic Farms, and 22-51% in Charles River rats). The expression of sigma-1 receptors in pituitary tumors had not been previously examined. **Chapter 4** describes microPET scans with ^{11}C-SA4503 in aged rats. Tracer uptake in healthy pituitary glands and pituitary tumors was compared and the impact of a pituitary tumor on ^{11}C-SA4503 uptake in the normal brain, thyroid and several peripheral organs was studied. Kinetic modeling was used to assess if increases of tracer uptake reflected an increased partition coefficient, an increased nondisplaceable binding potential or increases of both parameters. Pituitary tumors were well-visualized and the increased ^{11}C-SA4503 uptake in tumors (as compared to the normal pituitary) appeared to reflect both an increased partition coefficient and an

increased nondisplaceable binding potential of the tracer. Tracer uptake in brain tissue was increased in animals with pituitary tumors as compared to uptake in the brain of healthy rats. This increased brain uptake reflected an increased partition coefficient of the tracer, without significant change of tracer nondisplaceable binding potential. These findings may indicate that sigma-1 receptors are overexpressed in pituitary tumors compared to their tissue of origin and that ^{11}C-SA4503 is a suitable tracer for detection of pituitary adenomas, using PET.

The second part of this thesis concerns the use of sigma ligands for cancer treatment (either monotherapy or combination therapy with TRAIL). Sigma ligands are cytotoxic to cancer cells, but not toxic to most healthy cells. Relatively high concentrations (20-100 μM) of sigma ligands are required for this tumoricidal effect. This could be due to the fact that diffusion barriers must be passed to reach intracellular sites, or a large fraction of the sigma receptors must be occupied in order to induce a therapeutic effect. We have addressed this question in **Chapter 5**. Sigma receptor occupancies in rat glioma cells (C6) were correlated to oncolytic activity and metabolic changes in surviving cells, after *in vitro* treatment with various sigma ligands. A virtually complete occupancy of the entire sigma receptor population (both sigma-1 and sigma-2) appeared necessary for the therapeutic effect. Determination of sigma receptor levels and sigma receptor occupancy by therapeutic drugs (e.g. with ^{11}C-SA4503 and PET) may be possible in oncology patients and be employed for patient selection and prediction of the therapeutic dose of a sigma ligand. Examination of early metabolic changes following sigma ligand administration may indicate which tracer is most suitable for evaluation of tumor responses to sigma ligand therapy.

As a large increase of ^{18}F-FDG uptake was noted *in vitro* after treatment of tumor cells with sigma ligands, these compounds (like hormones) appear to induce a transient increase of glucose metabolism preceding cancer cell death, known as "metabolic flare". Since *in vitro* observations do not always match the *in vivo* situation, we examined if transient increases of ^{18}F-FDG uptake can also occur during sigma ligand treatment *in vivo* (**Chapter 6**). Mice bearing subcutaneous human A375M melanoma tumors were treated with the sigma ligand, rimcazole. Early tumor responses to treatment were monitored with ^{18}F-FDG and microPET. A375M tumors responded to the treatment by a strong (4-fold) reduction of their growth and ^{18}F-FDG uptake appeared to be initially increased. Thus, sigma ligands can affect glucose metabolism *in vivo*.

Malignant melanoma is characterized by early metastatic spread and pronounced therapy resistance. Cytokine-based therapy (interferon-gamma, IFNγ and soluble TNF-related apoptosis inducing ligand, sTRAIL) has thus far provided the most promising results for treatment of melanoma. Therefore, a novel immunotherapeutic fusion protein, designated anti-MCSP:TRAIL, in which an anti-tumor antibody fragment directed against

MSCP (scFvMCSP) is genetically fused to human soluble TRAIL, was developed in our institution. Anti-MCSP:TRAIL is conditionally inactive, but regains potent and tumor-selective pro-apoptotic activity after selective binding to tumor cell surface-expressed melanoma chondroitin sulfate proteoglycan (MCSP). MCSP is a cell surface transmembrane molecule that is selectively overexpressed on melanoma cells. Unfortunately, significant resistance of melanoma to sTRAIL was observed. Since sigma ligands have strong anti-melanoma activity and such compounds can overcome drug resistance in cancer and can synergistically enhance the anti-cancer effect of classic chemotherapeutics (e.g. doxorubicin, actinomycin D, vincristine, lomustin, paclitaxel and gemcitabine, see Chapter 2), we examined whether combination treatment of a sigma ligand, rimcazole, with anti-MCSP:TRAIL enhances apoptotic signaling and displays robust anti-cancer effects in human A375M melanoma (**Chapter 7**). In the following chapter (**Chapter 8**) we assessed early metabolic responses in cultured tumor (A375M melanoma) and determined the *in vitro* uptake of the PET tracers ^{18}F-FLT and ^{18}F-FDG. Combination of sigma ligands with TRAIL exerts robust anti-melanoma effects. ^{18}F-FLT and ^{18}F-FDG uptake can provide insight into underlying molecular events (inhibition of the cell cycle, decrease in cellular ATP levels).

In a pilot study described in **Chapter 9**, we evaluated the anti-cancer properties of rimcazole-TRAIL combination treatment on ovarian cancer cells, derived from ascites or a solid tumor of six patients. Patients were divided into two groups, responders and non-responders, based on the effect of combination treatment. In one sample, dose-dependency of the anti-tumor effect and caspase involvement were also studied. Based on the findings in this preliminary study, sigma ligands hold promise as adjuvants in chemotherapeutic protocols for ovarian cancer patients.

Chapter 10 summarizes the experimental results of this thesis and **Chapter 11** presents perspectives for future studies. **Chapter 12** is a summary in the Dutch and Polish language.

References

1 Stefansson V. Cancer: Disease Of Civilization? American Book-Stratford Press, Inc. 1960.

2 Jemal A, Bray F, Center MM, Ferlay J, Ward E, Forman D. Global cancer statistics. CA Cancer J Clin. 2011;61:69–90.

3 Anand P, Kunnumakkara AB, Kunnumakara AB, Sundaram C, Harikumar KB, Tharakan ST, et al. Cancer is a preventable disease that requires major lifestyle changes. Pharm Res. 2008;25:2097–116.

4 GLOBCAN 2008 [Internet]. (IARC) Section of Cancer Information. [cited 2011 Aug 5];Available from: http://globocan.iarc.fr/factsheets/populations/factsheet.asp?uno=900.

5 Hanahan D, Weinberg RA. The hallmarks of cancer. Cell. 2000;100:57–70.

6 Hanahan D, Weinberg RA. Hallmarks of cancer: the next generation. Cell. 2011;144:646–74.

7 Gillies RJ, Robey I, Gatenby RA. Causes and consequences of increased glucose metabolism of cancers. J Nucl Med. 2008;49 Suppl 2:24S-42S.

8 Kaufmann SH, Vaux DL. Alterations in the apoptotic machinery and their potential role in anticancer drug resistance. Oncogene. 2003;22:7414–30.

9 Fridman JS, Lowe SW. Control of apoptosis by p53. Oncogene. 2003;22:9030–40.

10 Foster FM, Traer CJ, Abraham SM, Fry MJ. The phosphoinositide (PI) 3-kinase family. J Cell Sci. 2003;116:3037–40.

11 Yuan TL, Cantley LC. PI3K pathway alterations in cancer: variations on a theme. Oncogene. 2008;27:5497–510.

12 Altomare DA, Testa JR. Perturbations of the AKT signaling pathway in human cancer. Oncogene. 2005;24:7455–64.

13 Shaw RJ. Glucose metabolism and cancer. Curr Opin Cell Biol. 2006;18:598–608.

14 Warbugr O. On the origin of cancer cells. Science. 1956;123:309–14.

15 Carmeliet P, Jain RK. Angiogenesis in cancer and other diseases. Nature. 2000;407:249–57.

16 Roninson IB. Tumor cell senescence in cancer treatment. Cancer Res. 2003;63:2705–15.

17 Nürnberg A, Kitzing T, Grosse R. Nucleating actin for invasion. Nat Rev Cancer. 2011;11:177–87.

18 Breasted JH. The Edwin Smith Surgical Papyrus. Oriental Institute Publications, University of Chicago: University of Chicago press; 1930.

19 Niederhuber JE. Abeloff's Clinical Oncology: Surgical interventions in cancer. 4th ed. Philadelphia: Pa: Elsevier Churchill Livingstone; 2008.

20 Curie M, Curie P. New Radio-Active Element in Pitchblende. Comptes Rendus. 1898;127:175–8.

21 Sherman AA. Translation of an historic paper. On a new, strongly radioactive substance, contained in pitchblende: by M.P. Curie, Mme P. Curie and M.G. Bémont; presented by M. Becquerel. J Nucl Med. 1970;11:269–70.

22 Urruticoechea A, Alemany R, Balart J, Villanueva A, Viñals F, Capellá G. Recent advances in cancer therapy: an overview. Curr Pharm Des. 2010;16:3–10.

23 Farber S, Diamond L, Mercer R, Sylvester R, Wolff J. Temporary remissions in acute leukemia in children produced by folic antagonist, 4-aminopteroylglutamic acid (aminopterin). N Eng J Med. 1948;238:787–93.

24 Gilman A. The biological actions and therapeutic applications of the B-chloroethyl amines and sulfides. Science. 1946;103:409–36.

25 Jordan VC. Tamoxifen: catalyst for the change to targeted therapy. Eur J Cancer. 2008;44:30–8.

26 Denis LJ, Griffiths K. Endocrine treatment in prostate cancer. Semin Surg Oncol. 18:52–74.

27 Lumachi F, Luisetto G, Basso SMM, Basso U, Brunello A, Camozzi V. Endocrine therapy of breast cancer. Curr Med Chem. 2011;18:513–22.

28 Peták I, Schwab R, Orfi L, Kopper L, Kéri G. Integrating molecular diagnostics into anticancer drug discovery. Nat Rev Drug Discov. 2010;9:523–35.

29 Khalil MM, Tremoleda JL, Bayomy TB, Gsell W. Molecular SPECT Imaging: An Overview. Int J Mol Imaging. 2011;2011:796025.

30 Gambhir SS. Molecular imaging of cancer with positron emission tomography. Nat Rev Cancer. 2002;2:683–93.

31 Phelps ME. PET: the merging of biology and imaging into molecular imaging. J Nucl Med. 2000;41:661–81.

32 Haberkorn U, Markert A, Mier W, Askoxylakis V, Altmann A. Molecular imaging of tumor metabolism and apoptosis. Oncogene. 2011;30:4141-51.

33 Chatziioannou AF. Molecular imaging of small animals with dedicated PET tomographs. Eur J Nucl Med Mol Imaging. 2002;29:98–114.

34 Judenhofer MS, Wehrl HF, Newport DF, Catana C, Siegel SB, Becker M, et al. Simultaneous PET-MRI: a new approach for functional and morphological imaging. Nat Med. 2008;14:459–65.

35 Van Waarde A, Elsinga PH. Proliferation markers for the differential diagnosis of tumor and inflammation. Curr Pharm Des. 2008;14:3326–39.

36 Valk PE, Bailey DL, Townsend DW, Maisey MN. Tracer Kinetic Modeling in PET: Characteristics of Radiotracers. In: Positron Emission Tomography: Basic Science and Clinical Practice. London, UK: Springer-Verlag; 2003. p. 149–50.

37 Van Waarde A, Jager PL, Ishiwata K, Dierckx RA, Elsinga PH. Comparison of sigma-ligands and metabolic PET tracers for differentiating tumor from inflammation. J Nucl Med. 2006;47:150–4.

Sigma receptors in oncology: therapeutic and diagnostic applications of sigma ligands

Chapter 2

Aren van Waarde[1], Anna A.Rybczynska[1], Nisha K. Ramakrishnan[1], Kiichi Ishiwata[2], Philip H.Elsinga[1] and Rudi A.J.O. Dierckx[1,3]

[1]Nuclear Medicine and Molecular Imaging, University Medical Center Groningen, University of Groningen, Groningen, The Netherlands

[2]Positron Medical Center, Tokyo Metropolitan Institute of Gerontology, Tokyo, Japan

[3]Nuclear Medicine, Ghent University, Ghent, Belgium

Current Pharmaceutical Design. 2010; 16: 3519-37.

Abstract

Sigma receptors (subtypes sigma-1 and sigma-2) are a unique class of binding sites expressed throughout the mammalian body. The endogenous ligand for these sites has not been identified, but steroid hormones (particularly progesterone), sphingolipidderived amines and N,N-dimethyltryptamine can bind with fairly high affinity. Sigma receptors are overexpressed in rapidly proliferating cells, like cancer cells. Particularly the sigma-2 subtype is upregulated when cells divide and down regulated when they become quiescent. Sigma ligands, especially sigma-2 agonists, can inhibit proliferation and induce apoptosis by a mechanism involving changes in cytosolic Ca^{2+}, ceramide and sphingolipid levels. Tumor cells are much more sensitive to such treatment than cells from their tissue of origin. Sigma ligands induce apoptosis not only in drug-sensitive but also in drug-resistant cancer cells (e.g., cells with p53 mutations, or caspase dysfunction). Moreover, sigma ligands may abrogate P-glycoprotein-mediated drug resistance and at subtoxic doses, they can potentiate the effect of conventional cytostatics. Thus, sigma-2 agonists may be developed as antineoplastic agents for the treatment of drug-resistant tumors. A large number of radiolabeled sigma ligands has been prepared for SPECT (single-photon emission computed tomography) and PET (positron emission tomography) imaging. Such radiopharmaceuticals can be used for tumor detection, tumor staging, and evaluation of anti-tumor therapy. There is still a need for the development of ligands with (1) high selectivity for the sigma-2 subtype, (2) defined action (agonist or antagonist) and (3) optimal pharmacokinetics (low affinity for P-glycoprotein, high and specific tumor uptake, and rapid washout from non-target tissues).

Keywords: sigma ligands, tumor imaging, proliferation markers, anti-tumor therapy, chemosensitizers, P-glycoprotein, apoptosis, multidrug resistance.

Introduction

Sigma receptors are unique proteins integrated in plasma, mitochondrial and endoplasmatic reticulum membranes of tissue derived from brain, kidney, liver, immune, endocrine and reproductive organs [1]. Sigma receptors were initially considered as members of the opioid family because the compound SKF 10,047 acts as an antagonist at mu-opioid and as an agonist at sigma sites [2]. However, when selective ligands became available, sigma receptors were shown to be unlike any other known neurotransmitter or hormone binding protein [3]. Even after 30 years of extensive research, understanding of the molecular cascade triggered by these transmembrane proteins is still rudimentary [4].

The two confirmed sigma receptor subtypes, 25 kDa sigma-1 and 21.5 kDa

Table 1. Expression of sigma receptors in human tumor cell lines

Cell Line	Origin	Radioligand	B_{max} (fmol/mg Protein or %)	Ref.
16HBE140	Bronchial epithelium (non-tumor line)	Real-time RT-PCR mRNA	4%	[42]
A375	Melanoma (amelanotic)	^{3}H-Pentazocine	34 (sigma-1)	[43]
A375	Melanoma (amelanotic)	^{3}H-DTG (+ 1 µM DEX)	3403 (sigma-2)	[43]
BE(2)-C	Neuroblastoma	^{3}H-Pentazocine	2980	[176]
H69	Small cell lung cancer	Real-time RT-PCR mRNA	51%	[42]
H209	Small cell lung cancer	Real-time RT-PCR mRNA	84%	[42]
H510	Small cell lung cancer	Real-time RT-PCR mRNA	76%	[42]
Jurkat	T-lymphocyte	^{3}H-Haloperidol	960	[177]
LNCaP	Prostate cancer	Real-time RT-PCR mRNA	18%	[42]
LNCaP.FGC	Prostate cancer	^{3}H-Pentazocine	1196 (sigma-1)	[43]
LNCaP.FGC	Prostate cancer	^{3}H-DTG (+ 1 µM DEX)	727 (sigma-2)	[43]
MCF-7	Breast adenocarcinoma	^{3}H-Pentazocine	0 (sigma-1 lacking)	[43]
MCF-7	Breast adenocarcinoma	^{3}H-DTG (+ 1 µM DEX)	2071 (sigma-2)	[43]
MCF-7	Breast adenocarcinoma	Real-time RT-PCR mRNA	16.6%	[42]
MCF-10A	Breast epithelium (non-tumor line)	Real-time RT-PCR mRNA	4%	[42]
MDA-MB-231	Breast cancer	Real-time RT-PCR mRNA	16%	[42]
NCI-H157	Non-small cell lung carcinoma	[^{3}H]SKF-10,047	674	[54]
NCI-H187	Small-cell lung carcinoma	[^{3}H]SKF-10,047	341 / 1820 (high / low affinity)	[54]
NCI-H727	Lung carcinoid	^{3}H-Pentazocine	26 (sigma-1)	[43]
NCI-H727	Lung carcinoid	^{3}H-DTG (+ 1 µM DEX)	2835 (sigma-2)	[43]
NCI-H727	Lung carcinoid	[^{125}I]PAB	Not specified	[178]
NCI-H838	Non-small cell lung carcinoma	[^{125}I]PAB	Not specified	[178]
NCI-H1299	Non-small cell lung carcinoma	[^{125}I]PAB	Not specified	[178]
PC-3	Prostate cancer	Real-time RT-PCR mRNA	33%	[42]
PNT2-C2	Prostate epithelium (non-tumor line)	Real-time RT-PCR mRNA	4%	[42]
SK-N-SH	Neuroblastoma	^{3}H-Pentazocine	975 (sigma-1)	[43]
SK-N-SH	Neuroblastoma	^{3}H-DTG (+ 1 µM DEX)	944 (sigma-2)	[43]
T47D	Breast ductal carcinoma	^{3}H-Pentazocine	108 (sigma-1)	[43]
T47D	Breast ductal carcinoma	^{3}H-DTG (+ 1 µM DEX)	1221 (sigma-2)	[43]
Th-P1	Leukemia	^{3}H-Pentazocine	1411 (sigma-1)	[43]
Th-P1	Leukemia	^{3}H-DTG (+ 1 µM DEX)	491 (sigma-2)	[43]
U-138MG	Glioblastoma	^{3}H-Pentazocine	1115 (sigma-1)	[43]
U-138MG	Glioblastoma	^{3}H-DTG (+ 1 µM DEX)	3136 (sigma-2)	[43]

Bmax values in % refer to the levels of mRNA compared to those of ß-actin

sigma-2 [5], are overexpressed in rapidly proliferating cells, like cancer cells from animal and human origin, as compared to healthy tissue (see Tables 1 and 2). While the sequence

Table 2. Expression of sigma receptors in rodent tumor cell lines

Cell Line	Origin	Radioligand	B_{max} (fmol/mg Protein)	Ref.
C6	Rat glioma	^{3}H-Pentazocine	42 (sigma-1)	[43]
C6	Rat glioma	^{3}H-DTG (+ 1 µM DEX)	5507 (sigma-2)	[43]
C6-BU-1	Rat glioma	^{3}H-DTG	10500 (sigma-2)	[179]
C6-BU-1	Rat glioma	^{3}H-DTG	6200 (sigma-2)	[180]
EMT-6	Mouse mammary carcinoma	^{3}H-Pentazocine	826 (sigma-1)	[167]
EMT-6	Mouse mammary carcinoma	^{3}H-DTG (+ 1 µM PEN)	740 (sigma-2)	[167]
N18TG2	Mouse neuroblastoma	^{3}H-DTG	11200	[180]
N1E-115	Mouse neuroblastoma	^{3}H-Pentazocine	41 (sigma-1)	[43]
N1E-115	Mouse neuroblastoma	^{3}H-DTG (+ 1 µM DEX)	3344 (sigma-2)	[43]
NB41A3	Mouse neuroblastoma	^{3}H-Pentazocine	76 (sigma-1)	[43]
NB41A3	Mouse neuroblastoma	^{3}H-DTG (+ 1 µM DEX)	7324 (sigma-2)	[43]
NCB-20	Rodent hybrid neurotumor	(+)-^{3}H-SKF10,047	11600	[181]
NCB-20	Rodent hybrid neurotumor	(+)-^{3}H-PPP	20900	[181]
NCB-20	Rodent hybrid neurotumor	(+)-^{3}H-SKF10,047	4100	[182]
NCB-20	Rodent hybrid neurotumor	(+)-^{3}H-SKF10,047	1000 (sigma-1), 69000 (sigma-2 ?)	[183]
NG108-15	Mouse neuroblastoma x rat glioma hybrid	^{3}H-DTG	15600 (sigma-2)	[184]
NG108-15	Mouse neuroblastoma x rat glioma hybrid	^{3}H-Pentazocine	95 (sigma-1)	[43]
NG108-15	Mouse neuroblastoma x rat glioma hybrid	^{3}H-DTG (+ 1 µM DEX)	3134 (sigma-2)	[43]
PC12	Rat pheochromocytoma	^{3}H-DTG, (+)-^{3}H-PPP	2025 and 1539 (sigma-2 ?)	[185]
PC12	Rat pheochromocytoma	^{3}H-NE100	3900 (sigma-1)	[186]
S20Y	Mouse neuroblastoma	^{3}H-DTG (+ 1 µM DEX)	2456 (sigma-2)	[43]

DEX = dextromethorphan, PEN = pentazocine

and partial structure of the sigma-1 receptor are established [6-8], the existence of the sigma-2 receptor has only been proven pharmacologically [9]. The sigma-1 receptor gene is located on human chromosome 9, band p13, a region associated with various psychiatric disorders [10].

Initial research on sigma receptors was focused on their role in the brain rather than in tumors.The endogenous ligand(s) for sigma receptors have not been identified with certainty. Early studies in extracts prepared from brain [11, 12] and liver [13] have indicated that such ligands exist. Various forms of stimulation (e.g., depolarization by veratradine or K^+, focal electrical stimulation) resulted in a transient, Ca^{2+}-dependent reduction of the binding of the sigma ligands ^{3}H-1,3-di-(2-tolyl)-guanidine (DTG) and ^{3}H-(+)-3-PPP to rat hippocampal slices [14, 15], suggesting that an endogenous sigma ligand is released after activation of granule cells, particularly in the dentate gyrus.

It has been proposed that neuropeptide Y and peptide YY are endogenous ligands for sigma receptors since these peptides competed with nanomolar affinity for ^{3}H-(+)-SKF 10,047 binding in rat brain homogenates [16], and intracerebral administration of

neuropeptide Y and peptide YY reduced the hippocampal binding of ^{3}H-(+)-SKF 10,047 in mouse brain *in vivo* [17]. However, this reduction was only minor (ca. 25%) and other research institutions could not reproduce the *in vitro* competition findings.

In contrast to neuropeptide Y, endogenous steroids such as progesterone, pregnenolone and testosterone were definitely shown to interact with rodent and human sigma-1 receptors, both *in vitro* and *in vivo* [18-27]. Two steroid-like binding domains have been identified in the sigma-1 receptor molecule [28-31].

In recent studies, endogenous compounds with an alkylamine structure were shown to act as sigma-1 ligands. Endogenous amines from the sphingolipid family (D-erythro-sphingosine, sphingamine) bind with sub-micromolar affinity to the sigma-1 receptor but not to the sigma-2 receptor protein. Because the phosphorylated form of such compounds (e.g., sphingosine-1-phosphate, S1P) has negligible affinity for both sigma receptor subtypes, the enzyme sphingosine kinase may inactivate the endogenous ligands. This hypothesis was confirmed by overexpression of sphingosine kinase in HEK- 293 cells. In kinase-overexpressing cells, D-erythro-sphingosine did not inhibit ^{3}H-pentazocine binding to sigma-1 receptors, whereas a prominent inhibition was observed in non-overexpressing control cells [32].

Another alkylamine, the hallucinogen N,N-dimethyltryptamine (DMT), has also been identified as an endogenous sigma-1 ligand [33]. A hypothetical signaling scheme triggered by the binding of DMT to sigma-1 receptors has been proposed. However, the Kd of DMT binding at sigma-1 receptors (10^{-5} M range) is much higher than the concentrations of DMT which are reached *in vivo*. Thus, the physiological relevance of DMT signaling through sigma-1 receptors is not yet clear [34].

Ionic zinc may function as an endogenous ligand for sigma-2 receptors. Zn^{2+} displaces ^{3}H-DTG bound to these sites (IC50 110 μM), is released from zinc-containing mossy fibers upon electrical stimulation resulting in a reduction of the binding of ^{3}H-DTG to hippocampal slices, and this reduction is blocked by the Zn^{2+} chelator, metallothionein peptide 1 [35].

Sigma-1 knockout mice have been generated [36]. These animals are viable and fertile and do not display any overt phenotype. However, sigma-1 knockout mice differ from wild-type animals in three important respects:

1. When challenged with sigma-1 agonists such as (+)SKF- 10,047 [36] or DMT [33], sigma-1 knockout mice do not display a hypermotility response, or only an attenuated response. Thus, the psychostimulant action of sigma-1 agonists is suppressed in these mice.
2. Formalin-induced tonic pain is strongly (approximately 55%) reduced in sigma-1 knockout mice [37] and in normal mice treated with the sigma-1 antagonist haloperidol [38]. A recent publication reported that increased sensitivity (allodynia)

Table 3. Expression of sigma receptors in tumors

Type of Tumor	Species	Radioligand	B_{max} (fmol/mg Protein)	Ref.
Normal brain (cerebral cortex)	Human	[^{3}H]DTG	249 (sigma-1 + sigma-2)	[44]
Meningioma	Human	[^{3}H]DTG	683 – 1260 (4 specimens)	[44]
Neuroblastoma SK-N-MC	Human (grown in mouse)	[^{3}H]DTG	10,710	[44]
Normal kidney	Human	[^{3}H]DTG	707 ± 112 (sigma-1 + sigma-2)	[45]
Renal carcinoma	Human	[^{3}H]DTG	1353 ± 134	[45]
Normal colon	Human	[^{3}H]DTG	638 ± 20 (sigma-1 + sigma-2)	[45]
Colon carcinoma	Human	[^{3}H]DTG	3095 ± 321	[45]
Sarcoma	Human	[^{3}H]DTG	954 ± 97	[45]
Normal bladder	Human	[^{3}H]DTG (+ 200 nM PEN)	943 – 1034 (sigma-2, 6 specimens)	[48]
Bladder carcinoma	Human	[^{3}H]DTG (+ 200 nM PEN)	930 – 4275 (sigma-2, 6 specimens)	[48]
Normal bladder	Cow	[^{3}H]DTG (+ 200 nM PEN)	370	[49]
Low-grade bladder carcinoma	Cow	[^{3}H]DTG (+ 200 nM PEN)	1370 ± 320	[49]
High-grade bladder carcinoma	Cow	[^{3}H]DTG (+ 200 nM PEN)	10900 ± 2800	[49]

DEX = dextromethorphan, PEN = pentazocine

to mechanical and thermal (cold) stimuli found after peripheral (sciatic) nerve injury is markedly attenuated or even absent in mice lacking sigma-1 receptors [39]. These experiments support a role for sigma-1 receptors in the regulation of non-acute pain.

3. Under certain forms of stress, sigma-1 receptor knockout mice display a depressive-like phenotype [40]. In wildtype mice, sigma-1 agonists are antidepressants [41].

Other studies (discussed below) have indicated that sigma receptors are not only implied in psychiatric disorders and in the sensation of pain, but also in mechanisms controlling cellular proliferation and survival. These data suggested possible applications of sigma ligands in oncology.

Receptor overexpression in tumors and tumor cell lines

As shown in Tables 1 and 2, sigma receptors are expressed at very high densities in many cancer cell lines. Malignant cells show higher receptor expression than non-malignant cells originatingfrom the same tissue [42]. The mRNA for sigma-1 receptors, for example, is 13- to 21-fold more abundant in small cell lung cancerthan in normal bronchial epithelium, and 8-fold more abundant inprostate cancer than in normal tissue from the prostate (Table 1). Sigma-2 receptor levels are generally much higher than those of the sigma-1 subtype [43].

In an initial screening of human brain tumors, sigma receptors were detected in 15 of 16 tumors examined. Very strong receptor expression was observed in a brain

metastasis from a lung adenocarcinoma and in a human neuroblastoma passaged in nude mice [44]. Sigma receptors were found to be 2- to 5-fold overexpressed in renal and colon carcinomas ([45], see Table 3). A much higher number of binding sites was observed for the non-subtype-selective sigma agonist [^{3}H]DTG than for the sigma-1-subtype selective agonist [^{3}H]3-PPP [45]. This may indicate that in renal and colon carcinomas, like in cancer cell lines, the sigma-2 receptor is more abundant than the sigma-1 subtype. Immunocytochemical staining detected sigma-1 receptors in the majority of human primary breast carcinomas, particularly in tumors with a positive progesterone receptor status [46, 47].

Over-expression (1.5- to 4-fold) of the sigma-2 receptor was observed in human high-grade carcinomas of the urinary bladder, in contrast to low-grade carcinomas where sigma-2 receptor densities were comparable to normal tissue [48]. In bovine high-grade carcinomas of the urinary bladder, a 25- to 44-fold overexpression of the sigma-2 receptor was observed, whereas low-grade carcinomas showed 3- to 5-fold higher sigma-2 receptor densities than the normal bladder wall [49].

The over-expression of sigma receptors in malignant tissue and the large number of copies of the receptor proteins per tumor cell suggested that sigma receptor expression could be a biomarker of cellular proliferation and that tumors might be visualized using radiolabeled sigma receptor ligands and medical imaging techniques.

Sigma receptor expression and cellular proliferation

The relationship of sigma-2 receptor density and cellular proliferation was explored in an important study from 1997. The authors used the 66 cell line (murine mammary adenocarcinoma) to acquire pure populations of proliferative and quiescent cells [50]. [^{3}H]DTG was used as the radioligand in the presence of 0.1 μM unlabeled (+)-pentazocine, to mask sigma-1 sites. Proliferative cells were found to have 10-times more sigma-2 receptors than quiescent cells, although full downregulation of the sigma-2 receptor was reached only several (> 3) days after the cells had become quiescent [50]. Thus, the half-life of the sigma-2 receptor appeared to be rather long (> 12 h).

A subsequent study examined the relationship between sigma-1 receptor expression and the cell cycle in human breast (T47D and MCF-7) and prostate cancer (DU-145) cell lines, using the sigma-1-subtype-selective radioligand [^{125}I]-PAB. When mitosis was stimulated by treating cells with insulin or by providing them with fresh serum, radioligand binding was increased. The highest binding of [^{125}I]-PAB was observed in cells arrested in the M-phase with colcemid, and the lowest binding in cells arrested in G1 by serum starvation. Cells synchronized in G1/S phase by aphidicolin had lower sigma-1 receptor binding than cells in M phase. These data suggest that sigma-1 receptors are upregulated prior to mitosis [51].

The impact of other factors than proliferation on sigma-2 receptor expression was later examined. Proliferative cells of the 67 line (aneuploid mouse mammary adenocarcinoma) were found to have 8 times more sigma-2 receptors than quiescent cells. Since this aneuploid line showed the same results as were previously reported in diploid 66 cells, ploidy appears to not substantially affect sigma-2 receptor expression [52]. Like 66 cells, 9L cells form a "plateau phase" in cell culture. However, unlike 66 cells, the plateau phase observed with 9L cells arises from a birth-death equilibrium, not through the formation of a quiescent population of cells. A similar density of sigma-2 receptors was observed in the plateau and exponential phases of 9L cells. This observation suggests that sigma-2 receptors are downregulated in quiescent (i.e., plateau phase) 66 cells vs. exponentially growing (i.e., proliferative) 66 cells. The reduction in sigma-2 receptors in plateau phase 66 cells was not due to some other environmental factor such as cell-cell contact, nutrient depletion, or altered metabolism since that would have also been observed in the 9L cells [52]. When quiescent 66 cells or quiescent 67 cells were seeded at low density in new culture flasks with fresh medium, the return from the quiescent to the proliferative state was accompanied by a rapid increase of sigma-2 receptor density [52]. Finally, when MCF-7 breast cancer cells were treated with low concentrations of the cytostatic drug, tamoxifen, the sigma-2 receptor density was decreased. The extent of this decrease was similar to the decrease of other biomarkers of cellular proliferation, like the Ki-67 and IdU labeling indexes or AgNOR scores [52]. Thus, sigma-2 receptor expression in cancer cells appears to reflect their proliferative status but not the ploidy, the metabolic status or the number of cell-cell contacts.

In a subsequent study, proliferating 66 and 67 cells grown as solid tumors in nude mice were labeled with BrdU. Tumor tissue was subsequently excised and dissociated. Sigma-2 receptor binding in the resulting cell suspension was found to be related to the fraction of proliferative cells, and calculated ratios of sigma-2 receptor expression in proliferative and quiescent cells were similar to those observed *in vitro*. Thus, sigma-2 receptor expression may be a biomarker of cellular proliferation in solid tumors [53].

Cytotoxic effect of sigma ligands

An early study showed that the growth of human lung cancer cells (non-small cell NCI-H157, and small-cell NCI-H187) was dose-dependently inhibited by SKF-10,047 at concentrations greater than 100 nM. Strong growth inhibition was observed at an 1 μM concentration of this prototypical sigma-1 agonist. The inhibition occurred within a few hours of exposure, and it was irreversible after 24 h. The growth inhibition seemed to be related to sigma rather than opioid receptors, since it could not be blocked by the opioid antagonist, naloxone [54]. In a later study, the sigma ligands 2-IBP, haloperidol, and IPAB were found to inhibit the growth of small cell lung cancer cells

(NCI-N417) at 10 μM concentration [55].

Neuroleptics in 100 μM concentration (particularly haloperidol, reduced haloperidol [RHAL], fluphenazine and perphenazine) induced marked changes in the morphology of C6 glioma cells within 3 h (rounding, retraction of cellular extensions). Prolonged incubation resulted in cessation of cell division and ultimately in cell death. The cytotoxic activity of neuroleptics was closely related to their binding affinity at sigma receptors. Dopamine, serotonin, NMDA, muscarinic or beta-adrenoceptor antagonists did not show this effect. Thus, sigma receptors appear to be involved in the regulation of cellular viability [56].

An Australian study examined the effect of the sigma ligands (+)-SKF10,047, (-)-SKF10,047, DTG, haloperidol, RHAL, rimcazole, (+)-pentazocine and (-)-pentazocine on proliferation of other cultured cells, *viz.* human mammary adenocarcinoma (MCF-7, MDA), colon carcinoma (LIM1215, WIDr) and melanoma (Chinnery) cells [57]. Dose-dependent rounding, detachment and cell death were observed in all cell lines. Rimcazole and RHAL were the most potent inhibitors of cellular proliferation. Ligands for dopamine receptors (SCH23390, raclopride), serotonin receptors (mianserin), NMDA receptors ((+)-MK801), beta-adrenoceptors (propranolol) or opioid receptors (naloxone) were generally ineffective, although mianserin and raclopride showed some effect in Chinnery and WIDr cells [57]. Ligands for the sigma-1 binding site produced much smaller effects than ligands binding to both sigma-1 and sigma-2 sites. Cells lines with long doubling times (e.g., 32 h) were less sensitive to treatment with sigma ligands than cells with shorter doubling time (e.g., 15 h). The morphological changes triggered by sigma ligands suggested an apoptotic rather than a necrotic mechanism of cell death [57].

Sigma ligands were found to have similar effects in SK-N-SH and SH-SY5Y neuroblastoma, NCB-20 hybridoma, NG108-15 neuroblastoma-glioma hybrid, COS-7 (immortalized green monkey kidney cells), MRS-5 (human lung cell line), and PC12 pheochromocytoma [58]. The pH of the culture medium was found to strongly affect the experimental outcome. EC50 values were lowered when the pH was increased from 7.3 to 8.4, and they were markedly increased when the pH was lowered from 7.3 to 6.6. Various mechanisms may be underlying this effect of medium pH. Most likely, only the deprotonated form of the ligands interacts with the sigma-1 receptor. Since all test compounds were amines, they were protonated at acidic and deprotonated at basic pH. Deprotonated molecules may also more easily cross the cell membrane and may then interact with intracellular sigma-1 sites (e.g. in the endoplasmatic reticulum or in mitochondria). Finally, a low pH can inhibit intracellular calcium fluxes and may thus interfere with the cytotoxic action of sigma ligands [58].

RHAL (50 and 100 μM) increased the levels of cytoplasmic free calcium in WIDr colon and MCF-7 breast adenocarcinoma cell lines, due to release of calcium from

intracellular stores (endoplasmatic reticulum and mitochondria). This disturbance of calcium homeostasis appears to trigger apoptosis [59]. Later, it was shown that the inositol 1,4,5-triphosphate (IP3) receptor is involved in the sigma-2-agonist induced release of intracellular calcium [60]. The increase of cytosolic Ca^{2+} is accompanied by a rapid drop of metabolic activity and cellular ATP concentrations (within 10 min) which finally results in cell death [60].

Receptor subtype involved in cell killing

Initially, a general correlation was reported between the cytotoxic potency of sigma ligands and their affinity at sigma-1 sites labeled with [^{3}H](+)-pentazocine [58]. However, later studies showed that the effects of sigma ligands on cellular morphology and apoptosis correlated much better with their affinity to sigma-2 rather than sigma-1 sites (see [61] and abstracts cited therein). In a study from our own institution on C6 glioma cells, competition binding assays were performed with the radioligand 1-(3,4-di-^{11}C-methoxy-phenethyl)-4-(3-phenylpropyl)piperazine (^{11}C-SA4503), and cell death was quantified after incubation with (+)-pentazocine (sigma-1 agonist), AC915 (sigma-1 antagonist), rimcazole (nonsubtype- selective sigma ligand) and haloperidol (non-subtypeselective sigma ligand). Cytotoxicity of the test drugs and changes of cellular metabolism (glycolytic rate, thymidine kinase 1 activity, choline kinase activity) were not observed at low drug doses associated with occupancy of the sigma-1 subpopulation, but only at high doses resulting in occupancy of all sigma receptors (both sigma-1 and sigma-2, for > 98%). Cytotoxicity of the test compounds was related to their affinity for sigma-2 but not sigma-1 receptors [62]. Thus, our PET data confirmed that in C6 cells, death is induced *via* sigma-2 receptors [61, 62]. The apoptotic component of haloperidol-induced cell death in rat pheochromocytoma (PC12) and mouse neuroblastoma (N2a) cells has also been shown to be mediated *via* sigma-2 receptors [63]. Therefore haloperidol, which is generally considered as a non-subtype-selective sigma antagonist, may in fact act as an agonist at sigma-2 receptors.

An Italian study examined growth inhibition by nine newly synthesized sigma ligands in two human breast cancer cell lines (MCF-7 and MDA-MB231). Compounds with significant sigma-2 affinity were found to be more potent than compounds which bind mainly to sigma-1 receptors. EC50 values were in the 40 to 100 μM range [64].

Very potent antitumoral activity was reported for the sigma ligand SR31747A in human epithelial breast and prostate cancer cell lines. Nanomolar concentrations of this compound already caused a dramatic inhibition of cell proliferation in both hormoneresponsive and unresponsive cells. However, since SR31747A binds to multiple sites including sigma-1 receptors, sigma-2 receptors, the enzyme sterol isomerase and SR37147A-binding protein-2, cytotoxicity of this drug may be based on other mechanisms

than its interaction with sigma receptors [65, 66].

An interesting study in SK-N-SH (human neuroblastoma) and C6 (rat glioma) cells correlated the antiproliferative and cytotoxic activities of sigma-2 agonists and sigma-1 antagonists to affinities of the test compounds at sigma receptors [67]. PB28 (sigma-2 agonist) was a potent inhibitor of growth, whereas AC927 (sigma-2 antagonist) was inactive. On the other hand, NE-100 (sigma-1 antagonist) inhibited proliferation while (+)-pentazocine (sigma-1 agonist) displayed a very low antiproliferative potential. The cytotoxic and antiproliferative effects of DTG and haloperidol reflected their sigma-1 antagonist and sigma-2 agonist activities. The antiproliferative activity of PB28 (sigma-2 agonist) could be partially blocked by pretreating cells with AC927 (sigma-2 antagonist). Apparently, sigma-2 receptor activation and sigma-1 receptor inhibition produce similar anti-cancer effects in cell proliferation and cytotoxicity assays [67]. Later studies confirmed that sigma-1 antagonists can be effective antitumor agents and can fully inhibit growth of A427 lung cancer cells at a concentration of 20 μM [68]. Bicyclic ligands with combined sigma-1 and sigma-2 affinity can be more potent than cisplatin [69].

Mechanisms underlying cytotoxicity

The mechanisms underlying cytotoxic effects of sigma-1 antagonists have been examined in detail. IPAG, rimcazole, BD1047, RHAL, and BD1063 showed pronounced anti-cancer effects. They mediated caspase activation *via* a rapid increase of cytoplasmic calcium resulting in apoptotic cell death. Sigma-1 agonists such as (+)-SKF10,047 and (+)-pentazocine attenuated these three processes. However, the sensitivity of cells towards sigma-1-antagonist triggered apoptosis appears to be not related to sigma-1 receptor expression but rather to coupling of existing receptors to the cell death pathway. Thus, sigma-1 receptor-rich neurons and several other normal cells such as fibroblasts and epithelial cells are resistant to sigma-1 antagonists, whereas tumor cells are susceptible. Cells that can promote autocrine survival such as lens epithelial and microvascular endothelial cells are equally susceptible as tumor cells [70]. The sensitivity of lens cells was confirmed in a later study which showed that their exposure to sigma-1 receptor antagonists (rimcazole, BD1047) leads to growth inhibition and the production of pigment granules. Apparently, the sigma-1 receptor has a protective function and it normally minimizes the harmful effects of photo-oxidation in the human eye [71]. The importance of sigma-1 receptors for cellular viability was further demonstrated by treating FHL124 human lens cells with sigma-1 receptor siRNA. Such treatment (72 h) led to a 70% loss of sigma-1 receptor mRNA, a 60% loss of receptor protein and a striking increase of caspasedependent cell death [72]. In a paper from another group, sigma antagonists like haloperidol and RHAL (1-10 μM range) were shown to induce an early decrease in the ATP content of melanoma cells (murine B16, human SK-MEL-28) and to cause G1 arrest [73].

The inhibitory effects of a sigma-1 antagonist (4-IBP) and of many psychiatric drugs with sigma-1 affinity on the duration of cell division and glioblastoma migration have recently also been examined with time-lapsed phase-contrast microscopic imaging [74, 75].

An interesting study from Italy examined the dose-dependent effects of PB28, a sigma-2 agonist and sigma-1 antagonist, in two breast cancer cell lines: MCF7 (low P-gp) and MCF7 ADR (high Pgp). The MCF7 line has a high sigma-2 receptor expression (1226 ± 150 fmol/mg protein) but a low expression of the sigma-1 subpopulation (434 ± 50 fmol/mg protein), whereas the MCF7 ADR line has a high expression of both the sigma-2 (1727 ± 150 fmol/mg protein) and the sigma-1 subtypes (1936 ± 200 fmol/mg protein). In both cell lines, PB28 strongly inhibited cell growth. The inhibitory effect did not occur within 24 h but it was evident after 48 h of treatment (IC50 15 to 25 nM). Cells were arrested in G0-G1 and they showed a significant increase of caspase-independent apoptosis. In addition to the apoptotic effect, PB28 (100 nM, 48 h treatment) also decreased the expression level of P-gp (by 60% in MCF7 cells and by 90% in MCF7 ADR cells, respectively). Due to the downregulation of P-gp, doxorubicin accumulation was strongly increased after treatment of cells with 20 nM PB28 (by 50% in MCF7 cells and by 75% in MCF7 ADR). Thus, sigma-2 agonists like PB28 can be applied either in monotherapy or in combination therapy with conventional cytotoxic drugs, and are potentially capable of overcoming P-gp-mediated multidrug resistance [76].

Besides P-gp, sigma ligands have been shown to modulate the activity and/or the expression of several other proteins involved in drug resistance, such as glucosylceramide synthase [77], Rho guanine nucleotide dissociation inhibitor [77], Akt kinase [78] and Bcl-2 family members [63]. Mutations in the TP53 gene, which are strong determinants of chemoresistance, do not affect the sensitivity of cancer cells to sigma-2-induced apoptosis [63, 79-81]. Moreover, sigma-2 induced apoptosis can be caspase-independent [80, 81] and may therefore also occur in cells with caspase dysfunction. However, the mechanism of cell death induced by sigma-2 ligands is dependent both on the type of ligand and the type of tumor cell. In pancreatic cells, the sigma-2 selective ligand, WC26, has been shown to induce caspase-dependent apoptosis [82]. Yet, the previously mentioned observations support the idea that sigma ligands in general, and sigma-2 agonists in particular, may be used to treat drug-resistant tumors and to reverse cancer cell resistance to chemotherapeutics.

Antitumor effect of sigma ligands in experimental animals

In an early pilot study, low doses of the sigma ligands IPAB or 2-IBP (4 mg/kg daily) were found to retard the proliferation of human small cell lung cancer xenografts in female athymic nude mice [55].

Later studies with SR31747A demonstrated potent growth inhibition of human

Table 4. Antitumor Effects of Sigma Ligands in Tumor-bearing Mice

Tumor Type	Animal Species	Treatment	Effect	Ref.
Small cell lung cancer NCI-N417	Athymic Balb/c nude mice	IPAB s.c. daily 4 mg/kg	Size after 1.5 wks reduced by 37 %	[55]
Small cell lung cancer NCI-N417	Athymic Balb/c nude mice	IBP s.c. daily 4 mg/kg	Size after 1.5 wks reduced by 19%	[55]
Mammary breast carcinoma MCF-7	Athymic Balb/c nude mice	SR31747A. daily 25 mg/kg i.p.	Alone ineffective, combined with tamoxifen (1 mg/kg/day) regression of tumor at > 40 d	[65, 66]
Idem, MDA-MB231	Athymic Balb/c nude mice	SR31747A. daily 25 mg/kg i.p	Growth reduction 60% after 67 d, 70% at 85 d	[65, 66]
Prostate cancer PC3	Athymic Balb/c nude mice	SR31747A. daily 25 mg/kg i.p	Growth reduction 50% after 45 d	[65, 66]
Prostate cancer DU145	Athymic Balb/c nude mice	SR31747A. daily 25 mg/kg i.p	Growth reduction 40% after 60 d	[65, 66]
Prostate cancer LNCaP	Athymic Balb/c nude mice	SR31747A. daily 25 mg/kg i.p	Growth reduction 45% after 75 d, combined with flutamide 70% reduction at day 75	[65, 66]
Breast carcinoma MDA-MB468	Outbred nude mice (Onu/Onu)	Rimcazole daily 10 mg/kg i.p.	Tumor stability in treated animals, in 30 d three-fold volume increase when untreated	[70]
Breast carcinoma MDA-MB435	NCr athymic mice	Rimcazole daily 15 mg/kg i.p.	Growth reduction 34% after 25 days	[70]
Breast carcinoma MCF-7	Outbred nude mice (Onu/Onu)	Rimcazole daily 40 mg/kg i.p.	Growth reduction 59% already after 14 days	[70]
Prostate cancer PC3M orthotopic	NCr athymic mice	Rimcazole daily 15 mg/kg i.p.	Growth reduction 42%	[70]
Lung carcinoma H1299	Outbred nude mice (Onu/Onu)	Rimcazole daily 40 mg/kg i.p.	Tumor stability in treated animals, when untreated 5-fold volume increase in 12 d and animal death	[70]
Orthotopic U373-MG glioblastoma	Nude mice	4-IBP (sigma-1 agonist) 2 mg/kg	Increased survival time from 80 to 100 d, in combination with temozolamide from 230 to 260 d	[77]
Orthotopic A549 NSCLC	Nude mice	4-IBP (sigma-1 agonist) 2 mg/kg	Alone ineffective, but survival time in combined treatment with irinotecan raised from 60 to 90 d	[77]
Murine pancreatic adenocarcinoma Panc-02	C57BL/6 mice	SV119 (sigma-2 ligand) 1 mg i.p., at 1 or 2d interval	Alone ineffective, but in combination with weekly gemcitabine (3 mg/mouse, for 2 wks) or daily paclitaxel (0.3 mg /mouse) tumor stability or regression	[85]
Orthotopic HS683 glioblastoma	Nude mice	Donepezil per os 2 mg/kg thrice per week for 3 wks	Alone ineffective, but in combination with temozolomide (40 mg/kg per os, thrice per week for 3 wks) an additive benefit (survival 41 rather than 34 d)	[75]

breast carcinoma (MDA-MB231) and various prostate cancer (PC3, DU145, LNCaP) xenografts in nude mice ([65, 66], see Table 4). Although SR31747A alone was not efficient at inhibiting growth of MCF-7 tumors, it induced tumor regression after 30-40 days of combination treatment with tamoxifen (1 mg/kg daily) and it prevented regrowth of MCF-7 tumors after > 50 days of tamoxifen treatment [65, 66]. In hormone-dependent LNCaP tumors, SR31747A acted synergistically with the anti-androgen flutamide ([65, 66], see Table 4). Thus, sigma ligands appear to have potential as chemotherapeutics, particularly in combination treatment.

In an animal model of lung cancer (murine alveolar cell carcinoma LIC2 cells implanted s.c. in the suprascapular area of BALB/c mice), sigma-1 receptor agonists (PRE-084, cocaine) were found to promote tumor growth and to induce expression of interleukin- 10 (IL-10) at the tumor site. Stimulation of tumor growth could be prevented by administration of anti-IL-10 neutralizing antibodies or by administration of a specific sigma-1 receptor antagonist (BD1047). Thus, sigma-1 receptor agonists, including cocaine, appear to augment tumor growth through an IL-10 dependent mechanism [83, 84].

In contrast, a seminal study from the UK demonstrated that systemic administration of sigma-1 antagonists (water-soluble rimcazole, but also *cis*-U50488 and haloperidol) significantly inhibits the growth of mammary carcinoma xenografts, orthotopic prostate tumors and lung carcinoma xenografts in immuno-compromised mice without adverse effects ([70], overview in Table 4). The authors suggested that sigma-1 receptors normally inhibit apoptosis, and that release of a sigma-1-receptor-mediated brake on apoptosis could be a novel approach to cancer treatment.

In an allograft model of pancreas cancer, daily treatment with the sigma-2 ligand SV119 (1 mg/kg) was not very effective in suppressing tumor growth and increasing animal survival. However, combination treatment of animals with SV119 and a relatively low dose of gemcitabine or paclitaxel led to tumor stability and in some cases even to tumor regression. All tumors resumed growing shortly after treatment was stopped, but the tumors in mice which had received combination treatment grew slower than tumors in untreated mice or in mice which had received monotreatment. Since SV119 potentiated conventional chemotherapy and lowered the rate of tumor regrowth after termination of treatment, and since no significant toxicities were observed in serum examination, immunohistochemistry and necropsy, these results suggest that SV119 may be a useful "chemosensitizer" for treatment of pancreatic cancer by cell cycle specific chemotherapeutic drugs [85].

Radiolabeled sigma ligands for SPECT

The development of radiotracers for tumor imaging has been an active area of research for at least two decades. Sigma receptorbinding radiotracers could combine high tumor uptake with low uptake in inflammatory tissue and provide valuable information about a tumor's proliferative status.

A SPECT ligand for sigma receptors was already developed in 1991, although the target to which the tracer bound was not known at that time (see Table 5). Michelot and co-workers prepared N-(2-diethylaminoethyl)-4-iodobenzamide (abbreviated as IDAB or IBZA) as an imaging agent for malignant melanoma. The compound was labeled both with ^{125}I (for biodistribution studies) and with ^{123}I (for imaging). In mice bearing murine

Table 5. Radiolabeled Sigma Ligands for SPECT

Ligand	Affinities (nM)	Application	Ref.
^{131}I/^{125}I/^{123}I-N-(2-diethylaminoethyl)-4-iodobenzamide (IDAB, IBZA)	6.9 (σ_1) 2900 (σ_2)	Melanoma. Very high tumor-to-muscle ratio (95) in melanoma-bearing mice. Useful for detection of melanoma, but not NSCLC.	[86-90]
^{131}I/^{125}I-(2-piperidinylaminoethyl)-4-iodobenzamide (IPAB)	1.7 (σ_1) 158 (σ_2)	Melanoma, lung carcinoma. Very high tumor-to-muscle ratio (95) in nude mice bearing human melanoma xenografts.	[90, 178, 187]
^{125}I-N-(N-benzylpiperidin-4-yl)-4-iodobenzamide (4-IBP)	1.7 (σ_1) 25 (σ_2)	Breast cancer. Specific binding in target organs of rats. Saturable binding to MCF-7 cells.	[91, 92]
^{125}I-N-[2-(4-iodophenyl)ethyl]-N-methyl-2-(1-piperidinyl)ethylamine (IPEMP)	0.8 (σ_1) 15 (σ_2)	Melanoma, breast cancer. Specific binding in target organs of rats, but rather poor target-to-nontarget ratios. Saturable binding to A375 and MCF-7 cells.	[93]
1-3-^{123}I-iodo-1-propyl-4-[2-(3,4-dichlorophenyl)-ethyl]piperazine	1.3 (σ_1)	Not tested in vivo	[111]
^{123}I-1-(2-hydroxyethyl)-4-(4-iodophenoxymethyl) piperidine	2.3 (σ_1) 139 (σ_2)	Melanoma. Tumor-to-muscle ratios > 30 at 48 h after injection in mice bearing B16 or A375 tumors. However, binding largely to a non-sigma site.	[94, 95]
^{99m}Tc-BAT-EN6	43.5	Breast cancer (T47D cells). Not evaluated for tumor imaging, but some specific binding (about 50%) to rat liver and kidney in vivo.	[96]
2-^{125}I-N-(N-benzylpiperidin-4-yl)-2-iodobenzamide (2-IBP)	1.6 (σ_1)	Prostate cancer. Specific binding to LnCAP cells and to DU-145 tumors in nude mice (>50% reduction after pretreatment of animals with haloperidol)	[97]
4-^{125}I-iodo-N-[2-(1'-piperidinyl)ethyl] benzene-sulfonamide (IPBS)	0.5 (σ_1) 206 (σ_2)	Melanoma. High uptake in B16 xenografts, at 24h good tumor-to-background contrast.	[98]
N-[2-(1'-piperidinyl)ethyl]-3-^{125}I/^{123}I-iodo-4-methoxybenzamide (PIMBA)	11.8 (σ_1) 206 (σ_2)	Breast cancer, prostate cancer. DU-145 tumor-to-muscle ratio 70 at 6 h after injection. Pilot study in patients with breast cancer was successful (8 of 10 tumors detected).	[99-101]
[(N-[2-((3'-N'-propyl-[3,3,1]aza-bicyclo-nonan-3alpha-yl)(2"-methoxy-5-methyl-phenylcarbamate)(2-mercaptoethyl)-amino)acetyl]-2-aminoethanethiolato] ^{99m}Tc (V) oxide)	2723 (σ_1) 22 (σ_2)	Breast cancer. Tumor-to-muscle ratio about 5, 4 h after injection. Binding in the (66) tumor at least partially to sigma-2 receptors.	[102,103]
5-^{125}I/^{123}I-iodo-2,3-dimethoxy-N-[2-(6,7-dimethoxy-3,4-dihydro-1H-isoquinolin-2-yl)-butyl]-benzamide	12,900 (σ_1) 8.2 (σ_2)	Breast cancer. EMT-6 tumor-to-muscle ratio about 7, 2 h after injection. Yet, tumors not visualized in microSPECT.	[104]
1-[2-(3,4-dimethoxyphenyl)ethyl]-4- (2-iodophenylpropyl)piperazine (o-BON)	6.4 (σ_1) 10.2 (σ_2)	Melanoma. Tumor-to-muscle ratios about 15 (B16) and 7 (A375) in nude mice, 24h after injection	[105]
^{99m}Tc-nitrido heterocomplex of 4-amino-N-benzylpiperidine	Not specified	Melanoma, fibrosarcoma. Tumor-to-muscle ratios only 2.0 to 3.5, but specific binding to sigma-1 receptors (40% of total tumor uptake).	[106]
(+)-2-[4-(4-^{125}I/^{131}I-iodophenyl) piperidino] cyclohexanol (pIV)	1.3 (σ_1) 20.4 (σ_2)	Prostate cancer. DU-145 tumor-to-muscle ratio > 20 after 48 h. Binding largely specific (for at least 60% to sigma-1 receptors). Prolonged high uptake in liver and kidneys may be problem.	[107]

B16 melanoma tumors, very high tumor-to-muscle ratios (of about 95) were reached at 24 h after injection [86]. This encouraging result prompted a phase II scintigraphic trial with ^{123}I-IDAB in 110 patients which indicated that ^{123}I-IDAB is useful for the diagnosis of malignant melanoma (sensitivity 81%, accuracy 87%, specificity 100%) [87]. A clinical follow-up study from the same group in 48 patients also reported positive results and it was concluded that IDAB scintigraphy is a useful tool for staging of malignant melanoma [88]. Less favorable results were reported in a study from Brussels, where twenty-six

patients with melanoma and eight patients with non-small-cell lung cancer (NSCLC) were examined with IDAB scintigraphy. That study indicated a lower sensitivity for the technique in malignant melanoma (64%). Hepatic lesions and lesions originating from an amelanotic melanoma could not be detected. The sensitivity of an IDAB scan for detecting mediastinal lymph nodes of NSCLC was very poor (22%). The authors concluded that IDAB scintigraphy may be used to confirm the melanoma nature of lesions that are not easily accessible to biopsy. However, in patients with NSCLC the value of IDAB-SPECT is questionable [89].

Other researchers discovered that IDAB is a potent and subtype-selective sigma-1 receptor ligand (Table 5) [90]. *In vivo* imaging and receptor blocking studies were performed with a structurally related radioiodinated benzamide, IPAB, which has been labelled with ^{125}I (for biodistribution studies) and with ^{131}I (for imaging). IPAB binds with very high affinity to sigma-1 receptors and with lower affinity to the sigma-2 subtype (Table 5). This tracer showed similar tumor-to-muscle ratios in nude mice with human malignant melanoma xenografts (A2058) as IDAB, i.e. about 95 at 24 h after injection. Binding of ^{125}I-IPAB to A2058 cells *in vitro* was dose-dependently blocked by the cold compound [90]. However, sigma-1 receptor binding may not be the only mechanism responsible for the high uptake of IDAB and IPAB in malignant melanomas, since these benzamide tracers can also interact with the melanin pigment [86, 87].

In a later study, three regioisomers of a single lead structure were prepared. The most promising ligand in terms of selectivity for sigma over dopamine D2 receptors was [^{125}I]-N-(N-benzylpiperidin-4-yl)-4-iodobenzamide (4-IBP, see Table 5). Saturable binding of the compound was demonstrated to sigma-2 receptors in human breast cancer cells (MCF-7, Bmax 4000 fmol/mg protein) [91]. The biodistribution of 4-^{125}I-IBP was also examined in healthy rats which were either untreated or pretreated with the sigma antagonist haloperidol. Specific binding of the tracer (up to 68% of total tissue uptake) was observed in brain, kidney, heart and lung. The authors concluded that 4-IBP had potential for imaging sigma receptors *in vivo* and could be tested for imaging of breast cancer [92] Another ligand, [^{125}I]N-[2-(4-iodophenyl)ethyl]-N-methyl-2-(1-piperidinyl) ethylamine (4-IPEMP) showed a highaffinity, saturable binding to melanoma (A375) and breast cancer (MCF-7) cells which could be blocked with a sigma receptor pharmacology. However, co-injection of non-radioactive 4-IPEMP with the radioiodinated compound resulted in only a small decrease of tracer uptake in rat liver and brain (37% and 35%, respectively) suggesting that the compound displays a rather strong nonspecific binding *in vivo* [93].

Waterhouse et al. developed several piperidine-based sigma ligands as melanoma imaging agents. The most promising derivative was ^{123}I-1-(2-hydroxyethyl)-4-(4-iodophenoxymethyl) piperidine, which showed very good tumor-to-muscle ratios (>

30) at 48 h after injection in nude mice bearing B16 or A375 tumors. However, blocking studies with the non-radioactive sigma ligand DuP734 produced unexpected results. Although a significant reduction of radioactivity was observed in organs known to possess sigma receptors such as brain, lung, heart and liver, the tumor uptake of the radioligand was significantly and strongly increased. These data suggest that tumor uptake of the radiolabeled piperidine is largely mediated by a mechanism other than sigma receptor binding [94, 95].

In an attempt to prepare a ^{99m}Tc-labeled sigma ligand for SPECT, Bowen and co-workers prepared ^{99m}Tc-BAT-EN6, a bisaminothiol (BAT) chelate appended with a sigma-receptor pharmacophore. The tracer showed a high degree of specific binding (> 90%) in human breast ductal carcinoma cells (T47D) *in vitro* and some specific binding to rat liver (31%) and kidney (54%) *in vivo* [96].

More promising results than with the previous compounds were obtained with a novel radioiodinated benzamide, 2-^{125}I-N-(Nbenzylpiperidin-4-yl)-2-iodobenzamide (2-IBP). This ligand showed a dose-dependent saturable binding to both sigma-1 and sigma-2 receptors in LnCAP human prostate tumor cells (Table 5). Biodistribution studies in nude mice bearing human prostate tumor xenografts (DU-145) indicated that the tumors had the highest uptake of radioactivity of all organs both at 4 and 24 h after injection. Tumor uptake was significantly reduced (for > 50%) after pretreatment of animals with the sigma antagonist haloperidol. These data suggest that 2-IBP labeled with ^{123}I or ^{131}I rather than ^{125}I may be a promising tracer for SPECT imaging of prostate tumors [97].

The same authors developed a novel class of sigma receptor ligands, the substituted halogenated arylsulfonamides. One of these, 4-iodo-N-[2-(1'-piperidinyl) ethyl]benzyl-sulfonamide (4-IPBS), was radiolabeled with ^{125}I and tested in cell binding and biodistribution studies. The compound has a > 400-fold higher affinity to sigma-1 than to sigma-2 receptors (Table 5). Competition studies suggested that exclusively sigma-1 receptors are labeled by 4-IPBS in brain homogenates. The imaging potential of 4-IPBS was assessed by biodistribution studies in C57 black mice bearing B16 melanoma xenografts. High tumor uptake and tumor retention of the tracer were observed up to 24 h after injection. Much lower uptake of radioactivity was noted in all other organs. Thus, radiohalogenated benzenesulfonamides like 4-IPBS could be useful for melanoma imaging [98].

With exception of IDAB, all previously mentioned sigma ligands were only evaluated in experimental animals. A more extensive evaluation (both in experimental animals and humans) was performed for N-[2-(1'-piperidinyl)ethyl]-3-iodo-4-methoxybenzamide (PIMBA). PIMBA binds with fairly high affinity to sigma-1 receptors and with lower affinity to the sigma-2 subtype (Table 5). In Lewis rats bearing syngeneic RMT breast cancers, tumor-tomuscle uptake ratios of about 3 were reached 4 h after injection [99]. Very good

results were obtained in biodistribution studies with ^{125}I-labeled PIMBA in BALB/c nude mice bearing human prostate tumor (DU145) xenografts. Tumor-to-muscle and tumor-to-blood ratios both reached a value of 70 in this animal model at 6 h after injection, due to prolonged retention of the tracer in the tumors compared to non-target tissues [100]. In a small pilot study with ^{123}I-labeled PIMBA in breast cancer patients, a focally increased tracer accumulation was observed in scintigraphic images of 8 out of 10 patients with histologically confirmed breast cancer (mean tumor-to-background ratio 2.04). No uptake was seen in a case of lymphatic adenitis. Thus, PIMBA accumulated in breast tumors but not in a benign lesion of the breast [101].

The first sigma-2 subtype-selective SPECT ligand was reported in 2001: [(N-[2-((3'-N'-propyl-[3,3,1]aza-bicyclononan-3alpha-yl)(2"-methoxy-5-methyl-phenylcarbamate) (2-mercaptoethyl)amino)acetyl]-2-aminoethanethiolato] ^{99m}Tc-technetium(V) oxide. The non-radioactive rhenium surrogate bound potently to sigma-2 receptors but showed much lower affinity for the sigma-1 subtype (Table 5). Biodistribution studies were performed in mice bearing a mouse mammary adenocarcinoma (cell line 66). Stereoselectivity of the binding was observed *in vivo*, as one of the two enantiomers showed significantly better tumor-to-blood and tumor-to-muscle ratios than the other enantiomer. Tumor-to-muscle ratios of the racemic compound reached a maximum of 4.8 at 4 h after injection. Tumor uptake of the tracer was reduced (by about 30%) after treatment of animals with haloperidol, and at 1 h after injection, tumor tissue contained only parent compound. Thus, it may be possible to visualize breast tumors with a sigma-2 subtype-selective SPECT ligand. However, a very strong uptake of radioactivity in liver, kidneys and bladder may be a problem in using the tracer for examination of the abdomen [102, 103].

The same authors also developed a radioiodinated sigma-2 ligand, 5-iodo-2,3-dimethoxy-N-[2-(6,7-dimethoxy-3,4-dihydro-1H-isoquinolin-2-yl)-butyl]-benzamide, which was labeled both with ^{125}I and ^{123}I. The non-radioactive bromine analog bound with high affinity to sigma-2 receptors and it showed very high subtype selectivity (~1600-fold, Table 5). Biodistribution studies in BALB/c mice bearing mouse mammary tumors (EMT6) indicated that tumor-to-muscle ratios of about 7 were reached 2 h after injection. However, in microSPECT scans the tumors were hardly visualized, suggesting that ligands with strong tumor uptake and very high target-to-nontarget ratios are required for successful microSPECT imaging [104].

Researchers from Japan prepared radioiodinated analogs of the sigma-1 agonist SA4503. 1-[2-(3,4-dimethoxyphenyl)ethyl]-4-(2-iodophenylpropyl) piperazine (*o*-BON) was most successful. This compound binds with high and virtually equal affinities to both sigma-1 and sigma-2 receptors (Table 5). Biodistribution studies in nude mice bearing human A375 melanoma tumors indicated that tumor-to-muscle ratios of around 7 were reached, 24 h after injection. Even higher values were reached in B16 melanomas (about

15) and lower values in SK-N-SH neuroblastomas, ME180 cervical carcinomas and C6 gliomas. A good relationship was observed between the accumulation of [^{125}I]*o*-BON and sigma receptor expression in the tumors (r = 0.84). This suggests that it may be possible to non-invasively assess sigma receptor density, using SPECT and a radioiodinated sigma ligand. However, the authors did not present any microSPECT images [105].

A group from India reported *in vivo* data for a ^{99m}Tc-nitrido heterocomplex of piperidine. Only moderate tumor-to-muscle ratios were reached at 24 h after injection in Swiss mice bearing fibrosarcoma tumors or C57BL6 mice bearing melanomas (2.0 and 3.5, respectively). Binding of the complex in the tumors appeared to be partially to sigma-1 receptors, since it was reduced by 40% after pretreatment of animals with 25 μg of (+)-pentazocine [106].

Outstanding tumor-to-muscle ratios (> 20 at 48 h after injection) have been reported for a radioiodinated analog of vesamicol, (+)-2-[4-(4-^{131}I-iodophenyl)piperidno] cyclohexanol, or (+)-pIV, in mice bearing human prostate tumors (DU-145). Tumor uptake of the radioligand was inhibited (for about 60%) after pretreatment of animals with non-radioactive sigma ligands (haloperidol, SA4503 or (+)-pIV). However, a prolonged high uptake of radioactivity in liver and kidneys may preclude use of this ligand for examination of the abdomen [107].

In conclusion:

1. Some early SPECT tracers showed very high tumor-to-background ratios in melanomas, but tracer accumulation was based upon another mechanism than sigma receptor binding;
2. A common finding with most sigma ligands has been prolonged high uptake of radioactivity in liver, kidneys and intestines. Thus there is a need for receptor-binding radiotracers with improved pharmacokinetics (e.g., rapid urinary excretion);
3. Sigma-1 subtype-selective, non-subtype-selective and sigma-2 subtype-selective SPECT ligands have been developed showing specific binding to sigma receptors in tumors and other target tissues *in vivo*;
4. Since some sigma-1 subtype-selective tracers (4-IPBS, o-BON) have produced nice results in preclinical studies (high uptake and specific binding in tumors), sigma-1 ligands may be useful for particular indications, e.g. detection of melanoma and breast cancer;
5. Yet, sigma-2 subtype-selective ligands may be the tracers of choice for SPECT studies in oncology because this subtype is overexpressed in virtually every tumor and generally most abundant, whereas sigma-1 overexpression is much less common.

Radiolabeled sigma ligands for PET

Since the early 1990s, radiochemists from several imaging institutions have also

tried to develop labeled sigma receptor ligands for positron emission tomography (PET, see Table 6 and Fig. 1). Interest in such tracers was primarily fuelled by the idea that PET studies of sigma receptors could lead to greater insight in the mechanisms underlying movement disorders and psychosis. Because of the overexpression of sigma receptors in many types of tumors, such radiotracers could also be employed as tumor-imaging agents.

Thus, initial research focused on imaging sigma receptors in the healthy brain rather than in tumors. Several ligands were labelled with positron emitters and evaluated for studies of the brain. These include ^{11}C-DTG [108], three radioactive derivatives of DTG (1-[4-([^{11}C]methoxy)phenyl]-3-(1-adamantyl) guanidine, 1-[4-([^{11}C] methoxy)-2-methylphenyl]-3-(1-adamantyl)guanidine and 1-[4-([^{18}F]-fluoro)-2-methylphenyl]-3-(1-adamantyl)guanidine) [109], ^{11}C-L-687,384 [110], 1-[3-^{18}F-fluoro-(1-propyl)-4-[2-(3,4-dichlorophenyl)ethyl]-piperazine [111, 112], ^{18}F-haloperidol [113, 114], ^{18}F-BMY14802 [115, 116], and (+)-^{11}C-*cis*-N-benzyl-normetazocine [117, 118] (see Table 6 for further details).

Encouraging results for tumor imaging were obtained with ^{18}F-1-(3-Fluoropropyl)-4-(4-cyanophenoxy-methyl)piperidine (FPS). This compound binds with sub-nM affinity and moderate subtype selectivity to sigma-1 receptors *in vitro* (Table 6) and it shows the optimal lipophilicity for uptake in the brain (logP at pH 7.5 = 2.8) [119]. As expected, the tracer showed high uptake in rat brain (2.5% ID/g). Moreover, uptake in target organs

Table 6. Radiolabeled Sigma Ligands for PET

Ligand	Affinities (nM)	Application / Selectivity	Ref.
^{11}C-DTG	17.9	Brain (does not pass blood-brain barrier)	[108]
Analogs of DTG labeled with ^{11}C or ^{18}F	10, 7 and 3.2	Brain (only in vitro data)	[109]
[^{11}C]L-687,384		Brain (no follow-up)	[110]
1-[3-^{18}F-fluoro-(1-propyl)-4-[2-(3,4-dichloro-phenyl)ethyl]piperazine	4.2	Brain (only in vitro tests)	[111, 112]
^{18}F-Haloperidol	3.3 (σ_1), 18.9 (σ_2)	Brain (in vivo binding largely nonspecific)	[113, 114]
(±)-^{18}F-BMY14802	28 (- enantiomer)	Brain (in vivo binding largely nonspecific)	[115, 116]
^{11}C-N-benzyl-N-normetazocine	0.7 (σ_1), >700 (σ_2)	Brain (promising results in preclinical studies in mice)	[117, 118]
^{18}F-1-(3-Fluoropropyl)-4-(4-cyanophenoxy-methyl)piperidine (FPS)	0.5 (σ_1), 17 (σ_2)	Melanoma, brain, kinetics not ideal for modeling	[26, 119-121]
^{18}F-1-(2-fluoroethyl)-4-[(4-cyanophenoxy)-methyl]piperidine (SFE)	5 (σ_1)	Brain, better kinetics than FPS	[122, 123]
2-[^{18}F](N-fluorobenzylpiperidin-4-yl)-4-iodobenzamide (FBI)	0.4 (σ_1), 20 (σ_2)	Brain (rather strong nonspecific binding)	[127]
N-(N-Benzylpiperidin-4-yl)-2-[^{18}F]fluorobenza-mide (FBP)	3.4 (σ_1), 408 (σ_2)	Breast cancer, Brain	[124-126]
^{11}C-NE100	1.2 (σ_1), 60 (σ_2)	Brain (rather strong nonspecific binding)	[129]

Table 6. Contd...

Ligand	Affinities (nM)	Application / Selectivity	Ref.
^{11}C-SA6298	6.9 (σ_1), 154 (σ_2)	Brain (rather strong nonspecific binding)	[130]
1-(4-[^{18}F]fluorobenzyl)-4-(4-cyano-phenoxy-methyl)piperidine (FBnCNE)	0.8 (σ_1), 6.2 (σ_2)	Brain (nonspecific binding in the rat only 10%, thus good results)	[128]
^{11}C-Nemonapride	4.2	Brain (extrastriatal areas. Successfully used for studies in PD patients)	[131, 132]
3-(4-chlorobenzyl)-8-[^{11}C]methoxy-1,2,3,4-tetrahydrochromeno[3,4-c]pyridin-5-one	105 (σ_1)	Brain (adequate results in rats and monkeys)	[133]
^{18}F-N-4'-Fluorobenzyl-4-(2-fluorophenyl)-acetamide	3.2 (σ_1), 144 (σ_2)	Brain (in the rat, nonspecific binding < 10%, thus good results)	[134]
^{18}F-N-4'-Fluorobenzyl-4-(3-bromophenyl)-acetamide	1.2 (σ_1), 6 (σ_2)	Breast cancer (rather poor results)	[135, 136]
^{11}C-SA4503	17 (σ_1), 1800 (σ_2)	Brain, glioma, non-small cell lung cancer	[137-159, 163, 164, 188-190]
(+)-p-[^{11}C]methylvesamicol	3 (σ_1), 40.7 (σ_2)	Brain, weaker signal than ^{11}C-SA4503	[165, 166]
^{11}C-SA5845	33 (σ_1), 9.5 (σ_2)	Rabbit VX2 carcinoma (slightly better results than ^{11}C-SA4503). .	[156, 188]
^{18}F-FESA5845	3.1 (σ_1), 6.8 (σ_2)	Brain, glioma, non-small cell lung cancer	[157, 161, 163, 164]
^{18}F-FESA4503	6.5 (σ_1), 2.1 (σ_2)	Brain, weaker signal than ^{11}C-SA4503	[160, 161]
^{18}F-FMSA4503	6.4 (σ_1), 250 (σ_2)	Brain. Good results in monkeys (binding > 80% specific after 3 h)	[162]
^{11}C-PB167	16.5 (σ_1), 0.3 (σ_2)	Breast cancer, failed during in vivo tests	[167, 168]
1-Cyclohexyl-4-[3-(5-[^{11}C]methoxy-1,2,3,4-tetrahydro-naphthalen-1-yl)-propyl]-piperazine (^{11}C-PB28)	12 (σ_1), 0.2 (σ_2)	Brain, failed during in vivo tests	[169]
^{11}C-PB183	10 (both σ_1 and σ_2)	Prostate cancer, only in vitro tests in Transgenic Mouse Prostate (TRAMP) cells	[170]
N-[^{18}F]4'-fluorobenzylpiperidin-4yl-(2-fluoro-phenyl) acetamide (FBFPA)	3.2 (σ_1), 140 (σ_2)	Brain. Good results in rats and monkeys (low nonspecific binding)	[27]
2-Methoxy-^{11}C-N-(4-(3,4-dihydro-6,7-dimethoxy-isoquinolin-2(1H)-yl)butyl)-5-methylbenzamide	3078 (σ_1), 10 (σ_2)	Breast cancer. Rather poor tumor-to-muscle ratios (max. 3.1)	[171]
5-^{76}Br-bromo-N-(4-(3,4-dihydro-6,7-dimethoxy-isoquinolin-2(1H)-yl)butyl)-2,3-dimethoxybenzamide	12900 (σ_1), 8.2 (σ_2)	Breast cancer. Good tumor-to-muscle ratios (almost 10 after 4 h)	[172]
N-(4-(6,7-dimethoxy-3,4-dihydroisoquinolin-2(1H)-yl)butyl)-2-(2-[^{18}F]-fluoroethoxy)-5-methylbenzamide	330 (σ_1), 6.9 (σ_2)	Breast cancer. Fair results (max. tumor-to-muscle ratios about 3.5)	[173]
N-(4-(6,7-dimethoxy-3,4-dihydroisoquinolin-2(1H)-yl)butyl)-2-(2-[^{18}F]-fluoro-ethoxy)-5-iodo-3-methoxybenzamide	2150 (σ_1), 0.26 (σ_2)	Breast cancer. Good tumor-to-muscle ratios (8 after 2 h)	[173]
^{18}F-WC-59	1711 (σ_1), 0.8 (σ_2)	Breast cancer. Rather poor tumor-to-muscle ratios (2.5 after 2 h)	[174]
^{18}F-WMS-1813	1.4 (σ_1), 837 (σ_2)	Brain. Good results in mice.	[191]

(brain, lung, heart, kidney) was significantly reduced after pretreatment of animals with nonradioactive sigma ligands (unlabeled FPS, DuP734, haloperidol) but not by dopamine

D2 [(-)-eticlopride], serotonin 5-HT2 (ritanserin) or muscarinic antagonists (atropine). In nude mice bearing B16 melanoma tumors, the tracer exhibited a tumor/blood ratio of 124 and a tumor/muscle ratio > 7 at 4 h after injection [120]. The binding of ^{18}F-FPS in several brain regions (cerebellum, striatum, hippocampus, hypothalamus, occipital cortex) and in peripheral target organs (lung, spleen, heart) proved sensitive to competition by endogenous steroids which are known to interact with sigma-1 receptors (progesterone, testosterone, DHEA) [26] Preclinical toxicity studies in three animal species (rats, rabbits, dogs) and dosimetry estimates indicated that ^{18}F-FPS can be safely used for imaging studies in humans up to doses of 5 mCi and 2.8 μg per injection [121]. The time course of ^{18}F-FPS binding appears to be not ideal for kinetic modeling, since there is no significant loss of radioactivity from rat (or human) brain during a 4 h study period [26, 120]. For this reason, a ligand with slightly lower affinity than FPS was developed, ^{18}F-1-(2-fluoroethyl)-4-[(4-cyanophenoxy)-methyl]piperidine (SFE), and that compound showed

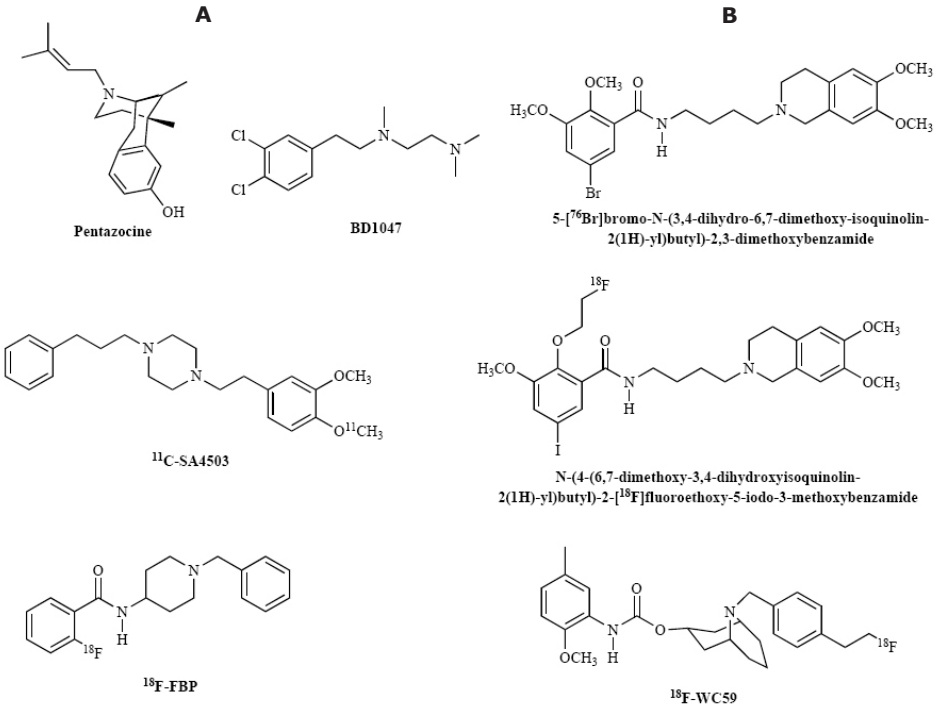

Fig. 1. Chemical structures of some sigma ligands discussed in this review: A) sigma-1 subtype-selective compounds (pentazocine, BD1047, ^{11}C-SA4503, ^{18}F-FBP); B) sigma-2 subtype-selective radioligands.

better kinetics in rodent brain (40% washout over a 90 min period) while retaining the favorable properties of FPS [122, 123]. No tumor imaging appears to have been performed with ^{18}F-SFE.

Nice results were also obtained with a structurally different radioligand, N-(N-benzylpiperidin-4-yl)-2-[^{18}F]fluorobenzamide (FBP). This compound binds with high affinity and reasonable subtype selectivity to sigma-1 receptors *in vitro* (Table 6). Blocking studies with haloperidol (2.5 mg/kg) in rats indicated that more than 90% of tracer uptake in various brain regions (striatum, cerebellum, hippocampus, brain stem) reflects binding to sigma receptors. In SCID mice bearing human breast tumors (MDA-MB231, or grown from primary explants) an adequate tumor-to-muscle contrast was observed (up to 7.8 at 1 to 2 h post injection), and this value was almost reduced to unity by pretreatment of animals with haloperidol. Thus, [^{18}F]-FBP is potentially useful for tumor imaging [124-126].

Analogs of FBP, such as 2-[^{18}F](N-fluorobenzylpiperidin-4-yl)-4-iodo-benzamide (FBI) [127], and analogs of FPS, such as 1-(4-[^{18}F]fluorobenzyl)-4-(4-cyanophenoxy-methyl)piperidine (FBnCNE) [128] have been prepared but these radioligands were never evaluated in tumor-bearing animal models (see Table 6). Several other ligands were also only evaluated for studies in the brain, such as the sigma-1 antagonist N,N-dipropyl-2-[4-methoxy-3-(2 phenylethoxy)phenyl]ethylamine (NE-100) which was labelled with ^{11}C in two different positions [129], the sigma-1 ligand [^{11}C]-SA6298 [130], the benzamide [^{11}C]-nemonapride (YM-09151-2) [131, 132] and the dopamine D4/sigma-1 antagonist 3-(4-chlorobenzyl)-8-[^{11}C]methoxy-1,2,3,4-tetrahydrochromeno[3,4-c]pyridin-5-one [133].

Tumor imaging has also been attempted with fluorinated acetamides. ^{18}F-N-4'-Fluorobenzyl-4-(2-fluorophenyl)-acetamide binds with high affinity and moderate selectivity to sigma-1 receptors *in vitro* (Table 6). Its uptake in rat brain was reduced for > 90% by pretreatment of animals with non-radioactive sigma receptor antagonists. Blocking studies with sigma-1 selective and nonsubtype- selective sigma ligands indicated that the tracer labels sigma-1 but not sigma-2 receptors *in vivo* [134]. ^{18}F-N-4'-Fluorobenzyl-4-(3-bromophenyl)-acetamide binds with high affinity to sigma-1 receptors, but its subtype selectivity is negligible (Table 6). This acetamide was evaluated in mice implanted with mouse mammary adenocarcinoma cells (line 66). A reasonable tumor-to-muscle ratio was observed (6.2 at 2 h post injection). The tumor-to-blood ratio was slightly reduced but tumor-to-muscle and tumor-to-lung ratios were significantly improved by pretreating mice with a cold sigma-1 ligand. These data suggest that for breast tumor imaging, a radiotracer with selectivity for the sigma-2 subtype should be better than a non-subtype-selective or sigma-1 subtype- selective ligand, since it will result in better tumor-to-background contrast [135, 136].

The sigma ligand which has been most widely used for PET imaging is ^{11}C-SA4503. This compound is a sigma-1 agonist with moderately high affinity and reasonable subtype selectivity (Table 6). Pre-, co- and postinjection of unlabeled SA4503 in rats decreased the uptake of ^{11}C-SA4503 in brain, spleen, heart, lung, kidney and skeletal muscle. Brain uptake of the ligand was also significantly reduced by pretreatment of animals with haloperidol (to about 30% of control). *Ex vivo* autoradiography confirmed that ^{11}C-SA4503 binding in rat brain is region-specific, a higher uptake being observed in cortex than in caudate putamen. No radioactive metabolites were detected in the brain at 30 min after injection, in contrast to plasma where approximately 20% of radioactivity represented metabolites [137]. In mouse brain, uptake of ^{11}C-SA4503 was reduced by 60-70% after co-injection of haloperidol or cold SA4503, but not affected by dopamine D2, histamine H1, muscarinic or serotonine 5-HT2 antagonists. In cat brain, about 60-65% of total uptake in cortex and cerebellum at 76 min after injection appeared to reflect specific binding [138]. ^{11}C-SA4503 is not a substrate for P-gp in the blood-brain barrier, in contrast to [^{3}H]-(+)-pentazocine [139]. Administration of non-radioactive SA4503 to mice results in a small reduction of cerebral binding of the dopamine D_2 receptor antagonist ^{11}C-raclopride probably because of increased release of dopamine from nerve endings in the striatum, but administration of non-radioactive raclopride does not affect cerebral binding of ^{11}C-SA4503 [140]. Thus, ^{11}C-SA4503 appears to be a suitable ligand for studies of sigma-1 receptors, both in the brain and in peripheral organs.

^{11}C-SA4503 has been successfully applied to PET studies of sigma-1 receptors in monkey [141, 142] and human [143-148] brain, including changes of receptor density in Alzheimer's disease [149], Parkinson's disease [150] or normal healthy ageing [142, 144], and assessment of sigma-1 receptor occupancy by CNS drugs [151-153].

The tracer was also used for studying sigma-1 receptors in rabbit eyes [154, 155] and in animal tumors [156, 157]. A study from our institution showed that the *in vivo* binding of ^{11}C-SA4503 to tumors is sensitive to competition by endogenous steroids. Tumor-to-muscle contrast is increased after steroid depletion and decreased after administration of exogenous progesterone [24]. In rats bearing a C6 glioma, a single treatment with doxorubicin (8 mg/kg i.p.) resulted in a significant 25-30% reduction of ^{11}C-A4503 uptake in the treated tumor with a corresponding decrease of sigma-1 receptor expression as determined by post mortem receptor assays [158]. However, a pilot PET study with ^{11}C-SA4503 in patients with NSCLC produced disappointing results [159]. Tumor lesions showing high FDG-uptake were cold spots in ^{11}C-SA4503 scans. In 3 tumors, a rim of increased uptake of ^{11}C-SA4503 was found surrounding the cold spots. In one patient many bone metastases were detected with FDG, while hot spots in the skeleton and bone marrow were also noted with ^{11}C-SA4503. Fused images showed that the FDG and ^{11}C-SA4503 hot spots were not at identical locations. In two patients, hot

spots in FDG-scans showed only slight uptake in ^{11}C-SA4503 scans with a surrounding cold region. Brain metastases detected with FDG were visible as cold spots in ^{11}C-SA4503 scans, whereas the surrounding healthy brain tissue showed a normal distribution pattern of sigma-1 receptors. Because of the high background uptake of ^{11}C-SA4503 in lung tissue and brain, and because an up-regulation of sigma-1 receptors was observed only in small areas of the tumors, ^{11}C-SA4503 appeared to be not suitable as a diagnostic tool for visualization of NSCLC and its brain metastases in cancer patients. Investigation of other tumor types is necessary to further elucidate the potency of sigma-1 receptor imaging of cancer. Two studies with ^{11}C-SA4503 in experimental animals suggest that a non-subtype-selective sigma ligand or a selective sigma-2 ligand may be more suited for tumor imaging than a selective sigma-1 agonist like ^{11}C-SA4503. In rat glioma cells, uptake of ^{18}F-FESA5845 (non-subtype-selective) but not of ^{11}C-SA4503 (sigma-1 selective) appeared to be strongly correlated to cellular proliferation [157]. In rabbits bearing VX-2 carcinomas, ^{11}C-SA5845 (non-subtype-selective) showed better target-to-background ratios than ^{11}C-SA4503 (sigma-1 selective), probably because of the fact that sigma-2 receptors are present at much higher densities than sigma-1 receptors in this tumor type [156].

Several radioligands for sigma receptors have been developed using SA4503 as lead compound, e.g. ^{18}F-FESA4503 [160, 161] and ^{18}F-FMSA4503 [162] but these tracers were never used for tumor imaging. ^{18}F-FESA5845 showed a similar distribution in conscious monkey brain as ^{18}F-FESA4503, but the binding potential of this ligand was 2- to 3-fold higher [161]. In receptor binding assays, FESA5845 showed high affinity for both sigma-1 and sigma-2 receptors (Table 6). Binding studies with ^{18}F-FESA5845 in C6 glioma cells indicated interaction of the ligand with two sites which could either be subtypes 1 and 2 of the sigma receptor, or sigma receptors located in different intracellular compartments. Biodistribution studies in tumor-bearing rats (Ham HSD RNU rnu with C6 gliomas in the right shoulder) indicated a tumor-to-muscle ratio of 4.9 after 60 min, which was reduced to 2.0 after pretreatment of animals with haloperidol [157]. In rats bearing both a C6 tumor and a sterile inflammation (induced by intramuscular injection of turpentine), ^{18}F-FESA5845 was found to accumulate in the tumor but hardly in the inflamed muscle [163]. The uptake of ^{18}F-FESA5845 in tumor cells was > 5-fold reduced when the cells moved from log phase to quiescence. In tumor-bearing animals, a significant reduction of tracer uptake was noted with increasing tumor size, probably because of growth inhibition in the center of the tumor. Thus, ^{18}F-FESA5845 showed some potential for tumor imaging and uptake of the tracer appeared to be related to cellular proliferation [157]. However, after 24 h of treatment of glioma cells with two cytostatic agents (doxorubicin, cisplatin), a paradoxical increase rather than a decrease of ^{18}F-FESA5845 uptake was noted, and treatment with a cytotoxic dose of 5-fluorouracil

did not affect ^{18}F-FESA5845 uptake at all [164].

(+)-p-Methylvesamicol, an analog of the vesicular acetylcholine transporter (VAChT) ligand vesamicol, is a sigma-1 antagonist and has been labeled with ^{11}C (Table 6). This compound has only been tested for studies of the brain [165, 166]. Another ligand with interesting *in vivo* properties, N-4'-fluorobenzylpiperidin-4yl (2-fluorophenyl) acetamide (FBFPA), was also only used for studies of the CNS [27].

Two cyclohexyl piperidine derivatives developed by Italian pharmacochemists have been labeled with ^{11}C and tested in experimental animals. PB167, a compound possessing high affinity to sigma-2 receptors and high or moderate affinity to sigma-1 receptors (Table 6) was labeled in the methoxy group and injected into mice bearing mammary tumors (EMT-6). Unfortunately, uptake in tumor tissue was found to be the same as in normal healthy muscle. This disappointing result may be due to the fact that PB167 is a substrate for P-gp and is actively expelled from tumors with a multi-drug-resistant (MDR) phenotype [167, 168]. Another cyclohexyl piperidine, ^{11}C-PB28, with a high affinity to sigma-2 receptors and a moderate affinity to the sigma-1 subtype (Table 6), has only been evaluated in healthy mice. The compound showed a rapid and homogeneous uptake in all brain structures, which could not be blocked by pretreatment of animals with unlabeled PB28 or with the sigma-2 ligand SM-21. Thus, ^{11}C-PB28 appears to be not suitable for sigma-2 receptor imaging since its *in vivo* binding is largely nonspecific [169]. A third compound, PB183, has been proposed for imaging of prostate adenocarcinoma, but thus far it has only been evaluated *in vitro* [170].

Mach *et al.* prepared four carbon-11 labeled ligands with high affinity and selectivity for sigma-2 receptors but different lipophilicities. The radiopharmaceuticals were evaluated in female BALB/C mice bearing EMT-6 breast tumors. Optimal tumor uptake was observed at a log P of + 2.75. The best results were obtained with 2-methoxy-^{11}C-N-(4-(3,4-dihydro-6,7-dimethoxy-isoquinolin-2(1H)-yl)butyl)-5-methylbenzamide (Table 6). Although tumor-to-muscle ratios were only fair (about 3 at 30 min post injection), they were better than those of the nucleoside ^{18}F-FLT. The poor results with ^{18}F-FLT may have been due to the fact that mice were not pretreated with phosphorylase in order to deplete them from endogenous thymidine [171].

Better results were obtained with a radiobrominated subtypeselective sigma-2 ligand, 5-^{76}Br-bromo-N-(4-(3,4-dihydro-6,7-dimethoxy-isoquinolin-2(1H)-yl)butyl)-2,3-dimethoxybenzamide. This compound binds with rather high affinity to the sigma-2 receptor and has negligible affinity for the sigma-1 subtype (Table 6). In mice bearing EMT-6 tumors, tumor-to-muscle ratios of almost 10 were reached at 4 h after injection and tumors were visualized. Tumor-to-muscle ratios were strongly reduced (from 8.6 to 3.6 at 2 h) after pretreatment of animals with a non-radioactive sigma ligand. Prolonged high uptake of radioactivity in the liver after injection of the radioligand will likely

prevent imaging of hepatic lesions. However, the high tumor-to-muscle ratios which were observed for implanted breast tumors suggest that it may be possible to image tumors in the lung, head and neck region, or the lower abdomen, using a radiolabeled sigma-2 ligand and PET [172].

Four fluorine-18 labeled benzamide analogues with high sigma-2 receptor selectivity were also prepared and evaluated for tumor imaging. One of these substances, N-(4-(6,7-dimethoxy-3,4-dihydroisoquinolin-2(1H)-yl)butyl)-2-(2-[^{18}F]-fluoroethoxy)-5-iodo-3-metho-xy-benzamide, showed almost equally good results in the EMT-6 tumor-bearing mouse model as the radiobrominated compound [173]. However, ^{18}F-WC-59, a subsequently developed radioligand with sub-nanomolar sigma-2 affinity and very high sigma-2 selectivity (Table 6) produced rather disappointing results (tumor-to-muscle ratio in the EMT-6 tumor-bearing mouse model maximally 2.5) [174]. ^{18}F-WC-59 is a radiolabeled [3.3.1]azabicyclononane. Azabicyclononane compounds do not appear to work as well as benzamide analogs *in vivo*, even though both classes of compounds have a high affinity and selectivity for sigma-2 versus sigma-1 receptors. The reason for this discrepancy is not known.

In conclusion:

1. Sigma-1 subtype-selective, non-subtype-selective and sigma-2 subtype-selective PET ligands have been developed showing specific binding to sigma receptors in tumors;
2. Radioligands for sigma-1 receptors may be useful for special indications (e.g. melanoma imaging), since some sigma-1 subtype-selective tracers (FPS) have produced good results in preclinical research;
3. Yet, for a variety of reasons, sigma-2-subtype-selective ligands may be the tracers of choice for PET imaging in oncology. First, this subtype is overexpressed in a much larger spectrum of tumors than the sigma-1 subtype. Second, sigma-2 receptors are usually much more abundant than sigma-1 receptors in tissues expressing both receptor subtypes. Sigma-2 ligands may therefore display greater tumor-to-background contrast than sigma-1-selective or non-subtype-selective radiotracers Third, sigma-2 receptor density appears to be more closely and strongly related to cellular proliferation than sigma-1 receptor expression. PET scans of the sigma-2 receptor may be a unique strategy to assess the ratio of proliferative over queiescent cells in individual tumors and may thus provide important information for therapy selection [175];
4. There is still opportunity for the development of positron-emitting ligands which combine high selectivity for the sigma-2 subtype with optimal pharmacokinetics.

Epilogue

Both sigma-1 and sigma-2 receptors are involved in the regulation of cellular proliferation and death or survival. Under normal conditions, sigma-1 receptors promote proliferation and inhibit apoptosis. Sigma-1 agonists stimulate tumor growth, whereas sigma-1 antagonists suppress growth and facilitate apoptosis. Release of a sigma-1-receptor-mediated brake on apoptosis could be a novel approach to cancer treatment. Sigma-2 agonists are powerful inducers of apoptosis in tumor cells but not in normal healthy tissue. The mechanism of apoptosis involves cytosolic calcium and can be caspase- and p53-independent. Therefore, sigma-2 agonists may kill both sensitive and drug-resistant tumor cells. Such compounds can also down-regulate P-gp, a key player in multidrug resistance, and they potentiate the antitumor effects of conventional cytostatics when administered at subtoxic doses. For these reasons, sigma-2 agonists and sigma-1 antagonists may be developed as antineoplastic agents and be used either in monotherapy or as adjuvants in chemotherapy.

The over-expression of sigma receptors in malignant tissue and the very large number of copies of the sigma-2 receptor protein per tumor cell suggest that tumors may be visualized using radiolabeled sigma ligands. Promising results have indeed been obtained in preclinical SPECT and PET imaging. Moreover, sigma-2 receptor expression was found to closely reflect the proliferative status but not the ploidy, the metabolic status or the number of cell-cell contacts of tumor cells and sigma-2 receptor density may be a biomarker of cellular proliferation in solid tumors. Radiopharmaceuticals which bind to sigma receptors may be used for tumor detection, tumor staging, and evaluation of anti-tumor therapy. However, there is still a need for novel ligands combining a high selectivity for the sigma-2 subtype, low affinity for P-gp, prolonged high uptake in tumor tissue and rapid washout from non-target organs.

References

1 Su TP. Sigma receptors. Putative links between nervous, endocrine and immune systems. Eur J Biochem 1991;200:633-42.

2 Martin WR, Eades CG, Thompson JA, Huppler RE, Gilbert PE. The effects of morphine- and nalorphine- like drugs in the nondependent and morphine-dependent chronic spinal dog. J Pharmacol Exp Ther 1976;197:517-32.

3 Quirion R, Chicheportiche R, Contreras PC, et al. Classification and nomenclature of phencyclidine and sigma receptor sites. Trends Neurosci 1987;10:444-6.

4 Hayashi T, Su TP. An update on the development of drugs for neuropsychiatric disorders: focusing on the sigma(1) receptor ligand. Expert Opin Ther Targets 2008; 12:45-58.

5 Hellewell SB, Bruce A, Feinstein G, Orringer J, Williams W, Bowen WD. Rat liver and kidney contain high densities of sigma 1 and sigma 2 receptors: characterization by ligand binding and photoaffinity labeling. Eur J Pharmacol 1994;268:9-18.

6 Hanner M, Moebius FF, Flandorfer A, et al. Purification, molecular cloning, and expression of the mammalian sigma1-binding site. Proc Natl Acad Sci U S A 1996; 93:8072-7.

7 Kekuda R, Prasad PD, Fei YJ, Leibach FH, Ganapathy V. Cloning and functional expression of the human type 1 sigma receptor (hSigmaR1). Biochem Biophys Res Commun 1996;229:553-8.

8 Mei JF, Pasternak GW. Molecular cloning and pharmacological characterization of the rat sigma(1) receptor. Biochem Pharmacol 2001;62:349-55.

9 Guitart X, Codony X, Monroy X. Sigma receptors: biology and therapeutic potential. Psychopharmacology (Berl) 2004;174:301-9.

10 Prasad PD, Li HW, Fei YJ, et al. Exon-intron structure, analysis of promoter region, and chromosomal localization of the human type 1 sigma receptor gene. J Neurochem 1998; 70(2): 443-51.

11 Su TP, Weissman AD, Yeh SY. Endogenous ligands for sigma opioid receptors in the brain ("sigmaphin"): evidence from binding assays. Life Sci 1986;38:2199-210.

12 Contreras PC, DiMaggio DA, O'Donohue TL. An endogenous ligand for the sigma opioid binding site. Synapse 1987;1:57-61.

13 Samovilova NN, Prokazova NV. [Search for an endogenous ligand for sigma receptors] Poisk endogennogo liganda sigma-retseptorov. Vopr Med Khim 1995;41:9-13.

14 Connor MA, Chavkin C. Focal stimulation of specific pathways in the rat hippocampus causes a reduction in radioligand binding to the haloperidol-sensitive sigma receptor. Exp Brain Res 1991;85:528-36.

15 Neumaier JF, Chavkin C. Calcium-dependent displacement of haloperidol-sensitive sigma receptor binding in rat hippocampal slices following tissue depolarization. Brain Res 1989;500:215-22.

16 Roman FJ, Pascaud X, Duffy O, Vauche D, Martin B, Junien JL. Neuropeptide Y and peptide YY interact with rat brain sigma and PCP binding sites. Eur J Pharmacol 1989;174:301-2.

17 Bouchard P, Dumont Y, Fournier A, St.Pierre S, Quirion R. Evidence for in vivo interactions between neuropeptide Y-related peptides and sigma receptors in the mouse hippocampal formation. J Neurosci 1993;13:3926-31.

18 Bergeron R, de Montigny C, Debonnel G. Pregnancy reduces brain sigma receptor function. Br J Pharmacol 1999;127:1769-76.

19 Maurice T. Neurosteroids and sigma1 receptors, biochemical and behavioral relevance. Pharmacopsychiatry 2004;37 Suppl 3:S171-82.

20 Maurice T, Phan VL, Urani A, Kamei H, Noda Y, Nabeshima T. Neuroactive neurosteroids as endogenous effectors for the sigma1 (sigma1) receptor: pharmacological evidence and therapeutic opportunities. Jpn J Pharmacol 1999;81:125-55.

21 Maurice T, Urani A, Phan VL, Romieu P. The interaction between neuroactive steroids and the sigma1 receptor function: behavioural consequences and therapeutic opportunities. Brain Res Brain Res Rev 2001;37:116-32.

22 Phan VL, Urani A, Romieu P, Maurice T. Strain differences in sigma(1) receptor-mediated behaviours are related to neurosteroid levels. Eur J Neurosci 2002;15: 1523-34.

23 Ramamoorthy JD, Ramamoorthy S, Mahesh VB, Leibach FH, Ganapathy V. Cocaine-sensitive sigma-receptor and its interaction with steroid hormones in the human placental syncytiotrophoblast and in choriocarcinoma cells. Endocrinology 1995; 136:924-32.

24 Rybczynska AA, Elsinga PH, Sijbesma JW, et al. Steroid hormones affect binding of the sigma ligand (11)C-SA4503 in tumour cells and tumour-bearing rats. Eur J Nucl Med Mol Imaging 2009;36:1167-75.

25 Su TP, London ED, Jaffe JH. Steroid binding at sigma receptors suggests a link between endocrine, nervous, and immune systems [see comments]. Science 1988; 240:219-21.

26 Waterhouse RN, Chang RC, Atuehene N, Collier TL. In vitro and in vivo binding of neuroactive steroids to the sigma-1 receptor as measured with the positron emission tomography radioligand [18F]FPS. Synapse 2007;61:540-6.

27 Mach RH, Gage HD, Buchheimer N, et al. N-[18F]4'- fluorobenzylpiperidin-4yl-(2-fluorophenyl) acetamide ([18F]FBFPA): a potential fluorine-18 labeled PET radiotracer for imaging sigma-1 receptors in the CNS. Synapse 2005;58:267-74.

28 Chen Y, Hajipour AR, Sievert MK, Arbabian M, Ruoho AE. Characterization of the cocaine binding site on the sigma-1 receptor. Biochemistry 2007;46(:3532-42.

29 Fontanilla D, Hajipour AR, Pal A, Chu UB, Arbabian M, Ruoho AE. Probing the steroid binding domain-like I (SBDLI) of the sigma-1 receptor binding site using N-substituted photoaffinity labels. Biochemistry 2008;47:7205-17.

30 Pal A, Chu UB, Ramachandran S, et al. Juxtaposition of the steroid binding domain-like I and II regions constitutes a ligand binding site in the sigma-1 receptor. J Biol Chem 2008;283:19646-56.

31 Pal A, Hajipour AR, Fontanilla D, et al. Identification of regions of the sigma-1 receptor ligand binding site using a novel photoprobe. Mol Pharmacol 2007;72: 921-33.

32 Ramachandran S, Chu UB, Mavlyutov TA, Pal A, Pyne S, Ruoho AE. The sigma1 receptor interacts with N-alkyl amines and endogenous sphingolipids. Eur J Pharmacol 2009;609:19-26.

33 Fontanilla D, Johannessen M, Hajipour AR, Cozzi NV, Jackson MB, Ruoho AE. The hallucinogen N,N-dimethyltryptamine (DMT) is an endogenous sigma-1 receptor regulator. Science 2009;323:934-7.

34 Su TP, Hayashi T, Vaupel DB. When the endogenous hallucinogenic trace amine N,N-dimethyltryptamine meets the sigma-1 receptor. Sci Signal 2009;2:e12.

35 Connor MA, Chavkin C. Ionic zinc may function as an endogenous ligand for the haloperidol-sensitive sigma 2 receptor in rat brain. Mol Pharmacol 1992;42:471-9.

36 Langa F, Codony X, Tovar V, et al. Generation and phenotypic analysis of sigma receptor type I (sigma 1) knockout mice. Eur J Neurosci 2003; 18(8): 2188-96.

37 Cendan CM, Pujalte JM, Portillo-Salido E, Montoliu L, Baeyens JM. Formalin-induced pain is reduced in sigma(1) receptor knockout mice. Eur J Pharmacol 2005;511: 73-4.

38 Cendan CM, Pujalte JM, Portillo-Salido E, Baeyens JM. Antinociceptive effects of haloperidol and its metabolites in the formalin test in mice. Psychopharmacology (Berl) 2005;182:485-93.

39 De la Puente B, Nadal X, Portillo-Salido E, et al. Sigma-1 receptors regulate activity-induced spinal sensitization and neuropathic pain after peripheral nerve injury. Pain 2009;145:294-303.

40 Sabino V, Cottone P, Parylak SL, Steardo L, Zorrilla EP. Sigma-1 receptor knockout mice display a depressive-like phenotype. Behav Brain Res 2009;198:472-6.

41 Bermack JE, Debonnel G. The role of sigma receptors in depression. J Pharmacol Sci 2005;97:317-36.

42 Aydar E, Onganer P, Perrett R, Djamgoz MB, Palmer CP. The expression and functional characterization of sigma (sigma) 1 receptors in breast cancer cell lines. Cancer Lett 2006;242:245-57.

43 Vilner BJ, John CS, Bowen WD. Sigma-1 and sigma-2 receptors are expressed in a wide variety of human and rodent tumor cell lines. Cancer Res 1995;55:408-13.

44 Thomas GE, Szucs M, Mamone JY, et al. Sigma and opioid receptors in human brain tumors. Life Sci 1990;46:1279-86.

45 Bem WT, Thomas GE, Mamone JY, et al. Overexpression of sigma receptors in nonneural human tumors. Cancer Res 1991;51:6558-62.

46 Simony-Lafontaine J, Esslimani M, et al. Immunocytochemical assessment of sigma-1 receptor and human sterol isomerase in breast cancer and their relationship with a series of prognostic factors. Br J Cancer 2000;82:1958-66.

47 Wang B, Rouzier R, Albarracin CT, et al. Expression of sigma 1 receptor in human breast cancer. Breast Cancer Res Treat 2004;87:205-14.

48 Colabufo NA, Berardi F, Contino M, et al. Correlation between sigma2 receptor protein expression and histopathologic grade in human bladder cancer. Cancer Lett 2006;237:83-8.

49 Roperto S, Colabufo NA, Inglese C, et al. Sigma-2 Receptor Expression in Bovine Papillomavirus-Associated Urinary Bladder Tumours. J Comp Pathol 2010;142:19-26.

50 Mach RH, Smith CR, al Nabulsi I, Whirrett BR, Childers SR, Wheeler KT. Sigma 2 receptors as potential biomarkers of proliferation in breast cancer. Cancer Res 1997; 57:156-61.

51 Zamora PO, Moody TW, John CS. Increased binding to sigma sites of N-[1'(2-piperidinyl)ethyl)-4-[I- 125]-iodobenzamide (I-125-PAB) with onset of tumor cell proliferation. Life Sci 1998;63:1611-8.

52 al Nabulsi I, Mach RH, Wang LM, et al. Effect of ploidy, recruitment, environmental factors, and tamoxifen treatment on the expression of sigma-2 receptors in proliferating and quiescent tumour cells. Br J Cancer 1999;81:925-33.

53 Wheeler KT, Wang LM, Wallen CA, et al. Sigma-2 receptors as a biomarker of proliferation in solid tumours. Br J Cancer 2000;82:1223-32.

54 Maneckjee R, Minna JD. Biologically active MK-801 and SKF-10,047 binding sites distinct from those in rat brain are expressed on human lung cancer cells. Mol Biol Cell 1992;3:613-9.

55 Moody TW, Leyton J, John C. Sigma ligands inhibit the growth of small cell lung cancer cells. Life Sci 2000;66:1979-86.

56 Vilner BJ, Bowen WD. Sigma receptor-active neuroleptics are cytotoxic to C6 glioma

cells in culture. Eur J Pharmacol 1993;244:199-201.

57 Brent PJ, Pang GT. Sigma binding site ligands inhibit cell proliferation in mammary and colon carcinoma cell lines and melanoma cells in culture. Eur J Pharmacol 1995; 278:151-60.

58 Vilner BJ, de Costa BR, Bowen WD. Cytotoxic effects of sigma ligands: sigma receptor-mediated alterations in cellular morphology and viability. J Neurosci 1995; 15:117-34.

59 Brent PJ, Pang G, Little G, Dosen PJ, Van Helden DF. The sigma receptor ligand, reduced haloperidol, induces apoptosis and increases intracellular-free calcium levels [Ca2+]i in colon and mammary adenocarcinoma cells. Biochem Biophys Res Commun 1996;219:219-26.

60 Cassano G, Gasparre G, Niso M, Contino M, Scalera V, Colabufo NA. F281, synthetic agonist of the sigma-2 receptor, induces Ca(2+) efflux from the endoplasmic reticulum and mitochondria in SK-N-SH cells. Cell Calcium 2009;45:340-5.

61 Kedjouar B, Daunes S, Vilner BJ, et al. Structural similitudes between cytotoxic antiestrogen-binding site (AEBS) ligands and cytotoxic sigma receptor ligands. Evidence for a relationship between cytotoxicity and affinity for AEBS or sigma-2 receptor but not for sigma-1 receptor. Biochem Pharmacol 1999;58:1927-39.

62 Rybczynska AA, Dierckx RA, Ishiwata K, Elsinga PH, Van Waarde A. Cytotoxicity of {sigma}-receptor ligands is associated with major changes of cellular metabolism and complete Occupancy of the {sigma}-2 subpopulation. J Nucl Med 2008;49: 2049-56.

63 Wei Z, Mousseau DD, Dai Y, Cao X, Li XM. Haloperidol induces apoptosis via the sigma2 receptor system and Bcl-XS. Pharmacogenomics J 2006;6:279-88.

64 Barbieri F, Sparatore A, Alama A, Novelli F, Bruzzo C, Sparatore F. Novel sigma binding site ligands as inhibitors of cell proliferation in breast cancer. Oncol Res 2003;13:455-61.

65 Berthois Y, Bourrie B, Galiegue S, et al. SR31747A is a sigma receptor ligand exhibiting antitumoural activity both in vitro and in vivo. Br J Cancer 2003;88:438-46.

66 Casellas P, Galiegue S, Bourrie B, Ferrini JB, Jbilo O, Vidal H. SR31747A: a peripheral sigma ligand with potent antitumor activities. Anticancer Drugs 2004;15:113-18.

67 Colabufo NA, Berardi F, Contino M, et al. Antiproliferative and cytotoxic effects of some sigma(2) agonists and sigma(1) antagonists in tumour cell lines. Naunyn Schmiedebergs Arch Pharmacol 2004;370:106-13.

68 Geiger C, Zelenka C, Weigl M, et al. Synthesis of Bicyclic sigma Receptor Ligands with Cytotoxic Activity. J Med Chem 2007;50:6144-53.

69 Holl R, Schepmann D, Frohlich R, Grunert R, Bednarski PJ, Wunsch B. Dancing of

the second aromatic residue around the 6,8-diazabicyclo[3.2.2]nonane framework: influence on sigma receptor affinity and cytotoxicity. J Med Chem 2009;52:2126-37.

70 Spruce BA, Campbell LA, McTavish N, et al. Small molecule antagonists of the sigma-1 receptor cause selective release of the death program in tumor and self-reliant cells and inhibit tumor growth in vitro and in vivo. Cancer Res 2004;64:4875-86.

71 Wang L, Prescott AR, Spruce BA, Sanderson J, Duncan G. Sigma receptor antagonists inhibit human lens cell growth and induce pigmentation. Invest Ophthalmol Vis Sci 2005;46:1403-8.

72 Wang L, Duncan G. Silencing of sigma-1 receptor induces cell death in human lens cells. Exp Cell Res 2006;312:1439-46.

73 Nordenberg J, Perlmutter I, Lavie G, et al. Anti-proliferative activity of haloperidol in B16 mouse and human SK-MEL-28 melanoma cell lines. Int J Oncol 2005;27: 1097-103.

74 Debeir O, Megalizzi V, Warzee N, Kiss R, Decaestecker C. Videomicroscopic extraction of specific information on cell proliferation and migration in vitro. Exp Cell Res 2008; 314:2985-98.

75 Megalizzi V, Decaestecker C, Debeir O, et al. Screening of antiglioma effects induced by sigma-1 receptor ligands: Potential new use for old anti-psychiatric medicines. Eur J Cancer 2009;45:2893-905.

76 Azzariti A, Colabufo NA, Berardi F, et al. Cyclohexylpiperazine derivative PB28, a sigma2 agonist and sigma1 antagonist receptor, inhibits cell growth, modulates P-glycoprotein, and synergizes with anthracyclines in breast cancer. Mol Cancer Ther 2006;5:1807-16.

77 Megalizzi V, Mathieu V, Mijatovic T, et al. 4-IBP, a sigma1 receptor agonist, decreases the migration of human cancer cells, including glioblastoma cells, in vitro and sensitizes them in vitro and in vivo to cytotoxic insults of proapoptotic and proautophagic drugs. Neoplasia 2007;9:358-69.

78 Dai Y, Wei Z, Sephton CF, Zhang D, Anderson DH, Mousseau DD. Haloperidol induces the nuclear translocation of phosphatidylinositol 3'-kinase to disrupt Akt phosphorylation in PC12 cells. J Psychiatry Neurosci 2007;32:323-30.

79 Achison M, Boylan MT, Hupp TR, Spruce BA. HIF-1alpha contributes to tumour-selective killing by the sigma receptor antagonist rimcazole. Oncogene 2007;26: 1137-46.

80 Crawford KW, Bowen WD. Sigma-2 receptor agonists activate a novel apoptotic pathway and potentiate antineoplastic drugs in breast tumor cell lines. Cancer Res 2002;62:313-22.

81 Ostenfeld MS, Fehrenbacher N, Hoyer-Hansen M, Thomsen C, Farkas T, Jaattela M. Effective tumor cell death by sigma-2 receptor ligand siramesine involves lysosomal

leakage and oxidative stress. Cancer Res 2005;65:8975-83.

82 Kashiwagi H, McDunn JE, Simon PO, Jr., et al. Selective sigma-2 ligands preferentially bind to pancreatic adenocarcinomas: applications in diagnostic imaging and therapy. Mol Cancer 2007;6:48.

83 Zhu LX, Sharma S, Gardner B, et al. IL-10 mediates sigma 1 receptor-dependent suppression of antitumor immunity. J Immunol 2003;170:3585-91.

84 Gardner B, Zhu LX, Roth MD, Tashkin DP, Dubinett SM, Sharma S. Cocaine modulates cytokine and enhances tumor growth through sigma receptors. J Neuroimmunol 2004;147:95-8.

85 Kashiwagi H, McDunn J, Simon PO, Jr., et al. Sigma-2 receptor ligands potentiate conventional chemotherapies and improve survival in models of pancreatic adenocarcinoma. J Transl Med 2009;7:24.

86 Michelot JM, Moreau MF, Labarre PG, et al. Synthesis and evaluation of new iodine-125 radiopharmaceuticals as potential tracers for malignant melanoma. J Nucl Med 1991;32:1573-80.

87 Michelot JM, Moreau MF, Veyre AJ, et al. Phase II scintigraphic clinical trial of malignant melanoma and metastases with iodine- 123-N-(2-diethylaminoethyl 4-iodobenzamide). J Nucl Med 1993;34:1260-6.

88 Rodot S, Darcourt J, Bussiere F, et al. A radiolabelled iodobenzamide for malignant melanoma staging. Melanoma Res 1994;4:307-12.

89 Everaert H, Flamen P, Franken PR, Verhaeghe W, Bossuyt A. Sigma-receptor imaging by means of I123-IDAB scintigraphy: clinical application in melanoma and non-small cell lung cancer. Anticancer Res 1997;17:1577-82.

90 John CS, Bowen WD, Saga T, et al. A malignant melanoma imaging agent: synthesis, characterization, in vitro binding and biodistribution of iodine-125-(2-piperidinylaminoethyl)4- iodobenzamide. J Nucl Med 1993;34:2169-75.

91 John CS, Vilner BJ, Bowen WD. Synthesis and characterization of [125I]-N-(N-benzylpiperidin-4- yl)-4- iodobenzamide, a new sigma receptor radiopharmaceutical: high-affinity binding to MCF-7 breast tumor cells. J Med Chem 1994;37:1737-9.

92 John CS, Vilner BJ, Gulden ME, et al. Synthesis and pharmacological characterization of 4-[125I]-N-(N- benzylpiperidin-4-yl)-4- iodobenzamide: a high affinity sigma receptor ligand for potential imaging of breast cancer. Cancer Res 1995;55:3022-7.

93 John CS, Gulden ME, Vilner BJ, Bowen WD. Synthesis, in vitro validation and in vivo pharmacokinetics of [125I]N-[2-(4- iodophenyl)ethyl]-N-methyl-2-(1-piperidinyl) ethylamine: a highaffinity ligand for imaging sigma receptor positive tumors. Nucl Med Biol 1996;23:761-6.

94 Waterhouse RN, Collier LT, O'Brien JC. Synthesis of a selective sigma receptor

radioligand for SPECT: [123I]-1-(2-Hydroxyethyl)- 4-(4-iodophenoxymethyl) piperidine. J Label Comp Radiopharm 1996;38:595-605.

95 Waterhouse RN, Chapman J, Izard B, et al. Examination of four 123I-labeled piperidine-based sigma receptor ligands as potential melanoma imaging agents: Initial studies in mouse tumor models. Nucl Med Biol 1997;24:587-93.

96 John CS, Lim BB, Geyer BC, Vilner BJ, Bowen WD. 99mTclabeled sigma-receptor-binding complex: synthesis, characterization, and specific binding to human ductal breast carcinoma (T47D) cells. Bioconjug Chem 1997;8:304-9.

97 John CS, Gulden ME, Li J, Bowen WD, McAfee JG, Thakur ML. Synthesis, in vitro binding, and tissue distribution of radioiodinated 2-[125I]N-(N-benzylpiperidin-4-yl)-2-iodo benzamide, 2-[125I]BP: a potential sigma receptor marker for human prostate tumors. Nucl Med Biol 1998;25:189-94.

98 John CS, Lim BB, Vilner BJ, Geyer BC, Bowen WD. Substituted halogenated arylsulfonamides: a new class of sigma receptor binding tumor imaging agents. J Med Chem 1998;41:2445-50.

99 John CS, Bowen WD, Fisher SJ, et al. Synthesis, in vitro pharmacologic characterization, and preclinical evaluation of N-[2-(1'- piperidinyl)ethyl]-3-[125I] iodo-4-methoxybenzamide(P[125I] MBA) for imaging breast cancer. Nucl Med Biol 1999;26:377-82.

100 John CS, Vilner BJ, Geyer BC, Moody T, Bowen WD. Targeting sigma receptor-binding benzamides as in vivo diagnostic and therapeutic agents for human prostate tumors. Cancer Res 1999;59:4578-83.

101 Caveliers V, Everaert H, John CS, Lahoutte T, Bossuyt A. Sigma receptor scintigraphy with N-[2-(1'-piperidinyl)ethyl]-3-(123)Iiodo- 4-methoxybenzamide of patients with suspected primary breast cancer: first clinical results. J Nucl Med 2002;43:1647-9.

102 Choi S, Yang B, Plossl K, et al. Development of a Tc-99m labelled sigma-2 receptor-specific ligand as a potential breast tumor imaging agent. Nucl Med Biol 2001; 28(6): 657-66.

103 Mach RH, Wheeler KT, Blair S, et al. Preparation of a technetium- 99m SPECT agent for imaging the sigma-2 receptor status of solid tumors. J Label Comp Radiopharm 2001; 44: 899-908.

104 Hou C, Tu Z, Mach R, Kung HF, Kung MP. Characterization of a novel iodinated sigma-2 receptor ligand as a cell proliferation marker. Nucl Med Biol 2006;33:203-9.

105 Hirata M, Mori T, Umeda T, Abe T, Yamamoto T, Ohmomo Y. Evaluation of radioiodinated 1-[2-(3,4-Dimethoxyphenyl)ethyl]-4- (2-iodophenylpropyl)piperazine as a tumor diagnostic agent with functional sigma receptor imaging by single photon emission computed tomography. Biol Pharm Bull 2008;31:879-83.

106 Satpati D, Bapat K, Sarma HD, Kothari K, Venkatesh M, Banerjee S. Synthesis of

(99m)tc-nitrido heterocomplex of piperidine and in vitro and in vivo evaluation of its affinity for sigma receptors. Cancer Biother Radiopharm 2008;23:34-42.

107 Ogawa K, Shiba K, Akhter N, et al. Evaluation of radioiodinated vesamicol analogs for sigma receptor imaging in tumor and radionuclide receptor therapy. Cancer Sci 2009;100:2188-92.

108 Westerberg G, Kärger W, Onoe H, Långström B. [11C]Cyanogen bromide in the synthesis of 1,3-di(2-tolyl)-[11C]guanidine. J Label Comp Radiopharm 1994; 34:691-6.

109 Wilson AA, Dannals RF, Ravert HT, Sonders MS, Weber E, Wagner HN-JR. Radiosynthesis of sigma receptor ligands for positron emission tomography: 11C- and 18F-labeled guanidines. J Med Chem 1991;34:1867-70.

110 Burns HD, Brenner NJ, Dannals RF, et al. Synthesis of a radiotracer for studying sigma recognition sites using positron emission tomography: [11C]L-687,384. J Label Comp Radiopharm 1993;32:338-9.

111 de Costa B, Radesca L, Dominguez C, Di Paolo L, Bowen WD. Synthesis and receptor binding properties of fluoro- and iodo- substituted high affinity sigma receptor ligands: identification of potential PET and SPECT sigma receptor imaging agents. J Med Chem 1992;35:2221-30.

112 Kiesewetter DO, de Costa B. Synthesis of N1-3-[18F]fluoropropyl-N4-2-([3,4-dichlorophenyl]ethyl)piperazine, a high affinity ligand for sigma receptor. J Label Comp Radiopharm 1993;33:639-43.

113 Schlyer DJ, Volkow ND, Fowler JS, et al. Regional distribution and kinetics of haloperidol binding in human brain: A PET study with [18F]haloperidol. Synapse 1992;11:10-9.

114 Yousef KA, Fowler JS, Volkow ND, et al. [18F]haloperidol binding in baboon brain in vivo. Nucl Med Biol 1996;23:47-52.

115 Shiue CY, Bai LQ, Shiue GG, et al. Synthesis of (+/-)-[18F]BMY 14802, its enantiomers and their anatomical distributions in rodents. Nucl Med Biol 1993;20:625-30.

116 Ding YS, Fowler JS, Dewey SL, et al. Synthesis and PET studies of fluorine-18-BMY 14802: A potential antipsychotic drug. J Nucl Med 1993;34:246-54.

117 Musachio JL, Scheffel U, Stathis M, Ravert HT, Mathews WB, Dannals RF. (+)-[C-11]-cis-N-benzyl-normetazocine: a selective ligand for sigma receptors in vivo. Life Sci 1994;55:PL225-32.

118 Musachio JL, Mathews WB, Ravert HT, Carroll FI, Dannals RF. Synthesis of a radiotracer for studying sigma receptors in vivo using PET: (+)-N-[11C]-benzyl-N-normetazocine (1S,5S,9S-(+)-cis-2-[11C]-benzyl-2'-hydroxy-5,9-dimethyl-6,7-benzomorphan). J Label Comp Radiopharm 1994;34:49-57.

119 Collier TL, O'Brien JC, Waterhouse RN. Synthesis of [18F]-1-(3-fluoropropyl)-4-(4-

cyanophenoxymethyl)-piperidine: A potential sigma-1 receptor radioligand for PET. J Label Comp Radiopharm 1996;38(9):785-94.

120 Waterhouse RN, Collier TL. In vivo evaluation of [18F]1-(3- fluoropropyl)-4-(4-cyanophenoxymethyl)piperidine: A selective sigma-1 receptor radioligand for PET. Nucl Med Biol 1997;24:127-34.

121 Waterhouse RN, Stabin MG, Page JG. Preclinical acute toxicity studies and rodent-based dosimetry estimates of the novel sigma-1 receptor radiotracer [(18)F]FPS. Nucl Med Biol 2003;30:555-63.

122 Waterhouse RN, Zhao J, Stabin MG, et al. Preclinical acute toxicity studies and dosimetry estimates of the novel sigma-1 receptor radiotracer, [18F]SFE. Mol Imaging Biol 2006;8:284-91.

123 Waterhouse RN, Chang RC, Zhao J, Carambot PE. In vivo evaluation in rats of [(18) F]1-(2-fluoroethyl)-4-[(4-cyanophenoxy) methyl]piperidine as a potential radiotracer for PET assessment of CNS sigma-1 receptors. Nucl Med Biol 2006;33:211-5.

124 Shiue CY, Shiue GG, Zhang SX, et al. N-(N-benzylpiperidin-4-yl)-2-[18F] fluorobenzamide: a potential ligand for PET imaging of sigma receptors. Nucl Med Biol 1997;24:671-6.

125 Shiue CY, Shiue GG, Benard F, Visonneau S, Santoli D, Alavi AA. N-(N-benzylpiperidin-4-yl)-2-[F-18]fluorobenzamide: A potential ligand for PET imaging of breast cancer. Nucl Med Biol 2000;27:763-7.

126 Shiue CY, Shiue GG, Benard F, Cesano A, Alavi A. N-(NBenzylpiperidin-4-yl)-2-[F-18] fluorobenzamide (2-FBP): A potential radioligand for PET imaging of human breast tumors in humans. Eur J Nucl Med 1998;25:854.

127 Dence CS, John CS, Bowen WD, Welch MJ. Synthesis and evaluation of [18F] labeled benzamides: High affinity sigma receptor ligands for PET imaging. Nucl Med Biol 1997; 24: 333-40.

128 Van Brocklin HF, Negash K, Kenski DM, Nagy D, Waterhouse RN. In vivo evaluation of 1-(4-[F-18]fluorobenzyl)-4-(4- cyanophenoxymethyl)piperidine ([F-18]FBnCNE): A high affinity sigma-1/sigma-2 receptor ligand for PET. J Nucl Med 1998;39:229P.

129 Ishiwata K, Noguchi J, Ishii SI, et al. Synthesis and preliminary evaluation of [11C] NE-100 labeled in two different positions as a PET sigma receptor ligand. Nucl Med Biol 1998;25:195-202.

130 Kawamura K, Ishiwata K, Tajima H, et al. Synthesis and in vivo evaluation of [11C] SA6298 as a PET sigma1 receptor ligand. Nucl Med Biol 1999;26:915-22.

131 Ishiwata K, Senda M. In vivo binding of [11C]nemonapride to sigma receptors in the cortex and cerebellum. Nucl Med Biol 1999;26:627-31.

132 Nimura T, Ando T, Yamaguchi K, et al. The role of sigmareceptors in levodopa-induced dyskinesia in patients with advanced Parkinson disease: a positron emission

tomography study. J Neurosurg 2004;100:606-10.

133 Zhang MR, Haradahira T, Maeda J, et al. Synthesis and evaluation of 3-(4-chlorobenzyl)-8-[11C]methoxy-1,2,3,4-tetrahydrochromeno [3,4-c]pyridin-5-one: a PET tracer for imaging sigma(1) receptors. Nucl Med Biol 2002;29:469-76.

134 Huang Y, Buchheimer N, Kuhner R, et al. [F-18]N-4'-fluorobenzyl-4-(2-fluorophenyl) acetamide for imaging sigma-1 receptors. J Label Comp Radiopharm 1999;42 Suppl 1:S167-9.

135 Mach RH, Huang Y, Buchheimer N, et al. [F-18]N-4'-fluorobenzyl-4-(3-bromophenyl) acetamide for imaging the sigma receptor status of tumors. J Label Comp Radiopharm 1999;42 Suppl 1:S258-60.

136 Mach RH, Huang Y, Buchheimer N, et al. [F-18]N-4`- fluorobenzyl-4-(3-bromophenyl) acetamide for imaging the sigma receptor status of tumors: comparison with [F-18] FDG and [I-125]IUDR. Nucl Med Biol 2001;28:451-8.

137 Kawamura K, Ishiwata K, Tajima H, et al. In vivo evaluation of [(11)C]SA4503 as a PET ligand for mapping CNS sigma(1) receptors. Nucl Med Biol 2000;27:255-61.

138 Kawamura K, Ishiwata K, Tajima H, et al. Preclinical evaluation of [11C]SA4503: Radiation dosimetry, in vivo selectivity and PET imaging of sigma1 receptors in the cat brain. Ann Nucl Med 2000;14:285-92.

139 Kawamura K, Kobayashi T, Matsuno K, Ishiwata K. Different brain kinetics of two sigma 1 receptor ligands, [3H](+)-pentazocine and [11C]SA4503, by P-glycoprotein modulation. Synapse 2003;48:80-6.

140 Ishiwata K, Kobayashi T, Kawamura K, Matsuno K, Senda M. [11C]Raclopride binding was reduced in vivo by sigma1 receptor ligand SA4503 in the mouse brain, while [11C]SA4503 binding was not by raclopride. Nucl Med Biol 2001;28:787-92.

141 Ishiwata K, Tsukada H, Kawamura K, et al. Mapping of CNS sigma1 receptors in the conscious monkey: Preliminary PET study with [11C]SA4503. Synapse 2001;40: 235-7.

142 Kawamura K, Kimura Y, Tsukada H, et al. An increase of sigma receptors in the aged monkey brain. Neurobiol Aging 2003;24:745-52.

143 Ishii K, Ishiwata K, Kimura Y, Kawamura K, Oda K, Senda M. Mapping of sigma-1 receptors in living human brain. Neuroimage 2001;13:S984.

144 Ishii K, Kimura Y, Kawamura K, Oda K, Sasaki T, Ishiwata K. Mapping of sigma1 receptors by 11C-SA4503-distribution and aging effect in normal human brain. Neuroimage 2002;16:S31.

145 Kimura Y, Naganawa M, Sakata M, et al. Distribution volume as an alternative to the binding potential for sigma(1) receptor imaging. Ann Nucl Med 2007;21:533-5.

146 Sakata M, Kimura Y, Naganawa M, et al. Mapping of human cerebral sigma1 receptors

using positron emission tomography and [11C]SA4503. Neuroimage 2007;35:1-8.

147 Ishiwata K, Ishii K, Kimura Y, et al. Successive positron emission tomography measurement of cerebral blood flow and neuroreceptors in the human brain: an (11)C-SA4503 study. Ann Nucl Med 2008;22:411-6.

148 Sakata M, Kimura Y, Naganawa M, et al. Shortened protocol in practical [(11)C] SA4503-PET studies for sigma (1) receptor quantification. Ann Nucl Med 2008; 22:143-6.

149 Mishina M, Ohyama M, Ishii K, et al. Low density of sigma1 receptors in early Alzheimer's disease. Ann Nucl Med 2008;22:151-6.

150 Mishina M, Ishiwata K, Ishii K, et al. Function of sigma1 receptors in Parkinson's disease. Acta Neurol Scand 2005;112:103-7.

151 Ishikawa M, Ishiwata K, Ishii K, et al. High occupancy of sigma-1 receptors in the human brain after single oral administration of fluvoxamine: a positron emission tomography study using [(11)C]SA4503. Biol Psychiatry 2007;62:878-83.

152 Ishikawa M, Sakata M, Ishii K, et al. High occupancy of sigma1 receptors in the human brain after single oral administration of donepezil: a positron emission tomography study using [11C]SA4503. Int J Neuropsychopharmacol 2009;12:1127-31.

153 Ishiwata K, Oda K, Sakata M, et al. A feasibility study of [11C]SA4503-PET for evaluating sigmal receptor occupancy by neuroleptics: the binding of haloperidol to sigma1 and dopamine D2-like receptors. Ann Nucl Med 2006;20:569-73.

154 Wang WF, Ishiwata K, Kiyosawa M, et al. Visualization of Sigma(1) Receptors in Eyes by ex vivo Autoradiography and in vivo Positron Emission Tomography. Exp Eye Res 2002;75:723-30.

155 Wang WF, Ishiwata K, Kiyosawa M, et al. Investigation of the use of positron emission tomography for neuroreceptor imaging in rabbit eyes. Ophthalmic Res 2004;36: 255-63.

156 Kawamura K, Kubota K, Kobayashi T, et al. Evaluation of [11C]SA5845 and [11C] SA4503 for imaging of sigma receptors in tumors by animal PET. Ann Nucl Med 2005;19:701-9.

157 Van Waarde A, Buursma AR, Hospers GA, et al. Tumor imaging with 2 sigma-receptor ligands, 18F-FE-SA5845 and 11C-SA4503: a feasibility study. J Nucl Med 2004; 45:1939-45.

158 Van Waarde A, Shiba K, de Jong JR, Ishiwata K, Dierckx RA, Elsinga PH. Rapid reduction of {sigma}1-receptor binding and 18F-FDG uptake in rat gliomas after in vivo treatment with doxorubicin. J Nucl Med 2007;48:1320-6.

159 Elsinga PH, Pruim J, Ishiwata K, Dierckx RA, Groen H. PET imaging of sigma receptors in non-small cell lung cancer patients. J Nucl Med 2006;47(Suppl 1):477P.

160 Elsinga PH, Kawamura K, Kobayashi T, et al. Synthesis and evaluation of [18F] fluoroethyl SA4503 as a PET ligand for the sigma receptor. Synapse 2002;43:259-67.

161 Elsinga PH, Tsukada H, Harada N, et al. Evaluation of [18F]fluorinated sigma receptor ligands in the conscious monkey brain. Synapse 2004;21:405-13.

162 Kawamura K, Tsukada H, Shiba K, et al. Synthesis and evaluation of fluorine-18-labeled SA4503 as a selective sigma(1) receptor ligand for positron emission tomography. Nucl Med Biol 2007;34:571-7.

163 Van Waarde A, Jager PL, Ishiwata K, Dierckx RA, Elsinga PH. Comparison of sigma-ligands and metabolic PET tracers for differentiating tumor from inflammation. J Nucl Med 2006;47:150-4.

164 Van Waarde A, Been LB, Ishiwata K, Dierckx RA, Elsinga PH. Early response of sigma-receptor ligands and metabolic PET tracers to 3 forms of chemotherapy: an in vitro study in glioma cells. J Nucl Med 2006;47:1538-45.

165 Shiba K, Ogawa K, Ishiwata K, Yajima K, Mori H. Synthesis and binding affinities of methylvesamicol analogs for the acetylcholine transporter and sigma receptor. Bioorg Med Chem 2006;14:2620-6.

166 Ishiwata K, Kawamura K, Yajima K, QingGeLeTu, Mori H, Shiba K. Evaluation of (+)-p-[11C]methylvesamicol for mapping sigma1 receptors: a comparison with [11C]SA4503. Nucl Med Biol 2006;33:543-8.

167 Colabufo NA, Berardi F, Contino M, et al. Distribution of sigma receptors in EMT-6 cells: preliminary biological evaluation of PB167 and potential for in-vivo PET. J Pharm Pharmacol 2005;57:1453-9.

168 Colabufo NA, Berardi F, Contino M, Niso M, Perrone R, Tortorella V. The potent sigma receptor ligand PB167, as a potential PET radiotracer for evaluating the mammary sarcoma in mice. Arkivoc 2006;viii:95-101.

169 Kassiou M, Dannals RF, Liu X, Wong DF, Ravert HT, Scheffel UA. Synthesis and in vivo evaluation of a new PET radioligand for studying sigma-2 receptors. Bioorg Med Chem 2005;13:3623-6.

170 Colabufo NA, Abate C, Contino M, et al. PB183, a sigma receptor ligand, as a potential PET probe for the imaging of prostate adenocarcinoma. Bioorg Med Chem Lett 2008;18:1990-3.

171 Tu Z, Dence CS, Ponde DE, et al. Carbon-11 labeled sigma(2) receptor ligands for imaging breast cancer. Nucl Med Biol 2005;32:423-30.

172 Rowland DJ, Tu Z, Xu J, Ponde D, Mach RH, Welch MJ. Synthesis and in vivo evaluation of 2 high-affinity 76Br-labeled sigma2- receptor ligands. J Nucl Med 2006;47:1041-8.

173 Tu Z, Xu J, Jones LA, et al. Fluorine-18-labeled benzamide analogues for imaging the

sigma2 receptor status of solid tumors with positron emission tomography. J Med Chem 2007;50:3194- 204.

174 Chu W, Xu J, Zhou D, et al. New N-substituted 9-azabicyclo [3.3.1]nonan-3alpha-yl phenylcarbamate analogs as sigma(2) receptor ligands: Synthesis, in vitro characterization, and evaluation as PET imaging and chemosensitization agents. Bioorg Med Chem 2009;17:1222-31.

175 Mach RH, Dehdashti F, Wheeler KT. PET Radiotracers for Imaging the Proliferative Status of Solid Tumors. PET Clin 2009;4:1-15.

176 Ryan Moro J, Chien CC, Standifer KM, Pasternak GW. Sigma binding in a human neuroblastoma cell line. Neurochem Res 1996;21:1309-14.

177 Ganapathy ME, Prasad PD, Huang W, Seth P, Leibach FH, Ganapathy V. Molecular and ligand-binding characterization of the sigma-receptor in the Jurkat human T lymphocyte cell line. J Pharmacol Exp Ther 1999;289:251-60.

178 John CS, Bowen WD, Varma VM, McAfee JG, Moody TW. Sigma receptors are expressed in human non-small cell lung carcinoma. Life Sci 1995;56:2385-92.

179 Georg A, Friedl A. Characterization of specific binding sites for [3H]-1,3-di-o- tolyl-guanidine (DTG) in the rat glioma cell line C6- BU-1. Glia 1992;6:258-63.

180 Barg J, Thomas GE, Bem WT, et al. In vitro and in vivo expression of opioid and sigma receptors in rat C6 glioma and mouse N18TG2 neuroblastoma cells. J Neurochem 1994;63:570-4.

181 Largent BL, Gundlach AL, Snyder SH. Sigma receptors on NCB-20 hybrid neurotumor cells labeled with (+)[3H]SKF 10,047 and (+)[3H]3-PPP. Eur J Pharmacol 1986; 124:183-7.

182 Kushner L, Zukin SR, Zukin RS. Characterization of opioid, sigma, and phencyclidine receptors in the neuroblastoma-brain hybrid cell line NCB-20. Mol Pharmacol 1988; 34:689-94.

183 Wu XZ, Bell JA, Spivak CE, London ED, Su TP. Electrophysiological and binding studies on intact NCB-20 cells suggest presence of a low affinity sigma receptor. J Pharmacol Exp Ther 1991;257:351-9.

184 Georg A, Friedl A. Identification and characterization of two sigma-like binding sites in the mouse neuroblastoma x rat glioma hybrid cell line NG108-15. J Pharmacol Exp Ther 1991;259:479-83.

185 Hellewell SB, Bowen WD. A sigma-like binding site in rat pheochromocytoma (PC12) cells: decreased affinity for (+)- benzomorphans and lower molecular weight suggest a different sigma receptor form from that of guinea pig brain. Brain Res 1990;527:244-53.

186 Sagi N, Yamamoto H, Yamamoto T, Okuyama S, Moroji T. Possible expression of a sigma 1 site in rat pheochromocytoma (PC12) cells. Eur J Pharmacol 1996;304:185-

90.

187 John CS, Baumgold J, Vilner BJ, McAfee JG, Bowen WD. [125I]N-(2-Piperidinylaminoethyl)-4-iodobenzamide and related analogs as sigma receptor imaging agents: High affinity binding to human malignant melanoma and rat C6 glioma cell lines. J Label Comp Radiopharm 1994;35:242-4.

188 Kawamura K, Elsinga PH, Kobayashi T, et al. Synthesis and evaluation of (11)C- and (18)F-labeled 1-[2-(4-alkoxy-3-methoxyphenyl) ethyl]-4-(3-phenylpropyl) piperazines as sigma receptor ligands for positron emission tomography studies. Nucl Med Biol 2003;30:273-84.

189 Kawamura K, Ishiwata K. Improved synthesis of [C-11]SA4503, [C-11]MPDX and [C-11]TMSX by use of [C-11]methyl triflate. Annals of Nuclear Medicine 2004; 18:165-8.

190 Toyohara J, Sakata M, Ishiwata K. Imaging of sigma1 receptors in the human brain using PET and [11C]SA4503. Cent Nerv Syst Agents Med Chem 2009;9:190-6.

191 Maestrup EG, Fischer S, Wiese C, et al. Evaluation of spirocyclic 3-(3-fluoropropyl)-2-benzofurans as sigma1 receptor ligands for neuroimaging with positron emission tomography. J Med Chem 2009;52:6062-72.

Steroid hormones affect binding of the sigma ligand ^{11}C-SA4503 in tumor cells and tumor-bearing rats

Anna A. Rybczynska,[1] Philip H. Elsinga,[1] Jurgen W. Sijbesma,[1] Kiichi Ishiwata,[2] Johan R. de Jong,[1] Erik F. de Vries,[1] Rudi A. Dierckx,[1,3] and Aren van Waarde[1]

[1]Nuclear Medicine and Molecular Imaging, University Medical Center Groningen, University of Groningen, Groningen, The Netherlands

[2]Positron Medical Center, Tokyo Metropolitan Institute of Gerontology, Tokyo, Japan

[3]Nuclear Medicine, Ghent University, Ghent, Belgium

Chapter 3

Eur J Nucl Med Mol Imaging. 2009; 36: 1167–1175.

Abstract

Sigma receptors are implicated in memory and cognitive functions, drug addiction, depression and schizophrenia. In addition, sigma receptors are strongly overexpressed in many tumors. Although the natural ligands are still unknown, steroid hormones are potential candidates. Here, we examined changes in binding of the sigma-1 agonist ^{11}C-SA4503 in C6 glioma cells and in living rats after modification of endogenous steroid levels. Methods: ^{11}C-SA4503 binding was assessed in C6 monolayers by gamma counting and in anaesthetized rats by microPET scanning. C6 cells were either repeatedly washed and incubated in steroid-free medium or exposed to five kinds of exogenous steroids (1 h or 5 min before tracer addition, respectively). Tumor-bearing male rats were repeatedly treated with pentobarbital (a condition known to result in reduction of endogenous steroid levels) or injected with progesterone. Results: Binding of ^{11}C-SA4503 to C6 cells was increased (~50%) upon removal and decreased (~60%) upon addition of steroid hormones (rank order of potency: progesterone > allopregnanolone = testosterone = androstanolone > dehydroepiandrosterone-3-sulphate, IC50 progesterone 33 nM). Intraperitoneally administered progesterone reduced tumor uptake and tumor-to-muscle contrast (36%). Repeated treatment of animals with pentobarbital increased the PET standardized uptake value of ^{11}C-SA4503 in tumor (16%) and brain (27%), whereas the kinetics of blood pool radioactivity was unaffected. Conclusions: The binding of ^{11}C-SA4503 is sensitive to steroid competition. Since not only increases but also decreases of steroid levels affect ligand binding, a considerable fraction of the sigma-1 receptor population in cultured tumor cells or tumor-bearing animals is normally occupied by endogenous steroids.

Keywords: steroid hormones, positron emission tomography (PET), glioma, sigma receptor ligand, ^{11}C-SA4503

Introduction

The use of positron emission tomography (PET) for imaging of cancer has a successful history spanning more than three decades. Suitable radiopharmaceuticals have been designed to track molecular events in the body, to monitor the time course of disease and to assess treatment outcome. Although ^{18}F-FDG and other metabolic PET tracers (^{18}F-FLT, ^{11}C-methionine, ^{11}C-choline, etc.) are widely available for the diagnosis of cancer and monitoring of treatment response, these tracers are not tumor specific and/or have only moderate cellular uptake [1,2]. For this reason, there is much interest in the

development and validation of novel radiopharmaceuticals with greater tumor selectivity. Attractive candidates are sigma ligands since sigma receptors are strongly overexpressed in rapidly proliferating cells [3–6].

Sigma receptors are proteins with a highly conserved sequence (87–92% identity and 90–93% homology for sigma-1 receptor) [7]. They are found in kidney, liver, immune, endocrine and reproductive organs [8]. Furthermore, sigma receptors are widely distributed in the brain and are implied in memory function, cognition, drug addiction, depression and schizophrenia [9]. Importantly, sigma receptors were demonstrated to play a role in tumor cell proliferation and cancer cell death. These binding sites are therefore important targets in the development of novel anti-cancer drugs [10]. Although the endogenous ligands for sigma receptors have not yet been identified, steroid hormones (in particular progesterone) are potential candidates [11,12].

Recent work has demonstrated regulation of sigma-1 receptor availability by endogenous steroids. Such steroids modulate the efficacy of a sigma-1 receptor agonist in stress and depression [12]. Binding of neurosteroids to sigma receptors affects the release of substance P from nociceptor endings in mice [13] and the release of glutamate and norepinephrine in rat prelimbic cortex and hippocampus [14,15]. Furthermore, such binding reduces subjective craving in cocaine addiction [16]. Based on their effects on substance P and norepinephrine release, progesterone was proposed to be a sigma antagonist, whereas dehydroepiandrosterone-3-sulphate (DHEA-S) and pregnenolone sulphate were considered as sigma agonists [13,15]. Multiple sequence analyses revealed the presence of two steroid-like binding domains (SBDLI and SBDLII) in the guinea pig sigma-1 receptor (amino acids 91–109 and 176–194, respectively) [17,18]. Recently, it was shown that administration of steroids reduces *in vivo* binding of the sigma-1 receptor ligand ^{18}F-FPS in rodent brain [19].

Although an interaction between cerebral sigma receptors and steroids has been established, our knowledge about competition between sigma ligands and endogenous steroids in cancer cells is still rudimentary. Moreover, it remains necessary to examine how steroid hormones affect the binding of radiopharmaceuticals other than ^{18}F-FPS, since sigma ligands may bind to different receptor subtypes [20] and to different binding sites within the sigma-1 receptor molecule (e.g. the agonist binding site and the phenytoin-binding site [21]).

Here, we examine the impact of steroid competition on binding of the sigma-1 agonist ^{11}C-SA4503. ^{11}C-SA4503 has been used extensively for PET studies of animal tumors [2,22–24] and the human brain [25–28]. For *in vitro* tests of steroid competition,

we used C6 rat glioma cells, a tumor line which expresses both sigma-1 and sigma-2 receptors [3]. As an *in vivo* model we used C6 glioma-bearing Wistar rats. Tumor cells were either repeatedly washed and incubated in steroid-free medium or exposed to five different exogenous steroids. Rats were either repeatedly injected with pentobarbital, a treatment known to reduce the levels of endogenous steroids [29], or injected with progesterone. If the binding of ^{11}C-SA4503 is sensitive to competition by endogenous steroids, we expected to find increased tracer binding after prolonged anaesthesia and decreased binding after steroid addition. Such competition, if present, could result in intrasubject variability of the binding potential of ^{11}C-SA4503 in women during the menstrual cycle and also in intersubject variability in aged subjects which may show widely different endogenous steroid concentrations.

Materials & Methods

Culture media and drugs

Dulbecco's minimum essential medium (DMEM), fetal calf serum (FCS) and trypsin were products of Invitrogen. Allopregnanolone acetate (5α-pregnan-3β-ol-20-one 3β-acetate), dehydroepiandrosterone 3-sulphate sodium salt (DHEA-S), haloperidol, progesterone (cell culture tested, P8783) and trypan blue (0.4% solution in phosphate-buffered saline) were purchased from Sigma. Androstanolone (5α-androstan-17β-ol-3-one) and testosterone were obtained from Fluka. MatrigelR came from Becton Dickinson. Arachid oil was a product of Levo BV, Franeker, Holland. Stock solutions of steroids and of haloperidol were prepared in ethanol unless otherwise indicated. The radioligand ^{11}C-SA4503 was prepared by reaction of ^{11}C-methyl iodide with the appropriate 4-O-methyl precursor [30]. The decay-corrected radiochemical yield was 9–11%, the specific radioactivity >11 TBq/mmol at the moment of injection and radiochemical purity >95%.

Cell culture

C6 rat glioma cells obtained from the American Type Culture Collection were grown as monolayers in DMEM (high glucose) supplemented with 7.5% FCS in a humidified atmosphere of 5% CO2/95% air at 37°C. Before each experiment, the cells were seeded in 12-well plates (Costar). An equal number of cells were dispensed in each well in 1.1 ml of serum-containing medium: DMEM (high glucose) supplemented with 7.5% FCS.

Binding studies

Binding studies were performed 48 h after seeding cells in 12-well plates when confluency had reached 80–90%. In some experiments, cells were steroid-depleted by removal of the normal medium, repeated (3 ×) washing with phosphate-buffered saline (PBS, 1 ml) and addition of DMEM (high glucose) without serum and phenol red, 1 h before addition of the radiotracer. Various concentrations of an unlabelled competitor (haloperidol or a steroid) were dispensed to the culture medium in the wells. Steroids investigated were allopregnanolone, androstanolone, DHEA-S, progesterone and testosterone. After 2 min, 4 MBq of ^{11}C-SA4503 in <30 µl of saline (containing 30% ethanol) were added to each well. After 45–60 min of incubation, the medium was quickly removed and the monolayer was washed 3 times with PBS. Cells were then treated with 0.2 ml of trypsin. When the monolayer had detached from the bottom of the well, 1 ml of DMEM (high glucose) supplemented with 7.5% FCS was added to stop the proteolytic action. Cell aggregates were resolved by repeated (at least tenfold) pipetting of the trypsin/DMEM mixture. Radioactivity in the cell suspension (1.2 ml) was assessed using a gamma counter (Compugamma 1282 CS, LKB-Wallac, Turku, Finland). A sample of the suspension was mixed with trypan blue solution (1:1 v/v) and was used for cell counting. Cell numbers were determined manually, using a phase contrast microscope (Olympus, Tokyo, Japan), a Bürker bright-line chamber (depth 0.1 mm; 0.0025 mm^2 squares) and a hand tally counter. All experiments were performed as a quadruplicate study with at least two repeats.

Animal model

The animal experiments were performed by licensed investigators in compliance with the Law on Animal Experiments of The Netherlands. The protocol was approved by the Committee on Animal Ethics of the University of Groningen.

C6 glioma cells [2.5 × 10^6, in a 1:1 mixture of Matrigel and DMEM (high glucose with 7.5% FCS)] were subcutaneously injected into the right shoulder of male Wistar rats. The animals were maintained at a 12 h light/12 h dark regime and were fed standard laboratory chow ad libitum. They were scanned after 9–10 days, when tumors had grown to above 0.5 g.

MicroPET scanning

Two rats were scanned simultaneously in each scan session, using a Siemens/Concorde microPET camera (Focus 220). A list mode protocol was used (60 min, brain,

Table 1. Effect of prolonged anaesthesia and progesterone administration on biodistribution of ^{11}C-SA4503.

Tissue	Control[a] (n=4)	Prolonged anaesthesia[b] (n=5)	Progesterone-treated* (n=4)	Effect of long anaesthesia (p)	Effect of progesterone (p)
Cerebellum	1.66±0.18	2.41±0.33	1.69±0.30	< 0.01	NS
Cerebral cortex	1.50±0.40	2.38±0.40	1.85±0.33	0.02	NS
Rest of brain	1.51±0.38	2.12±0.41	1.69±0.37	NS	NS
Adipose tissue	0.25±0.12	0.38±0.15	0.25±0.08	NS	NS
Bladder	0.67±0.16	0.80±0.31	0.55±0.17	NS	NS
Bone	0.27±0.08	0.42±0.09	0.34±0.11	< 0.05	NS
Bone marrow	1.56±0.36	2.15±0.23	1.17±0.20	< 0.05	NS
Heart	0.35±0.09	0.48±0.07	0.31±0.04	NS	NS
Large intestine	1.82±0.36	2.62±0.39	1.87±0.39	< 0.05	NS
Small intestine	2.35±0.28	3.48±0.86	2.73±0.53	NS	NS
Kidney	4.07±0.45	4.60±0.19	4.07±0.63	NS	NS
Liver	7.53±0.77	5.20±0.28	7.16±1.39	0.001	NS
Lung	2.21±0.59	2.51±0.62	1.92±0.50	NS	NS
Muscle	0.18±0.04	0.21±0.01	0.20±0.05	NS	NS
Pancreas	3.78±1.55	5.06±1.22	5.16±1.60	NS	NS
Plasma	0.09±0.03	0.10±0.02	0.09±0.01	NS	NS
Blood cells	0.05±0.01	0.07±0.01	0.05±0.01	< 0.05	NS
Spleen	2.26±0.39	3.76±0.95	2.07±0.41	< 0.05	NS
Submandibular gland	2.91±0.91	2.08±0.17	2.59±0.85	NS	NS
C6 tumour	0.83±0.11	1.52±0.36	0.57±0.14	< 0.05	< 0.05
Urine	0.48±0.20	0.75±0.76	0.92±0.29	NS	< 0.05

SUV values of ^{11}C, 60 min after injection of ^{11}C-SA4503
a Data were obtained from the control and progesterone-treated rats, respectively, after the PET scan of Fig. 4
b Data were obtained from the rats which had undergone the two PET scans of Fig. 3

tumor and upper half of both lungs in the field of view). These organs were clearly visualized, as reported previously [24]. The scanning was started during injection into the first rat; the second rat was injected 30 s later. Body temperature of anaesthetized animals in the scanner was kept at 37.5 ± 0.5°C, using rectal probes, individual temperature controllers and electronic heating (M2M Imaging).

Two microPET scans of five rats were made in order to explore the effect of anaesthesia duration on the *in vivo* binding of ^{11}C-SA4503 (23–27 MBq administered as a 0.3 ml bolus, tail vein catheter, mass <2 nmol). For the first scan, the tracer was injected shortly (<20 min) after the induction of pentobarbital anaesthesia (first scan = control condition). When this scan had been finished, the animal was kept under anaesthesia and remained at a fixed position in the microPET scanner. ^{11}C-SA4503 was once more injected after prolonged anaesthesia [four intraperitoneal injections of a sodium pentobarbital solution in water (60 mg/ml): first injection 1 ml/kg body weight, and then three subsequent 0.3 ml/kg body weight at 30–40 min intervals, total anaesthesia duration >3.5 h] in order to acquire the second scan.

For examination of the effect of an exogenous steroid on ^{11}C-SA4503 binding, microPET scans were made of four pairs of rats. One rat of each pair was treated with progesterone (three intraperitoneal injections of 10 mg each at 1.5 h intervals, in arachid oil, progesterone-treated group), whereas the other animal was treated with carrier (arachid oil) only (control group). In the arachid oil- and progesterone-treated rats, the tracer ^{11}C-SA4503 was injected shortly (< 20 min) after the induction of pentobarbital anaesthesia.

List mode data were reframed into a dynamic sequence of 4 × 60 s, 3 × 120 s, 4 × 300 s and 3 × 600 s frames. The data were reconstructed per time frame employing an interactive reconstruction algorithm (OSEM2D). The final data sets consisted of 95 slices with a slice thickness of 0.8 mm and an in-plane image matrix of 128 × 128 pixels of size 1 × 1 mm^2. Data sets were fully corrected for random coincidences, scatter and attenuation. A separate transmission scan was acquired for attenuation correction. This scan was performed right after the last emission scan.

Three-dimensional regions of interest (3-D ROIs) were manually drawn around the entire tumor, brain and peripheral area of the right lung, avoiding hilar structures, as described previously [24]. Time-activity curves (TACs) and volumes (cm^3) for the ROIs were calculated, using standard software (AsiPro VM 6.2.5.0, Siemens-Concorde, Knoxville, TN, USA). TACs were normalized for body weight and injected dose as indicated in the figure legends.

Biodistribution studies

After the scanning period, the anaesthetized animals were terminated. Blood was collected, and plasma and a cell fraction were obtained from the blood sample by short centrifugation (5 min at 1,000 g). Several tissues (see Table 1) were excised. The complete tumor was removed and separated from muscle and skin. All tissue samples were weighed. Radioactivity in tissue samples was measured using a gamma counter, applying a decay correction. The results were expressed as dimensionless standardized uptake values (SUVs). The parameter SUV is defined as: [tissue activity concentration (MBq/g) * body weight (g) / injected dose (MBq)].

Results

Cell experiments

The growth medium of C6 cells (DMEM-high) contains steroid hormones since

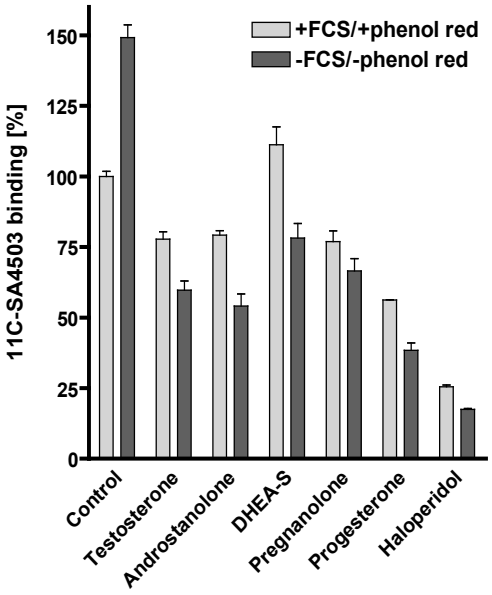

Fig.1. Competition of exogenous steroids (concentration 50 μM) and haloperidol (50 μM) with ^{11}C-SA4503 binding to C6 cells in normal culture medium and in steroid-free medium (expressed as a percentage of the binding to untreated cells in normal culture medium). All treatments resulted in a statistically significant effect on tracer binding, with exception of the DHEA-S effect in normal culture medium.

it is supplemented with FCS (7.5% v/v). This medium also contains the indicator phenol red which may interact with hormone binding sites, particularly estrogen receptors [31]. Yet, the addition of non-radioactive steroids to normal growth medium (50 μM of progesterone, allopregnanolone, testosterone or androstanolone) resulted in measurable competition with the radioligand ^{11}C-SA4503 for binding to cellular sigma receptors (Fig. 1). In contrast, the administration of 50 μM DHEA-S had no statistically significant effect.

C6 cells were depleted from endogenous steroids by removal of growth medium, repeated washing of the monolayer with PBS and addition of medium without FCS and phenol red. Such steroid depletion resulted in a significant (49 ± 4%) increase of the specific binding of ^{11}C-SA4503 to intact cells (Fig. 1).

When the steroid supplementation experiment was repeated in steroid-free medium, a stronger effect of exogenous steroids was observed than in the normal growth medium. Even 50 μM DHEA-S caused now a significant decrease of cellular ^{11}C-SA4503

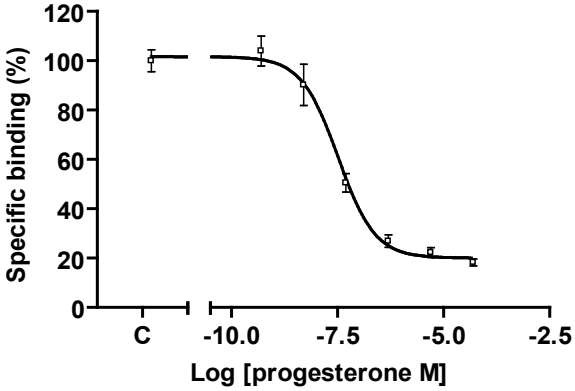

Fig.2. Dose-response plot of progesterone competition with ^{11}C-SA4503 binding to C6 cells in steroid-free medium. Specific binding was defined as total binding minus the residual binding observed in the presence of an excess of haloperidol (50 μM).

binding (Fig. 1). Both in normal and in steroid-depleted medium, the observed rank order of potency was: progesterone > androstanolone = testosterone = allopregnanolone > DHEA-S. A dose-response plot was made for the most potent steroid competitor, progesterone. The IC50 value of this compound for inhibition of cellular ^{11}C-SA4503 binding was 33 nM (Fig. 2).

Addition of the anaesthetic pentobarbital to C6 cells (up to concentrations of 1 mM in normal medium) did not result in any inhibition of ^{11}C-SA4503 binding (values not shown).

Animal data

No behavioural changes were observed in the animals up to 10 days after inoculation of C6 cells. Tumors appeared after 5 days and grew exponentially, as reported previously [24]. Body weight of the animals at the time of PET scanning was 326 ± 22 g. Tumor size was then 1.3 ± 0.7 g (mean ± SD, range 0.48–2.39 g). No significant tumor necrosis was observed, as reported previously [2].

MicroPET scans

Pentobarbital anaesthesia is known to affect steroid metabolism. A strong (> 70%) decline of endogenous steroid levels in the brain (progesterone, pregnenolone) occurs upon treatment of male rats with anaesthetic amounts of sodium pentobarbital (0.2 mmol/kg i.p., [29]). Plasma progesterone in female rats is also decreased after

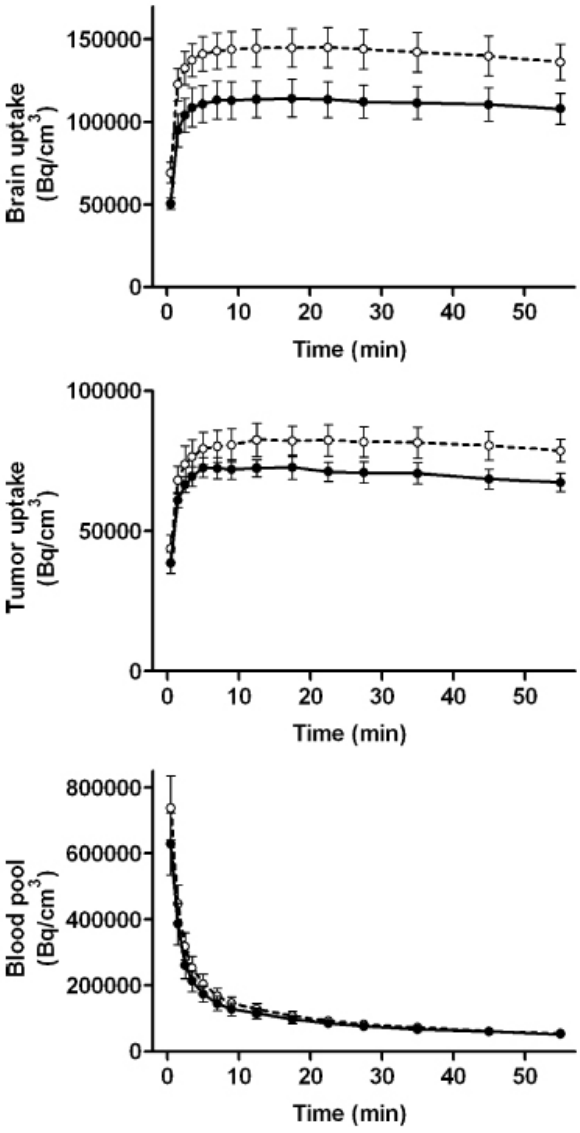

Fig.3. Time-activity curves of ^{11}C-SA4503-derived radioactivity in tumor, brain and blood pool. Solid line: animals scanned after short pentobarbital anaesthesia (< 20 min, control condition, n = 5); dotted line: same animals scanned after protracted pentobarbital anaesthesia (>3.5 h, n = 5). The PET data were normalized to a body weight of 330 g and an injected radioactivity dose of 20 MBq, as described previously [24]. The effect of protracted anaesthesia on brain uptake (after >10 min) and tumor uptake (after >20 min) was statistically significant, in contrast to the effect on radioactivity in the blood pool.

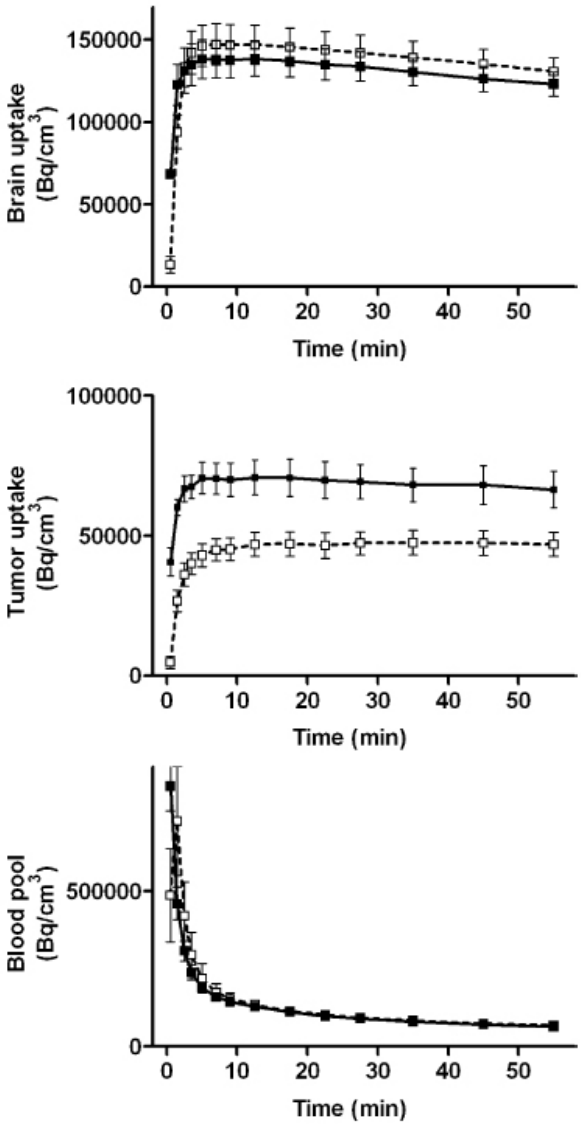

Fig.4. Time-activity curves of ^{11}C-SA4503-derived radioactivity in tumor, brain and blood pool. Solid line: animals scanned at baseline (treated with arachid oil only, control group, n = 4); dotted line: other animals scanned after repeated injections of progesterone in arachid oil (progesterone-treated group, n = 4). The PET data were normalized to a body weight of 330 g and an injected radioactivity dose of 20 MBq, as described previously [24]. The effect of progesterone addition on tumor uptake (but not brain or blood pool uptake) was statistically significant.

pentobarbital administration [32]. Thus, competition of endogenous steroids with ^{11}C-SA4503 binding in target organs was expected to be reduced after repeated treatment of Wistar rats with pentobarbital. A significant increase of tracer SUV in target organs (brain 27%, C6 tumor 16%) was indeed observed after prolonged anaesthesia (Fig. 3). However, anaesthesia duration did not significantly affect the kinetics of radioactivity in a blood pool from the right lung (Fig. 3).

Pretreatment of animals with a high dose of progesterone resulted in a significant decrease of ligand SUV in the C6 tumor (36 %), but did not significantly affect tracer kinetics in the brain or blood pool (Fig. 4).

MicroPET images of a single rat acquired after short and prolonged anaesthesia are shown in Fig. 5. Images of solvent (arachid oil)- and progesterone-pretreated animals are presented in Fig. 6.

Biodistribution studies

Biodistribution experiments confirmed the outcome of the microPET studies (Table 1). Prolonged anaesthesia with pentobarbital resulted in a significant increase of sigma ligand binding in C6 tumor, brain (particularly cerebellum and cerebral cortex), bone and bone marrow, large intestine, blood cells and spleen. Plasma levels of radioactivity were not changed under these conditions and the amount of radioactivity in the liver was significantly decreased.

Pretreatment of animals with progesterone caused a 31% decrease of sigma ligand binding in the C6 tumor, but did not significantly affect tracer uptake in any other organ or in plasma (Table 1).

Discussion

In vitro steroid competition

Although an interaction of steroid hormones with sigma receptors has been described in many publications, there are few reported observations of competition between endogenous steroids and sigma receptor ligands in intact cancer cells. Here, we demonstrate that altered steroid levels result in changes of ^{11}C-SA4503 binding to sigma receptors in the C6 glioma cell line. Steroid depletion (removal of FCS from the growth medium and washing of cells with steroid-free medium) resulted in a 49% increase of ^{11}C-SA4503 binding. Apparently, high steroid levels in the normal growth medium result in reduced tracer binding and can obscure the effects of steroids which bind with rather low

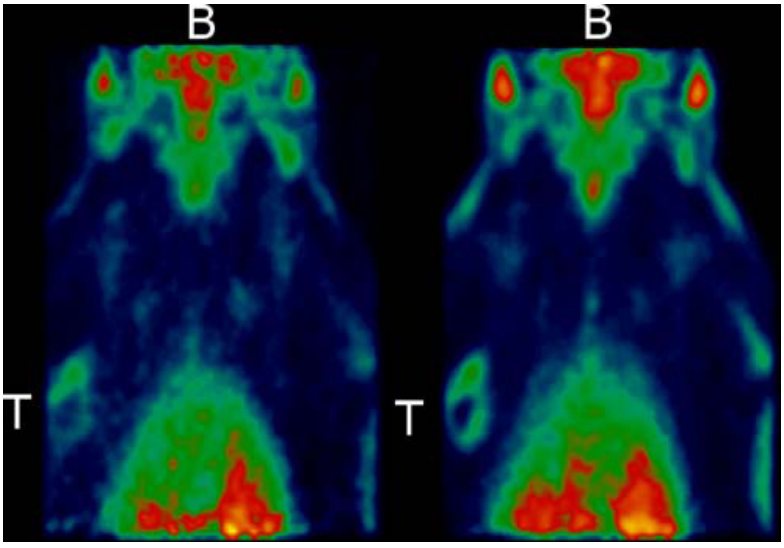

Fig.5. MicroPET images of a single animal scanned with ^{11}C-SA4503 after short (<20 min, left panel) and protracted (>3.5 h, right panel) pentobarbital anaesthesia. Images are summed data from 1 to 60 min after injection. The positions of tumor and brain are indicated by capitals T and B.

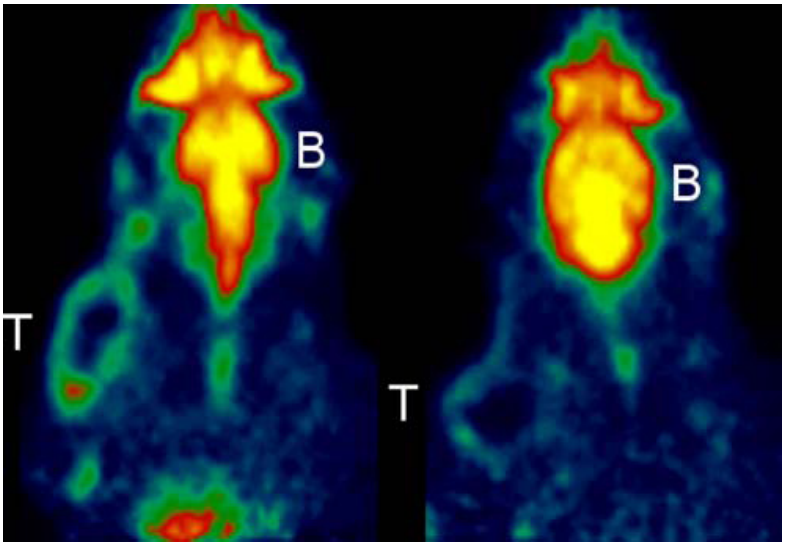

Fig.6. MicroPET images of two different rats scanned with ^{11}C-SA4503 after pretreatment with solvent (arachid oil, left panel) or progesterone (right panel). Images are summed data from 1 to 60 min after injection. The positions of tumor and brain are indicated by capitals T and B.

affinity to sigma receptor proteins. Enhanced competition of DHEA-S and other steroids with ^{11}C-SA4503 binding was observed when cells were washed and incubated in steroid-free medium, 1 h before tracer addition.

Testosterone (50 μM), an androgen secreted by the testis, caused a 40% reduction of radioligand binding to C6 cells in steroid-free medium. Androstanolone (dihydrotestosterone), a metabolite of testosterone which mediates many of the biological actions of testosterone, had a similar effect as the parent compound. Dehydroepiandrosterone sulphate, a steroid sigma agonist with antidepressant actions and an allosteric modulator of γ-aminobutyric acid (GABA)A receptors, was the weakest competitor for ^{11}C-SA4503 binding. The most potent steroid inhibitor proved to be progesterone (secreted by the corpus luteum in females) which reduced cellular ^{11}C-SA4503 binding by 60%. Allopregnanolone, an important metabolite of progesterone, was less potent than its parent compound, but still caused a 33% reduction of radioligand binding. Non-specific binding (defined as binding of the radioligand to C6 cells in the presence of an excess of haloperidol) was about 25% in normal growth medium and 18% in steroid-free medium (Fig. 1).

The results of our experiments in cancer are in accordance with previous studies which have employed different radioligands and have focused on healthy tissue. Progesterone and testosterone were shown to compete with the binding of ^{3}H-SKF-10,047 and ^{3}H-haloperidol to sigma receptors in homogenates from guinea pig brain and spleen [33]. These steroids were also potent inhibitors of the binding of ^{3}H-haloperidol to sigma-1 receptors in human placenta [11], and they reduced binding of the sigma-1 ligand ^{18}F-FPS to isolated membrane fragments and to the brain of intact rats [19]. Progesterone acted like a sigma-1 antagonist in the rat hippocampus, mimicking the effects of haloperidol on ^{3}H-norepinephrine release [15]. Progesterone but not dehydroepiandrosterone sulphate reduced the *in vivo* binding of ^{3}H-SKF-10,047 to sigma-1 receptors in the mouse hippocampus and cortex [34].

In vivo steroid competition

Progesterone supplementation reduced tumor SUV (from 0.83 ± 0.11 to 0.57 ± 0.14) and the tumor-to-muscle concentration ratio (from 4.6 to 2.8), as indicated by our biodistribution data (Table 1). TACs in microPET indicated a progesterone-mediated decrease of ^{11}C-SA4503 binding in the C6 tumor (by 36%), but not in the brain (Fig. 4). The reason for the absence of an effect of progesterone supplementation on radioligand binding in the brain of intact rats is unknown. P-glycoprotein (P-gp) function in the

blood-brain barrier hampers the entry of exogenous progesterone into the brain [35], whereas C6 tumors do not express P-gp (personal observations). Therefore, exogenous progesterone can freely enter the implanted C6 tumor, but can enter the brain only to a limited extent.

Our data suggest that not only steroid supplementation - as reported previously for other sigma ligands - but also removal of steroid is accompanied by changes of the *in vivo* binding of ^{11}C-SA4503. Repeated treatment of animals with pentobarbital increased tumor SUV (from 0.83 to 1.52) and the tumor to muscle ratio (from 4.6 to 7.2, Table 1). Tracer SUV in cerebellum and cerebral cortex was also increased (from 1.66 to 2.41 and from 1.50 to 2.38, respectively, Table 1). TACs in the microPET experiments indicated increased ^{11}C-SA4503 binding both in the C6 tumor (by 16%) and in the brain (by 27%, Fig. 3). Prolonged pentobarbital anaesthesia and progesterone supplementation were not accompanied by any significant change of the blood activity curves of ^{11}C-SA4503 (Figs. 2 and 3). Altered tracer binding to sigma-1 receptors in tumor and brain appears therefore to be related to changes within target tissue rather than to altered tracer delivery to the target organs. Since pentobarbital has multiple effects on cerebral biochemistry, our data do not prove that the effect of prolonged anaesthesia is due to an interference of pentobarbital with steroid metabolism. However, the information from our microPET and biodistribution studies is consistent with the hypothesis that prolonged pentobarbital anaesthesia results in reduced levels of endogenous steroid hormones.

Conclusion

Steroid competition affects binding of the sigma ligand ^{11}C-SA4503 in tumor cells and tumor-bearing rats. Progesterone, the most potent steroid competitor of ^{11}C-SA4503 binding, showed an IC50 value in tumor cells of 33 nM, or 10 ng/ml (Fig. 2). Similar levels of progesterone (3–28 ng/ml) are reached in human plasma during the luteal phase of the menstrual cycle [36] and even higher levels occur during hormone treatment. Moreover, steroid levels may change during chemotherapy, both in male and female patients [37–40]. Therefore, (patho)physiological variations of these levels can result in variability of the binding potential of ^{11}C-SA4503 and should be taken into account in PET studies of patients and healthy volunteers.

References

1 Strauss LG. Fluorine-18 deoxyglucose and false-positive results: a major problem in the diagnostics of oncological patients. Eur J Nucl Med 1996;23:1409–15.

2 van Waarde A, Jager PL, Ishiwata K, Dierckx RA, Elsinga PH. Comparison of sigma-ligands and metabolic PET tracers for differentiating tumor from inflammation. J Nucl Med 2006;47:150–4.

3 Vilner BJ, John CS, Bowen WD. Sigma-1 and sigma-2 receptors are expressed in a wide variety of human and rodent tumor cell lines. Cancer Res 1995;55:408–13.

4 Mach RH, Smith CR, al-Nabulsi I, Whirrett BR, Childers SR, Wheeler KT. Sigma 2 receptors as potential biomarkers of proliferation in breast cancer. Cancer Res 1997;57:156–61.

5 al-Nabulsi I, Mach RH, Wang LM, Wallen CA, Keng PC, Sten K, et al. Effect of ploidy, recruitment, environmental factors, and tamoxifen treatment on the expression of sigma-2 receptors in proliferating and quiescent tumour cells. Br J Cancer 1999;81:925–33.

6 Wheeler KT, Wang LM, Wallen CA, Childers SR, Cline JM, Keng PC, et al. Sigma-2 receptors as a biomarker of proliferation in solid tumours. Br J Cancer 2000;82:1223–32.

7 Maurice T, Gregoire C, Espallergues J. Neuro(active)steroids actions at the neuromodulatory sigma1 (sigma1) receptor: biochemical and physiological evidences, consequences in neuroprotection. Pharmacol Biochem Behav 2006;84:581–97.

8 Hellewell SB, Bruce A, Feinstein G, Orringer J, Williams W, Bowen WD. Rat liver and kidney contain high densities of sigma 1 and sigma 2 receptors: characterization by ligand binding and photoaffinity labeling. Eur J Pharmacol 1994;268:9–18.

9 Hashimoto K, Ishiwata K. Sigma receptor ligands: possible application as therapeutic drugs and as radiopharmaceuticals. Curr Pharm Des 2006;12:3857–76.

10 Vilner BJ, de Costa BR, Bowen WD. Cytotoxic effects of sigma ligands: sigma receptor-mediated alterations in cellular morphology and viability. J Neurosci 1995;15:117–34.

11 Ramamoorthy JD, Ramamoorthy S, Mahesh VB, Leibach FH, Ganapathy V. Cocaine-sensitive sigma-receptor and its interaction with steroid hormones in the human placental syncytiotrophoblast and in choriocarcinoma cells. Endocrinology 1995;136:924–32.

12 Maurice T, Phan VL, Urani A, Kamei H, Noda Y, Nabeshima T. Neuroactive neurosteroids as endogenous effectors for the sigma1 (sigma1) receptor: pharmacological evidence and therapeutic opportunities. Jpn J Pharmacol 1999;81:125–55.

13 Ueda H, Inoue M, Yoshida A, Mizuno K, Yamamoto H, Maruo J, et al. Metabotropic

neurosteroid/sigma-receptor involved in stimulation of nociceptor endings of mice. J Pharmacol Exp Ther 2001;298:703–10.

14 Dong Y, Fu YM, Sun JL, Zhu YH, Sun FY, Zheng P. Neurosteroid enhances glutamate release in rat prelimbic cortex via activation of alpha1-adrenergic and sigma1 receptors. Cell Mol Life Sci 2005;62:1003–14.

15 Monnet FP, Mahe V, Robel P, Baulieu EE. Neurosteroids, via sigma receptors, modulate the [3H]norepinephrine release evoked by N-methyl-D-aspartate in the rat hippocampus. Proc Natl Acad Sci USA 1995;92:3774–8.

16 Romieu P, Lucas M, Maurice T. Sigma1 receptor ligands and related neuroactive steroids interfere with the cocaine-induced state of memory. Neuropsychopharmacology 2006;31:1431–43.

17 Chen Y, Hajipour AR, Sievert MK, Arbabian M, Ruoho AE. Characterization of the cocaine binding site on the sigma-1 receptor. Biochemistry 2007;46:3532–42.

18 Pal A, Hajipour AR, Fontanilla D, Ramachandran S, Chu UB, Mavlyutov T, et al. Identification of regions of the sigma-1 receptor ligand binding site using a novel photoprobe. Mol Pharmacol 2007;72:921–33.

19 Waterhouse RN, Chang RC, Atuehene N, Collier TL. In vitro and in vivo binding of neuroactive steroids to the sigma-1 receptor as measured with the positron emission tomography radioligand [18F]FPS. Synapse 2007;61:540–6.

20 Quirion R, Bowen WD, Itzhak Y, Junien JL, Musacchio JM, Rothman RB, et al. A proposal for the classification of sigma binding sites. Trends Pharmacol Sci 1992;13:85–6.

21 Cobos EJ, Lucena G, Baeyens JM, Del Pozo E. Differences in the allosteric modulation by phenytoin of the binding properties of the sigma1 ligands [3H](+)-pentazocine and [3H]NE-100. Synapse 2006;59:152–61.

22 van Waarde A, Buursma AR, Hospers GA, Kawamura K, Kobayashi T, Ishii K, et al. Tumor imaging with 2 sigma-receptor ligands, 18F-FE-SA5845 and 11C-SA4503: a feasibility study. J Nucl Med 2004;45:1939–45.

23 Kawamura K, Kubota K, Kobayashi T, Elsinga PH, Ono M, Maeda M, et al. Evaluation of [11C]SA5845 and [11C]SA4503 for imaging of sigma receptors in tumors by animal PET. Ann Nucl Med 2005;19:701–9.

24 van Waarde A, Shiba K, de Jong JR, Ishiwata K, Dierckx RA, Elsinga PH. Rapid reduction of sigma1-receptor binding and 18F-FDG uptake in rat gliomas after in vivo treatment with doxorubicin. J Nucl Med 2007;48:1320–6.

25 Ishikawa M, Ishiwata K, Ishii K, Kimura Y, Sakata M, Naganawa M, et al. High occupancy of sigma-1 receptors in the human brain after single oral administration of fluvoxamine: A positron emission tomography study using [11C]SA4503. Biol Psychiatry 2007;62:878–83.

26 Sakata M, Kimura Y, Naganawa M, Oda K, Ishii K, Chihara K, et al. Mapping of

human cerebral sigma1 receptors using positron emission tomography and [11C] SA4503. Neuroimage 2007;35:1–8.

27 Mishina M, Ishiwata K, Ishii K, Kitamura S, Kimura Y, Kawamura K, et al. Function of sigma1 receptors in Parkinson's disease. Acta Neurol Scand 2005;112:103–7.

28 Mishina M, Ohyama M, Ishii K, Kitamura S, Kimura Y, Oda K, et al. Low density of sigma1 receptors in early Alzheimer's disease. Ann Nucl Med 2008;22:151–6.

29 Korneyev AY, Costa E, Guidotti A. During anesthetic-induced activation of hypothalamic pituitary adrenal axis, blood-borne steroids fail to contribute to the anesthetic effect. Neuroendocrinology 1993;57:559–65.

30 Kawamura K, Elsinga PH, Kobayashi T, Ishii S, Wang WF, Matsuno K, et al. Synthesis and evaluation of 11C- and 18F-labeled 1-[2-(4-alkoxy-3-methoxyphenyl)ethyl]-4-(3-phenylpropyl)piperazines as sigma receptor ligands for positron emission tomography studies. Nucl Med Biol 2003;30:273–84.

31 Berthois Y, Katzenellenbogen JA, Katzenellenbogen BS. Phenol red in tissue culture media is a weak estrogen: implications concerning the study of estrogen-responsive cells in culture. Proc Natl Acad Sci USA 1986;83:2496–500.

32 Lee CJ, Do BR, Kim JK, Yoon YD. Pentobarbital and ketamine suppress serum concentrations of sex hormones in the female rat. J Anesth 2000;14:187–90.

33 Su TP, London ED, Jaffe JH. Steroid binding at sigma receptors suggests a link between endocrine, nervous, and immune systems. Science 1988;240:219–21.

34 Maurice T, Roman FJ, Privat A. Modulation by neurosteroids of the in vivo (+)-[3H] SKF-10,047 binding to sigma 1 receptors in the mouse forebrain. J Neurosci Res 1996;46:734–43.

35 Cisternino S, Rousselle C, Debray M, Scherrmann JM. In situ transport of vinblastine and selected P-glycoprotein substrates: implications for drug-drug interactions at the mouse blood-brain barrier. Pharm Res 2004;21:1382–9.

36 Chiron Diagnostics ACS. Centaur Progesterone Assay Manual. 1998.

37 LeBlanc GA, Kantoff PW, Ng SF, Frei E, Waxman DJ. Hormonal perturbations in patients with testicular cancer treated with cisplatin. Cancer 1992;69:2306–10.

38 Nader S, Schultz P, Deinzer D, Samaan NA. Acute hormonal changes following chemotherapy for Hodgkin's disease in man. J Androl 1983;4:293–7.

39 Pribylova O, Springer D, Svobodnik A, Kyr M, Zima T, Petruzelka L. Influence of chemotherapy on hormonal levels in postmenopausal breast cancer patients. Neoplasma 2008;55:294–8.

40 Padmanabhan N, Wang DY, Moore JW, Rubens RD. Ovarian function and adjuvant chemotherapy for early breast cancer. Eur J Cancer Clin Oncol 1987;23:745–8.

MicroPET with a sigma ligand, ^{11}C-SA4503, detects spontaneous pituitary tumors in aged rats

Nisha K. Ramakrishnan,[1] Anna Rybczynska,[1] Anniek K.D. Visser,[1] Csaba J. Nyakas,[2] Chantal Kwizera,[1] Jurgen W.A. Sijbesma,[1] Phlip H. Elsinga,[1] Kiichi Ishiwata,[3] Jan Pruim,[1] Rudi A.J.O. Dierckx[1,4] and Aren van Waarde[1]

[1]Nuclear Medicine and Molecular Imaging, University Medical Center Groningen, University of Groningen, Groningen, The Netherlands

[2]Molecular Neurobiology, University of Groningen, Groningen, The Netherlands

[3]Positron Medical Center, Tokyo Metropolitan Institute of Gerontology, Tokyo, Japan

[4]Nuclear Medicine, Ghent University, Ghent, Belgium

Chapter 4

(submitted)

Abstract

Spontaneous pituitary tumors occur in rats over one year of age and are the most common cause of rodent death. In an ongoing study of changes of sigma-1 agonist binding related to ageing, several of our rats developed such tumors. The aim of the current study was to assess the kinetics of ^{11}C-SA4503 in tumor and brain, and to compare cerebral binding of the ligand in healthy and tumor-bearing animals. Methods: MicroPET scans of the brain region of male Wistar Hannover rats (age 18 to 32 months) were made, using a Siemens/Concorde Focus 220 camera and the agonist ^{11}C-SA4503. The time-dependent uptake of ^{11}C in the entire brain, individual brain regions, tumor or normal pituitary, and thyroid was measured. A cannula in a femoral artery was used for blood sampling and determination of the time course of activity in arterial plasma. Two-tissue compartment model (2TCM) was fitted to the PET data, using metabolite-corrected plasma radioactivity as input function. Results: (all values mean ± SEM): Pituitary tumors showed up as bright hot spots in the scans. The total distribution volume (V_T) of the tracer in malignant tissue (105.0 ± 47.6, n = 5) was significantly increased (P < 0.05) compared to the normal pituitary (11.6 ± 1.0, n = 8). Surprisingly, an increase in V_T was also seen in the brain (P < 0.001) and thyroid tissue (P < 0.01) of animals with pituitary tumors (25.5 ± 3.3; n = 5 and 39.3 ± 5.5; n = 4, respectively) compared to brain tissue of healthy rats (11.8 ± 1.2 and 23.1 ± 1.9, respectively; n = 8). Kinetic analysis showed that the increase in brain and thyroid was not related to a change of nondisplaceable binding potential (BP_{ND}) but rather to an increase of the partition coefficient (K_1/k_2 ratio) of ^{11}C-SA4503. The increase in V_T in the malignant tissue on the other hand was accompanied by a significant increase in BP_{ND} (10.7 ± 1.7, n = 5 vs 4.6 ± 0.5, n = 8, P < 0.01). Conclusion: Our results indicate that the BP_{ND} of ^{11}C-SA4503 to sigma-1 receptors is increased in pituitary tumors compared to their tissue of origin and that this tracer may have promise for the detection of pituitary adenomas, using PET.

Keywords: sigma receptor, ^{11}C-SA4503, spontaneous pituitary tumor, Wistar rats, kinetic analysis, microPET

Introduction

Pituitary tumors (adenoma of pituitary gland) are among five most common intracranial neoplasms [1,2]. Pituitary adenomas grow slowly and metastasize rarely [3]. Despite their benign nature, they can cause significant morbidity [4]. For example, pituitary tumors can lead to Cushing syndrome, pituitary hyperthyroidism, acromegaly, Nelson syndrome or impotence [5,6]. Unfortunately, pituitary tumors are very difficult to

diagnose and often remain undetected until post-mortem examination or during late-stage disease [7,8]. At late stages, the majority of pituitary tumors will be macroadenomas with a low surgical cure rate [3]. Diagnostic problems arise from the fact that they can manifest themselves by varying symptoms: 1. functioning tumors hypersecrete various hormones (e.g. prolactin, thyroid-stimulating hormone, and growth hormone), and 2. non-functioning tumors (non-secreting), grow usually undetected until they compress surrounding structures (e.g. optic nerves) or prevent normal functioning of the pituitary gland [9]. In addition, large pituitary tumors can cause occasionally fatal damage to the brain due to a sustained increase in the intracranial pressure [10].

Because hormonal or symptom examination gives a rather poor differential diagnosis, current diagnostic methods include imaging techniques such as computed tomography (CT) or magnetic resonance imaging (MRI). CT and MRI imaging allows avoidance of biopsies and improves significantly pituitary tumor localization [9,11,12]. However, CT and MRI cannot distinguish between tumor and scar tissue or monitor biochemical and functional aspects of the tumor.

There is no tracer of first choice for pituitary tumor imaging using nuclear medicine [4], although such lesions have been visualized also e.g. with ^{18}F-fluorodeoxyglucose (^{18}F-FDG), radioactively labeled somatostatin analogs, such as ^{111}In-pentetreotide, and dopamine D_2 receptor-targeting radiopharmaceuticals, such as ^{18}F-fluoroethyl-spiperone (^{18}F-FESP) [1,4,7]. The widespread use of ^{18}F-FDG in positron emission tomography (PET) imaging in the last two decades increased the detection of incidentalomas of the pituitary gland [7,13]. However, pituitary tumors are slowly growing and highly differentiated, which makes ^{18}F-FDG unsuitable for their imaging [4]. Furthermore, ^{18}F-FDG poorly distinguishes between non-/neoplastic lesion, benign/malignant lesions or inflammation, and accumulation of this tracer in pituitary gives an ambiguous interpretation [7,13-15]. Huyn et al. showed that only 40.8% of the patients with focal pituitary ^{18}F-FDG accumulation presented with pathologic lesions [7]. In addition, somatostatin receptor- and dopamine D_2 receptor-targeting radiopharmaceuticals have only limited clinical usefulness, because expression of these receptors is dependent on the hormones that the pituitary tumor secretes (e.g. higher expression of somatostatin receptors in tumors producing growth hormone/thyroid-stimulating hormone or higher expression of dopamine D_2 receptors in non-secretive tumors) [4,12,16].

Tumor cells frequently overexpress sigma receptors. Sigma receptors are unique transmembrane proteins, classified into two subtypes, sigma-1 and sigma-2 [17]. Sigma-1 receptors were studied in more detail than sigma-2 receptors since the sigma-1 gene has been sequenced and cloned [18], and selective ligands and antibodies are available for the sigma-1 but not for the sigma-2 subtype. Sigma-1 receptors were shown to be an intraorganelle signaling and cell survival modulator at the endoplasmic reticulum-

mitochondria junctions [19]. An increase of sigma-1 receptor expression counteracts the ER stress response, whereas a decrease in sigma-1 receptors can enhance apoptosis [19]. Sigma-1 receptor function is related to processes such as neuroplasticity and neuroprotection in the brain and cell death or survival in tumors [20,21].

Sigma-1 receptors are also expressed in the pituitary gland [22,23], where they were shown to be directly and functionally coupled to Kv1.4 K^+ channels [24,25]. In the rat posterior pituitary, sigma-1 receptor activation by agonistic ligands or co-expression of sigma-1 receptors and K^+ channels reduces the peak current amplitude of the neurohypophysial K^+ currents in a G protein-independent manner [26]. However, the presence of sigma-1 receptors in pituitary tumors has not yet been examined.

^{11}C-SA4503 (^{11}C-labeled 1-[2-(3,4-dimethoxyphenthyl)]-4-(3-phenylpropyl)-piperazine dihydrochloride) is a ligand with high affinity for sigma-1 receptors, IC50 = 17.4 nM, and commonly employed for PET [21]. We have previously reported that microPET with ^{11}C-SA4503 shows high tracer accumulation in the mammalian brain [27]. ^{11}C-SA4503 was already tested in healthy volunteers, and in patients with Alzheimer's disease [28,29] or Parkinson's disease [17,29,30]. Furthermore, microPET with ^{11}C-SA4503 in rats successfully detected subcutaneously-grown C6 gliomas, had 10-fold C6 tumor selectivity over a turpentine-induced sterile inflammation, and showed an early decrease in tumor uptake following systemic doxorubicin treatment which corresponded to a loss of sigma-1 receptors from the tumors [31,32].

In an ongoing study of changes of sigma-1 agonist binding related to ageing, several of our Wistar Hannover rats developed pituitary tumors. In the current study we examined if spontaneously developed pituitary tumors in aged rats (Figure 1) can

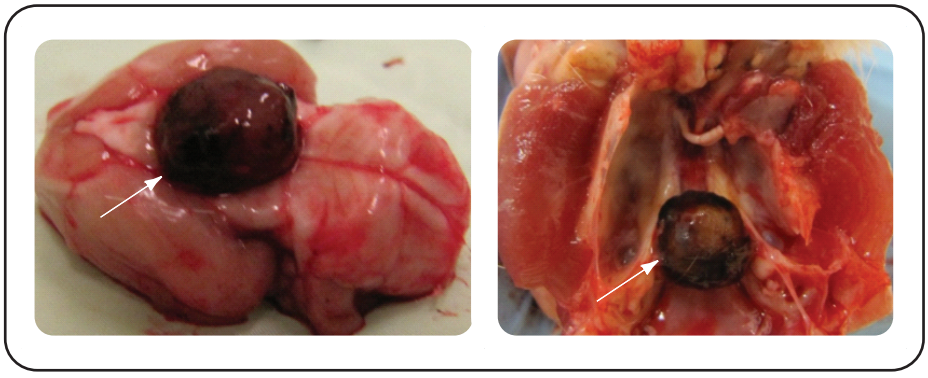

Fig.1. Brain specimens from aged rats with spontaneous pituitary tumors. Arrows indicate the position of the tumor.

be detected and distinguished from the normal pituitary by microPET imaging with ^{11}C-SA4503. Also, we performed kinetic analysis of tracer uptake in the brain, pituitary tumors and thyroid gland, using a 2-tissue compartment model (2TCM) to assess changes in partition coefficient (K_1/k_2), nondisplaceable binding potential ($BP_{ND} = k_3/k_4$) and total distribution volume (V_T). Finally, the impact of a pituitary tumor on uptake of ^{11}C-SA4503 in peripheral organs was examined.

Materials & Methods

^{11}C-SA503 Synthesis

The radioligand 1-[2-(3,4-dimethoxyphenethyl)]-4-(3-phenylpropyl)piperazine (^{11}C-SA4503) was prepared by reaction of ^{11}C-methyl iodide with 1-[2-(4-hydroxy-3-methoxy-penthyl)]-4-(3-phenylpropyl)piperazine dihydrochloride (4-O-demethyl SA4503), according to a published method [33]. The decay corrected radiochemical yield was ~ 24%, the specific radioactivity was > 100 TBq/mmol at the moment of injection and radiochemical purity > 98%. The ^{11}C-SA4503 solution had pH 6.0 to 7.0.

Animal Model

Experiments were performed in male Wistar Hannover rats (HsdHan™:WIST) aged 18 to 32 months. Animals were either purchased from Harlan (Boxmeer, The Netherlands) or acquired from Semmelweis University (Budapest, Hungary). It was previously reported that more than 37% of male Wistar Hannover rats above 1-year of age may develop pituitary tumors [34]. The rats were housed in Macrolon cages on a layer of wood shavings in a room with constant temperature (21 ± 2°C) and fixed 12-hour light-dark regime (light phase from 7:00 to 19:00 hours). Food (standard laboratory chow, RMH-B, Hope Farms, The Netherlands) and water were available ad libitum. After arrival the rats were acclimatized for at least seven days. Experiments were performed by licensed investigators in compliance with the Law on Animal Experiments in The Netherlands. The protocol was approved by the Committee on Animal Ethics of the University of Groningen. Animals were assigned to the healthy control (n = 8) or tumor-bearing group (n = 5) after autopsy.

Arterial Blood Sampling

Before microPET scanning, an arterial cannula was placed in each rat for blood sampling and determination of the time course of radioactivity in plasma. For this purpose, rats were anesthetized with isoflurane (Pharmachemie BV, The Netherlands, 5% in medicinal air for induction 2% for maintenance). An incision was made parallel to the femoral artery. The femoral artery was separated from the femoral vein and temporarily

ligated to prevent leakage of blood. A small incision was made in the artery and a cannula was inserted (0.8 mm outer, 0.4 mm inner diameter). The cannula was secured to the artery with a suture and attached to a syringe filled with heparinized saline.

From each rat, fifteen arterial blood samples (volume 0.1 to 0.15 ml) were collected at 0.25, 0.5, 0.75, 1, 1.25, 1.5, 2.0, 3, 5, 7.5, 10, 15, 30, 60 and 90 minutes after ^{11}C-SA4503 injection and start of the microPET scan. Plasma was obtained from the blood by centrifugation (5 min in Eppendorf-type centrifuge at 13,000 rpm). Radioactivity in plasma samples (25 µl) was determined using a calibrated gamma counter (CompuGamma CS 1282, LKB-Wallac, Turku, Finland). In a separate group of animals, larger volumes of blood (0.4 to 2 ml) were collected at 5, 10, 20, 40 and 60 min, and a metabolite analysis was performed by reversed-phase HPLC, using a previously published method for ^{11}C-SA4503 [35]. Plasma data was corrected for metabolites based on the age of the rat.

MicroPET Scan

Two rats were scanned simultaneously in each scan session, using a Siemens/Concorde microPET camera (Focus 220). They were positioned in the camera in transaxial position with their heads and neck in the field of view. First, a transmission scan of 515 seconds with a Co-57 point source was obtained for attenuation and scatter correction of 511 keV photons by tissue. Subsequently, the first rat was injected through the penile vein with ^{11}C-SA4503 (15-35 MBq, volume < 1 ml). The emission scan was started with tracer injection of the first rat; whereas the second animal was injected 16 min later. A list-mode protocol was used with 90 min acquisition time (analysis performed for first 74 min from tracer injection). Reconstructions were performed using microPET Manager 2.3.3.6; ASIPro 6.3.3.0 (Siemens). The list-mode data of the emission scans were reframed into a dynamic sequence of 8x30s, 3x60s, 2x120s, 2x180s, 3x300s, 3x600s, 1x720s, 1x960s frames. The data were reconstructed per time frame employing an interative reconstruction algorithm (OSEM2D with Fourier rebinning, 4 iterations and 16 subsets). The final datasets consisted of 95 slices with a slice thickness of 0.8 mm, and an in-plane image matrix of 128 x 128 pixels. Voxel size was 0.5 x 0.5 x 0.8 mm. The linear resolution at the center of the field-of-view was about 1.5 mm. Data sets were fully corrected for decay, random coincidences, scatter and attenuation.

MicroPET Data Analysis

The images obtained from the scan were co-registered with a MRI template [36] for drawing the three-dimensional regions of interest (ROIs) over the whole brain and healthy pituitary. ROIs were also drawn over the thyroid and pituitary tumor using Inveon Research Workplace software (Siemens Medical Solutions, Knoxville, TN). Time-activity curves (TACs) were calculated for each of these regions. Tracer uptake was expressed as

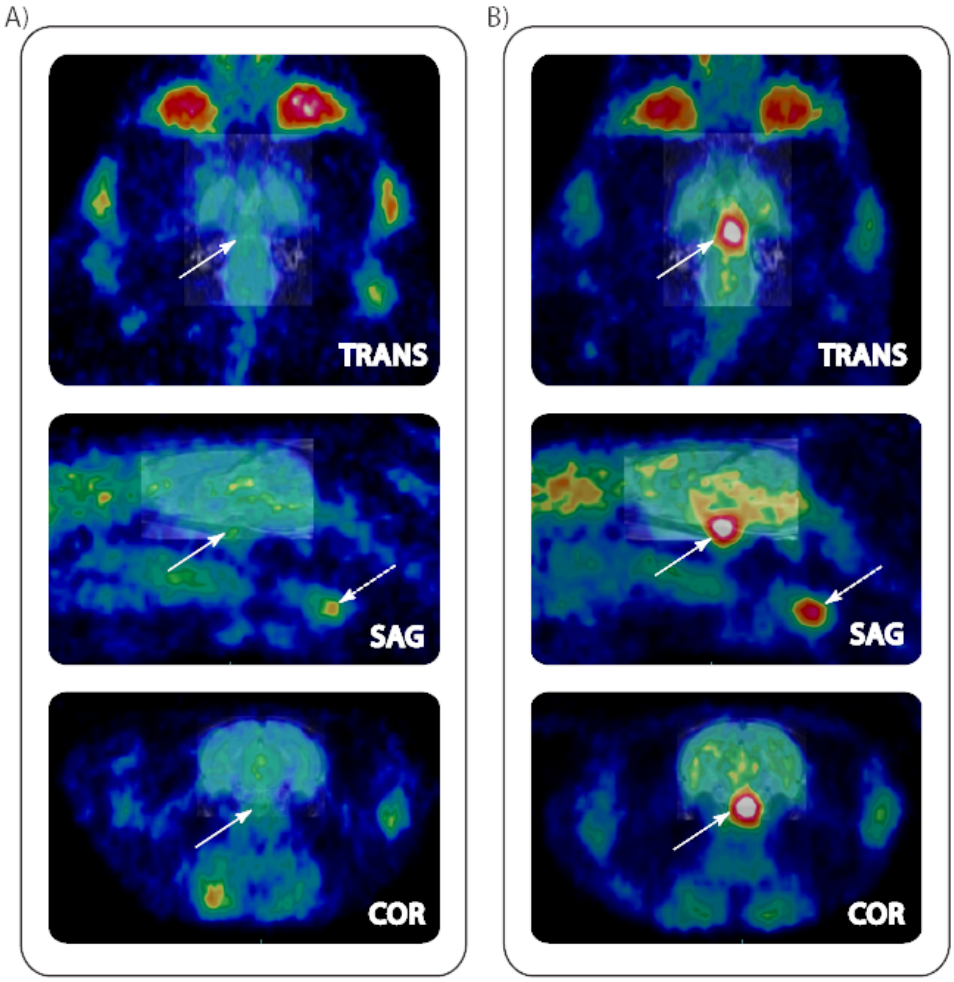

Fig.2. ^{11}C-SA4503 microPET images of: A) a healthy aged rat; B) an aged rat with spontaneous pituitary tumor weighing 17 mg. TRANS = transverse, COR = coronal, SAG = sagittal view. Solid arrows indicate the healthy pituitary or pituitary tumor, dashed arrow position of the thyroid gland.

a PET-$SUV_{(mean)}$, assuming a specific gravity of 1 g/cm^3 for brain tissue and blood plasma. The parameter SUV is defined as: [tissue activity concentration (MBq/g) × animal body weight (g) / injected dose (MBq)].

Kinetic analysis was performed by fitting a 2TCM to the dynamic PET data, using metabolite-corrected plasma radioactivity from arterial blood samples as input function.

Software routines for MatLab 7 (The MathWorks, Natick, MA), written by Dr. A.T.M. Willemsen (University Medical Center Groningen), were used to assess the K_1/k_2 and BP_{ND} = k_3/k_4 of ^{11}C-SA4503. The blood volume was fixed at 0.036. V_T was calculated as K1/k2 * (1+ k3/k4).

Ex vivo Biodistribution

After the scanning period, animals were terminated by extirpation of the heart. Blood was immediately collected, and plasma and a cell fraction were separated by short centrifugation (5 min at 1,000 × g). Several tissues (see Table 1) were excised. All tissue samples were weighed. Radioactivity in tissue samples and in a sample of the injected tracer solution (infusate) was measured using a gamma counter with automatic decay correction. The data are presented as SUV. Tissue-to-plasma, tumor-to-muscle and tumor-to-brain concentration ratios of radioactivity were calculated.

Statistics

The biodistribution results are expressed as mean ± SD and all other results are expressed as mean ± SEM. Differences between groups were examined by two-tailed unpaired t-test or 1-way ANOVA, followed by a post-hoc Bonferroni test, if applicable. A *P* value < 0.05 was considered statistically significant.

Results

Tumor visualization on PET images

Pituitary tumors apperared in approximately 45% of tested aminals. Spontaneous pituitary tumors were clearly visible in ^{11}C-SA4503 scans (Figure 2). The brains of animals with pituitary tumor appeared to take up more tracer than normal brain. Thyroid gland was visualized and it took up more of tracer in the tumor bearing rats than in the normal aged rats (Figure 2).

Kinetics of radioactivity in plasma and brain

Kinetics of radioactivity in the plasma after a bolus injection of ^{11}C-SA4503 is shown in Figure 3A. Plasma values from four of the normal rats were not included in this analysis; three due to non availability of plasma samples (failure of the cannula) and one due to changed kinetics because of a small depot during tracer injection. A rapid biexponential clearance was observed in both normal and tumor bearing animals. The presence of the pituitary tumor did not affect plasma kinetics of the tracer.

Kinetics of ^{11}C-SA4503 in pituitary and pituitary tumor, the brain and thyroid are presented in Figures 3B-D. Tracer uptake was rapid in normal brain, normal pituitary

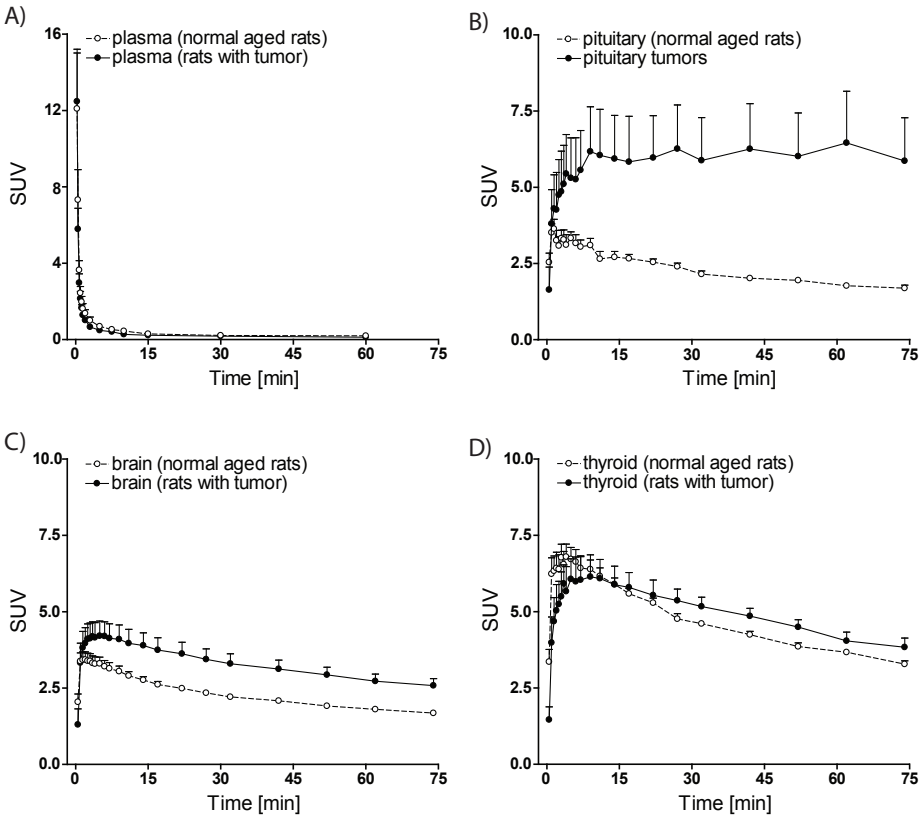

Fig.3. Time-activity curves of ^{11}C-SA4503 in: A) plasma of normal (n = 5) and tumor-bearing rats (n = 4); B) normal pituitary (n = 7) and pituitary tumors (n = 5); C) brain of normal (n = 7) and tumor-bearing rats (n = 5); D) thyroid of normal (n = 7) and tumor-bearing aged (n = 5). Data are expressed as mean ± SEM, differences were tested with repeated measures 2-way ANOVA and Bonferroni post hoc analysis.

and brain with tumor, with the peak appearing within 5 min of tracer injection and was followed by a slow washout. The pituitary tumor uptake while also rapid, reached a plateau within 10 min and no appreciable washout was seen within the scan duration. The brain uptake of the tracer in the tumor-bearing rats was about 50% higher than in normal aged rats. The tumor uptake was significantly higher (P ranging from <0.05 to <0.001) than the normal pituitary 7 min onwards and was about 3-fold higher by the end of the scan. It was also significantly higher (P ranging from <0.05 to <0.01) than the brain uptake in tumor bearing rats from 30 min onwards and was about 2-fold higher by the end of the scan.

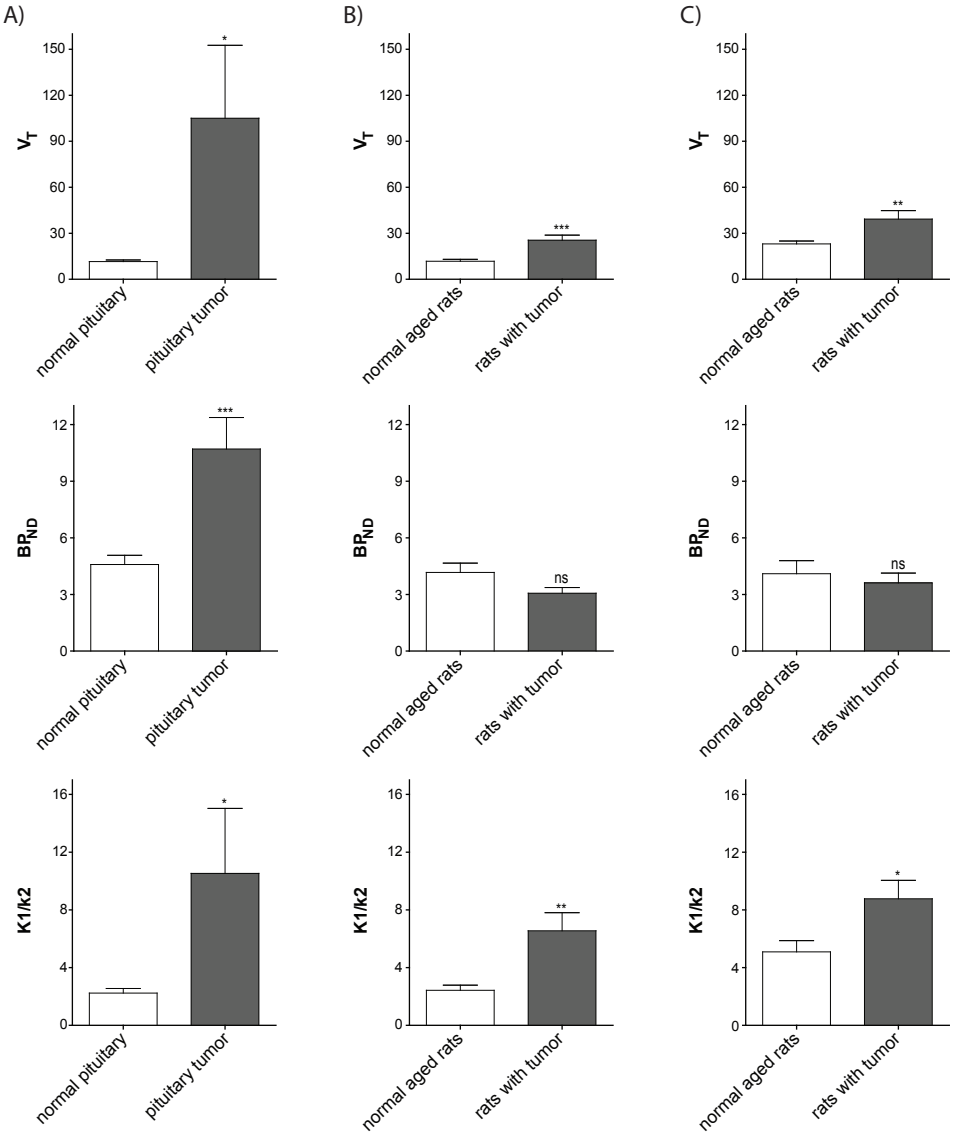

Fig.4. Kinetic modeling parameters of ^{11}C-SA4503 in: A) normal pituitary (n = 8) and pituitary tumor (n = 5); B) brain of normal (n = 8) and tumor bearing (n = 5) rats; C) thyroid of normal (n = 8) and tumor bearing (n = 5) rats. Data are expressed as mean ± SEM and were tested with unpaired, two-tailed t-test.

Kinetic analysis

2TCM was fitted to ROIs drawn around whole brain, normal pituitary, pituitary tumor and thyroid using metabolite-corrected arterial plasma as input. Where plasma data was not available, a population mean values corrected for injected dose and weight of individual animal was used as input. The V_T (Figure 4A) of the tracer was significantly increased ($P < 0.05$) in malignant tissue (105.0 ± 47.6) compared to the normal pituitary (11.6 ± 1.0). An increase in V_T was also seen in the brain tissue of animals with pituitary tumors compared to brain tissue of normal rats (25.5 ± 3.3 vs 11.8 ± 1.2, $P < 0.001$) (Figure 4B) and in thyroid of rats with pituitary tumors compared to thyroid of normal rats (39.3 ± 5.5 vs 23.1 ± 1.9, $P < 0.01$) (Figure 4C).

Further analysis showed that the increase of V_T in the brain was not related to a change in BP_{ND}, but rather to an increase in partition coefficient (K_1/k_2) of ^{11}C-SA4503 (6.6 ± 1.3 vs 2.4 ± 0.4, $P < 0.01$, Figure 4B). Similarly, the increase in V_T in the thyroid was related to an increase in K_1/k_2 (8.8 ± 1.3 vs 5.1 ± 0.8, $P < 0.05$, Figure 4C) rather than BP_{ND}. V_T, BP_{ND} and K_1/k_2 between brain and thyroid were well correlated (Figures 5A-C). Particularly V_T and K_1/k_2 showed a close correlation ($R^2 > 0.8$). However, increases of V_T in the tumor were associated with significant increases in both BP_{ND} (10.7 ± 1.7 vs 4.6 ± 0.5, $P < 0.01$) and K_1/k_2 (10.5 ± 4.5 vs 2.2 ± 0.3, $P < 0.05$) (Figures 3B and 3C). The values for K_1/k_2 (but not V_T and BP_{ND}) from brain and pituitary or tumor had a significant correlation ($R^2 = 0.38$, $P < 0.05$; data not shown).

Biodistribution

The mass of a normal pituitary was 12.7 ± 3.3 mg (mean ± SD, n = 5, range 8.6 to 17.7 mg). Spontaneous pituitary tumors weighed 70.5 ± 93.1 mg (mean ± SD, n = 8, range 14.0 to 274.7 mg). Representative specimens of pituitary tumors are shown in

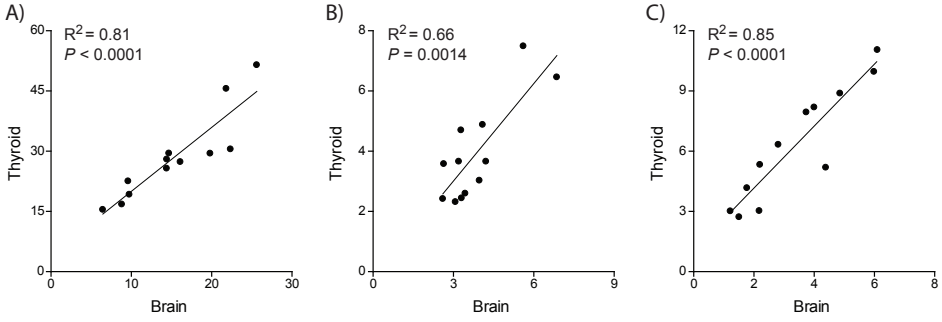

Fig.5. Correlation of ^{11}C-SA4503 kinetic parameters (A: VT, B: BP_{ND}, C: K_1/k_2) in the thyroid and brain.

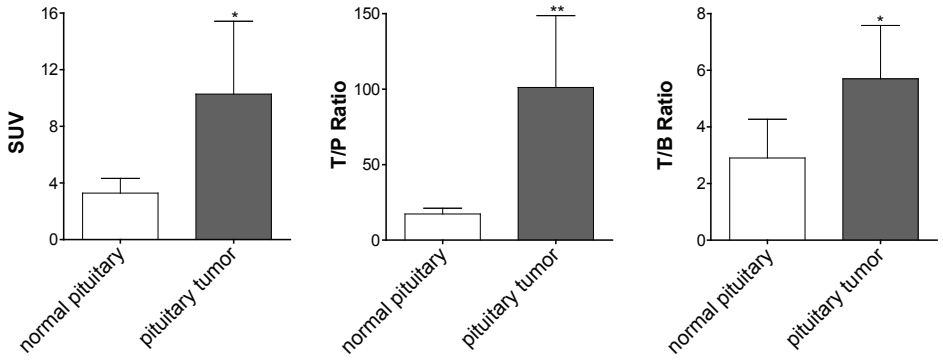

Fig.6. Tracer SUV, tissue-to-plasma (T/P) and tissue-to-brain (T/B) ratio of ^{11}C-SA4503 in the normal pituitary (n = 5) and spontaneous pituitary tumors (n = 6, two rats which had large necrotic tumors were not included in this analysis). Data are expressed as mean ± SD and were tested with unpaired, two-tailed t-test.

Figure 1. The figure shows one of the larger tumors (143 mg) still attached to the skull, and the position of the tumor with respect to the brain.

Biodistribution data for the brain areas and peripheral organs are listed in Table 1. The presence of the pituitary tumor was associated with a significant increase in the SUV and tissue-to-plasma ratio of the tracer in all brain areas. SUV values in peripheral organs of normal and tumor-bearing rats were not significantly different, but tissue-to-plasma ratios in brain, small intestine, liver and spleen of tumor-bearing animals were significantly increased.

Biodistribution data of ^{11}C 90 min after injection of ^{11}C-SA4503 showed a significantly higher uptake (SUV), tissue-to-plasma ratio and tissue-to-brain ratio in pituitary tumors than the normal pituitary (Figure 6).

Discussion

This study demonstrates that spontaneous pituitary tumors in aged rats can be detected and distinguished from normal pituitary and brain by microPET imaging with the sigma-1 ligand, ^{11}C-SA4503 (Figure 2B). To the best of our knowledge, this is the first report identifying sigma-1 receptors in pituitary tumors.

For a good visualization of tumor lesions, the ratio of tracer uptake in tumor versus surrounding tissue must be >> 1. In biodistribution experiments, we observed a rapid uptake, retention and high accumulation of ^{11}C-SA4503 in spontaneous intracranial pituitary tumors (SUV 10.3 ± 2.1) (Figures 3B and Figure 6B). Accumulation of ^{11}C-

Table.1. Biodistribution of ^{11}C-SA4503 in various tissues derived from normal aged (n = 7) and tumor-bearing (n = 5) aged rats.

	SUV			T/P Ratio		
Tissue	**Normal Aged**	**With Tumor**	*P#*	**Normal Aged**	**With Tumor**	*P#*
Cerebellum	1.21 ± 0.32	2.08 ± 0.57	<0.001	7.06 ± 2.67	20.67 ± 4.29	<0.001
Cerebral cortex	1.55 ± 0.14	2.31 ± 0.36	<0.01	8.97 ± 2.09	23.30 ± 4.76	<0.001
Rest of brain	1.28 ± 0.13	1.87 ± 0.41	<0.05	7.41 ± 1.85	18.55 ± 2.54	<0.001
Adipose tissue	0.32 ± 0.26	0.38 ± 0.43	NS	1.91 ± 1.73	3.59 ± 3.89	NS
Bladder	3.09 ± 3.41	2.28 ± 2.08	NS	19.81 ± 24.50	22.82 ± 19.28	NS
Bone	0.43 ± 0.21	0.62 ± 0.18	NS	2.48 ± 1.46	6.45 ± 2.68	NS
Bone marrow	3.55 ± 2.92	2.72 ± 2.01	NS	18.77 ± 13.46	28.00 ± 19.50	NS
Heart	0.61 ± 0.13	0.93 ± 0.12	NS	3.49 ± 0.97	9.43 ± 2.24	NS
Large intestine	2.41 ± 0.70	2.94 ± 0.35	NS	14.30 ± 6.22	30.74 ± 11.58	NS
Small intestine	3.50 ± 1.00	5.41 ± 1.18	NS	20.26 ± 8.13	55.59 ± 18.85	<0.01
Kidney	3.50 ± 0.66	4.08 ± 1.24	NS	20.40 ± 6.20	41.62 ± 15.14	NS
Liver	11.05 ± 1.67	11.68 ± 2.59	NS	63.83 ± 15.44	115.42 ± 14.92	<0.001
Lung	2.21 ± 0.38	3.85 ± 1.35	NS	12.71 ± 3.13	39.32 ± 15.51	NS
Muscle	0.30 ± 0.16	0.47 ± 0.19	NS	1.70 ± 0.86	4.83 ± 2.07	NS
Pancreas	5.74 ± 2.67	5.31 ± 1.72	NS	33.23 ± 18.07	55.07 ± 22.99	NS
Plasma	0.18 ± 0.04	0.10 ± 0.02	NS	1.00	1.00	
Red blood cells	0.09 ± 0.05	0.06 ± 0.02	NS	0.50 ± 0.27	0.64 ± 0.14	NS
Spleen	4.10 ± 0.76	5.77 ± 1.72	NS	24.13 ± 8.29	58.12 ± 17.49	<0.01
Submandibular gland	6.67 ± 2.20	4.90 ± 2.17	NS	37.24 ± 10.40	53.76 ± 36.77	NS
Urine	4.76 ± 5.47	3.68 ± 3.77	NS	31.26 ± 39.06	40.07 ± 41.19	NS

Data are expressed as mean ± SD and were tested with 2-way ANOVA followed by Bonferroni posttest (brain and peripheral organs were analyzed separately).

SA4503 in tumor tissue was ~ 6-fold higher than in the adjacent brain, ~ 3-fold higher than in the normal pituitary gland and ~ 100-fold higher than in blood plasma (Figure 6B). Kinetic modeling indicated that V_T in pituitary tumors is increased (by 10-fold) with respect to the normal pituitary. These changes in V_T result from increases in both BP_{ND} and K_1/k_2 (2.3-fold and 4.9-fold, respectively) (Figure 4A).

Increases of the partition coefficient of the tracer in pituitary tumors could be caused by increased vascularization. However, an increase of K_1/k_2 was observed not only in the tumor, but also in the brain and thyroid. Tracer V_T in the brain of pituitary tumor-bearing rats was increased (by 2.4-fold) compared to brain of healthy rats, due to an increase in K_1/k_2 (by 2.7-fold), whereas BP_{ND} was unaltered (Figure 4B). This observation suggests that increases of V_T are not limited to tumor tissue and are therefore related to changes of vascular permeability or altered blood flow rather than increased vascularization. A 1.7-fold increase of K_1/k_2 (but not BP_{ND}) was also observed in the

thyroid gland (Figure 4C). Since BP_{ND} values in the brain and thyroid of tumor-bearing rats were not increased in contrast to K_1/k_2, sigma-1 receptor expression in these organs appears to be not affected by a pituitary tumor.

An increased partition coefficient of ^{11}C-SA4503 in the brain and thyroid of tumor-bearing animals may be caused by altered blood flow or blood pressure rather than increased permeability of the vascular endothelium. Pituitary tumors are known to exert global effects on blood flow [37]. Regional blood pressure can either be increased or decreased since levels of e.g. adrenocorticotropic hormone, vasopressin or thyroid-stimulating hormone are significantly altered [37]. If the permeability-surface area product of a tracer remains constant, decreased perfusion will lead to increased tracer extraction and rises of V_T because of slower transit of the tracer through the capillary bed. A global reduction of perfusion is suggested by the fact that the presence of a pituitary tumor is associated with significant increases of the tissue-to-plasma ratio of ^{11}C-SA4503 in the brain, small intestine, liver and spleen ($P << 0.01$) (Figure 6A).

If the affinity of ^{11}C-SA4503 to sigma-1 receptors remains constant during malignant transformation, as has been reported for nonneural tumors [38], the observed increase of BP_{ND} in tumor tissue should reflect upregulation of sigma-1 receptors in pituitary tumors, consistent with the moderate (generally 2-3-fold) overexpression of sigma-1 receptors in other tumor tissues [21,38,39]. The reason for upregulation of sigma-1 receptors in tumor tissue is still unclear but it may provide the tumor cells with an additional brake on apoptosis [40].

In this study, we did not find any correlation between BP_{ND} and tumor size (data not shown). Similarly, in a study on 95 breast cancer patients no correlation was observed between sigma-1 receptor levels and tumor size, histological grade or expression of the proliferation marker, Ki-67, although a positive correlation was reported between sigma-1 receptor levels, hormone receptor positivity (in particular progesterone receptor), Bcl-2 expression and the period of disease-free survival [41]. Low ratios (< 1) of pro-survival Bcl-2 and pro-apoptotic Bax expression predominate in non-functioning pituitary tumors and pituitary microadenomas [42].

The very high uptake of ^{11}C-SA4503 in pituitary adenomas indicates that it may be worthwhile to test ^{11}C-SA4503-PET in a clinical setting. Even very small tumors were clearly detected (the mass of the specimen in Figure 2 was 17 mg). This suggests that ^{11}C-SA4503 may be applied for the detection of microadenomas. Future studies are needed to answer the question whether ^{11}C-SA4503-PET can detect pituitary adenomas and can discriminate between symptomatic, hormone-secreting and non-functioning (non-symptomatic, non-secretive) tumors. Clinical experiments may be performed rapidly, because of the frequent occurrence and re-growth of pituitary tumors and the fact that ^{11}C-SA4503 has been previously used in human volunteers.

Conclusions

Our results indicate that the BP_{ND} of ^{11}C-SA4503 to sigma-1 receptors is increased in pituitary tumors compared to their tissue of origin and that this tracer may have promise for the detection of pituitary adenomas, using PET.

References

1 Lucignani G, Losa M, Moresco RM, Del Sole A, Matarrese M, Bettinardi V, et al. Differentiation of clinically non-functioning pituitary adenomas from meningiomas and craniopharyngiomas by positron emission tomography with [18F]fluoro-ethyl-spiperone. Eur J Nucl Med Mol Imaging. 1997;24:1149–55.

2 Jane JA, Laws ER. The management of non-functioning pituitary adenomas. Neurol India. 2003;51:461–5.

3 Fougner SL, Lekva T, Borota OC, Hald JK, Bollerslev J, Berg JP. The expression of E-cadherin in somatotroph pituitary adenomas is related to tumor size, invasiveness, and somatostatin analog response. J Clin Endocrinol Metab. 2010;95:2334–42.

4 Bombardieri E, Seregni E, Villano C, Chiti A, Bajetta E. Position of nuclear medicine techniques in the diagnostic work-up of neuroendocrine tumors. Q J Nucl Med Mol Imaging. 2004;48:150–63.

5 Lafferty AR, Chrousos GP. Pituitary tumors in children and adolescents. J Clin Endocrinol Metab. 1999;84:4317–23.

6 Monson JP. The epidemiology of endocrine tumours. Endocr Relat Cancer. 2000;7:29–36.

7 Hyun SH, Choi JY, Lee K-H, Choe YS, Kim B-T. Incidental focal 18F-FDG uptake in the pituitary gland: clinical significance and differential diagnostic criteria. J Nucl Med. 2011;52:547–50.

8 Heaney AP. Pituitary Carcinoma: Difficult Diagnosis and Treatment. J Clin Endocrinol Metab. 2011;96:3649-60.

9 Bergström M, Muhr C, Lundberg PO, Långström B. PET as a tool in the clinical evaluation of pituitary adenomas. J Nucl Med. 1991;32:610–5.

10 Stanley T, Prabhakaran R, Misra M. Sellar and Pituitary Tumors in Children. In: Brooke S, Biller B, editors. (Contemporary Endocrinology) Diagnosis and management of pituitary disorders. Totowa, NJ: Human Press Inc. 2008. p. 412.

11 Buchfelder M, Schlaffer S-M. Modern imaging of pituitary adenomas. Front Horm Res. 2010;38:109–20.

12 Drevelegas A, editor. Imaging of Brain Tumors with Histological Correlations. II. Berlin, Heidelberg: Springer Berlin Heidelberg; 2011.

13 Jeong SY, Lee S-W, Lee HJ, Kang S, Seo J-H, Chun KA, et al. Incidental pituitary uptake on whole-body 18F-FDG PET/CT: a multicentre study. Eur J Nucl Med Mol Imaging. 2010;37:2334–43.

14 Ryu SI, Tafti BA, Skirboll SL. Pituitary adenomas can appear as hypermetabolic lesions in (18) F-FDG PET imaging. J Neuroimaging. 2010 Oct;20:393–6.

(submitted)

15 Ryu JS, Um JW, Min BW. Inflammatory pseudotumour of the spleen: the findings on F-18 fluorodeoxyglucose positron emission tomography/computed tomography (FDG-PET/CT). ANZ J Surg. 2010;80:650–2.

16 Chiewvit S, Chiewvit P, Pusuwan P, Sriussadaporn S, Ratanamart V. Somatostatin receptor tumor imaging (Tc 99m P829) in pituitary adenoma. J Med Assoc Thai. 1999;82:1208–13.

17 Hashimoto K, Ishiwata K. Sigma receptor ligands: possible application as therapeutic drugs and as radiopharmaceuticals. Curr Pharm Des. 2006;12:3857–76.

18 Kekuda R, Prasad PD, Fei YJ, Leibach FH, Ganapathy V. Cloning and functional expression of the human type 1 sigma receptor (hSigmaR1). Biochem Biophys Res Commun. 1996;229:553–8.

19 Hayashi T, Su T-P. Sigma-1 receptor chaperones at the ER-mitochondrion interface regulate Ca(2+) signaling and cell survival. Cell. 2007;131:596–610.

20 Van Waarde A, Ramakrishnan NK, Rybczynska AA, Elsinga PH, Ishiwata K, Nijholt IM, et al. The cholinergic system, sigma-1 receptors and cognition. Behav Brain Res. 2011;221:543–54.

21 Van Waarde A, Rybczynska AA, Ramakrishnan N, Ishiwata K, Elsinga PH, Dierckx RAJO. Sigma receptors in oncology: therapeutic and diagnostic applications of sigma ligands. Curr Pharm Des. 2010;16:3519–37.

22 Wolfe SA, Culp SG, De Souza EB. Sigma-receptors in endocrine organs: identification, characterization, and autoradiographic localization in rat pituitary, adrenal, testis, and ovary. Endocrinology. 1989;124:1160–72.

23 Iyengar S, Mick S, Dilworth V, Michel J, Rao TS, Farah JM, et al. Sigma receptors modulate the hypothalamic-pituitary-adrenal (HPA) axis centrally: evidence for a functional interaction with NMDA receptors, in vivo. Neuropharmacology. 1990;29:299–303.

24 Aydar E, Palmer CP, Klyachko VA, Jackson MB. The sigma receptor as a ligand-regulated auxiliary potassium channel subunit. Neuron. 2002;34:399–410.

25 Soriani O, Vaudry H, Mei YA, Roman F, Cazin L. Sigma ligands stimulate the electrical activity of frog pituitary melanotrope cells through a G-protein-dependent inhibition of potassium conductances. J Pharmacol Exp Ther. 1998;286:163–71.

26 Lupardus PJ, Wilke RA, Aydar E, Palmer CP, Chen Y, Ruoho AE, et al. Membrane-delimited coupling between sigma receptors and K+ channels in rat neurohypophysial terminals requires neither G-protein nor ATP. J Physiol. 2000;526 Pt 3:527–39.

27 Van Waarde A, Buursma AR, Hospers GAP, Kawamura K, Kobayashi T, Ishii K, et al. Tumor imaging with 2 sigma-receptor ligands, 18F-FE-SA5845 and 11C-SA4503: a feasibility study. J Nucl Med. 2004;45:1939–45.

28 Mishina M, Ohyama M, Ishii K, Kitamura S, Kimura Y, Oda K-ichi, et al. Low density of

sigma1 receptors in early Alzheimer's disease. Ann Nucl Med. 2008;22:151–6.

29 Toyohara J, Sakata M, Ishiwata K. Imaging of sigma1 receptors in the human brain using PET and [11C]SA4503. Cent Nerv Syst Agents Med Chem. 2009;9:190–6.

30 Mishina M, Ishiwata K, Ishii K, Kitamura S, Kimura Y, Kawamura K, et al. Function of sigma1 receptors in Parkinson's disease. Acta Neurol Scand. 2005;112:103–7.

31 Van Waarde A, Shiba K, de Jong JR, Ishiwata K, Dierckx RA, Elsinga PH. Rapid reduction of sigma1-receptor binding and 18F-FDG uptake in rat gliomas after in vivo treatment with doxorubicin. J Nucl Med. 2007;48:1320–6.

32 Van Waarde A, Jager PL, Ishiwata K, Dierckx RA, Elsinga PH. Comparison of sigma-ligands and metabolic PET tracers for differentiating tumor from inflammation. J Nucl Med. 2006;47:150–4.

33 Kawamura K, Elsinga PH, Kobayashi T, Ishii S-ichi, Wang W-F, Matsuno K, et al. Synthesis and evaluation of 11C- and 18F-labeled 1-[2-(4-alkoxy-3-methoxyphenyl) ethyl]-4-(3-phenylpropyl)piperazines as sigma receptor ligands for positron emission tomography studies. Nucl Med Biol. 2003;30:273–84.

34 Weber K, Razinger T, Hardisty JF, Mann P, Martel KC, Frische EA, et al. Differences in rat models used in routine toxicity studies. Int J Toxicol. 2011;30:162–73.

35 Sakata M, Kimura Y, Naganawa M, Oda K, Ishii K, Chihara K, et al. Mapping of human cerebral sigma1 receptors using positron emission tomography and [11C]SA4503. Neuroimage. 2007;35:1–8.

36 Schweinhardt P, Fransson P, Olson L, Spenger C, Andersson JLR. A template for spatial normalisation of MR images of the rat brain. J Neurosci Methods. 2003;129:105–13.

37 Schaeffer M, Hodson DJ, Lafont C, Mollard P. Functional importance of blood flow dynamics and partial oxygen pressure in the anterior pituitary. Eur J Neurosci. 2010;32:2087–95.

38 Bem WT, Thomas GE, Mamone JY, Homan SM, Levy BK, Johnson FE, et al. Overexpression of sigma receptors in nonneural human tumors. Cancer Res. 1991;51:6558–62.

39 Thomas GE, Szücs M, Mamone JY, Bem WT, Rush MD, Johnson FE, et al. Sigma and opioid receptors in human brain tumors. Life Sci. 1990;46:1279–86.

40 Spruce BA, Campbell LA, McTavish N, Cooper MA, Appleyard MVL, O'Neill M, et al. Small molecule antagonists of the sigma-1 receptor cause selective release of the death program in tumor and self-reliant cells and inhibit tumor growth in vitro and in vivo. Cancer Res. 2004;64:4875–86.

41 Simony-Lafontaine J, Esslimani M, Bribes E, Gourgou S, Lequeux N, Lavail R, et al. Immunocytochemical assessment of sigma-1 receptor and human sterol isomerase in breast cancer and their relationship with a series of prognostic factors. Brit J

Cancer. 2000;82:1958–66.

42 Sambaziotis D, Kapranos N, Kontogeorgos G. Correlation of bcl-2 and bax with apoptosis in human pituitary adenomas. Pituitary. 2003;6:127–33.

Cytotoxicity of sigma ligands is associated with major changes of cellular metabolism and complete occupancy of the sigma-2 subpopulation.

Anna A. Rybczynska,[1] Rudi A. Dierckx,[1,2] Kiichi Ishiwata,[3] Philip H. Elsinga,[1] and Aren van Waarde[1]

[1]Nuclear Medicine and Molecular Imaging, University Medical Center Groningen, University of Groningen, Groningen, The Netherlands

[2]Nuclear Medicine, Ghent University, Ghent, Belgium

[3]Positron Medical Center, Tokyo Metropolitan Institute of Gerontology, Tokyo, Japan

Chapter 5

Journal of Nuclear Medicine. 2008; 49: 2049-2056.

Abstract

Tumor cells can be selectively killed by application of sigma ligands; high concentrations (20–100 μM) are often required, however, because either diffusion barriers must be passed to reach intracellular sites or the entire sigma receptor population should be occupied to induce cell death. We measured receptor occupancies associated with the cytotoxic effect and dose-dependent changes of cellular metabolism in a tumor cell line. Methods: C6 cells (rat glioma) were grown in monolayers and exposed to (+)-pentazocine (sigma-1 agonist), AC915 (sigma-1 antagonist), rimcazole (sigma-1/sigma-2 antagonist), or haloperidol (sigma-1/sigma-2 antagonist). Occupancy of sigma receptors by the test drugs was measured by studying the competition of the test drugs with cellular binding of the ligand ^{11}C-SA4503. Metabolic changes were quantified by measuring cellular uptake of ^{18}F-FDG, ^{18}F-FLT, ^{11}C-choline, or ^{11}C-methionine. Cytotoxicity was assessed by cellular morphology observation and cell counting after 24 h. Results: IC50 values (drug concentrations resulting in 50% occupancy of the available binding sites) of the test drugs for inhibition of cellular ^{11}C-SA4503 binding were 6.5, 7.4, 0.36, and 0.27 μM for (+)-pentazocine, AC915, rimcazole, and haloperidol, respectively. EC50 values (dose required for a 50% reduction of cell number after 24 h) were 710, 819, 31, and 58 μM, for pentazocine, AC915, rimcazole, and haloperidol, respectively. Cytotoxic doses of sigma ligands were generally associated with increased uptake of ^{18}F-FDG, decreased uptake of ^{18}F-FLT and ^{11}C-choline, and little change in ^{11}C-methionine uptake per viable cell. Conclusion: IC50 values of the test drugs reflect their in vitro affinities to sigma-2 rather than to sigma-1 receptors. Because cytotoxicity occurred at concentrations 2 orders of magnitude higher than IC50 values for inhibition of cellular ^{11}C-SA4503 binding, high (99%) occupancy of sigma-2 receptors is associated with loss of cell viability. ^{18}F-FLT, ^{11}C-choline, and ^{18}F-FDG responded most strongly to drug treatment and showed changes corresponding to the cytotoxicity of the test compounds.

Keywords: PET, sigma receptor occupancy, cellular proliferation, glioma cells, ^{18}F-FLT, ^{18}F-FDG, ^{11}C-choline, ^{11}C-methionine

Introduction

Sigma receptors are unique proteins integrated in plasma and endoplasmatic reticulum membranes of tissue derived from immune, endocrine, and reproductive organs; kidney; liver; and brain [1]. Sigma receptors were initially considered as a subtype of the opioid receptor but were later shown to be unlike any other known neurotransmitter or hormone binding site [2]. After 30 years of extensive research, understanding of the

molecular cascade triggered by these transmembrane proteins is still rudimentary [3]. The two confirmed sigma receptor subtypes, 25 kDa sigma-1 and 21.5 kDa sigma-2 [4], are strongly overexpressed in rapidly proliferating cells, for example, in cancer cells from animals and humans, as compared with healthy tissue [5–7]. Although the sequence and partial structure of the sigma-1 receptor are already established [8,9], the existence of the sigma-2 receptor has been proven only pharmacologically [10].

Many natural substances from plant extracts and newly synthesized compounds were tested for sigma receptor binding, resulting in the availability of a broad range of sigma receptor ligands today [11]. Interestingly, some of these compounds were shown to be effective antineoplastic agents [12,13]. Later, *in vitro* [14–16] and *in vivo* [17,18] studies confirmed that sigma ligands, such as haloperidol and rimcazole, inhibit growth of both cultured cancer cells and *in vivo* tumors, whereas they do not affect proliferation or survival of the noncancer tissue [18]. These studies highlighted the potency of sigma ligands to kill cancer cells with minimal side effects. In most cell lines, including in C6 rat glioma, cell death was observed only after administration of high concentrations (20–100 μM) of a sigma-1 receptor antagonist or a sigma-2 receptor agonist [12,13]. The reason for the requirement of high concentrations is unknown. Possibly biomembranes limit drug access to intracellular sites, or a high fraction of the sigma receptor population should be occupied to kill tumor cells.

If a suitable radioligand for sigma receptors is available, dose-dependent occupancy of the receptor population by an exogenous ligand can be assessed by performing a competition assay in intact cells. Measured occupancy values can be subsequently compared with the dose-dependent effects of test drugs on cellular morphology and growth. The sigma-1 agonist SA4503, labeled with the positron emitter ^{11}C, is available for this purpose [19]. We used C6 cells as an *in vitro* model for the measurement of both sigma receptor occupancy and cytotoxic effects. This rat glioma cell line has been used extensively in previous research because it expresses high densities of both sigma-1 and sigma-2 receptors [6]. Rimcazole (sigma-1/sigma-2 receptor antagonist), haloperidol (sigma-1/sigma-2 receptor antagonist), (+)-pentazocine (sigma-1 receptor agonist), and AC915 (sigma-1 receptor antagonist) were chosen as our model compounds because these drugs are commercially available and are potent sigma receptor ligands [20–23]. Several metabolic PET tracers, such as ^{18}F-FDG, 3′-deoxy-3′-fluorothymidine (^{18}F-FLT), ^{11}C-choline, and ^{11}C-methionine, are routinely produced in our laboratory. These radiopharmaceuticals track changes in cellular metabolism and may show altered uptake kinetics after antitumor therapy [24]. Thus, we could assess the dose-dependent effects of sigma ligands on cellular biochemistry.

The present study aimed to answer the following questions: Which concentrations of sigma ligands should be administered to occupy a substantial fraction of the intracellular

receptor population and kill C6 cells? At which level of receptor occupancy does cell death occur? Can PET tracers detect any changes of cellular metabolism after sigma ligand binding? Which PET tracer is the most sensitive indicator of reduced cellular viability?

Materials & Methods

Culture Medium and Drugs

Dulbecco's minimum essential medium (DMEM), fetal calf serum (FCS), and trypsin were products of Invitrogen. AC915, haloperidol, (+)-pentazocine, rimcazole, and trypan blue (0.4% solution in phosphate-buffered saline) were purchased from Sigma. AC915 was dissolved in water with slight heating, and haloperidol and rimcazole were dissolved in ethanol. Stock solutions of (+)-pentazocine were made in 0.1N hydrochloric acid.

RadiopharmaceuticalsL

^{11}C-methionine, ^{11}C-choline, ^{18}F-FLT, and ^{18}F-FDG were prepared by standard procedures reported in the literature [25]. ^{11}C-SA4503 was prepared by reaction of ^{11}C-methyl iodide with the appropriate 4-O-methyl precursor [26]. Specific radioactivity at the end of synthesis was greater than 22 TBq/mmol. All radiochemical purities were greater than 95%.

Cell Culture

C6 rat glioma cells obtained from the American Type Culture Collection were grown as monolayers in DMEM (high glucose) supplemented with 7.5% FCS in a humidified atmosphere of 5% CO_2/95% air at 37°C. Before each experiment, the cells were seeded in 12-well plates (Costar). An equal number of cells was dispensed in each well and was supplied with 1.1 mL of DMEM (high glucose) supplemented with 7.5% FCS.

Binding Studies

Binding studies were performed 48 h after seeding cells in 12-well plates, when confluency reached 80%–90%. Various concentrations of an unlabeled competitor (AC915, haloperidol, (+)-pentazocine, or rimcazole; range, 10^{-8} to 10^{-3} M, in triplicate) were dispensed to the culture medium in the wells. After 2 min, 4 MBq of ^{11}C-SA4503 in less than 30 µL of saline (containing 30% ethanol) were added to each well. After about 45 min of incubation, the medium was quickly removed, and the monolayer was washed 3 times with phosphate-buffered saline. Cells were then treated with 0.2 mL of trypsin. When the monolayer had detached from the bottom of the well, 1 mL of DMEM (high glucose) supplemented with 7.5% FCS was applied to stop the proteolytic

action. Cell aggregates were resolved by repeated (at least 10-fold) pipetting of the trypsin/DMEM mixture. Radioactivity in the cell suspension (1.2 mL) was assessed using a gamma-counter (Compugamma 1282 CS; LKB-Wallac). A sample of the suspension was mixed with trypan blue solution (1:1 v/v) and used for cell counting. Cell numbers were manually determined, using a phase-contrast microscope (Olympus), a Bürker bright-line chamber (depth, 0.1 mm; 0.0025 mm^2 squares), and a hand-tally counter.

Uptake of radioactivity normalized to the number of viable cells was plotted against the logarithm of the dose of the competing drug (in [M]). A 3-parameter curve (single-site competition model) was fitted to these data, using the following equation:

$$Y = \text{bottom} + (\text{top} - \text{bottom}) / (1 + 10^{(X - \log IC50)}),$$

where IC50 is drug concentration resulting in 50% occupancy of the available binding sites. GraphPad Prism (GraphPad Software) was used for curve fitting and graphical presentation of data. Less than 6% (in most wells << 5%) of the administered tracer dose was bound to the cells under these conditions.

Treatment with Sigma Ligands and Scoring of Morphologic Effects

Sigma ligands were administered 24 h after seeding cells in 12-well plates when confluency had reached 40–45%. Final concentrations in culture medium were 1, 3, 10, 30, and 100 (in some cases also 300) times the IC50 value of the test drug for inhibition of ^{11}C-SA4503 binding to cellular sigma receptors (determined as described above).

After 20–24 h of incubation with sigma ligands, the cells were monitored by phase-contrast microscopy. The effect of each compound and concentration was scored relative to a control receiving only solvent vehicle. Scoring was performed as described previously [12]. Experiments were performed in quadruplicate and repeated at least twice. Decreases of cell number after drug treatment were quantified by harvesting and resuspending cells in medium containing FCS, followed by manual counting as described above.

Uptake Studies

Cellular uptake of metabolic PET tracers was determined after 24 h of treatment with either vehicle or a sigma ligand. Experiments were performed in quadruplicate and repeated at least twice. At time zero, a PET tracer (4 MBq of ^{11}C-methionine or ^{11}C-choline or 2 MBq of ^{18}F-FDG or ^{18}F-FLT in <20 µL of saline) was added to each well. After 45 min of incubation, cells were washed, and cellular radioactivity was assessed as described above. Less than 1% (^{11}C-methionine), 2% (^{18}F-FDG), or 4% (^{11}C-choline and ^{18}F-FLT) of the administered tracer dose was taken up by the cells under these conditions.

Statistics

Differences between groups were examined using 1-way ANOVA. A *P* value of less than 0.05 was considered statistically significant.

Results

Receptor Occupancy

Curves describing competition between the test drugs and the radioligand ^{11}C-SA4503 for cellular sigma receptors are presented in Figure 1. The data were best fitted by a 1-site competition model. IC50 values were either in the submicromolar range (rimcazole, 0.36 μM; haloperidol, 0.27 μM) or in the micromolar range ((+)-pentazocine, 6.5 μM; AC915, 7.4 μM).

Subtype Involvement

Table 1 lists literature values for the affinities (Kd) of the test compounds to sigma-1 and sigma-2 receptors, determined by *in vitro* binding assays using membrane

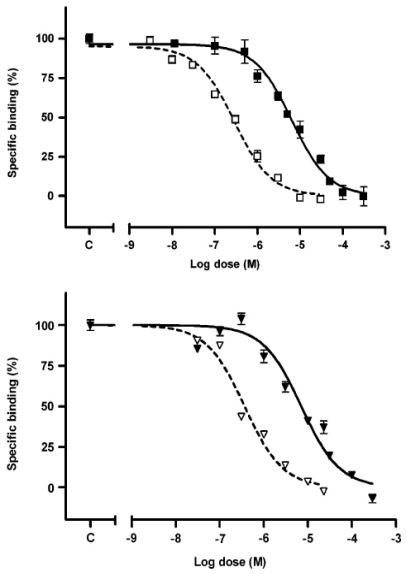

Fig.1. Dose-dependent increase of cellular ^{11}C-SA4503 binding by (+)-pentazocine (■), haloperidol (❒), AC915 (▼), and rimcazole (▽). Error bars indicate SEM. Specific binding was calculated by subtracting nonspecific binding (i.e., residual binding of radioligand in presence of highest dose of competing drug) from total binding; it amounted to 70%–80% of total radioactivity uptake by cells.

Table 1. Binding of Test Compounds to Sigma Receptor Subtypes

Test drug	K_d (nM)		IC_{50} for inhibition of ^{11}C-SA4503 binding in C6 cells (nM)	IC_{50}/K_d	
	σ_1-receptor	σ_2-receptor		σ_1-receptor	σ_2-receptor
AC915	4.9 (rat liver) (*22*)	>10,000 (rat liver) (*22*)	7,358	1,502	0.7
(+)-Pentazocine	7.0 (rat brain) (*21*); 5.5 (rat brain) (*23*)	2,470 (rat liver) (*23*); 1,923 (rat liver) (*38*)	6,495	928–1,181	2.6–3.4
Haloperidol	4.7 (rat brain) (*39*); 2.6 (rat brain) (*23*)	167 (rat liver) (*23*)	274	58–105	1.6
Rimcazole	690 (guinea pig brain) (*20*)	180 (guinea pig brain) (*20*)	356	0.5–0.8	2.0

fragments isolated from rodent tissues. We observed much higher (60- to 1,500-fold) IC50 values in intact cells than known Kd values at sigma-1 receptors, particularly in the case of AC915, (+)-pentazocine, and haloperidol. However, IC50 values of all test compounds corresponded closely to their Kd values at sigma-2 receptors. Here, only minor (<3-fold) differences were observed. Therefore, IC50 values for inhibition of ^{11}C-SA4503 binding to intact cells corresponded to the sigma-2 Kd rather than to the sigma-1 Kd of the test compounds.

Cytotoxicity

When the sigma-antagonists rimcazole, haloperidol, or AC915 were applied to C6 cells in culture, a dose-dependent growth inhibition was observed after 24 h (Fig. 2). Low doses of the test drugs did not affect cellular growth. Above a certain threshold concentration (rimcazole, 20 μM; haloperidol, 25 μM; and AC915, 220 μM), a reduction in cell number became apparent. EC50 values of the test compounds (effective concentrations resulting in 50% cell loss) were somewhat higher than the threshold for cytotoxicity (rimcazole, 31 μM; haloperidol, 58 μM; and AC915, 819 μM). Virtually complete cell death was observed after 24 h of treatment with either 100 μM rimcazole or 150 μM haloperidol (Fig. 2). Even 200 μM sigma-1 agonist (+)-pentazocine did not yet affect cell division or viability. Here, the EC50 value for growth inhibition was 710 μM.

Receptor Occupancy at Cytotoxic Dose

By comparing EC50 values of the test compounds with their IC50 values for inhibition of ^{11}C-SA4503 binding in intact cells, sigma receptor occupancies at cytotoxic doses of the test drugs could be estimated, using the curves presented in Figure 1 or the formula for a single-site competition model (see "Materials and Methods"). Because EC50 values were about 2 orders of magnitude higher than the corresponding IC50 values of the test drugs, cell death appeared to be associated with virtually complete (i.e., 99%) occupancy of the sigma receptor population (Table 2).

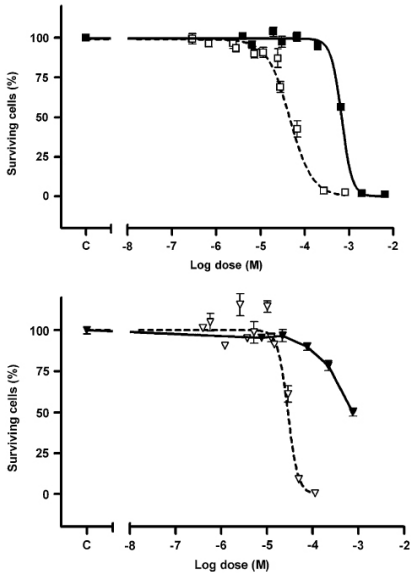

Fig.2. Dose-dependent cell loss after 24 h of incubation with (+)-pentazocine (■), haloperidol (❐), AC915 (▼), and rimcazole (▽). Note that x-axis scales of Figures 1 and 2 are different. Error bars indicate SEM.

Table 2. Receptor Occupancy at Cytotoxic Dose

Test drug	IC_{50} for inhibition of ^{11}C-SA4503 binding in C6 cells (μM)	EC_{50} for cell killing (within 24 h; μM)	EC_{50}/IC_{50}	Receptor occupancy (%)
AC915	7.4	819	110	99.1
(+)-Pentazocine	6.5	710	109	99.1
Haloperidol	0.27	58	215	99.5
Rimcazole	0.36	31	86	98.9

Changes of Cellular Metabolism

The metabolic PET tracers that we used responded differently to treatment of C6 cells with sigma receptor ligands. Cytotoxic doses of (+)-pentazocine, haloperidol, and rimcazole were generally associated with increases of the uptake of ^{18}F-FDG, decreases of the uptake of ^{18}F-FLT and ^{11}C-choline, and little change of ^{11}C-methionine uptake per viable cell (Figs. 3–6).

Significant increases of ^{18}F-FDG uptake were observed only when a certain threshold concentration was exceeded. The threshold dose for haloperidol and rimcazole was 10 μM but in the case of (+)-pentazocine was 30 μM (Fig. 3). Maximal increases of ^{18}F-FDG uptake (+111%, +150%, and +166% for haloperidol, rimcazole, and (+)-pentazocine, respectively; all statistically significant) occurred at doses of 100 μM

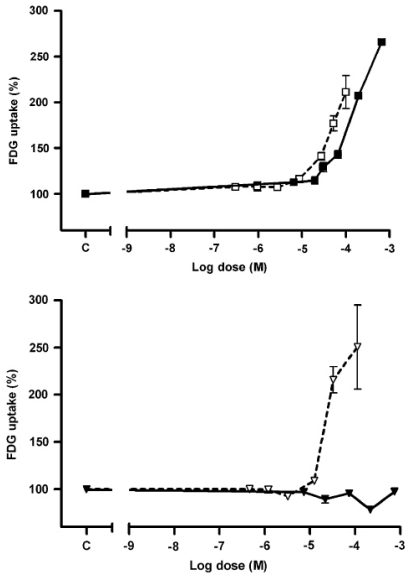

Fig.3. Dose-dependent increase of cellular ^{18}F-FDG uptake by (+)-pentazocine (■), haloperidol (❒), AC915 (▼), and rimcazole (▽).

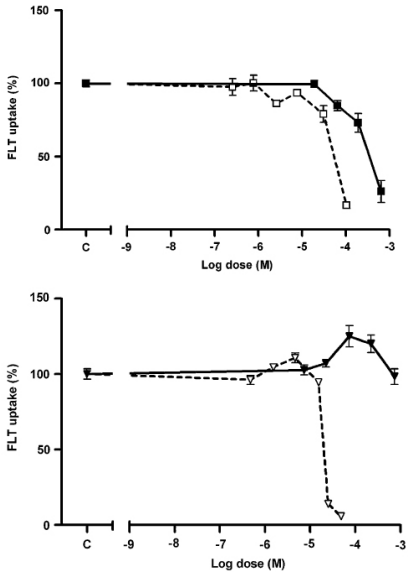

Fig.4. Dose-dependent inhibition of cellular ^{18}F-FLT uptake by (+)-pentazocine (■), haloperidol (❒), AC915 (▼), and rimcazole (▽).

for haloperidol, 112 μM for rimcazole, and 660 μM for (+)-pentazocine. Higher doses of test drug could not be examined, because these resulted in a complete loss of cells after 24 h. In contrast to the previously mentioned sigma ligands, AC915 in doses of up to 776 μM did not increase cellular ^{18}F-FDG uptake. A slight but statistically significant decline (–21%) of ^{18}F-FDG uptake was observed after incubation of cells with 220 μM AC915 (Fig. 3).

Treatment of C6 cells with rimcazole, (+)-pentazocine, and haloperidol resulted in a dose-dependent depression of ^{18}F-FLT uptake when drug concentrations exceeded threshold values of 20, 50, and 80 μM, respectively (Fig. 4). Strong and statistically significant depression of ^{18}F-FLT uptake was observed after a 24-h incubation of the cells with 50 (rimcazole), 100 (haloperidol), or 645 μM ((+)-pentazocine), to 6%, 17%, and 26% of the control, respectively. In contrast to the previously mentioned sigma ligands, AC915 did not depress cellular ^{18}F-FLT uptake but caused a biphasic increase with a maximum occurring at a drug dose of 74 μM (Fig. 4).

Cellular uptake of ^{11}C-choline was depressed by all drug treatments (Fig. 5). A decline occurred when the ligand concentration of (+)-pentazocine and AC915 exceeded 70 μM (20 μM for haloperidol and 15 μM for rimcazole). At concentrations of 650 ((+)-pentazocine), 711 (AC915), or 45 μM (rimcazole), ^{11}C-choline uptake was reduced more than 80%, whereas a concentration of 60 μM for haloperidol resulted in a 55% decline (Fig. 5).

No statistically significant changes of ^{11}C-methionine uptake occurred after 24 h of treatment of C6 cells with (+)-pentazocine, haloperidol, or AC915 (Fig. 6). In contrast, rimcazole at concentrations greater than 10 μM depressed uptake of the amino acid up to 40% (Fig. 6).

Discussion

Competition Assays

^{11}C-SA4503 has been reported to bind preferentially to sigma-1 receptors (IC50, 17.4 nM at the sigma-1 and 1,784 nM at the sigma-2 subtype [27]; IC50, 4.7 nM at sigma-1 and 63.1 nM at sigma-2 receptors in a later study [28]). Therefore, we expected that the potent sigma-1 selective ligands (+)-pentazocine and AC915 would compete more efficiently (i.e., at lower IC50 values) with cellular binding of ^{11}C-SA4503 than would the non–subtype-selective antagonists rimcazole and haloperidol, which bind less potently to sigma-1 receptors. In reality, however, rimcazole and haloperidol inhibited ^{11}C-SA4503 binding more potently (IC50 values, 0.36 and 0.27 μM, respectively) than did (+)-pentazocine and AC915 (IC50 values, 6.5 and 7.4 μM, respectively; Fig. 1). The IC50 values corresponded closely to the sigma-2 Kd but not to the sigma-1 Kd of the test

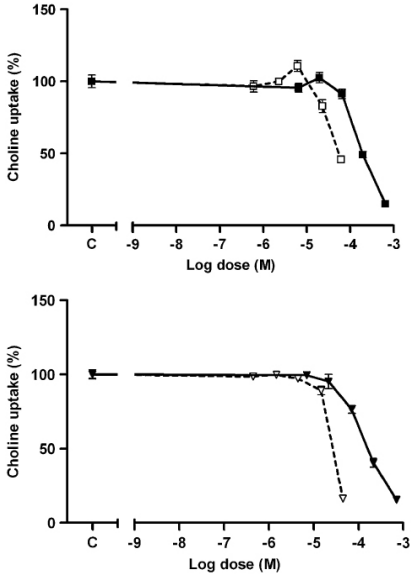

Fig.5. Dose-dependent increase of cellular ^{11}C-choline uptake by (+)-pentazocine (■), haloperidol (❐), AC915 (▼), and rimcazole (▽).

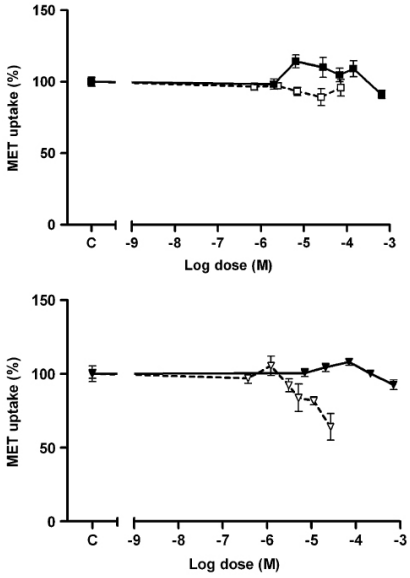

Fig.6. Dose-dependent increase of cellular ^{11}C-methionine uptake by (+)-pentazocine (■), haloperidol (❐), AC915 (▼), and rimcazole (▽). MET = methionine.

compounds (Table 1).

This outcome of our competition assays can be understood when the applied mass of ^{11}C-SA4503 is considered. To have acceptable count statistics even at high doses of a competing drug after 60 min of incubation, it was necessary to add 4 MBq of ^{11}C-SA4503. At a specific radioactivity of 22 TBq/mmol, this corresponds to a ligand mass of 0.2 nmol and a ligand concentration of 200 nM in each well. The receptor Kd reported by Matsuno *et al.* [27] predict that at this radioligand concentration, saturation of sigma-1 receptors will occur and specific binding will be observed mainly at the sigma-2 subtype.

Thus, the methods described in this article investigated the relationship between cytotoxicity and sigma-2 receptor occupancy, using the relatively low affinity of ^{11}C-SA4503 for sigma-2 receptors. During *in vivo* scans with ^{11}C-SA4503 in humans, ligand concentrations in the 10^{-8} or 10^{-7} M range will never be reached. Human SA4503-PET scans will, therefore, reflect the regional distribution of sigma-1 rather than sigma-2 receptors.

Cytotoxic Effects

According to the literature, relatively high doses of sigma-antagonists (20–100 μM for rimcazole or haloperidol [12,13]) are required for the killing of glioma cells. Our data confirm these reports (EC50, 31 μM for rimcazole and 58 μM for haloperidol; Fig. 2). Even higher doses of (+)-pentazocine and AC915 were necessary to induce cell death (EC50 values, 710 and 819 μM, respectively; Fig. 2). Such high doses are not required because diffusion barriers limit drug access to intracellular sites, for half-maximal occupancy of the sigma receptor population is reached already at concentrations 100-fold lower than the EC50 for cell killing (Table 2). Because we observed a decrease in cellular viability only at drug concentrations 2 orders of magnitude higher than the corresponding IC50 values for inhibition of ^{11}C-SA4503 binding, our data indicate that cell death is associated with virtually complete (>98%) occupancy of the sigma receptor population. Because ^{11}C-SA4503 binding occurred mainly at sigma-2 receptors under the conditions of our assay, the data also suggest that cell death is induced via the sigma-2 rather than via the sigma-1 subtype if the observed cytotoxic effects are really mediated through sigma receptors.

The curves describing cell loss after 24 h of treatment with rimcazole and (+)-pentazocine have a steep slope, indicating rapid cell killing when the drug dose exceeds a sharp threshold concentration (Fig. 2). In contrast, cell death induced by haloperidol and AC915 occurs more gradually (Fig. 2). These different curve shapes may signify that haloperidol and AC915 are partial agonists at sigma-2 receptors, whereas rimcazole and (+)-pentazocine are full agonists. It is also possible that rimcazole and (+)-pentazocine induce cell death via an additional mechanism, which occurs in parallel

and independently of occupancy of the sigma-2 receptor population. Sigma-2 receptor–mediated cell death is suggested by the fact that losses of cell viability always occur at concentrations 2 orders of magnitude higher than the IC50 of the 4 test compounds for inhibition of ^{11}C-SA4503 binding to cellular sigma-2 receptors (Table 2). An additional mechanism of cell death is suggested by the different shapes of the cell-loss curves (Fig. 2) and by a cellular morphology that is different after treatment of the cells with different sigma ligands (data not shown).

On the basis of these data, rimcazole appears to be the most interesting compound for further study as an anticancer drug.

Metabolic Changes

In our *in vitro* model, we observed a large increase of ^{18}F-FDG uptake after 24 h of incubation with sigma ligands (Fig. 3). A similar increase of ^{18}F-FDG uptake has been observed after some forms of chemo- and radiotherapy in which the increase of uptake preceded cell death [29,30]. This increase may be a "metabolic flare" due to increased energy consumption as a consequence of DNA and membrane repair [29]. Glucose transporters (glucose transporter 1 and sodium-dependent glucose transporter 1) are known to be overexpressed after various cellular stresses, including hypoxia and heat shock [31]. Rimcazole and (+)-pentazocine interfered strongly with cellular ^{18}F-FDG uptake, whereas haloperidol and AC915 had smaller effects on glucose metabolism (Fig. 3).

^{18}F-FLT traces the salvage pathway of DNA synthesis. The retention of this nucleoside is a measure of thymidine kinase 1 activity within the cells [32,33]. After treatment of C6 cells with sigma ligands, we observed striking decreases of ^{18}F-FLT uptake. (+)-Pentazocine, rimcazole, and haloperidol induced more than a 70% decline of cellular ^{18}F-FLT uptake at a dose 100 times greater than the IC50 for inhibition of cellular ^{11}C-SA4503 binding (Fig. 4). However, AC915 caused a less marked inhibition of ^{18}F-FLT uptake, which is consistent with a smaller reduction of cellular proliferation (Fig. 4). The rank order of drug effects on ^{18}F-FLT uptake was the same as for ^{18}F-FDG. In the range of 3–30 times IC50 for inhibition of cellular ^{11}C-SA4503 binding, AC915 induced a small increase of ^{18}F-FLT uptake, which may reflect activation of repair processes within the cells.

We tested ^{11}C-choline uptake after treatment of C6 cells with sigma ligands because total choline levels and phosphatidylcholine synthesis are known to be elevated in cancers of different origin, as compared with healthy tissue, and are related to cellular proliferation. We observed the expected strong decrease of ^{11}C-choline uptake when cells were treated with sigma ligands (Fig. 5). Above the threshold rimcazole concentration, the uptake of ^{11}C-choline was reduced rapidly, whereas (+)-pentazocine, AC915, and

haloperidol resulted in slower but progressive inhibition of phospholipid metabolism. These results are consistent with the fact that ^{11}C-choline uptake by cancer cells is related to the activity of the enzyme choline kinase [34], which is generally directly proportional to the proliferative status of the cell.

In contrast to ^{18}F-FLT and ^{11}C-choline, ^{11}C-methionine did not behave as a proliferation marker, and ^{11}C-methionine uptake per viable cell showed hardly any change (Fig. 6). Thus, ^{11}C-methionine appeared to trace cell number rather than cellular viability after sigma ligand treatment. The methyl group of methionine, which contains the ^{11}C label, is implicated in many metabolic processes such as protein synthesis, transmethylation, and polyamine synthesis. Therefore, ^{11}C-methionine has a complex metabolism, and uptake of ^{11}C-methionine by tumor cells may be a reflection of several processes, which are affected differently by anticancer treatment, some being increased and others showing a decrease [35]. The lack of change in ^{11}C-methionine uptake may also indicate unaltered transport of this amino acid through the cell membrane and slow transmethylation processes [31].

Our data indicate that ^{18}F-FLT and ^{11}C-choline are the tracers of choice for evaluation of the effects of sigma ligands on cellular proliferation. ^{18}F-FDG may also provide useful information, but ^{11}C-methionine uptake is a reflection of the cell number rather than the proliferation state.

Growth reduction of glioma cells and changes of cellular metabolism were observed only at ligand concentrations more than 30-fold higher than those required for 50% occupancy of the sigma-2 receptor population. Strong decreases of the number of viable cells occurred at drug concentrations greater than or equal to 100-fold higher than the IC50 for inhibition of ^{11}C-SA4503 binding. Thus, cell death was associated with virtually complete (99%) occupancy of the intracellular sigma-2 receptor pool.

Although high levels of receptor occupancy and drug doses in the 10^{-5} M range are required for rapid cell killing, sigma ligands appear to have potential as cancer therapeutics for the following reasons. First, preliminary studies, both from our own laboratory and from other institutions [18], have demonstrated that cell death is limited to tumor cells and occurs only at much higher concentrations in healthy normal cells. Adverse effects could be further diminished by local application or selective drug targeting. Second, significant inhibition of *in vivo* tumor growth has been observed in a variety of tumor models in response to sigma ligands given systemically [17,18]. Third, because sigma-2 ligands trigger cell death both by caspase-dependent and caspase-independent mechanisms, such compounds may be suitable for treatment of a wide variety of tumors, including caspase-deficient tumor types [36]. Last, subtoxic doses of sigma ligands can be applied in combination therapy and can potentiate the antitumor effects of "classic" cytostatic agents [36,37]. Because of the therapeutic potential of sigma

ligands, radiopharmaceuticals for sigma receptors may be used not only as diagnostic imaging agents but also as tools to assess sigma receptor occupancy during experimental tumor therapy.

Conclusion

In the present study, treatment of tumor cells with cytotoxic doses of sigma ligands resulted in strong increases of the uptake of ^{18}F-FDG and decreases of ^{18}F-FLT and ^{11}C-choline uptake per viable cell. Cell-specific uptake of ^{11}C-methionine was largely unaltered under these conditions. ^{18}F-FLT, ^{11}C-choline, and ^{18}F-FDG responded strongly to drug treatment and were suitable tools in the evaluation of the cytotoxicity of the test compounds. These PET tracers may, therefore, be used in future *in vivo* studies.

References

1 Su TP. Sigma receptors: putative links between nervous, endocrine and immune systems. Eur J Biochem. 1991;200:633–642.

2 Quirion R, Chicheportiche R, Contreras PC, et al. Classification and nomenclature of phencyclidine and sigma binding receptor sites. Trends Neurosci. 1987;10:444–446.

3 Hayashi T, Su TP. An update on the development of drugs for neuropsychiatric disorders: focusing on the 1 receptor ligand. Expert Opin Ther Targets. 2008;12:45–58.

4 Hellewell SB, Bruce A, Feinstein G, Orringer J, Williams W, Bowen WD. Rat liver and kidney contain high densities of sigma 1 and sigma 2 receptors: characterization by ligand binding and photoaffinity labeling. Eur J Pharmacol. 1994;268:9–18.

5 Aydar E, Onganer P, Perrett R, Djamgoz MB, Palmer CP. The expression and functional characterization of sigma 1 receptors in breast cancer cell lines. Cancer Lett. 2006;242:245–257.

6 Vilner BJ, John CS, Bowen WD. Sigma-1 and sigma-2 receptors are expressed in a wide variety of human and rodent tumor cell lines. Cancer Res. 1995;55:408–413.

7 Thomas GE, Szucs M, Mamone JY, et al. Sigma and opioid receptors in human brain tumors. Life Sci. 1990;46:1279–1286.

8 Kekuda R, Prasad PD, Fei YJ, Leibach FH, Ganapathy V. Cloning and functional expression of the human type 1 sigma receptor (hSigmaR1). Biochem Biophys Res Commun. 1996;229:553–558.

9 Mei JF, Pasternak GW. Molecular cloning and pharmacological characterization of the rat sigma1 receptor. Biochem Pharmacol. 2001;62:349–355.

10 Guitart X, Codony X, Monroy X. Sigma receptors: biology and therapeutic potential. Psychopharmacology (Berl). 2004;174:301–319.

11 Newman AH, Coop A. Medicinal chemistry: new chemical classes and subtype-selective ligands. In: Matsumoto RR, Bowen WD, Su TP, eds. Sigma Receptors: Chemistry, Cell Biology and Clinical Implications. Berlin, Germany: Springer Verlag; 2007:25–44.

12 Vilner BJ, de Costa BR, Bowen WD. Cytotoxic effects of sigma ligands: sigma receptor-mediated alterations in cellular morphology and viability. J Neurosci. 1995;15:117–134.

13 Brent PJ, Pang GT. Sigma binding site ligands inhibit cell proliferation in mammary and colon carcinoma cell lines and melanoma cells in culture. Eur J Pharmacol. 1995;278:151–160.

14 Brent PJ, Pang G, Little G, Dosen PJ, Van Helden DF. The sigma receptor ligand, reduced haloperidol, induces apoptosis and increases intracellular-free calcium levels [Ca2+]i in colon and mammary adenocarcinoma cells. Biochem Biophys Res Commun. 1996;219:219–226.

15 Colabufo NA, Berardi F, Contino M et al. Antiproliferative and cytotoxic effects of some 2 agonists and 1 antagonists in tumour cell lines. Naunyn Schmiedebergs Arch Pharmacol. 2004;370:106–113.

16 Nordenberg J, Perlmutter I, Lavie G, et al. Anti-proliferative activity of haloperidol in B16 mouse and human SK-MEL-28 melanoma cell lines. Int J Oncol. 2005;27:1097–1103.

17 Moody TW, Leyton J, John C. Sigma ligands inhibit the growth of small cell lung cancer cells. Life Sci. 2000;66:1979–1986.

18 Spruce BA, Campbell LA, McTavish N, et al. Small molecule antagonists of the sigma-1 receptor cause selective release of the death program in tumor and self-reliant cells and inhibit tumor growth in vitro and in vivo. Cancer Res. 2004;64:4875–4886.

19 Kawamura K, Ishiwata K, Tajima H, et al. In vivo evaluation of [11C]SA4503 as a PET ligand for mapping CNS sigma1 receptors. Nucl Med Biol. 2000;27:255–261.

20 Ferris RM, Harfenist M, McKenzie GM, Cooper B, Soroko FE, Maxwell RA. BW 234U, (cis-9-(3,5-dimethyl-1-piperazinyl)propyl]carbazole dihydrochloride): a novel antipsychotic agent. J Pharm Pharmacol. 1982;34:388–390.

21 Cagnotto A, Bastone A, Mennini T. [3H](+)-pentazocine binding to rat brain sigma 1 receptors. Eur J Pharmacol. 1994;266:131–138.

22 Maeda DY, Williams W, Bowen WD, Coop A. A sigma-1 receptor selective analogue of BD1008: a potential substitute for (+)-opioids in sigma receptor binding assays. Bioorg Med Chem Lett. 2000;10:17–18.

23 Ishiwata K, Kawamura K, Yajima K, QingGeLeTu, Mori H, Shiba K. Evaluation of (+)-p-[11C]methylvesamicol for mapping sigma1 receptors: a comparison with [11C]SA4503. Nucl Med Biol. 2006;33:543–548.

24 Van Waarde A, Been LB, Ishiwata K, Dierckx RA, Elsinga PH. Early response of sigma-receptor ligands and metabolic PET tracers to 3 forms of chemotherapy: an in vitro study in glioma cells. J Nucl Med. 2006;47:1538–1545.

25 Van Waarde A, Jager PL, Ishiwata K, Dierckx RA, Elsinga PH. Comparison of sigma-ligands and metabolic PET tracers for differentiating tumor from inflammation. J Nucl Med. 2006;47:150–154.

26 Kawamura K, Elsinga PH, Kobayashi T, et al. Synthesis and evaluation of 11C- and 18F-labeled 1-[2-(4-alkoxy-3-methoxyphenyl)ethyl]-4-(3-phenylpropyl)piperazines as sigma receptor ligands for positron emission tomography studies. Nucl Med Biol. 2003;30:273–284.

27 Matsuno K, Nakazawa M, Okamoto K, Kawashima Y, Mita S. Binding properties of SA4503, a novel and selective sigma 1 receptor agonist. Eur J Pharmacol. 1996;306:271–279.

28 Lever JR, Gustafson JL, Xu R, Allmon RL, Lever SZ. 1 and 2 receptor binding affinity and selectivity of SA4503 and fluoroethyl SA4503. Synapse. 2006;59:350–358.

29 Slosman DO, Pugin J. Lack of correlation between tritiated deoxyglucose, thallium-201 and technetium-99m-MIBI cell incorporation under various cell stresses. J Nucl Med. 1994;35:120–126.

30 Furuta M, Hasegawa M, Hayakawa K, et al. Rapid rise in FDG uptake in an irradiated human tumour xenograft. Eur J Nucl Med. 1997;24:435–438.

31 Clavo AC, Wahl RL. Effects of hypoxia on the uptake of tritiated thymidine, L-leucine, L-methionine and FDG in cultured cancer cells. J Nucl Med. 1996;37:502–506.

32 Rasey JS, Grierson JR, Wiens LW, Kolb PD, Schwartz JL. Validation of FLT uptake as a measure of thymidine kinase-1 activity in A549 carcinoma cells. J Nucl Med. 2002;43:1210–1217.

33 Barthel H, Perumal M, Latigo J, et al. The uptake of 3'-deoxy-3'-[18F]fluorothymidine into L5178Y tumours in vivo is dependent on thymidine kinase 1 protein levels. Eur J Nucl Med Mol Imaging. 2005;32:257–263.

34 Yoshimoto M, Waki A, Obata A, Furukawa T, Yonekura Y, Fujibayashi Y. Radiolabeled choline as a proliferation marker: comparison with radiolabeled acetate. Nucl Med Biol. 2004;31:859–865.

35 Vaalburg W, Coenen HH, Crouzel C, et al. Amino acids for the measurement of protein synthesis in vivo by PET. Int J Rad Appl Instrum B. 1992;19:227–237.

36 Crawford KW, Bowen WD. Sigma-2 receptor agonists activate a novel apoptotic pathway and potentiate antineoplastic drugs in breast tumor cell lines. Cancer Res. 2002;62:313–322.

37 Azzariti A, Colabufo NA, Berardi F, et al. Cyclohexylpiperazine derivative PB28, a sigma2 agonist and sigma1 antagonist receptor, inhibits cell growth, modulates P-glycoprotein, and synergizes with anthracyclines in breast cancer. Mol Cancer Ther. 2006;5:1807–1816.

38 Choi S-R, Yang B, Plössl K, et al. Development of a Tc-99m labeled sigma-2 receptor-specific ligand as a potential breast tumor imaging agent. Nucl Med Biol. 2001;28:657–666.

39 Barnes JM, Barnes NM, Barber PC, et al. Pharmacological comparison of the sigma recognition site labelled by [3H]haloperidol in human and rat cerebellum. Naunyn Schmiedebergs Arch Pharmacol. 1992;345:197–202.

In vivo responses of human A375M melanoma to a sigma ligand: FDG-PET imaging

Anna A. Rybczynska,[1] Marco de Bruyn,[2] Nisha K. Ramakrishnan,[1] Philip H. Elsinga,[1] Wijnand Helfrich,[2] Rudi A.J.O. Dierckx,[1,3] Aren van Waarde[1]

[1]Nuclear Medicine and Molecular Imaging, University Medical Center Groningen, University of Groningen, Groningen, The Netherlands

[2]Surgery, Surgical Research Laboratories, University Medical Center Groningen, University of Groningen, Groningen, The Netherlands

[3]Nuclear Medicine, Ghent University, Ghent, Belgium

Chapter 6

(submitted)

Abstract

Sigma ligands can kill tumor cells. Previously we have shown that a short incubation of tumor cells with sigma ligands (24 h) results in a dose-dependent increase of cellular ^{18}F-FDG uptake, and that the magnitude of this increase is predictive of subsequent cell death. Here, we aimed to assess if the sigma ligand, rimcazole, inhibits growth of A375M melanoma xenografts in mice, and if rimcazole treatment changes ^{18}F-fluorodeoxyglucose (^{18}F-FDG) uptake in vivo. Methods: Athymic mice were inoculated with A375M melanoma cells in matrigel. After two weeks, tumors had appeared and had reached a size of 0.041 ± 0.006 cm^3. We then started a 14-day treatment schedule with daily drug dosing. Control animals were intraperitoneally injected with water, treated animals with rimcazole (26 mg/kg) in water. Three microPET scans with ^{18}F-FDG were made: on day 0, 7 and 14 of treatment. After the last scan, animals were terminated and a biodistribution study was performed. Results: Rimcazole treatment resulted in a > 4-fold reduction of tumor weight in comparison to controls at day 14 (0.100 ± 0.026 vs 0.436 ± 0.117 g, respectively, P < 0.03). Treatment did not affect the levels of (non-radioactive) glucose in blood, animal weight, behavior or appearance. Anti-tumor activity of rimcazole was accompanied by a "metabolic flare" manifested by a temporary increase of ^{18}F-FDG uptake in the tumor (measured at day 7). Significant increase of ^{18}F-FDG uptake at day 14 was observed in liver and pancreas. Conclusion: Rimcazole strongly inhibited the growth of A375M melanoma xenografts. This growth inhibition may be predicted from the early increase of ^{18}F-FDG uptake in the tumor.

Keywords: sigma receptors, rimcazole, melanoma, fluorodeoxyglucose, microPET, metabolic flare

Introduction

Melanoma, a neoplasm arising from pigment-producing melanocytes, is highly metastatic and the most deadly dermatologic malignancy. If spread to distant sites, patients have a median survival rate of 6 months. This is because the disease is frequently diagnosed in the advanced stages and metastasized melanoma is refractory to current therapeutic modalities (such as radiotherapy, chemotherapy, and immunotherapy) [1]. Therefore, new targets which can induce melanoma cell death and/or overcome melanoma resistance may lead to improved treatment of refractory melanomas.

Melanomas can be divided, based on their ability to produce the pigment (melanin), into melanotic melanomas and, more aggressive, amelanotic melanomas [2]. Both melanoma types possess moderate to high levels of sigma receptors, as shown by

a pronounced uptake of several sigma ligands labeled for positron emission tomography (PET) [3], single photon emission computed tomography (SPECT) [4-6] and by immunohistochemical (IHC) staining of sigma-1 receptors in primary human melanomas (www.proteinatlas.com).

Sigma receptors are proteins integrated into cell membrane, endoplasmic reticulum, mitochondrial membrane, nuclear envelope and lysosomes [7,8]. There are two identified sigma receptor subtypes, sigma-1 receptors and sigma-2 receptors [9,10]. Sigma-1 receptors are upregulated with the onset of cancer cell proliferation [11]. Also, sigma-2 receptors are 10-fold more abundant in rapidly proliferating cancer cells than in quiescent cancer cells derived from mouse mammary adenocarcinoma *in vitro* and *in vivo* [12]. A 3- to 5-fold overexpression of sigma-2 receptors has been observed in low grade bovine bladder carcinomas, whereas a marked 25- to 44-fold overexpression is found in high-grade bovine bladder carcinomas [13]. These data are consistent with the participation of sigma receptors in cellular proliferation and indicates that sigma ligands may be useful diagnostic agents and radiotracers for cancer imaging.

Sigma ligands (sigma-1 antagonists and sigma-2 agonists) have strong anti-cancer properties, but they exert only minor effects on non-cancerous tissue [14]. In addition, sigma ligands can repress or overcome therapy resistance in cancer cells and, thus, enhance the anti-cancer effect of chemotherapeutics (reviewed in [15]). This observation has resulted in several *in vitro* and *in vivo* studies with sigma ligands as anti-cancer agents including clinical trials with rimcazole (Modern Biosciences), siramesine (H Lundbeck A/S), SR31747A (Sanofi-Aventis) and ANAVEX 1007 (Anavex Life Sciences).

Sigma ligands can activate multiple cell death pathways dependent on the cancer type and ligand concentration. The mechanism by which a sigma ligand induces cytotoxicity is partially p53- and caspase-independent [16]. However, it involves disturbance of the cell cycle (particularly arrest of cancer cells in G1 phase) [17,18], changes in calcium homeostasis [19,20] and modulation of the ceramide/sphingolipid ratios [21]. The key pathway in these processes could be PI3K/Akt, since both downregulation of sigma-1 receptors and treatment with sigma ligands (e.g. IPAG, rimcazole and haloperidol) affects Akt phosphorylation [14,22-25]. Furthermore, haloperidol was shown to inhibit proliferation of B16 and SK-MEL-28 melanotic melanoma cell lines [17]. Sigma receptors are, therefore, an appealing target for melanoma treatment.

Previously, we have demonstrated a strong anti-cancer activity of the sigma-ligand, rimcazole, in cultured human A375M amelanotic melanoma cells and rat C6 glioma [26,27]. In addition, our *in vitro* results showed that cytotoxic doses of sigma-ligands were generally associated with increased uptake of 2-deoxy-2-(^{18}F)fluoro-D-glucose (^{18}F-FDG) [27].

Although sigma receptors are abundant in melanoma and the sigma ligands,

rimcazole and haloperidol, showed superior activity towards melanoma cells in culture [19,26], the effect of rimcazole on the *in vivo* growth of a melanoma xenograft was never documented. Furthermore, while sigma ligands are currently being tested in clinical trials for cancer treatment, there is lack of a non-invasive technique, like positron emission tomography (PET), for monitoring of *in vivo* responses during sigma receptor targeted anti-cancer therapy.

^{18}F-FDG may be a suitable PET probe for this purpose, for the following reasons:

1. ^{18}F-FDG, the most commonly used tracer in oncology, monitors the cellular metabolic rate of glucose, which is an indirect reflection of tumor growth. ^{18}F-FDG uptake is mainly determined by the activity of glucose transporters (GLUTs) and the first enzyme of the glycolytic pathway, hexokinase (HK). Overexpression and increased activity of GLUTs and HK isozymes is a characteristic feature of rapidly dividing cancer cells.
2. In cancer cells grown *in vitro*, ^{18}F-FDG uptake shows strong changes which reflect sigma ligand-induced cancer cell death. We noticed an increased rather than a decreased uptake 24h after treatment. Such a response is known in the literature as a "metabolic flare" and is frequently observed in tumors after hormonal drug administration.

In the current study we assessed the *in vivo* activity of rimcazole against human A375M melanoma subcutaneously xenografted in athymic nude mice, using ^{18}F-FDG and microPET (FDG-PET). Tumor growth was monitored with calipers and FDG-PET scans were made on d0, d7 and d14 of rimcazole treatment to test whether the treatment-induced changes in tumor growth are accompanied by changes in glucose metabolism.

Material & Methods

Culture Media and Drugs

DMEM (high-glucose) medium was purchased from Sigma. Fetal calf serum (FCS) was obtained from Bodinco (Alkmaar, The Netherlands), trypsin was a product of Invitrogen (Breda, The Netherlands), and matrigel was from Becton Dickinson (Breda, The Netherlands). Water-soluble form of rimcazole (BW234U; 9-[3-(*cis*-3,5-Dimethyl-1-piperazinyl)propyl]-9*H*-carbazole dihydrochloride) was purchased from Tocris Bioscience (Bristol, United Kingdom), diluted accordingly to ~ 4,7 mg/ml stock, aliquoted and frozen at -20°C. Isoflurane was from Pharmachemie BV (Haarlem, The Netherlands). Anti-Ki-67 antibody (ab9260) was from Chemicon/Milipore (Amsterdam, The Netherlands). Antibody for human sigma-1 receptor (OPRS1, polyclonal, ab89655) was from Abcam (Cambridge,

UK). Secondary antibodies goat-anti-rabbit-peroxidase (GaR^{PO}, P0448) and rabbit-anti-goat-peroxidase (RaG^{PO}, P0160) were from Dako (Glostrup, Denmark).

Radiopharmaceuticals

Synthesis and quality control of ^{18}F-FDG were performed according to the standard procedures reported in the literature. ^{18}F-FDG was prepared by an automated synthesis module, using the Hamacher method [28]. The specific radioactivity was always more than 10 (usually between 50 and 100) TBq/mmol. ^{18}F-FDG was sterile and its radiochemical purities were always greater than 95%.

Cell Culture

The malignant human melanoma cell line A375M was purchased from the American Type Culture Collection (ATCC). A375M cells were cultured as monolayers in DMEM (high-glucose) supplemented with 10% FCS at 37°C and incubated in a humidified atmosphere (5% CO_2 in air). Cells were passaged 1:10 twice a week. For *in vivo* experiments, cells in exponential phase of growth were used. The A375 cell line, which is parental to A375M, was previously characterized for high sigma receptor content (sigma-1: Bmax = 34 fmol/mg protein, sigma-2: Bmax = 3403 fmol/mg protein [29]).

Animal Model

A375M tumor xenografts were established in athymic nude-nu mice (Hsd:Athymic Nude-Fox1nu; Harlan, The Netherlands, aged 6 weeks) by s.c. injection of 2×10^6 cells in 100 µl matrigel into the right shoulder of the animal. Animals were randomly assigned to treatment groups. In treated mice (n = 5), rimcazole (26 mg/kg of body weight, in ~ 150 µl water) was administered by daily i.p. injection from day 14 after tumor inoculation (when tumor size reached 0.041 ± 0.006 cm^3) and was continued for the remaining 14 days (Fig. 1A). Control mice (n = 5) received i.p. water injections. Animal welfare, behavior and body weight were checked at daily intervals. At the same time, tumor size measurements were performed using digital calipers and tumor size was calculated using the formula V = 0.5234 x [H] x [L] x [W], where H, L and W are respectively height, length and width. On d14 of treatment, mice were sacrificed, and tumors were excised and weighed. Experiments were performed by licensed investigators in compliance with the Law on Animal Experiments in The Netherlands. The protocol was approved by the Committee on Animal Ethics of the University of Groningen. Mice were maintained in IVC cages (2 mice per cage) under a regime of 12 h of light and 12 h of dark cycle and were fed standard laboratory chow *ad libitum*.

MicroPET Study

All mice were scanned three times with ^{18}F-FDG: scan 1, baseline on d0; scan 2, treatment evaluation on d7; and scan 3, follow-up on d14 of treatment (Fig. 1A). Before each scan, mice were anesthetized with isoflurane (induction 3%, maintenance 1.5%), thereafter, animal weight and blood glucose levels (One-Touch Ultra2 Blood Glucose Meter; LifeScan Inc.; CA, USA) were determined. ^{18}F-FDG (8.74 ± 0.69 MBq, pH 6.6-7.0, volume < 0.1 ml) was injected through the penile vein. The camera (microPET Focus 220; CTI Siemens, Munich, Germany) was started 8 minutes after tracer injection. Two animals were scanned simultaneously in each scan session. Heating mats were used to maintain body temperature of the mice at 37°C. A list-mode protocol was used (44 minutes acquisition time, whole body scan). Reconstructions were performed using microPET Manager 2.3.3.6. List-mode data were processed by a static reconstruction (94 slices with a slice thickness of 0.796 mm, and an in-plane image matrix of 128 x 128 pixels of size 0.47 x 0.47 mm^3). Emission sinograms were iteratively reconstructed (OSEM2D) after being normalized, corrected for attenuation, and corrected for decay of radioactivity. A separate transmission scan (515 sec) with a Co-57 point source was acquired for attenuation correction of 511 keV photons by tissue.

^{18}F-FDG Uptake Analysis

After image reconstruction, Inveon Research Workplace software (Siemens, USA) was used to manually draw 3D regions of interest (ROIs) around the tumor. Necrotic areas of tumors, identified by histopathologic evaluation of hematoxylin and eosin-stained tissue section, were included in the ROI. The data is presented as the mean uptake in Bq/cc normalized to a blood glucose level of 7.8 mmol/L, body weight of 27 g and injected dose of 10 MBq, assuming a tissue density of 1 g/cm^3.

Ex vivo Biodistribution

Following scan 3, animals were terminated via cervical dislocation under anesthesia and a biodistribution study was performed (Fig. 1A). Blood was collected, and plasma and a cell fraction were obtained from the blood sample by short centrifugation (5 min at 1,000 x g). Several tissues (see Table 1) were excised and stored on ice. Radioactivity in tissue samples and in infusate was measured using a gamma counter (CompuGamma CS 1282, LKB-Wallac, Turku, Finland), applying a decay correction. All samples were weighed. The results were expressed as dimensionless standardized uptake values (SUVs) normalized to a blood glucose level of 7.8 mmol/L. The parameter SUV is defined as: [tissue activity concentration (MBq/g) * body weight (g) / injected dose (MBq)]. Tissue-to-plasma and tumor-to-muscle concentration ratios of radioactivity were also calculated.

Histology and Immunohistochemistry

Liver samples were formalin-fixed for 24 h, embedded in paraffin, cut into 4 µm sections and stained with hematoxylin-eosin. Liver histopathology (hepatic tissue injury and inflammation) was evaluated by an independent researcher who was blinded to all data (Dr. Arjan Diepstra, Department of Pathology, University Medical Center Groningen, The Netherlands).

Tumor samples were rapidly frozen and stored at -80°C until further analyses. For staining, tumors were cut into 5.5 µm sections and fixed in acetone. A two-step immunoperoxidase technique was used. Sections were stained with selected primary antibodies (dilution 1:50, 45', RT). Subsequently, endogenous peroxidase was blocked with H_2O_2, followed by staining with the secondary antibody (GaRPO, dilution 1:100, 30', RT) and the tertiary antibody (RaGPO, dilution 1:100, 30', RT). The reaction was developed using brown/red 3-Amino-9-Ethyl-Carbazole/H_2O_2. Sections were counterstained using Mayer's Hematoxylin Solution (Merck, Darmstadt, Germany). A negative control was obtained by omission of the primary antibody.

Statistics

All results are expressed as mean ± SEM. Differences between groups were examined both by two-tailed unpaired t-test and 1-way ANOVA, followed by a post hoc Tukey's Multiple Comparison Test, if applicable. A P value < 0.05 was considered statistically significant.

Results

Sigma-1 receptors in established A375M xenografts

All A375M melanoma xenografts maintained sigma-1 receptor expression after 4 weeks of growth in athymic nude mice (Fig. 1B). Sigma-1 receptor staining was found generally in cytoplasmic compartment, but occasionally also a ring around the nucleus (possibly part of endoplasmic reticulum or nuclear membrane) was stained. Furthermore, we detected a comparable staining in control tumors and rimcazole-treated tumors suggesting that expression of sigma-1 receptors is preserved after two weeks of rimcazole treatment. Sigma-2 receptor expression was not evaluated because no antibodies exist for staining sigma-2 receptors.

Effects of rimcazole treatment on tumor growth

In all studied mice, A375M tumor formed palpable masses 11-12 days after inoculation. Treatment of the control group (n = 5) and rimcazole group (n = 5) started on day 14 after inoculation, when the tumor reached a size of 0.041 ± 0.006 cm^3. Tumor size at the beginning of treatment was not significantly different between control and

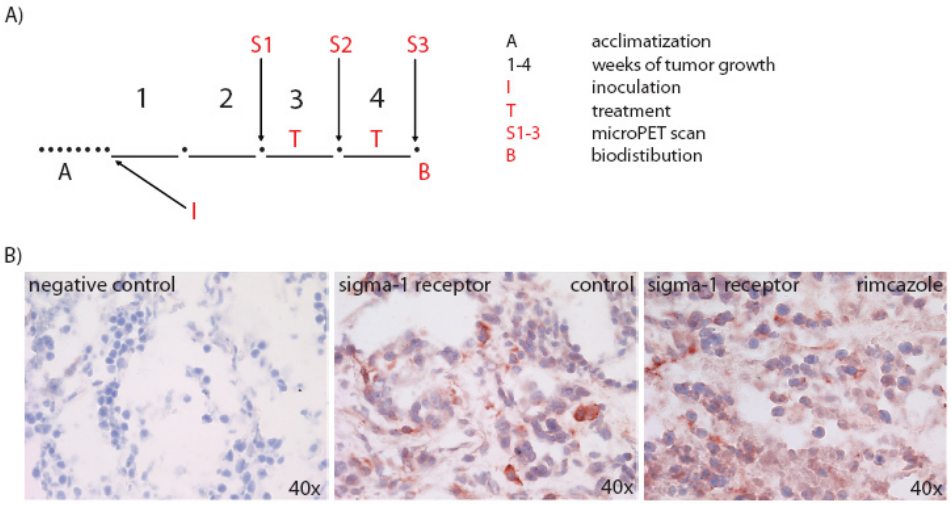

Fig.1. Experimental design: A) study plan; B) sigma-1 receptors are present in human A375M melanoma grown for 4 weeks in athymic nude mice and sigma-1 receptor levels appear to be preserved after 14 days of rimcazole treatment.

rimcazole-treated group. The tumor growth curve obtained from caliper measurements indicated that rimcazole rapidly inhibited tumor growth (Fig. 2A). The significant reduction in tumor growth was observed already at the 4th day of treatment and onwards. On the last day of rimcazole treatment tumor volume from caliper measurements in rimcazole-treated group was 4.8-fold (79%) smaller than in control group ($P < 0.0001$). These volumes corresponded well with tumor weight determined on the last day of treatment, which showed a > 4.4-fold (77%) reduction (from 0.436 ± 0.117 cm^3 to 0.100 ± 0.026 cm^3, $P < 0.03$). Since sigma ligands have both tumoricidal and anti-proliferative activity, we used a proliferation marker, Ki-67, to check whether reduced tumor size by rimcazole is due to a growth inhibitory effect of this drug. Tumor samples derived from all rimcazole-treated mice showed a decrease in nuclear expression of Ki-67 in comparison to control tumor slices (Fig. 2B).

Adverse-effects of rimcazole treatment

Aside from strongly retarded tumor growth, mice treated with 26 mg/kg rimcazole did not show any changes in behavior and appearance. However, one mouse from the rimcazole-treated group contracted diarrhea of unknown origin on day 6/7 of treatment, which persisted until the end of the experiment. None of the rimcazole-treated mice experienced treatment-related death. The body weight of both vehicle- and rimcazole-

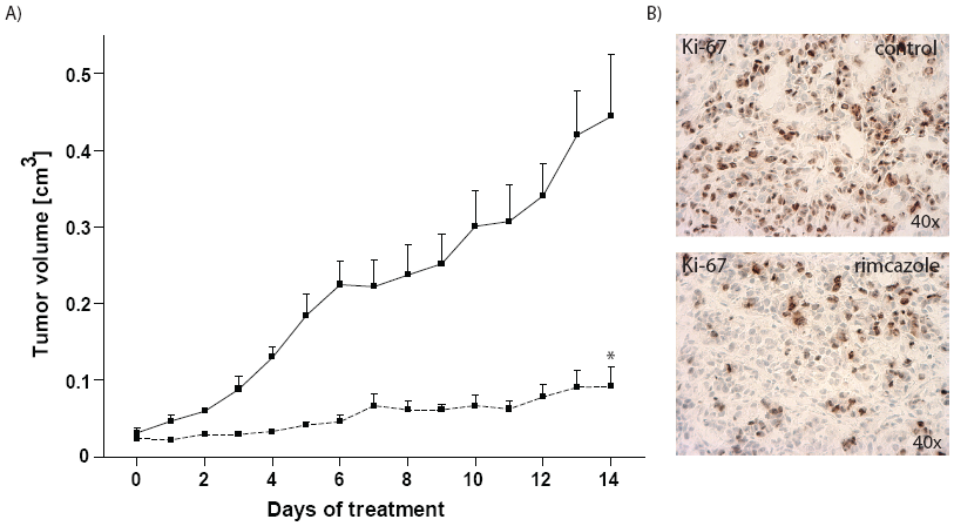

Fig.2. Rimcazole-induced growth inhibition of human A375M melanoma: A) tumor size determined by caliper measurements in the control (n = 5, solid line) and rimcazole-treated (n = 5, dashed line) groups; B) decrease of Ki-67 expression in A375M melanoma determined by IHC staining after 14 days of rimcazole treatment. Asterisk indicates significant difference, $P < 0.0001$

treated group remained constant during the period of treatment (Fig. 3A). Blood glucose levels in the control group (8.26 ± 0.24 mmol/L) and the rimcazole-treated group (7.83 ± 1.46 mmol/L) were not significantly different.

One of the organs with the highest sigma receptor expression is liver. If the amount of sigma receptors determines the cytotoxic effect of sigma ligands, liver could be especially susceptible to treatment-induced side-effects. Examination of the H&E-stained liver sections from the control and rimcazole-treated group revealed no obvious hepatic injury or inflammation, although a slight increase in hepatocyte mitosis was noticed in the rimcazole-treated group (Fig. 3B).

Effects of rimcazole treatment on tumor ^{18}F-FDG uptake

a) MicroPET scans

^{18}F-FDG visualized all A375M tumors. The tracer showed a heterogeneous distribution in tumors, with low uptake in the necrotic regions. Necrotic center in the tumor was visible in PET images in 3 out of 5 control animals and in 1 out of 5 rimcazole-treated mice. Generally necrosis was found in A375M tumors bigger than 250 mm^3. The fraction of necrosis in tumors appeared to be related to tumor volume but was not proportional to changes of ^{18}F-FDG-SUV (data not shown). Tumor volumes from manually

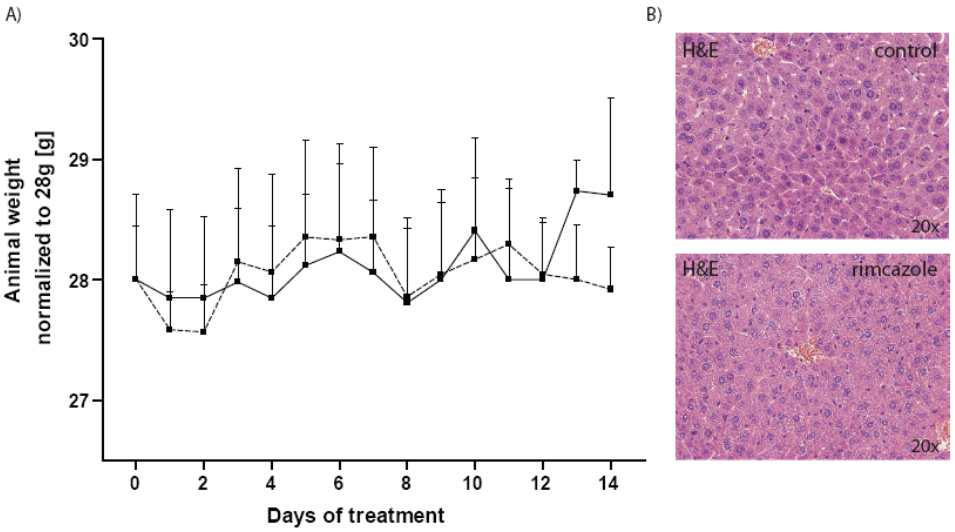

Fig.3. Lack of adverse effects after rimcazole treatment: A) body weights in the control (solid line) and rimcazole-treated (dashed line) groups were not significantly different; B) no hepatic injury or inflammation were detected by H&E staining of formalin-fixed liver sections after 14 days of rimcazole treatment

drawn 3D ROIs corresponded to the volumes estimated from tumor weight or, in case of scan 1 and scan 2, caliper measurements. However, in one control animal tumor size was underestimated by caliper measurements because the tumor had grown into the underlying muscle tissue.

On d7 (scan 2) of treatment, ^{18}F-FDG uptake corrected for blood glucose levels showed an increase in 3 animals and a decrease in 2 animals from the rimcazole–treated group, whereas it was unchanged in 1 animal and decreased in 4 animals from the control group, all with respect to ^{18}F-FDG uptake in scan 1 (before treatment). These increases or decreases were not related to changes in tumor volume. One of the two animals from the rimcazole-treated group showing a decrease of ^{18}F-FDG uptake on day 7 was the mouse with diarrhea. When mean ^{18}F-FDG uptake in control and rimcazole-treated groups on day 7 and day 1 were compared, no statistically significant differences were noted. However, the ratio of mean ^{18}F-FDG uptake in rimcazole-treated to control animals was significantly (2-fold) increased on d7 of treatment (from 0.68 ± 0.08 in scan 1 to 1.36 ± 0.19 in scan 2, $P < 0.02$) (Fig. 4B). The mean tumor uptake of ^{18}F-FDG can be underestimated when the necrotic center, especially of a larger extent, is included in the analysis. On the contrary, the max uptake of ^{18}F-FDG is not sensitive to inclusion or exclusion of the

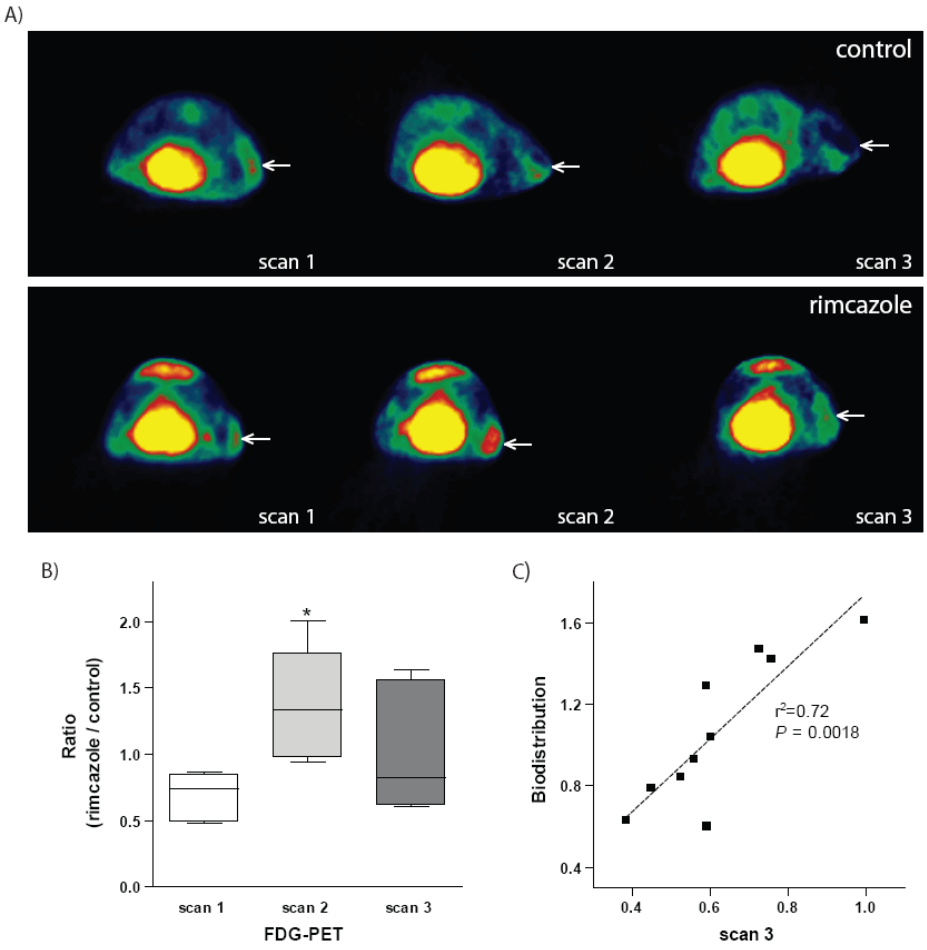

Fig.4. ^{18}F-FDG uptake at different time points after rimcazole treatment: A) transverse ^{18}F-FDG microPET images of a single control (upper row) and rimcazole-treated mouse (lower row). The position of the tumor is indicated by an arrow. B) a rimcazole-induced "metabolic flare" is manifested by a temporary increase of ^{18}F-FDG uptake in the tumor at day 7 of treatment; C) ^{18}F-FDG uptake calculated from manually drawn regions of interest in microPET images corresponds rather closely to ^{18}F-FDG uptake measured in a biodistribution study. Asterisks indicate a significant difference, $P < 0.05$.

necrotic center from the analysis. Comparison of the max ^{18}F-FDG uptake in control and rimcazole-treated groups gave similar results as comparison of the mean ^{18}F-FDG uptake (data not shown). However, the increase in ratio of max ^{18}F-FDG uptake in rimcazole-treated to control animals on d7 of treatment was still significant (1.7-fold, $P = 0.045$).

Table 1. Effect of 14-day lasting rimcazole treatment on biodistribution of ^{18}F-FDG

	SUV $_{GLU}$				Tissue / Plasma $_{GLU}$		
Tissue	Control	Rimcazole		Tissue	Control	Rimcazole	
Brain	**1.19** ± 0.15	**1.57** ± 0.28	ns	Brain	**7.00** ± 0.45	**7.12** ± 1.06	ns
Tumor	**0.97** ± 0.17	**1.36** ± 0.21	ns	Tumor	**5.57** ± 0.40	**6.22** ± 0.88	ns
Lungs	**1.90** ± 0.28	**2.30** ± 0.09	ns	Lungs	**11.38** ± 1.59	**10.84** ± 0.82	ns
Kidney	**2.91** ± 0.13	**3.03** ± 0.69	ns	Kidney	**18.16** ± 2.39	**13.62** ± 2.39	ns
Liver	**0.37** ± 0.03	**0.72** ± 0.10	*P<0.02	Liver	**2.34** ± 0.38	**3.34** ± 0.46	ns
Bone	**0.58** ± 0.07	**0.63** ± 0.10	ns	Bone	**3.46** ± 0.27	**2.82** ± 0.29	ns
Colon	**2.47** ± 0.57	**3.00** ± 0.62	ns	Colon	**13.84** ± 1.39	**13.35** ± 2.32	ns
Duodenum	**2.40** ± 0.31	**2.94** ± 0.56	ns	Duodenum	**14.30** ± 1.55	**13.50** ± 2.52	ns
Fat	**0.58** ± 0.26	**0.83** ± 0.28	ns	Fat	**3.44** ± 1.74	**3.63** ± 0.97	ns
Heart	**26.71** ± 2.80	**28.71** ± 5.49	ns	Heart	**171.25** ± 34.68	**131.23** ± 18.64	ns
Ileum	**2.13** ± 0.19	**2.62** ± 0.47	ns	Ileum	**13.11** ± 1.70	**11.78** ± 1.80	ns
Muscle	**0.31** ± 0.07	**0.25** ± 0.02	ns	Muscle	**1.69** ± 0.23	**1.17** ± 0.10	P=0.06
Pancreas	**0.46** ± 0.06	**0.86** ± 0.10	*P<0.01	Pancreas	**2.71** ± 0.30	**4.06** ± 0.54	P=0.06
Plasma	**0.17** ± 0.02	**0.22** ± 0.03	ns	Plasma	**1.00**	**1.00**	ns
RBC	**0.16** ± 0.02	**0.31** ± 0.06	P=0.07	RBC	**0.99** ± 0.10	**1.42** ± 0.30	ns
Spleen	**1.81** ± 0.32	**2.08** ± 0.28	ns	Spleen	**10.42** ± 0.81	**9.60** ± 0.99	ns
Trachea	**0.97** ± 0.15	**1.38** ± 0.22	ns	Trachea	**6.36** ± 1.71	**6.30** ± 0.87	ns
Urine	**39.81** ± 7.06	**38.92** ± 20.57	ns	Urine	**236.43** ± 37.40	**164.02** ± 70.73	ns

SUV-values and tissue/plasma ratios of 18F with blood glucose correction, ~ 2h after injection of 18F-FDG
Data were obtained from the control (n=5) and rimcazole-treated (n=5) mice, respectively, after the PET scan of Figure 4.

On d14 (scan 3), ^{18}F-FDG uptake corrected for blood glucose levels showed a decrease in 4 animals and a small increase in 1 animal from the rimcazole–treated group, whereas in the control group a decrease was noted in 4 animals and no change was seen in 1 animal (the same as in scan 2), all with respect to ^{18}F-FDG uptake in scan 1. The decrease in ^{18}F-FDG uptake was statistically significant in the control group but not in the rimcazole-treated group. The ratio of mean ^{18}F-FDG uptake in rimcazole-treated to control animals at scan 3 was not changed compared to the ratio at scan 1 (Fig. 4B).

Tumor SUV values obtained from a PET scan and tumor SUV values obtained from the later biodistribution study were closely correlated (P < 0.002, R^2 = 0.72) (Fig. 4C).

b) Biodistribution

The biodistribution study which was performed on day 14 indicated that rimcazole treatment had little impact on ^{18}F-FDG uptake in most tissues (Table 1). A small but significant increase of SUV was observed in liver and pancreas (P < 0.02 and P < 0.01, respectively) after correction for blood glucose level, and a small but not statistically significant decrease in SUV and tissue-to-plasma ratio was observed in muscle. Rimcazole treatment tended to increase the tumor-to-muscle uptake ratio of ^{18}F-FDG (from

3.18 ± 0.79 to 5.50 ± 0.79, $P = 0.07$), as a consequence of the slightly decreased SUV in muscle after treatment.

Discussion

In the present study, we assessed whether treatment-resistant human A375M melanoma cells subcutaneously xenografted in athymic nude mice are sensitive to rimcazole treatment. In addition, we investigated the *in vivo* changes of ^{18}F-FDG uptake in tumor and non-tumor tissue at different time points of rimcazole treatment.

Anti-melanoma effects

We observed that rimcazole (at 26 mg/kg) causes a 4.4- to 4.8-fold reduction of human A375M melanoma tumor growth compared to control by the end of the (14 day) treatment (Fig. 2). This marked reduction of tumor size was, at least in part, due to a growth inhibitory effect of rimcazole as indicated by decreased staining of the proliferation marker Ki-67 in rimcazole-treated A375M tumors in comparison to vehicle-treated control tumors (Fig. 2). A similar rimcazole effect has been observed in three mammary carcinomas (MDA-MB 468, MDA-MB 435, MCF-7), one lung cancer (HT1299) and one prostate cancer (PC3M) xenograft [14]. Similar inhibition of tumor growth as we observed in A375M tumors was seen in MCF-7 carcinomas (3-fold reduction of tumor growth after 14 days of treatment), whereas a stronger tumoricidal effect was noted in a H1299 cancer (> 10-fold reduction). However, the concentration of rimcazole used in these studies was higher (40 mg/kg) than the concentration used by us (26 mg/kg).

We noticed that A375M melanoma maintains its expression of sigma-1 receptors after being xenografted into athymic nude mice (Fig. 1B). No changes of sigma-1 receptor staining were seen between tumors treated with water and tumors treated with rimcazole. Sigma-2 receptor changes were not examined. Earlier communications have shown that repeated haloperidol treatment decreases sigma-1 receptor but not sigma-2 receptor binding without affecting sigma-1 receptor mRNA levels in guinea pig brain [30]. Previous data from our institution have shown that sigma-1 receptor binding and sigma-1 receptor densities are reduced (both by 26-27 %) within 1 or 2 days after *in vivo* treatment of rat gliomas with doxorubicin [31]. The observation that sigma receptor binding is maintained or only slightly decreased in melanomas during *in vivo* treatment with sigma ligands may have important implications for using such drugs in melanoma patients. In other words, the molecular target for sigma receptor ligand treatment is preserved and melanoma cells probably did not develop resistance within these treatment period.

Absence of adverse-effects

During our daily monitoring of animal welfare no apparent adverse effects were noted in mice treated for 14 days with rimcazole (Fig. 3). This is consistent with the low toxicity of sigma ligands towards non-tumor tissue in concentrations toxic for cancer cells [14,29]. The only documented exception is lens epithelial cells, where sigma-1 receptor antagonists cause growth inhibition and pigment formation [22]. Rimcazole is known to be rapidly accumulated in tissues, particularly liver [14,32]. In a previous study it was reported that peak concentrations of the drug in the liver were 20 to 30 times higher and peak concentrations in tumors were 20 to 100 times higher than those in plasma [14]. Yet, we detected no signs of fibrosis or steatosis after histological examination of liver slices and we observed no loss of hepatic tissue but rather a slightly increased population of dividing hepatocytes after 14 days of rimcazole treatment. Thus, a rimcazole dose which strongly inhibited tumor growth did not result in any liver damage.

^{18}F-FDG uptake in melanomas

Based on the documented effect of blood glucose levels on ^{18}F-FDG uptake, we used a glucose normalization procedure to compare ^{18}F-FDG data of individual animals and scans performed on different days.

We observed an increase of ^{18}F-FDG uptake (metabolic flare) in 60% of the rimcazole-treated animals and none of the control animals after 7 days of treatment (see the PET images presented in Fig. 4A). The magnitude of the increase in the rimcazole-treated group was variable, perhaps because scan 2 was always made after 7 days whereas the timing of the flare may be different in different animals. We did not observe any correlation between the magnitude of the rimcazole-induced increase of ^{18}F-FDG uptake and rimcazole-induced inhibition of tumor growth (data not shown). It may be necessary to perform ^{18}F-FDG scans earlier after rimcazole treatment (e.g., after 1 or 2 rather than 7 days) to predict later reduction of tumor growth from the size of the metabolic flare.

Because of a large inter-individual variability in ^{18}F-FDG uptake, the mean SUV of ^{18}F-FDG in the control and rimcazole-treated groups was not significantly different. The effect of drug treatment on tumor metabolism is better visible when ratios of ^{18}F-FDG uptake in treated and untreated animals are compared at different time points (Fig. 4B). After 7 days of treatment, this ratio was significantly increased when compared to the ratio before treatment. After 14 days, the ratio had returned to the pretreatment level (Fig. 4B). In an *in vitro* study from our institution, we observed a marked increase in the ^{18}F-FDG uptake of glioma cells after 24 h of sigma ligand (haloperidol, rimcazole, (+)-pentazocine) treatment [27]. Apparently, rimcazole increases ^{18}F-FDG uptake in the early stage of treatment both *in vivo* and *in vitro*, although the mechanisms underlying

increased glucose consumption should still be examined.

A "metabolic flare" of ^{18}F-FDG frequently occurs in tumors during hormonal therapy or radiotherapy and was proposed to be an indicator of hormone responsiveness in breast cancer [33,34]. This effect has been explained by the assumption that inflammatory processes occur or that the therapeutic drugs are partial agonists. Since the athymic mice which we used do not have functional T-lymphocytes, it is unlikely that the rimcazole-induced flare was due to an inflammatory process. Since rimcazole binds to both subtypes of sigma receptors, it may activate several downstream signaling cascades and act in some as a partial agonist. In cultured A375M cells, we previously observed a marked decrease of cellular ATP after 24 h treatment with rimcazole (unpublished results). Other groups have also reported decreases of ATP levels in neuroblastoma and melanoma cell lines treated with sigma ligands [17,20]. Tumor cells depleted of ATP may try to restore their initial energy levels by increasing the expression of GLUTs and/or glucose metabolism enzymes, like HK, which will result in increased uptake of ^{18}F-FDG.

^{18}F-FDG uptake in peripheral organs

Our biodistribution data indicate increased SUV but not tissue/plasma ratios of ^{18}F-FDG in liver and pancreas after treatment with rimcazole (Table 1). Uptake of ^{18}F-FDG in muscle and red blood cells (RBC) tended to decrease but this trend was not statistically significant.

Hepatocytes have high and pancreatic exocrine glandular and skeletal muscle cells have moderate sigma-1 receptor expression (www.proteinatlas.com). High affinity binding sites for the selective sigma-1 receptor ligand, (+)-pentazocine, are present in outer mitochondrial membranes of rat liver [35]. These binding sites have been called "sigma-1 like receptors", because they are pharmacologically distinct from sigma-1 receptors in the brain and show a higher affinity to typical sigma-1 ligands.

The first possible explanation for increased glucose uptake in the liver is a slightly increased mitotic division and, therefore, increased energy requirements of hepatocytes (see above). Another possible mechanism is a stimulating effect of rimcazole on glycogenesis. Increased levels of blood glucose activate glycogen production in the liver. We did not observe any changes in blood glucose levels during rimcazole treatment, but blood glucose was measured just before each microPET scan and at least 16 h after the last rimcazole administration. If rimcazole causes a transient increase of blood glucose, our measurements would fail to detect this response. Such increases of plasma glucose have been reported in humans after treatment with the sigma ligand, haloperidol [36]. Two other sigma ligands, (+)-3-PPP ((+)-3-(3-Hydroxyphenyl)-N-(1-propyl)-piperidine) and DTG (1,3-di-o-tolylguanidine), have been shown to affect insulin secretory responses in rat islets of Langerhans in an imidazoline-independent but glucose-dependent manner.

Insulin increases the uptake of glucose from the blood by liver and muscle (for production of glycogen) and by adipose tissue (for the production of fat). A third explanation for increased glucose uptake may thus be activation of hepatic glycogenesis by insulin. Increased glucose uptake in the pancreas could be related to increased energy demand of this organ for insulin production.

Conclusion

Rimcazole strongly inhibited the growth of A375M melanoma *in vivo*. A transient increase of ^{18}F-FDG uptake was seen on day 7 in most rimcazole-treated tumors but not in control tumors. This early increase may be related to tumor response and later growth inhibition. Pilot studies in melanoma patients may be facilitated by the fact that some sigma ligands (e.g., haloperidol) have already been registered for human use. In these studies, FDG-PET imaging may be applied for predicting early responses to sigma ligand treatment and the possibility of a metabolic flare should be considered.

Acknowledgements

We wish to thank Dr Arjan Diepstra and Ms. Janneke Wiersema-Buist for their support in analyzing the histological specimens, and Mr. Jurgen Sijbesma for his excellent technical assistance with animal imaging.

References

1 Miller AJ, Mihm MC. Melanoma. N Engl J Med. 2006;355:51–65.

2 Notani K, Shindoh M, Yamazaki Y, Nakamura H, Watanabe M, Kogoh T, et al. Amelanotic malignant melanomas of the oral mucosa. Br J Oral Maxillofac Surg. 2002;40:195–200.

3 Waterhouse RN, Collier TL. In vivo evaluation of [18F]1-(3-fluoropropyl)-4-(4-cyanophenoxymethyl)piperidine: a selective sigma-1 receptor radioligand for PET. Nucl Med Biol. 1997;24:127–34.

4 Michelot JM, Moreau MF, Labarre PG, Madelmont JC, Veyre AJ, Papon JM, et al. Synthesis and evaluation of new iodine-125 radiopharmaceuticals as potential tracers for malignant melanoma. J Nucl Med. 1991;32:1573–80.

5 John CS, Bowen WD, Saga T, Kinuya S, Vilner BJ, Baumgold J, et al. A malignant melanoma imaging agent: synthesis, characterization, in vitro binding and biodistribution of iodine-125-(2-piperidinylaminoethyl)4-iodobenzamide. J Nucl Med. 1993;34:2169–75.

6 Hirata M, Mori T, Umeda T, Abe T, Yamamoto T, Ohmomo Y. Evaluation of Radioiodinated 1-[2-(3,4-Dimethoxyphenyl)ethyl]-4-(2-iodophenylpropyl)piperazine as a Tumor Diagnostic Agent with Functional Sigma Receptor Imaging by Single Photon Emission Computed Tomography. Biol Pharm Bull. 2008;31:879–83.

7 Hayashi T, Su T-P. Sigma-1 receptor chaperones at the ER-mitochondrion interface regulate Ca(2+) signaling and cell survival. Cell. 2007;131:596–610.

8 Zeng C, Vangveravong S, Xu J, Chang KC, Hotchkiss RS, Wheeler KT, et al. Subcellular localization of sigma-2 receptors in breast cancer cells using two-photon and confocal microscopy. Cancer Res. 2007;67:6708–16.

9 Hellewell SB, Bowen WD. A sigma-like binding site in rat pheochromocytoma (PC12) cells: decreased affinity for (+)-benzomorphans and lower molecular weight suggest a different sigma receptor form from that of guinea pig brain. Brain Res. 1990;527:244–53.

10 Quirion R, Bowen WD, Itzhak Y, Junien JL, Musacchio JM, Rothman RB, et al. A proposal for the classification of sigma binding sites. Trends Pharmacol Sci. 1992 Mar;13(3):85–6.

11 Zamora PO, Moody TW, John CS. Increased binding to sigma sites of N-[1'(2-piperidinyl)ethyl)-4-[I-125]-iodobenzamide (I-125-PAB) with onset of tumor cell proliferation. Life Sci. 1998;63:1611–8.

12 Mach RH, Smith CR, Al-Nabulsi I, Whirrett BR, Childers SR, Wheeler KT. Sigma 2 receptors as potential biomarkers of proliferation in breast cancer. Cancer research. 1997;57:156–61.

13 Roperto S, Colabufo NA, Inglese C, Urraro C, Brun R, Mezza E, et al. Sigma-2 receptor expression in bovine papillomavirus-associated urinary bladder tumours. J Comp Pathol. 2010;142:19–26.

14 Spruce BA, Campbell LA, McTavish N, Cooper MA, Appleyard MVL, O'Neill M, et al. Small molecule antagonists of the sigma-1 receptor cause selective release of the death program in tumor and self-reliant cells and inhibit tumor growth in vitro and in vivo. Cancer Res. 2004;64:4875–86.

15 van Waarde A, Rybczynska AA, Ramakrishnan N, Ishiwata K, Elsinga PH, Dierckx RAJO. Sigma receptors in oncology: therapeutic and diagnostic applications of sigma ligands. Curr Pharm Des. 2010;16:3519–37.

16 Crawford KW, Bowen WD. Sigma-2 receptor agonists activate a novel apoptotic pathway and potentiate antineoplastic drugs in breast tumor cell lines. Cancer research. 2002;62:313–22.

17 Nordenberg J, Perlmutter I, Lavie G, Beery E, Uziel O, Morgenstern C, et al. Anti-proliferative activity of haloperidol in B16 mouse and human SK-MEL-28 melanoma cell lines. Int J Oncol. 2005;27:1097–103.

18 Azzariti A, Colabufo NA, Berardi F, Porcelli L, Niso M, Simone GM, et al. Cyclohexylpiperazine derivative PB28, a sigma2 agonist and sigma1 antagonist receptor, inhibits cell growth, modulates P-glycoprotein, and synergizes with anthracyclines in breast cancer. Mol Cancer Ther. 2006;5:1807–16.

19 Brent PJ, Pang G, Little G, Dosen PJ, Van Helden DF. The sigma receptor ligand, reduced haloperidol, induces apoptosis and increases intracellular-free calcium levels [Ca2+]i in colon and mammary adenocarcinoma cells. Biochem Biophys Res Commun. 1996;219:219–26.

20 Cassano G, Gasparre G, Niso M, Contino M, Scalera V, Colabufo NA. F281, synthetic agonist of the sigma-2 receptor, induces Ca2+ efflux from the endoplasmic reticulum and mitochondria in SK-N-SH cells. Cell calcium. 2009;45:340–5.

21 Crawford KW, Coop A, Bowen WD. Sigma(2) Receptors regulate changes in sphingolipid levels in breast tumor cells. Eur J Pharmacol. 2002;443(:207–9.

22 Wang L, Prescott AR, Spruce BA, Sanderson J, Duncan G. Sigma receptor antagonists inhibit human lens cell growth and induce pigmentation. Invest Ophthalmol Vis Sci. 2005 Apr;46(4):1403–8.

23 Dai Y, Wei Z, Sephton CF, Zhang D, Anderson DH, Mousseau DD. Haloperidol induces the nuclear translocation of phosphatidylinositol 3'-kinase to disrupt Akt phosphorylation in PC12 cells. J Psychiatry Neurosci. 2007;32:323–30.

24 Wei Z, Mousseau DD, Dai Y, Cao X, Li X-M. Haloperidol induces apoptosis via the sigma2 receptor system and Bcl-XS. Pharmacogenomics J. 2006;6:279–88.

25 Wei Z, Qi J, Dai Y, Bowen WD, Mousseau DD. Haloperidol disrupts Akt signalling to reveal a phosphorylation-dependent regulation of pro-apoptotic Bcl-XS function.

Cellular signalling. 2009 Jan;21(1):161–8.

26 de Bruyn M, Rybczynska AA, Wei Y, Schwenkert M, Fey GH, Dierckx RAJO, et al. Melanoma-associated Chondroitin Sulfate Proteoglycan (MCSP)-targeted delivery of soluble TRAIL potently inhibits melanoma outgrowth in vitro and in vivo. Mol Cancer. 2010;9:301.

27 Rybczynska AA, Dierckx RA, Ishiwata K, Elsinga PH, van Waarde A. Cytotoxicity of sigma-receptor ligands is associated with major changes of cellular metabolism and complete occupancy of the sigma-2 subpopulation. 2008;49:2049–56.

28 Hamacher K, Coenen HH, Stöcklin G. Efficient stereospecific synthesis of no-carrier-added 2-[18F]-fluoro-2-deoxy-D-glucose using aminopolyether supported nucleophilic substitution. J Nucl Med. 1986;27:235–8.

29 Vilner BJ, John CS, Bowen WD. Sigma-1 and sigma-2 receptors are expressed in a wide variety of human and rodent tumor cell lines. Cancer research. 1995;55:408–13.

30 Inoue A, Sugita S, Shoji H, Ichimoto H, Hide I, Nakata Y. Repeated haloperidol treatment decreases sigma(1) receptor binding but does not affect its mRNA levels in the guinea pig or rat brain. Eur J Pharmacol. 2000;401:307–16.

31 van Waarde A, Shiba K, de Jong JR, Ishiwata K, Dierckx RA, Elsinga PH. Rapid reduction of sigma1-receptor binding and 18F-FDG uptake in rat gliomas after in vivo treatment with doxorubicin. J Nucl Med. 2007;48:1320–6.

32 Gilmore DL, Liu Y, Matsumoto RR. Review of the pharmacological and clinical profile of rimcazole. CNS drug reviews. 2004;10:1–22.

33 Mortimer JE, Dehdashti F, Siegel BA, Trinkaus K, Katzenellenbogen JA, Welch MJ. Metabolic flare: indicator of hormone responsiveness in advanced breast cancer. J Clin Oncol. 2001;19:2797–803.

34 Dehdashti F, Mortimer JE, Trinkaus K, Naughton MJ, Ellis M, Katzenellenbogen JA, et al. PET-based estradiol challenge as a predictive biomarker of response to endocrine therapy in women with estrogen-receptor-positive breast cancer. Breast Cancer Res Treat. 2009;113:509–17.

35 Klouz A, Sapena R, Liu J, Maurice T, Tillement J-P, Papadopoulos V, et al. Evidence for sigma-1-like receptors in isolated rat liver mitochondrial membranes. Br J Pharmacol. 2002;135:1607–15.

36 Chan SL, Morgan NG. Sigma receptor ligands and imidazoline secretagogues mediate their insulin secretory effects by activating distinct receptor systems in isolated islets. Eur J Pharmacol. 1998;350:267–72.

Melanoma-associated Chondroitin Sulfate Proteoglycan (MCSP)-targeted delivery of soluble TRAIL potently inhibits melanoma outgrowth *in vitro* and *in vivo*

Anna A Rybczynska,#[1] Marco de Bruyn,#[2] Yunwei Wei,[2,3] Michael Schwenkert,[4] Georg H Fey,[4] Rudi AJO Dierckx,[1,5] Aren van Waarde,[1] Wijnand Helfrich,[2] and Edwin Bremer,[2]

#Contributed equally.

[1]Nuclear Medicine and Molecular Imaging, University Medical Center Groningen, University of Groningen, Groningen, The Netherlands

[2]Surgery, Surgical Research Laboratories, University Medical Center Groningen, University of Groningen, Groningen, The Netherlands

[3]Third Department of General Surgery, First Clinical Hospital of Harbin, Medical University Harbin, Harbin, China

[4]Genetics, University of Erlangen, Nuremberg, Erlangen, Germany

[5]Nuclear Medicine, Ghent University, Ghent, Belgium

Chapter 7

Molecular Cancer 2010; 9: 301.

Abstract

Advanced melanoma is characterized by a pronounced resistance to therapy leading to a limited patient survival of ~6 - 9 months. Here, we report on a novel bifunctional therapeutic fusion protein, designated anti-MCSP:TRAIL, that is comprised of a melanoma-associated chondroitin sulfate proteoglycan (MCSP)-specific antibody fragment (scFv) fused to soluble human TRAIL. MCSP is a well-established target for melanoma immunotherapy and has recently been shown to provide important tumorigenic signals to melanoma cells. TRAIL is a highly promising tumoricidal cytokine with no or minimal toxicity towards normal cells. Anti-MCSP:TRAIL was designed to 1. selectively accrete at the cell surface of MCSP-positive melanoma cells and inhibit MCSP tumorigenic signaling and 2. activate apoptotic TRAIL-signaling. Results: Treatment of a panel of MCSP-positive melanoma cell lines with anti-MCSP:TRAIL induced TRAIL-mediated apoptotic cell death within 16 h. Of note, treatment with anti-MCSP:TRAIL was also characterized by a rapid dephosphorylation of key proteins, such as FAK, implicated in MCSP-mediated malignant behavior. Importantly, anti-MCSP:TRAIL treatment already inhibited anchorage-independent growth by 50% at low picomolar concentrations, whereas > 100 fold higher concentrations of non-targeted TRAIL failed to reduce colony formation. Daily i.v. treatment with a low dose of anti-MCSP:TRAIL (0.14 mg/kg) resulted in a significant growth retardation of established A375M xenografts. Anti-MCSP:TRAIL activity was further synergized by co-treatment with rimcazole, a sigma ligand currently in clinical trials for the treatment of various cancers. Conclusions: Anti-MCSP:TRAIL has promising pre-clinical anti-melanoma activity that appears to result from combined inhibition of tumorigenic MCSP-signaling and concordant activation of TRAIL-apoptotic signaling. Anti-MCSP:TRAIL alone, or in combination with rimcazole, may be of potential value for the treatment of malignant melanoma.

Keywords: melanoma, fusion protein, melanoma-associated chondroitin sulfate proteoglycan, tumor necrosis factor-related apoptosis inducing ligand, synergy, rimcazole

Introduction

Patients diagnosed with localized melanoma have a 10-year survival rate of up to 95%. In contrast, the life expectancy of patients with metastasized melanoma is limited to only 6 - 9 months [1]. The poor survival of patients with advanced melanoma is largely attributable to resistance towards current treatment modalities such as chemo- and radiotherapy [2]. Therefore, the development of novel therapeutic approaches that can trigger melanoma-selective cell death appears warranted.

One target molecule of potential relevance for the tumorigenicity of melanoma is the melanoma chondroitin sulfate proteoglycan (MCSP), also known as high molecular weight melanoma associated antigen (HMW-MAA). MCSP is highly expressed on the cell surface of both benign dysplastic nevi and on over 85% of malignant melanomas [3].

Importantly, over-expression of MCSP correlates with an unfavorable prognosis [4]. Expression of MCSP on normal tissue is mainly restricted to cells of the melanocyte lineage, but has also been detected in basal cells of the epidermis and within the hair follicle, in pericytes, chondrocytes and smooth muscle cells [3]. Recent studies have revealed that MCSP expression may provide important tumorigenic signals to melanoma cells. MCSP signaling stimulates growth, motility, and tissue invasion by melanoma cells, e.g. by enhancing integrin function [5], activation of Focal Adhesion Kinase (FAK) [6], mitogenic ERK signaling [7] and matrix metalloproteinase 2 [8]. Furthermore, non-metastatic radial growth tumor cells acquired anchorage-independent growth characteristics upon ectopic expression of MCSP [6]. Of note, anti-MCSP antibody treatment can partly inhibit MCSP-tumorigenic signaling *in vitro*, as evidenced by a pronounced inhibition of FAK [6].

Thus, MCSP appears to be important for melanoma tumorigenicity and appears to be a promising target for both naked monoclonal antibody (mAb) as well as immunotoxin-based strategies [9,10]. Notably, anti-MCSP mAbs proved to have beneficial effects on the clinical course of the disease of melanoma patients [3,11].

In recent years, we have demonstrated that scFv antibody fragment-targeted delivery of the immuno cytokine TRAIL holds particular promise for tumor-selective induction of apoptosis in various cancer types. TRAIL (Tumor Necrosis Factor Related Apoptosis Inducing Ligand) is a highly promising anti-cancer agent with pronounced pro-apoptotic activity towards various malignant cell types, including melanoma. Importantly, TRAIL essentially lacks activity towards normal cells [12]. Based on these characteristics, recombinant soluble TRAIL (sTRAIL) preparations have recently entered clinical trials, with promising preliminary reports on anti-tumor activity and safety [13].

Antibody fragment-mediated targeting of TRAIL can further selectively enhance the anti-tumor activity of TRAIL towards various types of cancer, including carcinomas and Acute Myeloid Leukemia [12,14-20]. Briefly, genetic fusion of TRAIL to a scFv antibody fragment allows for the selective delivery of TRAIL to a pre-selected tumor-associated antigen at the tumor cell surface. The resulting high levels of tumor cell surface bound TRAIL then efficiently activate apoptotic signaling via the agonistic TRAIL-receptors TRAIL-R1 and TRAIL-R2 in a mono- and/or bi/multicellular manner [14-18,20]. Of note, non-targeted sTRAIL has no intrinsic tumor-selective binding activity and is less efficient in cross-linking and activating TRAIL-R2 [21].

Here we preclinically evaluated the anti-melanoma activity of MCSP-targeted delivery of TRAIL, using fusion protein anti-MCSP:TRAIL. Anti-MCSP:TRAIL was designed to selectively bind to MCSP at the cell surface of melanoma cells and simultaneously inhibit tumorigenic signaling by MCSP. Once bound to MCSP-expressing melanoma cells, the anti-MCSP:TRAIL fusion protein can activate apoptotic TRAIL-signaling. Since TRAIL resistance has been reported for melanoma [22] we further evaluated a combinatorial

strategy in which anti-MCSP:TRAIL treatment was combined with rimcazole. Rimcazole is a sigma receptor ligand currently in clinical trials for various cancers that has shown potent single-agent anti-tumor activity towards glioma and breast cancer [23,24]. Sigma ligand-based therapy may also be of value for the treatment of melanoma since the two subtypes of sigma receptors, sigma-1 receptors and sigma-2 receptors, are strongly overexpressed in this tumor [25,26].

MCSP targeting with anti-MCSP:TRAIL indeed appeared to inhibit MCSP-signaling and activated TRAIL-apoptotic signaling in melanoma cells *in vitro* and *in vivo*. Furthermore, TRAIL-apoptotic signalling in melanoma cells can be further increased by combinatorial treatment with rimcazole. The dual anti-melanoma activity of anti-MCSP:TRAIL alone, or in combination with rimcazole, may be of interest for treatment of melanoma.

Materials & Methods

Reagents

MAb 9.2.27 is a murine IgG2a with high binding affinity for human MCSP [10]. TRAIL-neutralizing mAb 2E5 was purchased from Alexis (10P's, Breda, The Netherlands). Caspase inhibitors zVAD-fmk and zLEHD-fmk were from Calbiochem (VWR International B.V., Amsterdam, The Netherlands) and dissolved at 10 mM in DMSO. Rimcazole (BW 239U) and (+)-pentazocine were from Sigma Aldrich (Sigma-Aldrich Chemie B.V. Zwijndrecht, Netherlands). Stock solutions of rimcazole (3.9 mM in ethanol) and (+)-pentazocine (10 mM in 0.1 N hydrochloric acid) were freshly prepared for each experiment.

Cell lines

MCSP-positive/EpCAM-negative melanoma cell lines A375M, A2058 and SK-MEL-28 were obtained from and characterized (STR profiling, karyotyping, isoenzyme analysis) by the American Tissue Culture Collection (ATCC). The MCSP-negative melanoma cell line M14 and transfectant cell line M14.MCSP were provided by Prof. Dr. G.H. Fey. Expression of MCSP was determined by flow cytometry using anti-MCSP mAb 9.2.27 and a FITC-conjugated goat-anti-mouse mAb. A375M.FADD-DED cells were generated by transfection of parental A375M cells using Fugene (Roche BV, Woerden, The Netherlands). All cell lines were cultured at 37°C, in a humidified 5% CO_2 atmosphere. A375M, A2058, SK-MEL-28 and M14 cells were cultured in RPMI 1640 medium (Cambrex Bio Science, Verviers, France) supplemented with 10% fetal calf serum. M14.MCSP cells were cultured in RPMI 1640 medium supplemented with 10% fetal calf serum and 400 μg/ml Geneticin. A375M.FADD-DED cells were cultured in RPMI 1640 medium supplemented with 10% fetal calf serum and 500 μg/ml Geneticin.

Primary human hepatocytes (PHH) and melanocytes

Cryopreserved human hepatocytes and melanocytes (Tebu-bio bv, Heerhugowaard, The Netherlands) were isolated according to standard protocol using hepatocyte isolation kit and melanocyte isolation kit, respectively (tebu-bio bv, Heerhugowaard, The Netherlands). For experiments, hepatocytes and melanocytes were seeded in a 48-well plate at a density of 0.5×10^6 cells/ml.

Construction of fusion protein anti-MCSP:TRAIL

A scFv antibody fragment in the VH-VL format was derived from mAb 9.2.27 using standard antibody-phage display technology [10]. Fusion protein anti-MCSP:TRAIL was constructed by cloning the cDNA of antibody fragment MCSP in frame with soluble TRAIL into in-house constructed vector pEE14 using unique SfiI and NotI restriction enzyme sites, yielding plasmid pEE14-anti-MCSP:TRAIL. Fusion protein anti-MCSP:TRAIL was produced in CHO-K1 cells using previously described methods [14,16]. Culture medium containing anti-MCSP:TRAIL was cleared by centrifugation (10 000 x g, 10 min), filter sterilized, and stored at -80°C until further use. Fusion protein anti-MCSP:TRAIL was purified via the N-terminal Hemagglutinin (HA)-tag using anti-HA affinity chromatography. Fusion protein scFvC54:sTRAIL [14], for reasons of clarity hereafter renamed into anti-EpCAM:TRAIL, is a fusion protein that is essentially identical to anti-MSCP:TRAIL except that it contains an anti-EpCAM scFv instead of an anti-MSCP scFv.

Assessment of apoptosis

MCSP-restricted induction of apoptosis by anti-MCSP:TRAIL was assessed on a panel of melanoma cell lines. Briefly, melanoma cells were pre-cultured in a 48-well plate at a concentration of 3×10^4 cells/well. Subsequently, cells were treated as indicated and apoptosis was assessed by: Loss of mitochondrial membrane potential (ψ); ψ was analyzed by DiOC6 staining (Eugene, The Netherlands) as previously described [16]. After 16 h treatment, cells were harvested and incubated for 20 min with DiOC6 (0.1 µM) at 37°C, harvested (1000 x g, 5 min.), resuspended in PBS, and assessed for staining by flow cytometry. Caspase-8, caspase-9 and caspase-3/-7 activity; caspase activity was assessed using the Caspase-Glo 8, 9 and 3/7 Assay according to manufacturer's instructions (Promega Benelux BV, Leiden, The Netherlands). The assay is based on the cleavage of non-luminescent substrates by activated caspases into a luminescent product. Luminescence was quantified using a Victor3 multi-label plate reader (Perkin Elmer, Groningen, The Netherlands)

Soft agar colony forming assay

Soft agar colony forming assays were performed in 24-well plates pre-coated

with 0.5 ml solidified 0.4% agarose in RPMI 1640 medium. Cells were resuspended at a density of 1×10^4 cells/well in 0.6% agarose in RPMI 1640 medium supplemented with 20% fetal calf serum and layered on the solidified 0.4% agarose in a 24-well plate. Tumor cell containing agarose was allowed to solidify for 10 minutes at 4°C before addition of 1 ml of RPMI 1640 medium supplemented with 20% fetal calf serum. Cells were treated as indicated and subsequently cultured at 37°C, in a humidified 5% CO_2 atmosphere. Colony formation was assessed 21 days after start of treatment. Assays were performed in quadruplicate. Number of colonies was quantified and percentage of colony growth was calculated with the formula: Percentage of colony growth = (number of colonies in experimental condition)/(number of colonies in medium control) × 100%. For A375M cells, the number of colonies in untreated samples ranged from 30 ± 5 to 262 ± 35 between individual experiments.

Proteome Profiler array

The effect of MCSP targeting on protein tyrosine kinase activity was assessed by the Human Phospho-Kinase Array Kit (R&D Systems) according to the manufacturer's recommendations. Briefly, per condition 1×10^7 cells were treated for 0, 30, 60, or 240 min. at 37°C as indicated. Lysate (500 µg/condition) was added to the NC-membranes containing spotted Phospho-Kinase (PK) antibodies. Subsequently, secondary Biotin-conjugated anti-Kinase antibodies and Horseradish Peroxidase-conjugated Streptavidin were added to detect the presence of phosphorylated kinases. Between incubation steps, membranes were rigorously washed. Blots were developed by standard chemoluminescence (Roche). Luminescent signals were quantified using the IVIS Spectrum bioluminescent imager (Caliper Biosciences) as photons/sec/sr/cm^2. After background luminescence subtraction, the relative kinase activity in treated conditions was calculated by the formula: (PK activity experimental condition/PK activity medium control) × 100%.

A375M xenograft mouse model

Experiments involving animals were performed in accordance with the experimental protocol approved by the Committee for Research and Animal Ethics of the UMCG. Six week old healthy male athymic mice (n = 8) were purchased from Harlan (Harlan Netherlands B.V., Horst, The Netherlands). Mice were housed in IVC cages and fed ad libitum. Subsequently, mice were subcutaneously inoculated with 2×10^6 A375M cells suspended in 100 µl matrigel. Tumor growth was monitored daily by electronic caliper measurements. After reaching tumor size of ~ 50 ± 6 mm^3, mice were randomly assigned into two groups with a sample size of 4. Mice received daily i.v. saline injections or anti-MCSP:TRAIL injections (0.14 mg/kg). After two weeks of treatment, mice were sacrificed by cervical dislocation. Tumor size was calculated by the formula:

$V = 0,5234 \times H \times L \times W$ [mm^3]. Tumor size was expressed as the percentage of maximum tumor size in Sham-treated mice.

Liver histopathology

Formalin-fixed liver samples were embedded in paraffin, sectioned into 5 µm thickness and stained with hematoxylin-eosin and microscopically inspected for hepatic tissue damage and inflammation.

Combination treatment with anti-MCSP:TRAIL and σ-ligands

Cells were plated at 3.0×10^4 cells/well in a 48-well plate and allowed to adhere overnight. Cells were concurrently treated for 24 h with anti-MCSP:TRAIL with or without rimcazole (15 µM), and (+)-pentazocine (200 nM). Synergy was assessed by calculating the cooperativity index (CI) in which the sum of apoptosis induced by single-agent treatment is divided by apoptosis induced by combination treatment. When CI was less than 1, treatment was considered synergistic; when CI equaled 1, treatment was considered additive; when CI was greater than 1, treatment was considered antagonistic.

Statistical analysis

Data reported are mean values ± standard error of the mean of at least three independent experiments. Statistical analysis was performed by one-way ANOVA followed by Tukey-Kramer post test or by two-sided unpaired Student's t-test. $P < 0.05$ was defined as a statistically significant difference.

Results and Discussion

MCSP-restricted induction of apoptosis by anti-MCSP:TRAIL

We and others have previously demonstrated that selective delivery of the cytokine TRAIL by genetic fusion to an appropriate tumor-selective scFv antibody fragment significantly enhances the anti-tumor activity of TRAIL towards the corresponding type of cancer [14-20]. Here, we adapted this targeted approach to malignant melanoma by exploiting an anti-MCSP scFv antibody fragment that was derived from the well-established monoclonal antibody (mAb) 9.2.27. The resultant fusion protein, anti-MCSP:TRAIL, was equipped to selectively accrete at the cell surface of MCSP-positive cells only and subsequently trigger TRAIL-mediated apoptosis.

Indeed, treatment of MCSP-transfected M14 melanoma cells (M14.MCSP) with anti-MCSP:TRAIL resulted in dose-dependent activation of apoptosis within 16 h, whereas parental MCSP-negative M14 cells were resistant to treatment with anti-MCSP:TRAIL (Fig. 1A). Similarly, treatment of a series of MCSP-positive cell lines (A375M, A2058 and

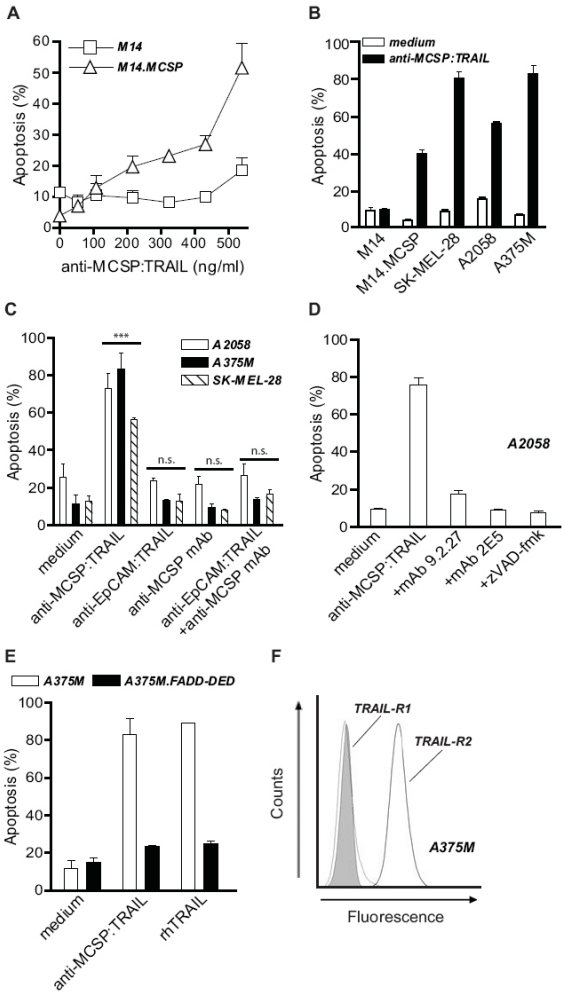

Fig.1. MCSP-restricted induction of apoptosis by anti-MCSP:TRAIL: A) M14 and M14.MCSP cells were treated with increasing concentrations of anti-MCSP:TRAIL for 16 h and apoptosis was assessed by Δψ; B) MCSP-negative cell line M14 and MCSP-positive cell lines M14. MCSP, SK-MEL-28, A2058 and A375M were treated with 500 ng/ml anti-MCSP:TRAIL for 16 h and apoptosis was assessed by Δψ; C) A375M, A2058 and SK-MEL-28 cells were treated with equimolar concentrations of anti-MCSP:TRAIL, anti-EpCAM:TRAIL, anti-MCSP mAb or anti-EpCAM:TRAIL + anti-MCSP mAb for 16 h and apoptosis was assessed by Δψ; D) A2058 cells were treated with 500 ng/mL anti-MCSP:TRAIL in the absence or presence of parental MCSP-blocking mAb 9.2.27, TRAIL-neutralizing mAb 2E5 or pan-caspase inhibitor zVAD-fmk for 16 h and apoptosis was assessed by Δψ; E) A375M and A375M. FADD-DED cells were treated with anti-MCSP:TRAIL or rhTRAIL for 16 h and apoptosis was assessed by Δψ; F) A375M cells were incubated with anti-TRAIL-R1 (thin line) or anti-TRAIL-R2 (thick line) mAb and expression of TRAIL-R1 and TRAIL-R2 was analyzed by flow cytometry. Shaded area indicates the fluorescence signal when cells were incubated with fluorescent-labeled secondary antibody alone.

SK-MEL-28) with anti-MCSP:TRAIL resulted in a marked induction of apoptosis (Fig. 1B). In a control experiment we treated the same series of melanoma cells with fusion protein anti-EpCAM:TRAIL, a fusion protein that is essentially identical to anti-MCSP:TRAIL except that it contains an anti-EpCAM scFv instead of an anti-MCSP scFv antibody fragment [14]. EpCAM is a well established carcinoma-associated cell surface target antigen that is not expressed on melanoma cells. Indeed, no signs of apoptosis were observed when A375M, A2058 or SK-MEL-28 cells were treated with anti-EpCAM:TRAIL (Fig. 1C and Fig. 2A).

Treatment of MCSP-positive A375M, A2058 or SK-MEL-28 cells with the parental anti-MCSP antibody mAb 9.2.27 failed to induce any signs of apoptosis (Fig. 1C). Importantly, also co-treatment with MAb 9.2.27 and anti-EpCAM:TRAIL did not induce any significant signs of apoptosis (Fig. 1C). Thus, treatment of MCSP-positive melanoma cells with fusion protein anti-MCSP:TRAIL efficiently activates apoptosis that is MCSP-restricted and that is superior to combined treatment with TRAIL and the parental anti-MCSP mAb 9.2.27.

Induction of apoptosis by anti-MCSP:TRAIL was abrogated when treatment was performed in the presence of the parental mAb 9.2.27 (Fig. 1D). Thus, anti-MCSP:TRAIL activity is strictly dependent on binding to cell surface-expressed MCSP on malignant cells. Furthermore, addition of the TRAIL-neutralizing mAb 2E5 fully abrogated the apoptotic effect of anti-MCSP:TRAIL (Fig. 1D), indicating that induction of apoptosis is dependent on interaction of TRAIL with its agonistic TRAIL-receptors. In addition, induction of apoptosis was inhibited when treatment is performed in the presence of pan-caspase-inhibitor zVAD-fmk (Fig. 1D), further suggesting involvement of TRAIL-mediated apoptotic signaling. Indeed, treatment of melanoma cells with anti-MCSP:TRAIL was characterized by time-dependent activation of initiator caspase-8 (Fig. 2B) as well as effector caspases 3 and 7 (Fig. 2C).

To further confirm that TRAIL-signaling is involved, the mutant cell line A375M.FADD-DED that ectopically overexpresses a dominant negative mutant of the adaptor protein FADD, was produced. FADD is a pivotal adaptor protein in TRAIL-receptor signaling. The mutant FADD protein lacks the so-called DED domain, which results in a general and strong resistance against TRAIL-mediated apoptosis. Indeed, TRAIL-mediated apoptotic signaling was fully halted in A375M.FADD-DED cells, as is evidenced by the fact that these cells were fully resistant to ubiquitously active recombinant human TRAIL (rhTRAIL) (Fig. 1E). Likewise, A375M.FADD-DED cells were also fully resistant to treatment with anti-MCSP:TRAIL (Fig. 1E). Taken together, these data clearly demonstrate that the pro-apoptotic activity of anti-MCSP:TRAIL is TRAIL-mediated.

Previously, we and others have shown that upon binding to the respective target antigen, scFv:TRAIL fusion proteins can efficiently activate TRAIL-R2, whereas untargeted sTRAIL preparations have a markedly reduced capacity to activate TRAIL-R2 signaling.

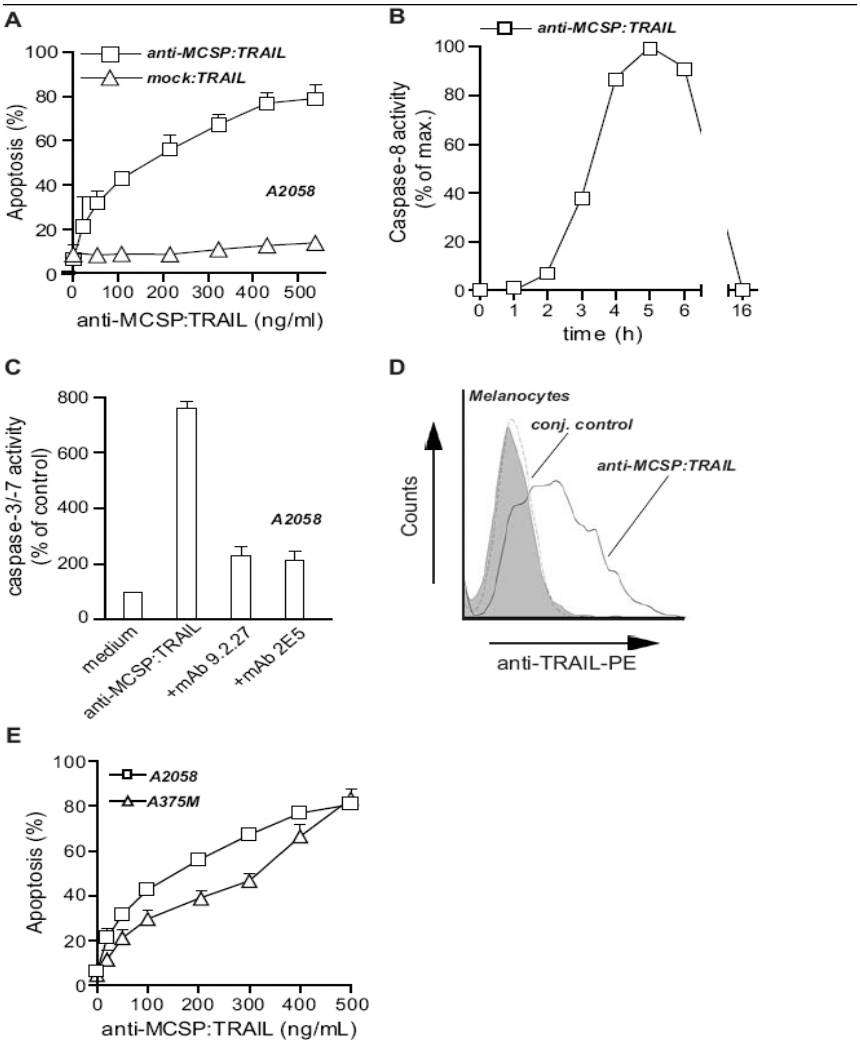

Fig.2. A) A2058 cells were treated with increasing concentrations of anti-MCSP:TRAIL or anti-EpCAM:TRAIL for 16 h and apoptosis was assessed by Δψ; B) A375M cells were treated with 500 ng/ mL anti-MCSP:TRAIL for the time-points indicated and caspase-8 activation was assessed; C) A2058 cells were treated with 500 ng/mL anti-MCSP:TRAIL in the absence or presence of parental MCSP-blocking mAb 9.2.27 or TRAIL-neutralizing mAb 2E5 and caspase-3/-7 activation was assessed; D) MCSP-restricted binding of anti-MCSP:TRAIL to melanocytes was assessed. Specific binding was demonstrated by pre-incubating melanocytes with mAb 9.2.27 followed by incubation with anti-MCSP:TRAIL. Binding of anti-MCSP:TRAIL was assessed by flow cytometry using a PE-conjugated anti-TRAIL mAb; E) A2058 and A375M cells were treated with increasing concentrations of anti-MCSP:TRAIL for 16 h and apoptosis was assessed by Δψ.

Indeed A375M cells, that solely express TRAIL-R2 at the cell surface (Fig. 1F) are sensitive to treatment with anti-MCSP:TRAIL (Fig. 1B, Fig. 2E), indicating that anti-MCSP:TRAIL can potently activate TRAIL-R2 signaling in MCSP-positive melanoma cells. This feature may be of special relevance for melanoma since TRAIL-R2 is the most prevalent agonistic TRAIL-receptor expressed on melanoma cells [27].

Potent inhibition of anchorage-independent growth by anti-MCSP:TRAIL

The MCSP antibody fragment used in this study was derived from mAb 9.2.27. In earlier studies, mAb 9.2.27 partly inhibited MCSP-tumorigenic signaling *in vitro*, as evidenced by inhibition of FAK [9]. Since ectopic expression of MCSP was also recently shown to induce anchorage-independent growth capacity, anti-MCSP:TRAIL was evaluated for its effect on anchorage-independent growth of melanoma cells. In a soft agar assay, treatment of the MCSP-positive cell lines A375M and A2058 cells with anti-MCSP:TRAIL abrogated colony outgrowth in a dose-dependent manner (Fig. 3A). Of note, anti-MCSP:TRAIL reduced colony formation by 50% already at very low concentrations (0.1 ng/ml and 1 ng/ml for A375M and A2058 cells, respectively). Induction of apoptosis by anti-MCSP:TRAIL at these concentrations in adherent growth conditions was marginal (see Fig. 2E for dose-response curves of apoptosis induction). In contrast, treatment with similar concentrations of anti-EpCAM:TRAIL or with anti-MCSP mAb 9.2.27 only marginally reduced colony formation (Fig. 3B). Importantly, also combinatorial treatment with equimolar concentrations of anti-EpCAM:TRAIL and mAb 9.2.27 failed to significantly inhibit colony outgrowth of A375M cells at the highest concentrations tested (Fig. 3B). Furthermore, rhTRAIL failed to significantly reduce colony outgrowth (Fig. 3C). Thus, anti-MCSP:TRAIL uniquely and efficiently prevents colony outgrowth.

Treatment of A375M cells with anti-MCSP:TRAIL in the presence of the TRAIL-neutralizing mAb 2E5 largely blocked the effect of anti-MCSP:TRAIL on colony outgrowth (Fig. 3D). Similarly, treatment of cells with anti-MCSP:TRAIL in the presence of the parental anti-MCSP mAb 9.2.27 inhibited anti-MCSP:TRAIL activity, although the number of colonies still remained significantly lower than medium control (Fig. 3D). Of note, co-incubation with pan-caspase inhibitor zVAD-fmk abrogated the inhibitory effect of anti-MCSP:TRAIL on colony outgrowth (Fig. 3D), suggesting that apoptotic signaling is required for the inhibitory effect of anti-MCSP:TRAIL.

To further evaluate whether TRAIL-induced caspase-signaling was required for the inhibitory effect of anti-MCSP:TRAIL on colony outgrowth, TRAIL-resistant A375M.FADD-DED cells were treated with anti-MCSP:TRAIL. Importantly, colony formation of A375M.FADD-DED cells was inhibited by anti-MCSP:TRAIL treatment although ~50- to 100-fold higher concentrations were required to obtain the same magnitude of inhibition as observed for parental A375M cells (Fig. 3E). Of note, treatment of A375M.

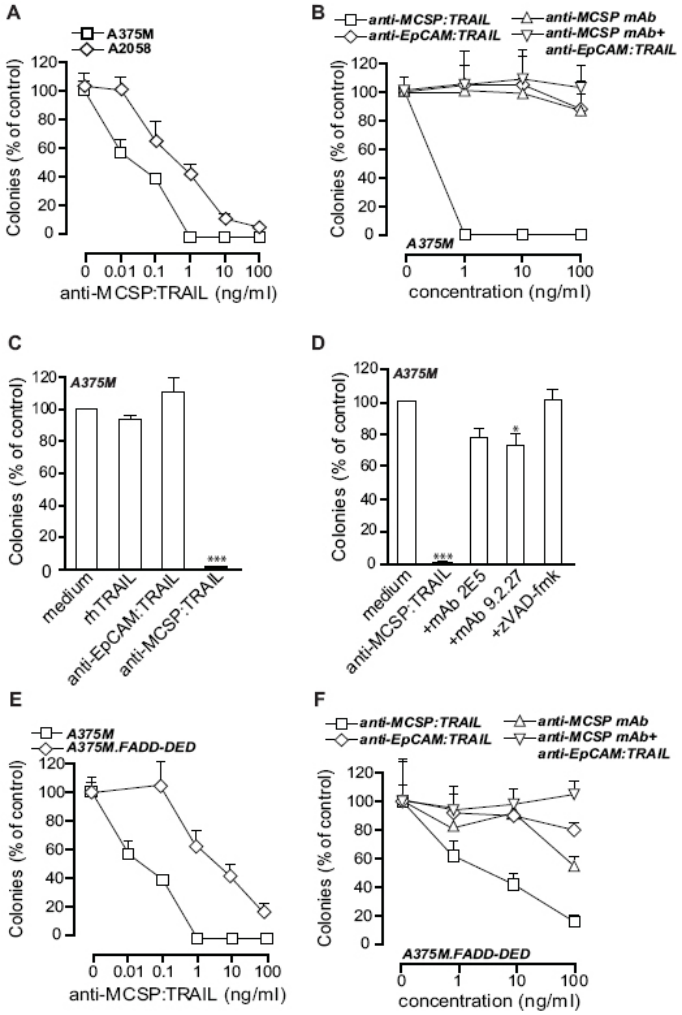

Fig.3. Inhibition of anchorage-independent growth by anti-MCSP:TRAIL: A) A375M and A2058 cells were treated with increasing concentrations of anti-MCSP:TRAIL for 21 days and colony formation was assessed; B) A375M cells were treated with increasing concentrations of anti-MCSP:TRAIL, anti-EpCAM:TRAIL, anti-MCSP mAb or anti-EpCAM:TRAIL+anti-MCSP mAb for 21 days and colony formation was assessed; C) A375M cells were treated with rhTRAIL, anti-EpCAM:TRAIL or anti-MCSP:TRAIL for 21 days and colony formation was assessed; D) A375M cells were treated with 100 ng/ml anti-MCSP:TRAIL in the absence or presence of TRAIL-neutralizing mAb 2E5, parental anti-MCSP mAb 9.2.27 or pancaspase inhibitor zVAD-fmk for 21 days and colony formation was assessed; E) A375M and A375M.FADD-DED cells were treated with increasing concentrations of anti-MCSP:TRAIL for 21 days and colony formation was assessed; F) A375M.FADD-DED cells were treated with increasing concentrations of anti-MCSP:TRAIL, anti-EpCAM:TRAIL, anti-MCSP mAb or anti-EpCAM:TRAIL+anti-MCSP mAb for 21 days and colony formation was assessed.

Table 1. Kinases downregulated by anti-MCSP:TRAIL, the percentage of inhibition after 1 h treatment with anti-MCSP:TRAIL and their role in oncology

Kinase	Phosphorylation site	anti-MCSP:TRAIL	*P*-value	Function in oncology
Fyn	Y420	69±8	<0.01	Src family kinase member involved in integrin-mediated cell adhesion [34,35]
FAK	Y397	75±6	<0.01	focal adhesion kinase involved in cell adhesion and spreading [36-38]
Src	Y419	59±9	<0.01	Src family kinase members involved in cell adhesion, invasion, proliferation, survival and angiogenesis during tumor formation [38-39]
Hck	Y411	57±10	<0.01	
Lyn	Y397	81±12	<0.05	
Yes	Y426	67±10	<0.01	
AMPKα1	T174	61±10	<0.01	AMP-activated protein kinase involved in energy homeostasis [40-41]
AMPKα2	T172	50±18	<0.01	
STAT2	Y689	47±17	<0.01	signal transducer and activator of transcription family members involved in cytokine and growth factor signaling [42-43]
STAT3	Y705	43±19	<0.01	
STAT5a	Y699	55±22	<0.01	
STAT5b	Y699	55±18	<0.01	
STAT5a/b	Y699	55±15	<0.01	
STAT6	Y641	54±19	<0.01	
β-catenin	-	32±8	<0.01	signaling molecule involved in the Wnt pathway [44-45]
p53	S392	56±4	<0.01	phosphorylation site involved in nucleolar localization and DNA-binding affinity of p53 [46]
p53	S46	63±9	<0.01	phosphorylation site involved in regulation of pro-apoptotic gene transcription [47]
p53	S15	77±7	<0.01	
Chk-2	T68	62±3	<0.01	involved in cell cycle control and p53 phosphorylation [48-50]
Jnk	T183/Y185, T221/Y223	59±11	<0.01	mitogen-activated protein kinase involved in regulation of apoptosis [51-52]
TOR	S2448	62±21	<0.05	involved in cell cycle control and p53 phosphorylation [47,53]
Erk-1/-2	T202/Y204, T185/Y187	124±48	n.s.	mitogen-activated protein kinase involved in MCSP-signaling [36,54]

FADD-DED cells with anti-EpCAM:TRAIL did not inhibit colony formation (Fig. 3F), nor did combination treatment of anti-EpCAM:TRAIL and mAb 9.2.27 (Fig. 3F). In contrast, mAb 9.2.27 alone did significantly inhibit colony outgrowth in this cell line, although to a lesser extent than anti-MCSP:TRAIL (Fig. 3F). Together, these experimental data suggest that the simultaneous interaction of anti-MCSP:TRAIL with MCSP and TRAIL-receptors uniquely blocks anchorage-independent growth of melanoma cells at low concentrations.

Anti-MCSP:TRAIL dephosphorylates proteins involved in cell proliferation and apoptosis resistance

The efficacy of anti-MCSP:TRAIL on inhibition of colony formation by melanoma cells in 3D-culture suggests that antibody fragment-dependent sensitization of cells to concurrent TRAIL-signaling may contribute to its therapeutic effect. Previously, we generated proof of concept data for such dual therapeutic signaling with scFv:TRAIL fusion proteins, using an scFv:TRAIL fusion protein that targeted the Epidermal Growth Factor Receptor [16,19]. Here, the EGFR-inhibitory antibody fragment blocked mitogenic EGFR-signaling and synergized TRAIL apoptotic signaling [16,19]. To assess whether the MCSP-specific antibody fragment might contribute to the anti-tumor activity of anti-MCSP:TRAIL, a focused set of 48 cellular phosphoproteins was examined for the level of phosphorylation after treatment with anti-MCSP:TRAIL (Fig. 4A and 4B), anti-MCSP mAb 9.2.27 (Fig. 4C) and rhTRAIL (Fig. 4D). Interestingly, although A375M cells were treated with anti-MCSP:TRAIL in adherent growth conditions in view of experimental

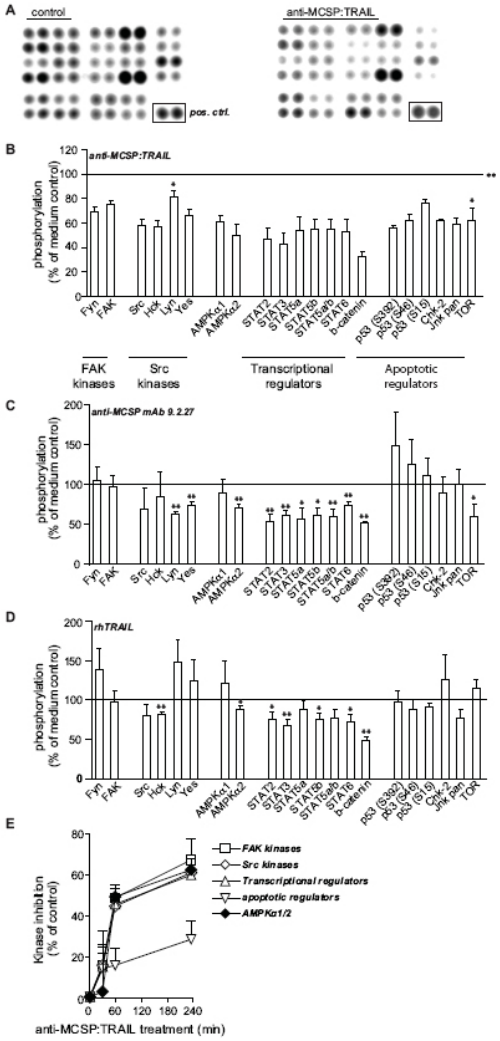

Fig.4. Anti-MCSP:TRAIL triggers dephosphorylation of cellular proteins. A375M cells were treated with anti-MCSP:TRAIL, anti-MCSP mAb 9.2.27, rhTRAIL or left untreated for 1 h. Whole cell lysates were analyzed for phosphorylation of 48 cellular kinases: A) Phosphorylation of 28 kinases in untreated cells (left panel) or anti-MCSP:TRAIL-treated cells (right panel) are depicted. Images are representative of three independent experiments. B-D) Changes in the phosphorylation of 21 kinases after treatment with: B) anti-MCSP:TRAIL, C) anti-MCSP mAb 9.2.27 or D) rhTRAIL are expressed as a percentage of the phosphorylation measured in untreated cells. E) A375M cells were treated with anti-MCSP:TRAIL for 0, 30, 60 or 240 min. Whole cell lysates were analyzed for phosphorylation of 48 cellular kinases. Changes in phosphorylation of the different kinase groups as indicated in panel B are depicted. *, $P < 0.05$; **, $P < 0.001$; ***, $P < 0.0001$.

limitations with 3D-cultures, significant dephosphorylation of various proteins involved in cell survival and proliferation was detected after 1 h of treatment (Fig. 4A, 4B and Table 1). This dephosphorylation induced by anti-MCSP:TRAIL was detectable within 30 minutes and increased for up to 4 h after start of treatment (Fig. 4E). Treatment with mAb 9.2.27 and rhTRAIL also triggered dephosphorylation of proteins at 1 h of treatment, but to a lesser extent and in a smaller panel (Fig. 4C and 4D, respectively).

First and foremost, the previously reported down-stream target of MCSP, FAK, was dephosphorylated by a factor 2 compared to medium control. The parental anti-MCSP mAb 9.2.27 has been shown to prevent association of MCSP with integrins, thereby preventing activation of FAK [6]. Thus, although not determined here for anti-MCSP:TRAIL, a similar inhibition of MCSP/integrin interaction by the mAb 9.2.27-derived antibody fragment may be responsible for the inhibitory effect of anti-MCSP:TRAIL on FAK. Intriguingly, cross-linking of MCSP by bead-coated mAb 9.2.27 has also been used to achieve activation of MCSP-signaling [6]. The different outcome of treatment with soluble *vs.* coated mAb suggests that the extent of cross-linking of MCSP by the antibody determines the activation or inhibition, respectively, of downstream signaling. It will be interesting to evaluate in future studies whether the three MCSP reading heads in trimeric anti-MCSP:TRAIL are perhaps better suited for inhibition of MCSP-signaling.

The activity of ERK1/2, another established downstream effector of MCSP signaling [6], was not affected after 1 h of treatment with anti-MCSP:TRAIL. One possible reason for this finding is a perhaps delayed effect of anti-MCSP:TRAIL on ERK1/2 signaling at later and not examined time-points. In addition, it has been shown that MCSP enhances FAK and Erk1/2 signaling by distinct mechanisms [6]. It is therefore also conceivable that FAK is dephosphorylated while Erk1/2 is not a target of inhibition by anti-MCSP:TRAIL.

In addition to the established MCSP-target FAK, a panel of other proteins was dephosphorylated upon anti-MCSP:TRAIL treatment, including the kinase Fyn, and the Src kinases Src, Hck, Lyn and Yes. The relative impact of these respective proteins on MCSP tumorigenic signaling is currently being evaluated in extended ongoing studies using e.g. constitutively active and/or dominant negative mutants as well as small inhibitory RNA-mediated silencing of the individual components. Importantly, the above-mentioned experiments need to be performed not only in 2D, but also in 3D-cultures, in order to reliably determine the relative importance of the here identified proteins for MCSP-dependent anchorage-independent growth of melanoma cells.

Perhaps counter intuitively, the proto-oncogene Beta-Catenin (β-Catenin) was also dephosphorylated by treatment with anti-MCSP:TRAIL, as well as by treatment with mAb 9.2.27 and rhTRAIL (Fig. 4B, 4C and 4D**,** respectively). Dephosphorylation of β-Catenin does not inactivate β-Catenin but actually prevents proteasomal degradation and increases cellular levels of β-Catenin. In turn, this leads to activation of pro-oncogenic

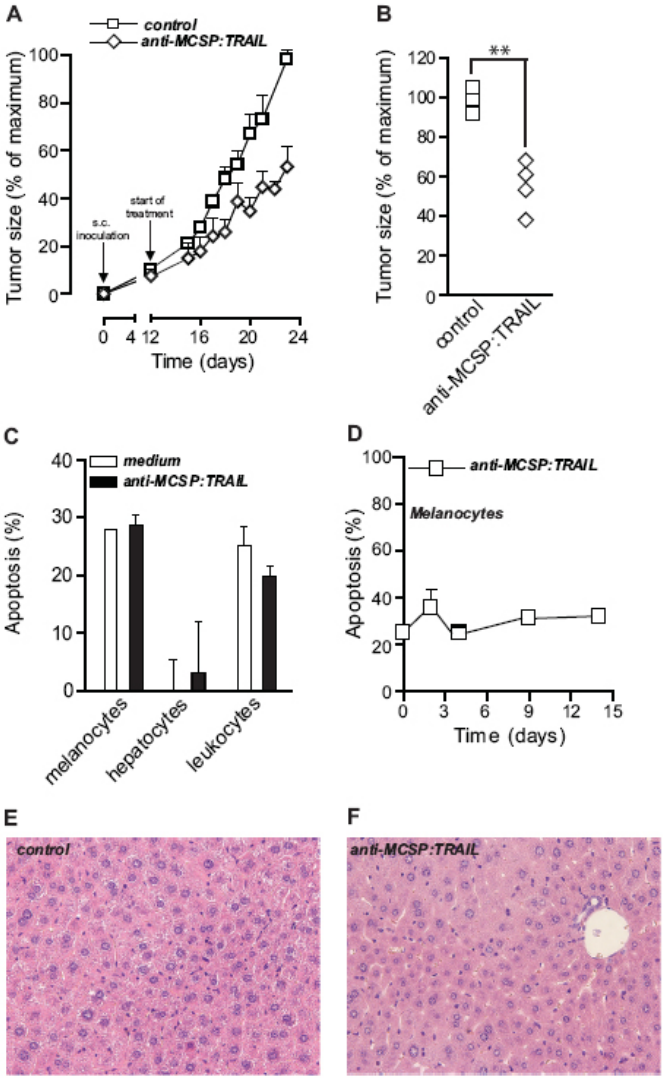

Fig.5. Anti-tumor activity of anti-MCSP:TRAIL towards A375M xenografts: A) mice were inoculated with A375M tumor cells at day 0 and developed xenografts of ~ 50 mm^3 after 12 days. Starting at day 12, mice were injected daily with saline (n = 4) or anti-MCSP:TRAIL (0.14 mg/kg, n = 4) and tumor size was measured daily using electronic caliper measurements; B) tumor size at day 23; C) MCSP-positive melanocytes and MCSPnegative leukocytes and hepatocytes were treated with 500 ng/ml anti-MCSP:TRAIL for 16 h and apoptosis was assessed by Δψ; D) melanocytes were treated with 4 μg/mL anti-MCSP:TRAIL for up to 14 days and apoptosis was assessed by Δψ at time points indicated; E-F) liver pathology of mice carrying A375M xenografts was examined for E) Sham-treated mice and F) anti-MCSP:TRAIL-treated mice.

gene transcription [28]. However, the exact role of β-Catenin-induced gene transcription in melanoma is still a matter of debate. Based on mouse models with activating mutations in β-Catenin, an oncogenic role of β-Catenin in melanoma was proposed [29]. On the other hand, others have shown that β-Catenin induces a transcriptional profile in melanoma cells that is reminiscent of normal melanocyte differentiation [30]. This transcriptional profile is moreover associated with increased patient survival and is lost upon malignant progression [30].

Taken together, anti-MCSP:TRAIL dephosphorylates a panel of established MCSP targets as well as newly identified proteins (see Table 1 for overview). Thus, the kinase array data support a dual anti-melanoma activity by anti-MCSP:TRAIL that partly relies on inhibition of tumorigenic signaling by the anti-MCSP antibody fragment.

Anti-tumor activity of low dose anti-MCSP:TRAIL towards A375M xenografts

To further characterize the anti-melanoma activity of anti-MCSP:TRAIL, A375M cells were xenografted subcutaneously in nude mice and allowed to form small tumors (~ 50 mm^3). Subsequently, mice were treated daily by intra-peritoneal injection with a low dose of anti-MCSP:TRAIL (~ 0.14 mg/kg) or with saline. Of note, anti-MCSP mAb 9.2.27 and therefore anti-MCSP:TRAIL do not cross-react with mouse MCSP [3]. Compared to sham-treated mice, tumor size of the anti-MCSP:TRAIL-treated mice was strongly retarded in time (Fig. 5A), with a 50% reduction in tumor size at the end of the experiment (Fig. 5B). Of note, earlier animal studies with A375M cells and non-targeted rhTRAIL were performed at > 300 times higher concentrations (50 mg/kg) compared to the here employed treatment regimen with anti-MCSP:TRAIL [31]. Thus, in analogy to the low dose required for therapeutic activity in colony formation assays, anti-MCSP:TRAIL already has potent *in vivo* anti-melanoma activity at a very low dose.

Anti-MCSP:TRAIL lacks apoptotic activity towards normal cells

Earlier studies have shown that tumor targeted delivery of TRAIL augments the tumor-specific activity of TRAIL, while not affecting the absence of toxicity on normal human cell types. Indeed, although anti-MCSP:TRAIL strongly bound to MCSP on normal human melanocytes (Fig. 2D), no apoptosis was induced in melanocytes even when treatment was performed with 4 μg/ml anti-MCSP:TRAIL (Fig. 5C). Also extended treatment (up to 8 days) of melanocytes with 4 μg/ml anti-MCSP:TRAIL did not yield significant increases in apoptosis compared to medium control (Fig. 5D). Similarly, normal human MCSP-negative hepatocytes were fully resistant to treatment with anti-MCSP:TRAIL (Fig. 5C). Hepatocytes have previously been shown to be one of the most vulnerable normal cell types to possible TRAIL-related toxicity [32]. Importantly, also in nude mice carrying A375M xenografts treatment with anti-MCSP:TRAIL had no deleterious effect on liver

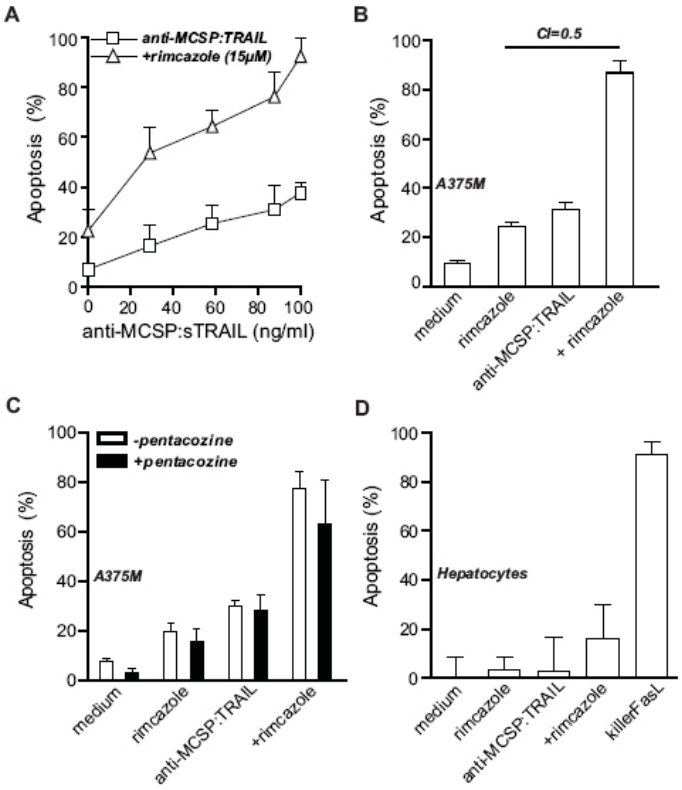

Fig.6. Synergistic induction of apoptosis by anti-MCSP:TRAIL and rimcazole: A) A375M cells were treated with increasing concentrations of anti-MCSP:TRAIL in the presence or absence of rimcazole for 16 h and apoptosis was assessed by Δψ; B) A375M cells were treated with rimcazole (15 μM), anti-MCSP:TRAIL (100 ng/ml) or both for 16 h, apoptosis was assessed by Δψ and the cooperativity index (CI) was calculated as indicated in the materials and methods section; C) A375M cells were treated with rimcazole (15 μM), anti-MCSP:TRAIL (100 ng/mL) or both in the presence or absence of pentacozine (200 nM) for 16 h and apoptosis was assessed by Δψ; D) Hepatocytes were treated with, rimcazole (15 μM), anti-MCSP:TRAIL (100 ng/ml) or both for 16 h and apoptosis was assessed by Δψ. KillerFasL (100 ng/ml)was used as a positive control for hepatocyte toxicity.

morphology, with morphology of liver sections comparable to the morphology of liver sections of Sham-treated mice (Fig. 5E and 5F). The here obtained data regarding the absence of activity of anti-MCSP:TRAIL towards normal cell types are in line with the large body of evidence in literature on the preclinical safety profile of sTRAIL. Indeed, ongoing clinical trials with rhTRAIL confirm the relative safety of TRAIL treatment with no serious adverse effects and no dose-limiting toxicity reported to date.

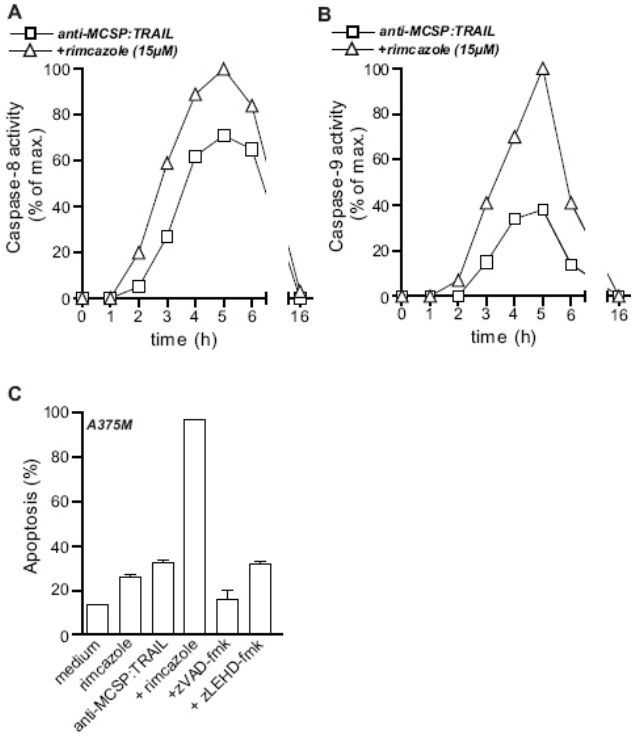

Fig.7. Activity of caspases: A) caspase-8 and B) caspase-9 was assessed in A375M cells after incubation with anti-MCSP:TRAIL in the presence or absence of rimcazole (15 μM) for 1, 2, 3, 4, 5, 6 or 16 h; C) A375M cells were treated for 16 h with 100 ng/mL of anti-MCSP:TRAIL and/or rimcazole (15 μM) in the presence or absence of zVAD-FMK (20 μM) or zLEHD-FMK and apoptosis was assessed by Δψ.

Synergistic induction of apoptosis by anti-MCSP:TRAIL and sigma ligands

Since resistance of melanoma cells towards sTRAIL has previously been reported [22] a combinatorial strategy was evaluated of anti-MCSP:TRAIL with rimcazole, a sigma ligand in clinical trials for various cancers. Sigma receptors are expressed in the central nervous, immune, endocrine, and reproductive systems, but also in peripheral organs like kidney, liver and gastrointestinal tract. Although the precise function of these receptors remains unknown, both sigma-1 and sigma-2 receptors are strongly overexpressed in rapidly proliferating cells such as melanoma and may be exploited as possible targets for melanoma therapy [26]. Treatment of A375M cells with the sigma-1/sigma-2 antagonist rimcazole synergistically enhanced induction of apoptosis by anti-MCSP:TRAIL (Fig. 6A and 6B). Of note, treatment in the presence of the sigma-1 agonist (+)-pentazocine did

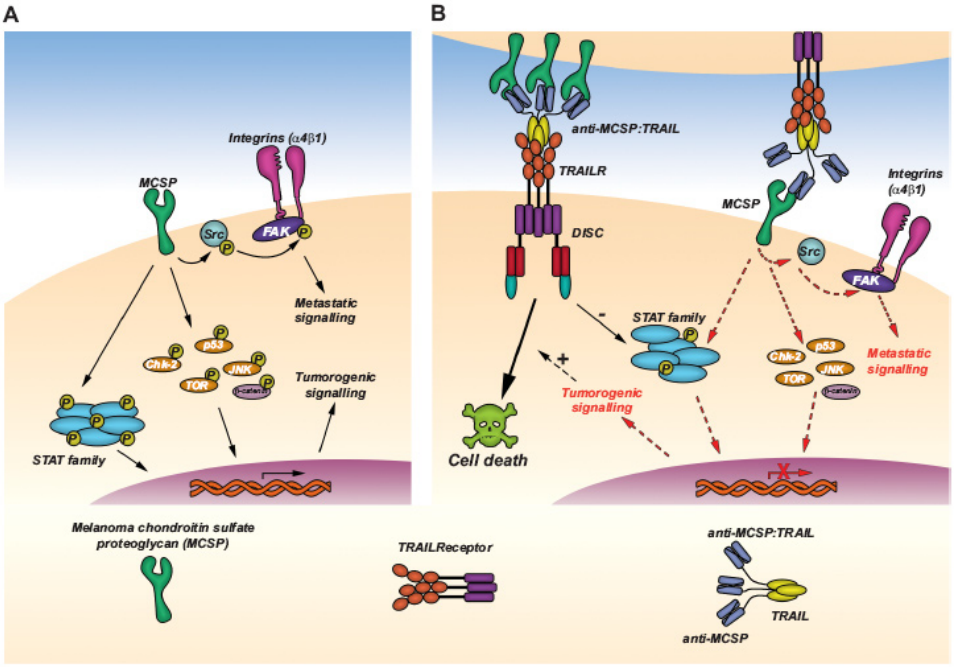

Fig.8. Schematic representation of the anti-melanoma activity of anti-MCSP:TRAIL: A) direct or indirect MCSP-mediated signaling involves (integrin-dependent) FAK and Src phosphorylation and maintains phosphorylation of downstream transcription factors and apoptotic modulators. MCSP thus contributes to pro-survival and metastatic signals; B) binding of anti-MCSP:TRAIL inhibits MCSP-mediated signaling and concomitant activation of pro-metastatic/-survival signals and thereby sensitizes cells to apoptosis induction via binding of the TRAIL moiety to TRAILR.

not abrogate synergy, suggesting that rimcazole synergizes with anti-MCSP:TRAIL activity via sigma-2 receptors (Fig. 6C). Rimcazole did not upregulate TRAIL-R1 or TRAIL-R2 expression (data not shown), but augmented the activation of initiator caspase-8 and initiator caspase-9 upon anti-MCSP:TRAIL treatment (Fig. 7A and 7B, respectively). Moreover, inhibition of either initiator caspase abrogated cytotoxic activity (Fig. 7C). Thus, rimcazole appears to synergize the activity of anti-MCSP:TRAIL by promoting caspase-8 activation. Of note, anti-MCSP:TRAIL in combination with rimcazole lacked apoptotic activity towards hepatocytes (Fig. 6D), suggesting that this combination retains the favorable toxicity profile associated with TRAIL and rimcazole alone.

Conclusions

We provide evidence that anti-MCSP:TRAIL, a TRAIL fusion protein targeted

to melanoma-expressed MCSP, inhibits MCSP tumorigenic signaling and simultaneously induces TRAIL apoptotic signaling. Consequently, fusion protein anti-MCSP:TRAIL potently inhibits outgrowth of melanoma cells both *in vitro* and *in vivo* and this effect can be further enhanced with the cytotoxic agent rimcazole. Based on the above, we postulate the following working model for anti-MCSP:TRAIL (see also Fig. 8A and 8B); anti-MCSP:TRAIL binds to MCSP and inhibits MCSP-signaling, which includes inhibition of src-kinases and FAK, the STAT transcription factors, and various anti-apoptotic modulators such as p53, TOR, JNK. Concurrently, interaction of the sTRAIL domain with its agonistic receptors TRAIL-R1 and TRAIL-R2 triggers potent induction of apoptosis. Notably, TRAIL/TRAIL-R interaction also triggers dephosphorylation of the STAT family, which may contribute to sensitization of cells to apoptosis [33,34]. Thus, melanoma cells are eliminated on the one hand by MCSP-mediated sensitization of melanoma cells to apoptosis and on the other hand by the concurrent activation of TRAIL-apoptotic signaling. Taken together, anti-MCSP:TRAIL is a novel immunotherapeutic agent that, either alone or in combination with rimcazole, may be of potential value for treatment of advanced melanoma.

Acknowledgements

This research was financially supported by the Melanoma Research Alliance (Young Investigator Award to EB), the Dutch Cancer Society (RUG 2009-4355 to EB, RUG2005-3358 and 2007-3784 to WH) and the Alexander von Humboldt Foundation (EB).

References

1 Balch C, Buzaid A, Soong S, Atkins M, Cascinelli N, Coit D, Fleming I, Gershenwald J, Houghton A, Kirkwood J. et al. Final Version of the American Joint Committee on Cancer Staging System for Cutaneous Melanoma. J Clin Oncol. 2001;19:3635–3648.

2 Helmbach H, Sinha P, Schadendorf D. Human melanoma: drug resistance. Recent Results Cancer Res. 2003;161:93–110.

3 Campoli MR, Chang CC, Kageshita T, Wang X, McCarthy JB, Ferrone S. Human high molecular weight-melanoma-associated antigen (HMW-MAA): a melanoma cell surface chondroitin sulfate proteoglycan (MSCP) with biological and clinical significance 1. Crit Rev Immunol. 2004;24:267–296.

4 Vergilis I, Szarek M, Ferrone S, Reynolds S. Presence and Prognostic Significance of Melanoma-Associated Antigens CYT-MAA and HMW-MAA in Serum of Patients with Melanoma. J Investig Dermatol. 2005;125:526–531.

5 Eisenmann KM, McCarthy JB, Simpson MA, Keely PJ, Guan JL, Tachibana K, Lim L, Manser E, Furcht LT, Iida J. Melanoma chondroitin sulphate proteoglycan regulates cell spreading through Cdc42, Ack-1 and p130cas. Nat Cell Biol. 1999;1:507–513.

6 Yang J, Price MA, Neudauer CL, Wilson C, Ferrone S, Xia H, Iida J, Simpson MA, McCarthy JB. Melanoma chondroitin sulfate proteoglycan enhances FAK and ERK activation by distinct mechanisms. J Cell Biol. 2004;165:881–891.

7 Yang J, Price MA, Li GY, Bar-Eli M, Salgia R, Jagedeeswaran R, Carlson JH, Ferrone S, Turley EA, McCarthy JB. Melanoma proteoglycan modifies gene expression to stimulate tumor cell motility, growth, and epithelial-to-mesenchymal transition. Cancer Res. 2009;69:7538–7547.

8 Iida J, Wilhelmson KL, Ng J, Lee P, Morrison C, Tam E, Overall CM, McCarthy JB. Cell surface chondroitin sulfate glycosaminoglycan in melanoma: role in the activation of pro-MMP-2 (pro-gelatinase A) Biochem J. 2007;403:553–563.

9 Chang CC, Campoli M, Luo W, Zhao W, Zaenker KS, Ferrone S. Immunotherapy of melanoma targeting human high molecular weight melanoma-associated antigen: potential role of nonimmunological mechanisms. Ann N Y Acad Sci. 2004;1028:340–350.

10 Schwenkert M, Birkholz K, Schwemmlein M, Kellner C, Kugler M, Peipp M, Nettelbeck DM, Schuler-Thurner B, Schaft N, Dorrie J. et al. A single chain immunotoxin, targeting the melanoma-associated chondroitin sulfate proteoglycan, is a potent inducer of apoptosis in cultured human melanoma cells. Melanoma Res. 2008;18:73–84.

11 Mittelman A, Chen ZJ, Yang H, Wong GY, Ferrone S. Human high molecular weight melanoma-associated antigen (HMW-MAA) mimicry by mouse anti-idiotypic monoclonal antibody MK2-23: induction of humoral anti-HMW-MAA immunity and prolongation of survival in patients with stage IV melanoma. Proceedings of the

National Academy of Sciences of the United States of America. 1992;89:466–470.

12 Ashkenazi A, Pai RC, Fong S, Leung S, Lawrence DA, Marsters SA, Blackie C, Chang L, McMurtrey AE, Hebert A. et al. Safety and antitumor activity of recombinant soluble Apo2 ligand. J Clin Invest. 1999;104:155–162.

13 Soria J, Smit E, Khayat D, Besse B, Yang X, Hsu C, Reese D, Wiezorek J, Blackhall F. Phase 1b Study of Dulanermin (recombinant human Apo2L/TRAIL) in Combination With Paclitaxel, Carboplatin, and Bevacizumab in Patients With Advanced Non-Squamous Non-Small-Cell Lung Cancer. J Clin Oncol. 2010;9:1527–1533.

14 Bremer E, Kuijlen J, Samplonius D, Walczak H, de Leij L, Helfrich W. Target cell-restricted and -enhanced apoptosis induction by a scFv:sTRAIL fusion protein with specificity for the pancarcinoma-associated antigen EGP2 1. Int J Cancer. 2004;109:281–290.

15 Bremer E, Samplonius D, Kroesen BJ, van Genne L, de Leij L, Helfrich W. Exceptionally potent anti-tumor bystander activity of an scFv:sTRAIL fusion protein with specificity for EGP2 toward target antigen-negative tumor cells. Neoplasia. 2004;6:636–645.

16 Bremer E, Samplonius DF, van Genne L, Dijkstra MH, Kroesen BJ, de Leij LF, Helfrich W. Simultaneous inhibition of epidermal growth factor receptor (EGFR) signaling and enhanced activation of tumor necrosis factor-related apoptosis-inducing ligand (TRAIL) receptor-mediated apoptosis induction by an scFv:sTRAIL fusion protein with specificity for human EGFR. J Biol Chem. 2005;280:10025–10033.

17 Bremer E, Samplonius DF, Peipp M, van Genne L, Kroesen BJ, Fey GH, Gramatzki M, de Leij LF, Helfrich W. Target cell-restricted apoptosis induction of acute leukemic T cells by a recombinant tumor necrosis factor-related apoptosis-inducing ligand fusion protein with specificity for human CD7. Cancer Res. 2005;65:3380–3388.

18 Bremer E, de Bruyn M, Samplonius DF, Bijma T, Ten Cate B, de Leij LF, Helfrich W. Targeted delivery of a designed sTRAIL mutant results in superior apoptotic activity towards EGFR-positive tumor cells. J Mol Med. 2008;86:909–924.

19 Bremer E, van Dam GM, de Bruyn M, van Riezen M, Dijkstra M, Kamps G, Helfrich W, Haisma H. Potent systemic anticancer activity of adenovirally expressed EGFR-selective TRAIL fusion protein. Mol Ther. 2008;16:1919–1926.

20 Stieglmaier J, Bremer E, Kellner C, Liebig TM, Ten Cate B, Peipp M, Schulze-Koops H, Pfeiffer M, Buhring HJ, Greil J. et al. Selective induction of apoptosis in leukemic B-lymphoid cells by a CD19-specific TRAIL fusion protein 274. Cancer Immunol Immunother. 2008;57:233–246.

21 Muhlenbeck F, Schneider P, Bodmer JL, Schwenzer R, Hauser A, Schubert G, Scheurich P, Moosmayer D, Tschopp J, Wajant H. The tumor necrosis factor-related apoptosis-inducing ligand receptors TRAIL-R1 and TRAIL-R2 have distinct cross-linking requirements for initiation of apoptosis and are non-redundant in JNK activation. J Biol Chem. 2000;275:32208–32213.

22 Ivanov VN, Bhoumik A, Ronai Z. Death receptors and melanoma resistance to

apoptosis. Oncogene. 2003;22:3152–3161. Brent PJ, Pang GT. [sigma] Binding site ligands inhibit cell proliferation in mammary and colon carcinoma cell lines and melanoma cells in culture. European Journal of Pharmacology. 1995;278:151–160.

23 Spruce BA, Campbell LA, McTavish N, Cooper MA, Appleyard MV, O'Neill M, Howie J, Samson J, Watt S, Murray K. et al. Small molecule antagonists of the sigma-1 receptor cause selective release of the death program in tumor and self-reliant cells and inhibit tumor growth in vitro and in vivo. Cancer Res. 2004;64:4875–4886.

24 Rybczynska AA, Dierckx RA, Ishiwata K, Elsinga PH, van Waarde A. Cytotoxicity of sigma-receptor ligands is associated with major changes of cellular metabolism and complete occupancy of the sigma-2 subpopulation. J Nucl Med. 2008;49:2049–2056.

25 Vilner BJ, John CS, Bowen WD. Sigma-1 and sigma-2 receptors are expressed in a wide variety of human and rodent tumor cell lines. Cancer Res. 1995;55:408–413.

26 Kurbanov BM, Geilen CC, Fecker LF, Orfanos CE, Eberle J. Efficient TRAIL-R1/DR4-mediated apoptosis in melanoma cells by tumor necrosis factor-related apoptosis-inducing ligand (TRAIL) 2. J Invest Dermatol. 2005;125:1010–1019.

27 Chien AJ, Moon RT. WNTS and WNT receptors as therapeutic tools and targets in human disease processes. Front Biosci. 2007;12:448–457.

28 O'Connell MP, Weeraratna AT. Hear the Wnt Ror: how melanoma cells adjust to changes in Wnt. Pigment Cell Melanoma Res. 2009;22:724–739.

29 Chien AJ, Moore EC, Lonsdorf AS, Kulikauskas RM, Rothberg BG, Berger AJ, Major MB, Hwang ST, Rimm DL, Moon RT. Activated Wnt/beta-catenin signaling in melanoma is associated with decreased proliferation in patient tumors and a murine melanoma model. Proc Natl Acad Sci USA. 2009;106:1193–1198.

30 Chawla-Sarkar M, Bauer J, Lupica J, Morrison B, Tang Z, Oates R, Almasan A, DiDonato J, Borden E, Lindner D. Suppression of NF-+¦B Survival Signaling by Nitrosylcobalamin Sensitizes Neoplasms to the Anti-tumor Effects of Apo2L/TRAIL. Journal of Biological Chemistry. 2003;278:39461–39469.

31 Gores GJ, Kaufmann SH. Is TRAIL hepatotoxic? Hepatology. 2001;34:3–6.

32 Ivanov V, Zhou H, Partridge M, Hei T. Inhibition of Ataxia Telangiectasia Mutated Kinase Activity Enhances TRAIL-Mediated Apoptosis in Human Melanoma Cells. Cancer Res. 2009;69:3510–3519.

33 Yoshida T, Zhang Y, Rivera Rosado L, Zhang B. Repeated Treatment with Subtoxic Doses of TRAIL Induces Resistance to Apoptosis through Its Death Receptors in MDA-MB-231 Breast Cancer Cells. Molecular Cancer Research. 2009;7:1835–1844.

34 Resh M. Fyn, a Src family tyrosine kinase. The International Journal of Biochemistry & Cell Biology 1998 Nov;30:1159-62.

35 Saito YD, Jensen AR, Salgia R, Posadas EM. Fyn: a novel molecular target in cancer.

Cancer 2010;116:1629-37.

36 Yang J, Price MA, Neudauer CL, Wilson C, Ferrone S, Xia H, et al. Melanoma chondroitin sulfate proteoglycan enhances FAK and ERK activation by distinct mechanisms. J Cell Biol 2004;165:881-91.

37 Schwock J, Dhani N, Hedley DW. Targeting focal adhesion kinase signaling in tumor growth and metastasis. Expert Opin Ther Targets 2010;14:77-94.

38 Zhao J, Guan JL. Signal transduction by focal adhesion kinase in cancer. Cancer Metastasis Rev 2009;28:35-49.

39 Kim L, Song L, Haura E. Src kinases as therapeutic targets for cancer. Nat Rev Clin Oncol 2009;6:587-95.

40 Koh H, Chung J. AMPK links energy status to cell structure and mitosis. Biochemical and Biophysical Research Communications 2007;362:789-92.

41 Shaw RJ. Glucose metabolism and cancer. Curr Opin Cell Biol 2006;18:598-608.

42 Yu H, Pardoll D, Jove R. STATs in cancer inflammation and immunity: a leading role for STAT3. Nat Rev Cancer 2009;9:798-809.

43 Lopez-Bergami P, Fitchman B, Ronai Z. Understanding signaling cascades in melanoma. Photochem Photobiol 2008;84:289-306.

44 O'Connell MP, Weeraratna AT. Hear the Wnt Ror: how melanoma cells adjust to changes in Wnt. Pigment Cell Melanoma Res 2009;22:724-39.

45 Moon R, Kohn A, Ferrari G, Kaykas A. WNT and [beta]-catenin signalling: diseases and therapies. Nat Rev Genet 2004;5:691-701.

46 Karni-Schmidt O, Friedler A, Zupnick A, McKinney K, Mattia M, Beckerman R, et al. Energy-dependent nucleolar localization of p53 in vitro requires two discrete regions within the p53 carboxyl terminus. Oncogene 2007;26:3878-91.

47 Castedo M, Ferri KF, Blanco J, Roumier T, Larochette N, Barretina J, et al. Human immunodeficiency virus 1 envelope glycoprotein complex-induced apoptosis involves mammalian target of rapamycin/FKBP12-rapamycin-associated protein-mediated p53 phosphorylation. J Exp Med 2001;194:1097-110.

48 Shieh S, Ahn J, Tamai K, Taya Y, Prives C. The human homologs of checkpoint kinases Chk1 and Cds1 (Chk2) phosphorylate p53 at multiple DNA damage-inducible sites. Genes & Development 2000;14:289-300.

49 Stracker TH, Usui T, Petrini JH. Taking the time to make important decisions: the checkpoint effector kinases Chk1 and Chk2 and the DNA damage response. DNA Repair (Amst) 2009;8:1047-54.

50 Stracker TH, Couto SS, Cordon-Cardo C, Matos T, Petrini JH. Chk2 suppresses the oncogenic potential of DNA replication-associated DNA damage. Mol Cell 2008;31:21-

32.

51 Lin A, Dibling B. The true face of JNK activation in apoptosis. Aging Cell 2002;1:112-6.

52 Dhanasekaran DN, Reddy EP. JNK signaling in apoptosis. Oncogene 2008;27:6245-51.

53 Hay N, Sonenberg N. Upstream and downstream of mTOR. Genes & Development 2004;18:1926-45.

54 Russo AE, Torrisi E, Bevelacqua Y, Perrotta R, Libra M, McCubrey JA, et al. Melanoma: molecular pathogenesis and emerging target therapies. Int J Oncol 2009;34:1481-9.

Cell cycle inhibition by sigma ligands enhances anti-MCSP:TRAIL-induced apoptosis in human melanoma cells: monitoring synergy with FDG and FLT

Anna A.Rybczynska,#[1] Marco de Bruyn,#[2]
Philip H. Elsinga,[1] Wijnand Helfrich,[2]
Rudi A.J.O. Dierckx,[1,3] and Aren van Waarde,[1]

#Contributed equally.

[1]Nuclear Medicine and Molecular Imaging, University Medical Center Groningen, University of Groningen, Groningen, The Netherlands

[2]Surgery, Surgical Research Laboratories, University Medical Center Groningen, University of Groningen, Groningen, The Netherlands

[3]Nuclear Medicine, Ghent University, Ghent, Belgium

Chapter 8

(submitted)

Abstract

Sub-toxic amounts of sigma ligands enhance apoptosis in A375M melanoma cells induced by sTRAIL (a tumor-selective pro-apoptotic protein). Although we have previously established a caspase-dependent mechanism of synergy, the precise mechanism of interaction remained elusive. In this study, we asked whether early metabolic responses to treatment, monitored with radioactively labeled thymidine and glucose analogs (^{18}F-FLT and ^{18}F-FDG) in cancer and non-cancer cells, reflect enhanced apoptotic signaling and can provide insight into underlying molecular events. Sigma ligands and anti-MCSP:TRAIL synergistically eliminated A375M and A2058 (human metastatic melanomas) but not HUVEC (human umbilical vein endothelial) cells. PI staining followed by FACS analyses showed that sigma ligand-treated A375M cells increased in G1/G0-phase and decreased in S-phase fraction in a dose-dependent manner. Addition of anti-MCSP:TRAIL abrogated both effects and increased the apoptotic cell fraction, as demonstrated by analysis of the cell cycle and the ^{18}F-FLT uptake. Cellular ATP levels quantified by bioluminescence additively decreased and ^{18}F-FDG uptake synergistically increased after co-treatment. ^{18}F-FLT and ^{18}F-FDG uptake studies demonstrate that a combination of sigma ligands with anti-MCSP:TRAIL changes cell cycle distribution and strongly depletes cellular energy levels in cancer cells. However, ^{18}F-FDG uptake is not a direct reflection of synergy and changes of ^{18}F-FLT uptake are too small to be easily quantified in vivo. Therefore, the mechanism of cooperation should be always considered when selecting a tracer for pre- and clinical studies.

Keywords: sigma receptor ligands, TRAIL, enhanced apoptotic signaling, cell cycle, ^{18}F-FDG, ^{18}F-FLT

Introduction

Melanoma is the most deadly dermatologic malignancy and is responsible for 80% of deaths from skin cancer. This high mortality is due to its high metastatic potential. Only during the early stages of malignant melanoma, surgical resection is a viable treatment option. However, metastatic melanoma does not respond to current therapies [1].

A promising compound for the safe elimination of melanoma cells is the immune effector molecule, Tumor Necrosis Factor Related Apoptosis Inducing Ligand (TRAIL) [2]. TRAIL selectively forces superfluous and potentially dangerous cells, such as cancer cells, to undergo programmed cell death, or apoptosis, with minimal or no activity towards normal cells [3]. The effectiveness and safety of TRAIL receptor ligand preparations (rhApo2L/TRAIL), alone or in combination with other anti-cancer agents, was already evaluated in human subjects. Interestingly, recombinant soluble TRAIL (sTRAIL) has shown tumoricidal activity towards melanoma cell lines resistant to therapy with other cytokine-based therapeutics and promises to be the most effective cytokine for treatment

of melanoma [4].

Previously, we genetically fused sTRAIL to an antibody fragment (scFv) directed against the human melanoma chondroitin sulfate proteoglycan (MCSP) [5]. The resulting anti-MCSP:TRAIL fusion protein selectively binds to and induces apoptosis in MCSP-positive cancer cells, with no toxicity towards normal cells [5].

However, many tumor cell lines and almost all primary tumor cells are TRAIL-resistant and require sensitization for sTRAIL-induced apoptosis [3]. The reason for this resistance is not completely clear, but alterations in cancer cell death pathways likely play a pivotal role. Therefore, a combination of two anti-cancer agents with different cellular targets, but intercalating mechanisms of action, is warranted to establish sensitization. Previously, we have demonstrated that promising compounds for combination treatment with anti-MCSP:TRAIL are sigma ligands, e.g. rimcazole [5] or haloperidol (unpublished results).

Sigma receptors are strongly over-expressed in rapidly proliferating cells, like cancer cells [6,7]. Recent studies have confirmed that sigma receptors play a pivotal role in regulating growth of both cultured cancer cells and *in vivo* tumors [8]. More importantly, *in vitro* and/or *in vivo* treatment with sigma ligands is very effective in killing a variety of cancer cells like melanoma, ovarian, colon, prostate cancer and leukemia cells [9]. Many sigma ligands are used in clinical practice (haloperidol for treatment of psychosis, fluvoxamine and opipramol for handling depression, donepezil and memantine for treatment of Alzheimer's disease, noscapine and dextromethorphan for suppression of cough). In addition, rimcazole was tested as an antipsychotic with reduced extrapyramidal side-effects, but it proved to lack the expected efficacy in schizophrenic patients. Currently rimcazole is being re-tested in clinical trials and re-profiled for treatment of cancer (Modern Biosciences). Sigma receptors are therefore relevant targets in the development of novel anti-cancer drugs [10]. Although the exact mechanism of action remains to be elucidated, the ability of sigma ligands to eliminate cancer cells is known to involve both caspase-dependent and caspase-independent mechanisms [11]. Moreover, sigma ligands (e.g. haloperidol or PB28) decrease expression and/or activity of p-glycoprotein (P-gp), a drug efflux pump implicated in multidrug resistance (MDR) [8]. Recent data show that sigma ligands can potentiate the action of several well known chemotherapeutic agents (e.g. haloperidol: doxorubicin, vinblastin, epirubicin and actinomycin D) [12,13]. Despite the broad utility, the dose of sigma ligands required for elimination of most adherent cancer cell lines is relatively high (20 -100 μM), a consequence of the fact that high sigma receptor occupancy is required for cell killing [14]. In combination therapy (as opposed to single agent therapy), lower (sub-toxic) doses of sigma ligands might be used.

Previously, we have shown that: 1. the cooperation between sTRAIL and sigma ligand, rimcazole, occurs exclusively in cancer cells, but not in normal cells like primary

human hepatocytes, and is based on increased caspase-8 and caspase-9 activation, 2. TRAIL-1 and TRAIL-2 receptor expression is not altered by rimcazole or haloperidol treatment, 3. the sigma-2 subpopulation participates in the cytotoxicity, and 4. the maximum synergistic effect between anti-MCSP:TRAIL and sigma ligands appears to occur at a sub-toxic dose of sigma ligands [5,14]. Although we and others speculated that binding of sigma-2 receptors by sigma ligands induces dose-dependent sensitization to apoptotic stimuli by repressing anti-apoptotic processes [5,15], the precise mechanism underlying the synergy remained unknown.

Here, we used ^{18}F-labeled metabolic tracers, ^{18}F-FLT (3'-deoxy-3'-fluorothymidine, measures thymidine kinase 1 activity) [16] and ^{18}F-FDG (fluorodeoxyglucose, measures glucose transport and/or metabolism) [17], to examine the manner in which a low dose of sigma ligand enhances sTRAIL-induced cancer cell death. Since tumors consist not only of tumor cells but to a large extension also of inflammatory tissue, *in vivo* assessment of the early metabolic responses of tumor cells to combination treatment can be difficult. Therefore, we selected an *in vitro* system to gain insight into the melanoma cell metabolism after sigma ligand and sTRAIL treatment, and for studying the mechanisms underlying synergy of this drug combination.

Materials & Methods

Culture Media and Drugs

DMEM (high-glucose) medium was purchased from Sigma. Fetal calf serum (FCS) was obtained from Bodinco, and trypsin was a product of Invitrogen. The pan-caspase inhibitor N-benzyloxycarbonyl-valyl-alanyl-aspartyl-fluoromethylketone (zVAD-fmk) was from Calbiochem, dissolved at 10 mM in DMSO and used at a final concentration of 10 μM. Rimcazole, haloperidol, α-tocopherol and trypan blue [0.4% solution in phosphate-buffered saline] were purchased from Sigma. Rimcazole and haloperidol stocks (3.9 mM and 4.8 mM) were prepared in ethanol with slight heating. α-tocopherol was dissolved in ethanol to 200 mg/ml and further in FSC to a stock concentration of 50 mg/ml. The synthesis and further production of anti-MCSP:TRAIL in CHO-K1 cells have been described previously [5].

Radiopharmaceuticals

^{18}F-FLT and ^{18}F-FDG were prepared by standard procedures reported in the literature [18]. ^{18}F-FLT was prepared according to Machulla *et al.* [19]. The specific activity of the final product was >10 TBq/mmol. ^{18}F-FDG was synthesized according to Hamacher *et al.* [20) by an automated synthesis module [21]. The specific radioactivity was always more than 10 (usually between 50 and 100) TBq/mmol. All radiopharmaceuticals were sterile and their radiochemical purities were greater than 95%.

Cell Culture

The malignant human melanoma cell lines A375M and A2058 (MCSP-positive) were purchased from and characterized (STR profiling, karyotyping, isoenzyme analysis) by the American Type Culture Collection (ATCC). A375M and A2058 were previously characterized for MCSP expression [5,22] and sigma receptor content [9,23]. Melanoma cell lines were cultured at 37°C, in a humidified 5% CO2 atmosphere, in DMEM (high-glucose) supplemented with 10% FCS. Before each experiment, the cells were seeded in 12-well plates (Costar). An equal number of cells was dispensed in each well and was supplied with 1.0 ml of complete cell culture medium. Human umbilical vein endothelial cells (HUVEC) were isolated as previously described [24]. HUVEC cells were used before culture passage number four and were grown in 6-well plates to 60% confluency before each experiment.

Uptake Studies

Drug treatment was performed 24 h after seeding cells in 12-well plates when confluency had reached 40 to 45%. Based on our previous results, cellular uptake of metabolic PET tracers was determined after 20-24 h incubation with sigma ligand (15 µM rimcazole, 38 µM haloperidol) and/or 100 ng/ml anti-MCSP:TRAIL [5,14]. For experiments involving α-tocopherol, A375M cells were incubated for 24 h with 48 µM haloperidol and/or 200 µg/ml α-tocopherol. Experiments were performed in 3-5 repeats for HUVEC and 6-16 repeats for A375M cells. At time zero, a PET tracer (2 MBq of ^{18}F-FDG or ^{18}F-FLT, in < 25 µl of saline) was added to each well. After 45 min of incubation the medium was quickly removed and the monolayers were washed 3 times with warm PBS. Cells were then treated for < 5 minutes with 0.2 ml of trypsin. When the monolayer had detached from the bottom of the well, 1 ml of complete cell culture medium was applied to stop the proteolytic action. Cell aggregates were resolved by repeated pipetting of the cell suspension. Radioactivity was assessed using a gamma counter (Compugamma 1282 CS; LKB-Wallac).

A sample of the suspension was mixed with trypan blue solution (1:1 v/v) and used for cell counting. Cell numbers were manually determined, using a phase-contrast microscope (Olympus), a Bürker bright-line chamber (depth 0.1 mm; 0.0025 mm^2 squares), and a hand-tally counter. Uptake of radioactivity was normalized to the number of viable cells. Less than 3% of administered ^{18}F-FDG or 7% of administered ^{18}F-FLT was taken up by the cells under these conditions.

Scoring of Cell Number Decrease after Treatment

Cytotoxicity experiments were performed in parallel with uptake studies. After assessment of tracer uptake with a gamma counter, a sample of the cell suspension was

mixed with trypan blue solution (1:1 v/v) and used for cell counting (see above).

Additive or synergistic apoptotic effects were determined using the cooperativity index (CI). CI was calculated by the following formula: the sum of the effects induced by both single-agent treatments divided by the effect induced by combination treatment. When CI ≤ 0.9, treatment was termed synergistic; when 0.9 < CI ≤ 1.1, treatment was termed additive; when CI > 1.1, treatment was termed antagonistic.

ATP Assay

Cellular ATP was measured with a kit based on firefly (Photinus pyralis) luciferase (ATPlite Luminescence ATP Detection Assay System; Perkin-Elmer). The bioluminescence was quantified using a Lumicount microplate luminometer (Packard Instruments Co.). A reaction blank and a standard curve with 9 concentrations of ATP were run in parallel. The assay was linear over a large range of ATP concentrations (10^{-7} to 10^{-4} mol/L) and of cell numbers in the assay. Cell samples were diluted to ensure that the concentration of ATP was within the range of the calibration curve.

Western Blot Analysis

A375M cells were plated in two T75 flasks and used for control experiment or rimcazole (15 μM, 24 h) treatment. Similarly to the tracer uptake studies, floating dead cells were removed by PBS washing. Remaining attached cells were lysed and centrifuged 14.000 rcf (10 min, 4°C). Nuclear fraction (pellet) was discarded. All supernatants were collected, analyzed for protein content by Bradford assay, boiled for 5 min and frozen in -80°C until use. Cellular proteins (30 μg) were size fractioned on a 7.5% SDS-PAGE (Biorad, Veenendaal, The Netherlands) and transferred onto activated PVDF membranes (Milipore, Etten-Leur, The Netherlands). Primary antibody: polyclonal anti-HKII antibody (diluted 1:200, Abcam) or monoclonal anti-GAPDH antibody (diluted 1:10000, Abcam); and secondary antibody: horseradish peroxidase-conjugated goat anti-rabbit or anti-mouse antibodies (diluted 1:1500, DAKO, Glostrup, Denmark) were used for detection by chemiluminescence (BM Chemiluminescence blotting kit, Roche Biochemicals, Mannheim, Germany). Quantification of the band intensity was performed using ImageJ software (version 1.43; NIH, USA). For determination of the expression levels of HK-II, the band intensity of HK-II was divided by the band intensity of GAPDH. The HK-II expression after rimcazole treatment was expressed as percent of control.

Propidium Iodide (PI) Staining and Flow Cytometric Analysis

A375M cells were plated at 3.0×10^4 cells/well in a 48-well plate containing 0.25 ml of culture medium and allowed to adhere overnight. Subsequently, cell medium was exchanged and the cells were concurrently treated with sigma ligands and/or

anti-MCSP:TRAIL in a total volume of 0.25 ml. After about 20h of incubation, the cells were washed with 0.25 ml of warm PBS, incubated in 0.1 ml trypsin and re-suspended in 0.2 ml of culture medium. Supernatants and trypsinized cells were collected into 2 ml tube and centrifuged (1800 rpm, 3 min.). The cell pellet was subsequently re-suspended in 1 ml PBS and fixed for 15 min on ice in 2.5 ml ethanol (final concentration approx. 70% v/v). Fixed cells were washed three times in PBS, where each washing step was followed by centrifugation (1500 rpm, 5 min), and stained with PI solution containing: 50 µg/ml PI, 0.01 mg/ml RNase A and 0.05% Triton X-100 in PBS (40 min, 37ºC). Cellular DNA content was determined with a FACSCalibur (Becton Dickinson). Data were plotted using CellQuest software (Becton Dickinson); at least 5,000 events were analyzed for each sample.

Statistics

Results are expressed as mean ± SEM. Statistical analyses were performed using SPSS 14.0 software and differences between groups were examined using 1-way ANOVA. When a significance of $P < 0.05$ was found, a post-hoc test for multiple comparisons was used (Bonferroni, $P < 0.05$). Significant changes are indicated with an asterisk.

Results

Synergistic Decrease in Melanoma Cell Number

Co-treatment of A375M and A2058 cells with sub-toxic doses of sigma ligands, rimcazole or haloperidol, and anti-MCSP:TRAIL for 24h resulted in a greater loss of viable cells than mono-treatment ($P < 0.001$) (Fig. 1). More importantly, the loss of viable cells after drug combination indicated synergy in A375M cells (Fig. 1A) and strong additive effect in A2058 cells (Fig. 1B). The cooperativity index (CI) for co-treatment of A375M cells with anti-MCSP:TRAIL and rimcazole was 0.77 compared to 0.51 for anti-MCSP:TRAIL and haloperidol. The cooperativity index (CI) for co-treatment of A2058 cells with anti-MCSP:TRAIL and rimcazole was 0.94.

Cell Cycle Arrest

Morphological changes, like dispersed cell localization and decrease in number of cell-cell contacts, in A375M cells following treatment with 15 µM rimcazole or 38 µM haloperidol appeared indicative of cell cycle arrest in addition to a loss of cell viability. Therefore, we examined the inhibition of A375M cell proliferation after administration of haloperidol. The inhibition of proliferation was dose-dependent (Fig. 2A) and occurred even at low concentrations of haloperidol that did not result in any loss of cell viability after 24 h. Furthermore, we studied the distribution of A375M cells among different phases of the cell cycle following treatment with 15 µM rimcazole or 38 µM haloperidol in

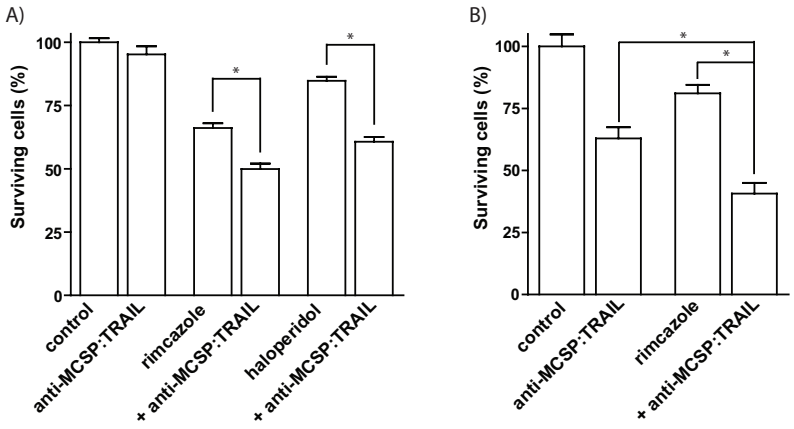

Fig. 1. Co-treatment reduces the number of A) A375M cells; B) A2780 cells.

the presence or absence of 100 ng/ml anti-MCSP:TRAIL. As expected, mono-treatment with anti-MCSP:TRAIL did not alter the cell cycle distribution (Fig. 2B). In contrast, treatment with rimcazole or haloperidol increased the fraction of G1/G0 cells by 12 to 16%. Co-treatment with anti-MCSP:TRAIL and rimcazole or haloperidol restored the percentage of G0/G1 cells to the control value (Fig. 2B). Treatment of A375M cells with sigma ligands and anti-MCSP:TRAIL in the presence of 10 μM of pan-caspase inhibitor zVAD-fmk abrogated the synergistic loss of viable cells (Figs. 2C and 2D), but did not affect cell death induced by sigma ligands alone [5]. In addition, analysis of the fraction of cells in G0/G1 phase demonstrated that addition of zVAD-fmk to anti-MCSP:TRAIL with haloperidol prevents restoration of the control values for the fraction of G0/G1 cells (Fig. 2E, right bar).

Changes in Metabolic Tracer Uptake

^{18}F-FLT: Treatment of A375M with anti-MCSP:TRAIL did not alter ^{18}F-FLT uptake per viable cell compared to control (Fig. 3A). However, treatment with both rimcazole and haloperidol resulted in a decrease of ^{18}F-FLT uptake per viable cell to 27.5 ± 2.1% and 30.4 ± 1.1% of the control value, respectively. Furthermore, co-treatment of A375M cells with anti-MCSP:TRAIL and rimcazole or haloperidol increased ^{18}F-FLT uptake up to 37.7 ± 1.0% ($P < 0.001$) and 41.1 ± 2.3% ($P < 0.05$) in comparison to treatment with these sigma ligands alone. Interestingly, changes in ^{18}F-FLT uptake after sigma ligand treatment and co-treatment closely monitored changes in the fraction of S-phase cells determined by PI staining ($P < 0.05$) (Fig. 3B).

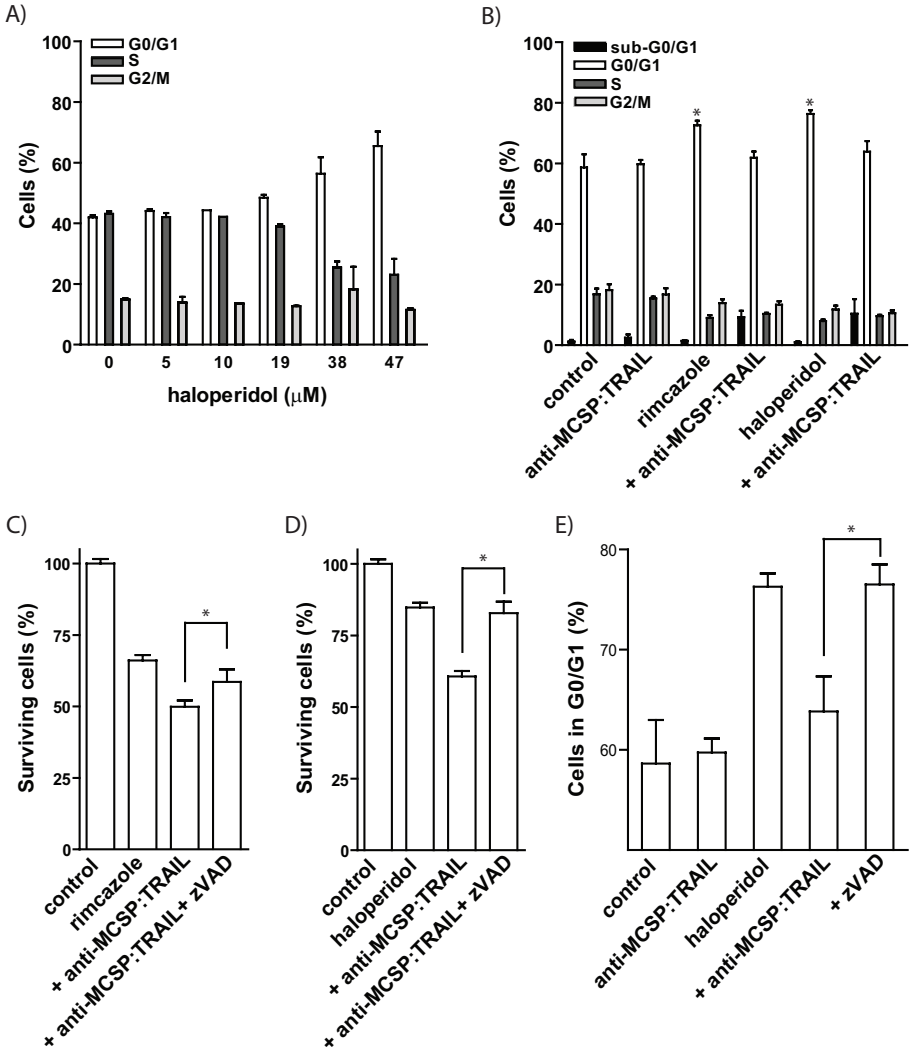

Fig. 2. Effect of treatment on cell proliferation: A) dose-dependent increase of G0/G1 fraction of A375M cells by haloperidol; B) synergy between sigma ligands and anti-MCSP:TRAIL depends on the G0/G1 stage of the cell cycle (sub-G0/G1 indicates the apoptotic cells); C) zVAD-fmk abrogates potentiating of anti-MCSP:TRAIL signaling by rimcazole; D) zVAD-fmk abrogates potentiating of anti-MCSP:TRAIL signaling by haloperidol; E) zVAD-fmk inhibits anti-MCSP:TRAIL-induced killing of cells arrested in G0/G1.

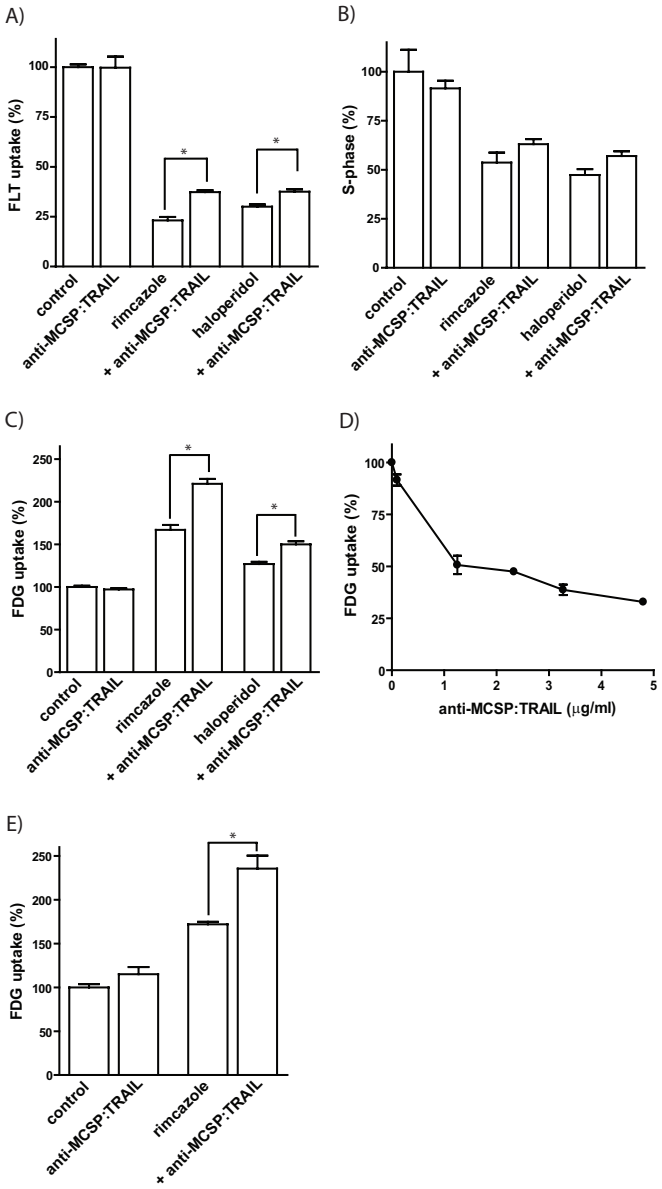

Fig. 3. Changes in: A) cellular ^{18}F-FLT uptake; B) fraction of cells in S-phase; C) cellular ^{18}F-FDG uptake after co-treatment of A375M with sigma ligands and anti-MCSP:TRAIL or D) mono-treatment of A375M cells with anti-MCSP:TRAIL; E) cellular ^{18}F-FDG uptake after co-treatment of A2058 with rimcazole and anti-MCSP:TRAIL.

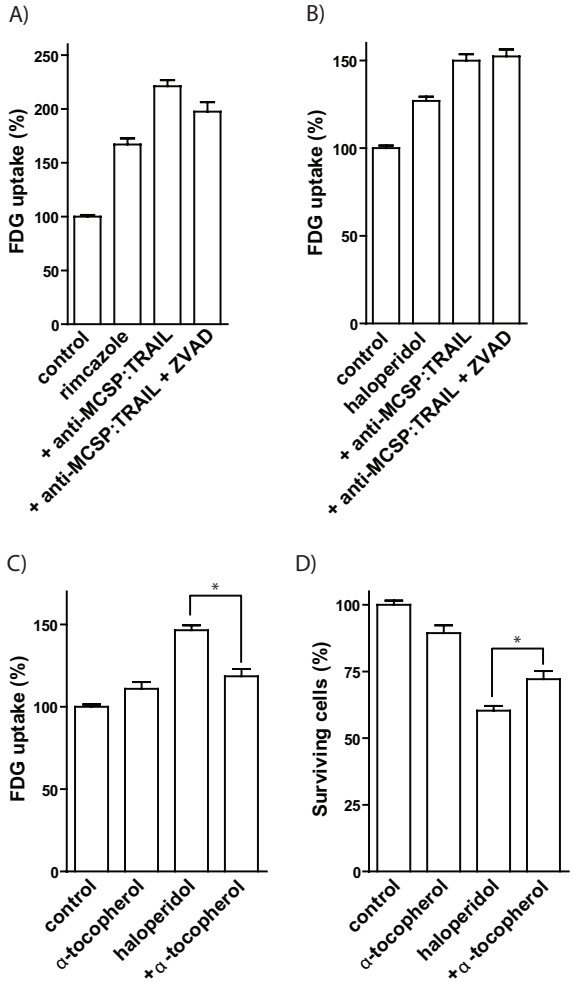

Fig. 4. ZVAD-fmk does not block the increase of ^{18}F-FDG uptake after co-treatment with anti-MCSP:TRAIL and A) rimcazole, B) haloperidol. α-tocopherol C) reduces increase of ^{18}F-FDG uptake and D) increases viability in A375M cells after haloperidol treatment.

^{18}F-FDG: Incubation of A375M cells with rimcazole and haloperidol resulted in a significant increase of ^{18}F-FDG uptake per viable cell (by 66.9 ± 5.8% and 26.9 ± 2.5%, respectively). In contrast, treatment with a sub-toxic concentration of anti-MCSP:TRAIL did not alter the uptake of ^{18}F-FDG (Fig. 3C). The synergistic decrease in viable A375M cells was reflected by a synergistic increase of ^{18}F-FDG uptake by 121 ± 5.8% and 49.9 ± 3.7% ($P << 0.05$) with CI values of 0.55 and 0.54 for co-treatment with rimcazole

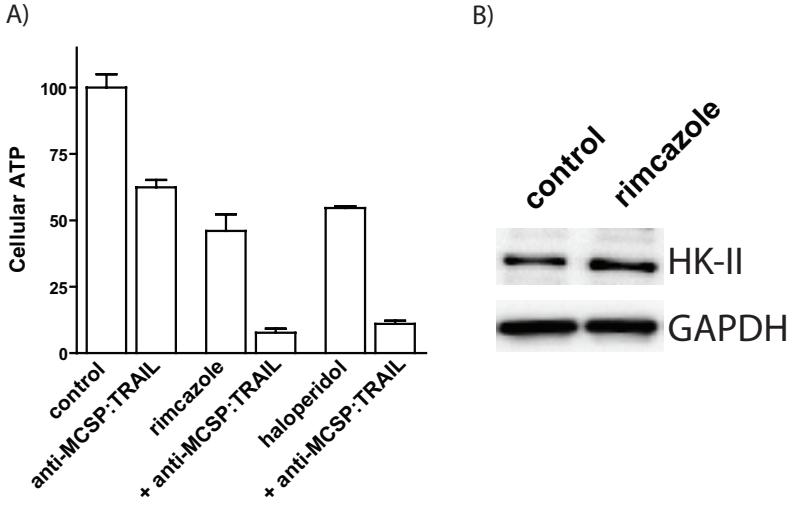

Fig. 5. Changes in A) cellular ATP content after single-agent and co-treatment, B) cellular HEX-II expression after rimcazole treatment.

or haloperidol, respectively. Interestingly, incubation with increasing concentrations of anti-MCSP:TRAIL induces a dose-dependent decrease in ^{18}F-FDG uptake (Fig. 3D). ZVAD-fmk did not significantly block the synergistic increase of ^{18}F-FDG uptake (Figs. 4A and 4B). Interestingly, α-tocopherol blocked the increase of ^{18}F-FDG uptake in A375M cells treated with a high dose of haloperidol by 28% ($P < 0.001$) (Fig. 4C) and increased the survival of these cells by 12 % ($P < 0.05$) (Fig. 4D). Similarly, in A2058 cells rimcazole treatment increased ^{18}F-FDG uptake per viable cell by 73 ± 2.9%, anti-MCSP:TRAIL did not alter the uptake of ^{18}F-FDG and co-treatment with rimcazole and anti-MCSP:TRAIL resulted in a synergistic increase of ^{18}F-FDG uptake by 136 ± 14.7% ($P < 0.001$) with CI value of 0.65 (Fig. 3E).

Changes of cellular ATP levels

The large increase of glucose consumption after co-treatment could indicate changes in cellular energy levels. Therefore, we determined ATP content in A375M cells after drug treatment. Incubation with anti-MCSP:TRAIL, haloperidol or rimcazole for 24h decreased the amount of ATP per cell to 62.5 ± 2.8%, 54.6 ± 0.7% and 46 ± 6.3% of control, respectively. Furthermore, co-treatment with haloperidol or rimcazole resulted in further dramatic decrease of cellular ATP content to 11.1 ± 1.2% and 7.7 ± 1.5% of control, respectively (Fig. 5A). However, drug-induced ATP depletion displayed no synergy (CIs ≈ 1).

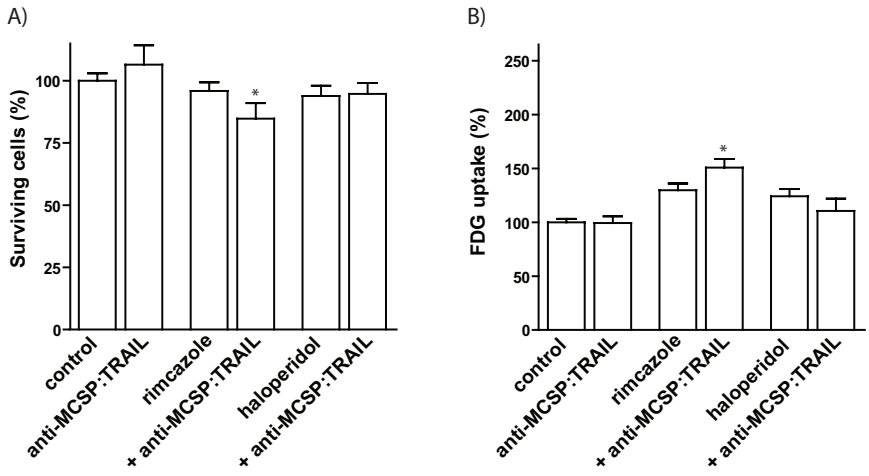

Fig. 6. Responses of HUVEC to single-agent and combination treatment: A) surviving cells, B) ^{18}F-FDG uptake.

Changes hexokinase-II expression

Decrease of cellular ATP by sigma ligands may activate a survival cascade in the cell and increase the expression of hexokinase-II (HK-II), a first enzyme on a glycolytic pathway of ^{18}F-FDG. Incubation of A375M cells with rimcazole for 24 h increased the expression of HK-II by 28-55% (Fig. 5B).

Synergy does not affect HUVEC Cells

To determine the effect of co-treatment in untransformed cells, we used healthy human umbilical vein endothelial cells (HUVEC). Doses of sigma ligands and anti-MCSP:TRAIL which resulted in elimination of A375M cells did not affect the viability of HUVEC (Fig. 6A). The combination of rimcazole and anti-MCSP:TRAIL did not significantly decrease the number of HUVEC cells ($P > 0.05$).

In contrast to A375M cells, HUVEC cells treated with haloperidol or co-treated with haloperidol and anti-MCSP:TRAIL did not respond with increased ^{18}F-FDG uptake (Fig. 6B). However, moderate, but significant, (29.8 ± 6.3% ($P < 0.01$) and 50.8 ± 8% ($P < 0.001$)) increases in ^{18}F-FDG uptake were observed after both single agent treatment with rimcazole and co-treatment with rimcazole and anti-MCSP:TRAIL, respectively. The increases of ^{18}F-FDG uptake in HUVEC cells were more than two fold smaller than those observed in A375M melanoma.

Discussion

Previously, we have observed that sigma ligands strongly enhance apoptosis triggered by the newly developed melanoma-targeted anticancer agent, anti-MCSP:TRAIL. As it is of interest to get further insight into the mechanism of action of this promising drug combination, we employed metabolic tracers, ^{18}F-FLT and ^{18}F-FDG, in an *in vitro* assay and showed that combination of sigma ligands with anti-MCSP:TRAIL changes cell cycle distribution and strongly depletes cellular energy levels in cancer cells.

Cell cycle

Previously, Azzariti *et al.* reported that the sigma ligand, PB28, inhibits breast cancer cell proliferation by increasing the G1 population by ~ 20% in a dose- and time-independent manner [25]. Here we show that the sigma ligand, haloperidol, similarly inhibits proliferation of A375M melanoma cells by simultaneously increasing G0/G1-phase and decreasing S-phase population, but in a dose-dependent manner (Fig. 2A). The same effect was observed after rimcazole treatment (data not published). Co-treatment with anti-MCSP:TRAIL and rimcazole or haloperidol eliminated this arrested population by a mechanism which involves caspases, since the elimination is inhibited by zVAD-fmk (Fig. 2, C-E).

These findings are consistent with earlier work by Jin *et al.* [26] demonstrating increased susceptibility of H460 lung cancer and SW480 colon cancer cells to TRAIL-mediated apoptosis when cells were arrested in G0/G1. Their data suggest no changes in the levels of Bcl-2, Bcl-XL, FADD, DcR2, FLIP, IAPs or alteration in TRAIL-1 and TRAIL-2 receptor expression. Similarly, we observed no changes in TRAIL receptor expression level [5]. Therefore, synergy between sigma ligands and anti-MCSP:TRAIL likely relies on molecular changes that occur in cells arrested during the cell cycle. However, the precise mechanism of interaction needs further investigation.

^{18}F-FLT

The first metabolic PET tracer which we used to monitor effects of single agent and combination treatment on tumor cell metabolism was the nucleoside ^{18}F-FLT. Uptake of ^{18}F-FLT into tumor cells is related to the activity of the principal enzyme in the salvage pathway of DNA synthesis, thymidine kinase 1 (TK1). After being taken up by the cell, ^{18}F-FLT is phosphorylated by TK1 into ^{18}F-FLT-monophosphate, which is trapped in the cell. This activity is a biomarker of cell proliferation, as it is very low in the G0 and early G1 phase and reaches a maximum in the late G1 and S-phase of the cell cycle [27]. In our experiments, ^{18}F-FLT uptake per viable cell showed a strong decline after treatment of A375M cells with rimcazole and haloperidol (Fig. 3A), in accordance with the observed

cell cycle arrest at G0/G1 and a decrease mainly of the S-phase population (Figs. 2B, and 3B). Co-treatment with anti-MCSP:TRAIL attenuated this decrease (Fig. 3A), due to preferential elimination of G0/G1-arrested cells and a resulting slight increase of the S-phase fraction of the remaining cell population. Thus, the uptake of ^{18}F-FLT reflected changes of the S-phase fraction of A375M cells after combination treatment (Figs. 3A and 3B).

^{18}F-FDG

The second tracer which we employed was the glucose analog ^{18}F-FDG. The uptake of ^{18}F-FDG depends on the activity and expression of glucose transporters (GLUTs) and the enzymes performing the first step in glycolysis, hexokinases (HKs). ^{18}F-FDG uptake is used to indirectly assess population doubling time and cell viability. Measurement of changes in the tumor uptake of ^{18}F-FDG is considered a promising technique to monitor treatment response in various forms of cancer [28-30]. Previously, we have reported that sigma ligands increase glucose uptake in rat C6 glioma cell line after 16-20 h treatment despite their anticancer properties [14]. Treatment of A375M and A2058 melanoma cells with sigma ligand also resulted in increases of cellular ^{18}F-FDG uptake (Fig. 3C). In contrast, incubation of A375M cells with increasing anti-MCSP:TRAIL concentrations decreased the uptake of glucose (Fig. 3D). Finally, the synergistic decrease of cell numbers which was observed after co-treatment was accompanied by a significant and synergistic increase in ^{18}F-FDG uptake per viable cell in A375M and A2058 (Figs. 3C and 3E), but not in HUVEC (Fig. 6B). The increase in ^{18}F-FDG uptake after sigma ligand treatment was related at least partially to increased hexokinase II (HK-II) expression (Fig. 5B). However, the involvement also of glucose transporting systems (e.g. GLUT-1, GLUT-3) in the increase of ^{18}F-FDG uptake cannot be excluded.

Incubation with zVAD-fmk did not abrogate the increase of ^{18}F-FDG uptake after combination treatment (Figs. 4A and 4B) in contrast to the increase of apoptosis (Figs. 2C and 2D). Thus, although synergistic changes of ^{18}F-FDG uptake were observed after the combination treatment, ^{18}F-FDG uptake was no direct reflection of cell killing by the tested drug combinations.

In contrast, α-tocopherol partially prevented increase of ^{18}F-FDG uptake and decrease of viability in A375M cells triggered by a high dose of haloperidol (Figs. 4C and 4D). α-tocopherol is the major lipophilic chain breaking antioxidant which can regulate also protein expression, ROS and other free radical production and mitochondrial function. Oxidative stress and cellular ATP depletion have been reported to affect glucose uptake [31,32]. ROS production and early (24 h) ATP depletion have been shown in SK-MEL-28 melanoma after treatment with sigma ligands (haloperidol > ifenprodil tartrate >> carbetapentane citrate) [33]. We have observed a decrease of cellular ATP in

A375M melanoma following rimcazole or haloperidol treatment and a marked decrease in ATP after 24 h of co-treatment with sigma ligand and anti-MCSP:TRAIL. Such a strong decrease in cellular ATP (i.e. exceeding 50%) indicates excessive mitochondrial DNA damage and damage to respiratory complexes [34], as could be expected following a substantial induction of apoptosis. Because cells try to compensate for any loss of ATP, glucose uptake will be strongly increased if cellular ATP levels show a significant decline. Furthermore, a reduction of cellular ATP results in a reduction of the levels of cyclin D1 and cell cycle arrest, as was demonstrated after oligomycin-induced inhibition of mitochondrial ATPase [35]. Thus, cell cycle arrest and the observed increases of ^{18}F-FDG uptake may have a common origin.

Conclusion

Addition of anti-MCSP:TRAIL to rimcazole- and haloperidol-treated A375M cells preferentially eliminates cells arrested in G0/G1 by these sigma ligands. By this mechanism, sub-toxic doses of sigma ligands can potentiate caspase activation and the anti-tumor effects of recombinant sTRAIL, which may offer important therapeutic advantages: reduced sTRAIL dosing, limited side effects in patients undergoing cancer therapy, and increased chances of therapeutic success.

The uptake of ^{18}F-FDG and ^{18}F-FLT is differently affected after co-treatment. ^{18}F-FLT reflects the fraction of cells in S-phase and, therefore, the impact of combination therapy on tumor cell cycling. Synergistic changes of ^{18}F-FDG uptake after the combination treatment paralleled the synergistic induction of apoptosis. However, ^{18}F-FDG uptake was no direct reflection of treatment-induced apoptosis, since the increases of ^{18}F-FDG uptake were based on a caspase-independent mechanism.

References

1 Miller A, Mihm M. Melanoma. N Engl J Med 2006;3551:51-65.

2 McCarthy M, DiVito K, Sznol M, Kovacs D, Halaban R, Berger A, et al. Expression of Tumor Necrosis Factor-Related Apoptosis-Inducing Ligand Receptors 1 and 2 in Melanoma. Clin Cancer Res 2006;1212:3856-63.

3 Koschny R, Walczak H, Ganten TM. The promise of TRAIL--potential and risks of a novel anticancer therapy. J Mol Med 2007;859:923-35.

4 Griffith T, Chin W, Jackson G, Lynch D, Kubin M. Intracellular Regulation of TRAIL-Induced Apoptosis in Human Melanoma Cells. J Immunol 1998;1616:2833-40.

5 de Bruyn M, Rybczynska A, Wei Y, Schwenkert M, Fey G, Dierckx R, et al. Melanoma-associated Chondroitin Sulfate Proteoglycan (MCSP)-targeted delivery of soluble TRAIL potently inhibits melanoma outgrowth in vitro and in vivo. Molecular Cancer 2010;91:301.

6 Aydar E, Onganer P, Perrett R, Djamgoz MB, Palmer CP. The expression and functional characterization of sigma (sigma) 1 receptors in breast cancer cell lines. Cancer Lett 2006;2422:245-57.

7 Wheeler KT, Wang LM, Wallen CA, Childers SR, Cline JM, Keng PC, et al. Sigma-2 receptors as a biomarker of proliferation in solid tumours. Br J Cancer 2000;826:1223-32.

8 Colabufo N, Berardi F, Contino M, Niso M, Abate C, Perrone R, et al. Antiproliferative and cytotoxic effects of some sigma(2) agonists and sigma(1) antagonists in tumour cell lines. Naunyn-Schmiedeberg's Archives of Pharmacology 2004;3702:106-13.

9 Vilner BJ, John CS, Bowen WD. Sigma-1 and sigma-2 receptors are expressed in a wide variety of human and rodent tumor cell lines. Cancer Res 1995;55:408-13.

10 Vilner BJ, de Costa BR, Bowen WD. Cytotoxic effects of sigma ligands: sigma receptor-mediated alterations in cellular morphology and viability. J Neurosci 1995;15:117-34.

11 Zeng C, Vangveravong S, Xu J, Chang KC, Hotchkiss RS, Wheeler KT, et al. Subcellular localization of sigma-2 receptors in breast cancer cells using two-photon and confocal microscopy. Cancer Res 2007;6714:6708-16.

12 Kashiwagi H, McDunn JE, Simon PO, Jr., Goedegebuure PS, Vangveravong S, Chang K, et al. Sigma-2 receptor ligands potentiate conventional chemotherapies and improve survival in models of pancreatic adenocarcinoma. J Transl Med 2009;7:24.

13 Kataoka Y, Ishikawa M, Miura M, Takeshita M, Fujita R, Furusawa S, et al. Reversal of vinblastine resistance in human leukemic cells by haloperidol and dihydrohaloperidol. Biol Pharm Bull 2001;246:612-7.

14 Rybczynska A, Dierckx R, Ishiwata K, Elsinga P, van Waarde A. Cytotoxicity of {sigma}-Receptor Ligands Is Associated with Major Changes of Cellular Metabolism and Complete Occupancy of the {sigma}-2 Subpopulation. J Nucl Med 2008;4912:2049-56.

15 Spruce BA, Campbell LA, McTavish N, Cooper MA, Appleyard MV, O'Neill M, et al. Small molecule antagonists of the sigma-1 receptor cause selective release of the death program in tumor and self-reliant cells and inhibit tumor growth in vitro and in vivo. Cancer Res 2004;6414:4875-86.

16 Rasey JS, Grierson JR, Wiens LW, Kolb PD, Schwartz JL. Validation of FLT uptake as a measure of thymidine kinase-1 activity in A549 carcinoma cells. J Nucl Med 2002;439:1210-7.

17 Herholz K, Rudolf J, Heiss WD. FDG transport and phosphorylation in human gliomas measured with dynamic PET. J Neurooncol 1992;122:159-65.

18 Van Waarde A, Jager PL, Ishiwata K, Dierckx RA, Elsinga PH. Comparison of sigma-ligands and metabolic PET tracers for differentiating tumor from inflammation. J Nucl Med 2006;471:150-4.

19 Machulla HJ, Blocher A, Kuntzsch M, Piert M, Wei R, Grierson JR. Simplified Labeling Approach for Synthesizing 3'-Deoxy-3'-[18F]fluorothymidine ([18F]FLT). Journal of Radioanalytical and Nuclear Chemistry 2000;2432:843-6.

20 Hamacher K, Coenen HH, Stocklin G. Efficient stereospecific synthesis of no-carrier-added 2-[18F]-fluoro-2-deoxy-D-glucose using aminopolyether supported nucleophilic substitution. J Nucl Med 1986;272:235-8.

21 Medema J, Luurtsema G, Keizer H, Tilkema SP, Elsinga PH, Vaalburg W. Performance of a fully automated and unattended production system of [18F]FDG. J Labelled Compds Radiopharm. 42, s853-s855. 1999.

22 Schwenkert M, Birkholz K, Schwemmlein M, Kellner C, Kugler M, Peipp M, et al. A single chain immunotoxin, targeting the melanoma-associated chondroitin sulfate proteoglycan, is a potent inducer of apoptosis in cultured human melanoma cells. Melanoma Res 2008;182:73-84.

23 John CS, Bowen WD, Saga T, Kinuya S, Vilner BJ, Baumgold J, et al. A Malignant Melanoma Imaging Agent: Synthesis, Characterization, In Vitro Binding and Biodistribution of Iodine-125-(2-Piperidinylaminoethyl)4-Iodobenzamide. J Nucl Med 1993;3412:2169-75.

24 Mulder A, Blom N, Smit J, Ruiters M, Meer J, Halie MR, et al. Basal tissue factor expression in endothelial cell cultures is caused by contaminating smooth muscle cells. Reduction by using chymotrypsin instead of collagenase. Thrombosis Research 1995;805:399-411.

25 Azzariti A, Colabufo NA, Berardi F, Porcelli L, Niso M, Simone GM, et al. Cyclohexylpiperazine derivative PB28, a sigma2 agonist and sigma1 antagonist receptor, inhibits cell growth, modulates P-glycoprotein, and synergizes with

anthracyclines in breast cancer. Mol Cancer Ther 2006;57:1807-16.

26 Jin Z, Dicker DT, El Deiry WS. Enhanced sensitivity of G1 arrested human cancer cells suggests a novel therapeutic strategy using a combination of simvastatin and TRAIL. Cell Cycle 2002;11:82-9.

27 Direcks WGE, Lammertsma AA, Molthoff CFM. 3'-Deoxy-3'-18F-Fluorothymidine as a tracer of proliferation in positron emission tomography. In: Deoxynucleoside Analogs in Cancer Therapy , 441-462. 2006. Totowa, NJ: Humana Press Inc., Peters GJ (ed).

28 Geus-Oei LF, Vriens D, van Laarhoven HW, van der Graaf WT, Oyen WJ. Monitoring and predicting response to therapy with 18F-FDG PET in colorectal cancer: a systematic review. J Nucl Med 2009;50 Suppl 1:43S-54S.

29 Hicks RJ. Role of 18F-FDG PET in assessment of response in non-small cell lung cancer. J Nucl Med 2009;50 Suppl 1:31S-42S.

30 Schwarz JK, Grigsby PW, Dehdashti F, Delbeke D. The role of 18F-FDG PET in assessing therapy response in cancer of the cervix and ovaries. J Nucl Med 2009;50 Suppl 1:64S-73S.

31 Knowles H, Harris A. Hypoxia and oxidative stress in breast cancer: Hypoxia and tumourigenesis. Breast Cancer Res 2001;35:318-22.

32 Xing Y, Musi N, Fujii N, Zou L, Luptak I, Hirshman MF, et al. Glucose metabolism and energy homeostasis in mouse hearts overexpressing dominant negative alpha2 subunit of AMP-activated protein kinase. J Biol Chem 2003;27831:28372-7.

33 Nordenberg J, Perlmutter I, Lavie G, Beery E, Uziel O, Morgenstern C, et al. Anti-proliferative activity of haloperidol in B16 mouse and human SK-MEL-28 melanoma cell lines. Int J Oncol 2005;274:1097-103.

34 Rossignol R, Faustin B, Rocher C, Malgat M, Mazat JP, Letellier T. Mitochondrial threshold effects. Biochem J 2003;370Pt 3:751-62.

35 Gemin A, Sweet S, Preston TJ, Singh G. Regulation of the cell cycle in response to inhibition of mitochondrial generated energy. Biochem Biophys Res Commun 2005;3324:1122-32.

Treatment of ovarian carcinoma with sigma receptor ligands: preliminary data and perspectives

Chapter 9

Anna A.Rybczynska,[1] Marco de Bruyn,[2] Philip H. Elsinga,[1] Wijnand Helfrich,[2] Rudi A.J.O. Dierckx,[1,3] Ate G.J. van der Zee,[4] and Aren van Waarde,[1]

[1]Nuclear Medicine and Molecular Imaging, University Medical Center Groningen, University of Groningen, Groningen, The Netherlands

[2]Surgery, Surgical Research Laboratories, University Medical Center Groningen, University of Groningen, Groningen, The Netherlands

[3]Nuclear Medicine, Ghent University, Ghent, Belgium

[4]Gynecological Oncology, University Medical Center Groningen, University of Groningen, Groningen, The Netherlands

Introduction

Ovarian carcinoma (OC) remains the leading cause of gynecologic cancer deaths and its long-term survival rate has not improved in recent years [1,2]. Furthermore, while OC is highly responsive to platinum-based therapy after initial cytoreductive surgery, there is a very high risk (approx. 75%) for recurrences of refractory disease [3,4]. This is because OC acquires drug resistance [4,5]. Therefore, development and clinical implementation of novel targets for treatment and/or repression of drug resistance in advanced OC may improve disease-free survival.

Sigma ligands possess low toxicity towards normal cells, while they activate unique (caspase- and p53-independent) mechanisms of cancer cell death that slow down cancer cell proliferation and overcome therapy resistance (Chapter 2 and Chapter 8, [6-15]). Furthermore, sigma ligands can enhance the anti-cancer activity of various conventional chemotherapeutic agents [7,8,12] and novel tumor-selective, pro-apoptotic therapeutics (see Chapter 7-8 for anti-MCSP:TRAIL). As such, sigma ligands may be highly suitable, alone or in drug combination, for improving treatment outcome of refractory OC. In this chapter, we present preliminary data indicating that sigma ligand-based approaches may be of value for the treatment of OC and we discuss plans for future experiments.

Materials & Methods

Culture Medium and Reagents

RPMI 1640 medium was from Cambrex Bio Science (Verviers, France). DiOC6 was purchased from Eugene (The Netherlands). Primary anti-human sigma-1 receptor antibody (ab89655) was from Abcam. Secondary PE-labeled goat anti-rabbit antibody was from Southern Biotech. Rimcazole (BW 239U) and haloperidol were from Sigma Aldrich (Sigma-Aldrich Chemie B.V. Zwijndrecht, Netherlands). Stock solutions of rimcazole (3.9 mM in ethanol) and haloperidol (4.8 mM in ethanol) were freshly prepared for each experiment.

ScFv425:sTRAIL production

ScFv425:sTRAIL was produced as described previously [16]. Briefly, the high affinity antibody fragment scFv425 (Vh-(G4S)3-Vl format) (provided by Merck), was directionally inserted in the first multiple cloning site of vector pEE14, using the unique SfiI and NotI restriction enzyme sites. A PCR-truncated 593-bp DNA fragment encoding the extracellular domain of human TRAIL (sTRAIL) was cloned in-frame in the second multiple cloning site using restriction enzymes XhoI and HindIII, yielding plasmid pEE14-scFv425:sTRAIL. Expression plasmid pEE14-scFv425:sTRAIL was transfected into

Chinese hamster ovary K1 (CHO-K1) cells using FuGENE 6 reagent (Roche Diagnostics) according to the manufacturer's instructions. Successfully transfected cells were selected by the glutamine synthetase system. Single cell sorting using the MoFlo high speed cell sorter (Cytomation, Fort Collins, CO) established clone 100F1, stably secreting 2.4 µg/ml scFv425:sTRAIL into the culture medium.

Culture of ovarian cancer cell lines and primary ovarian cancer

OVCAR-3 and SKOV-3 were obtained from the American Tissue Culture Collection (ATCC). Both cell lines were cultured as monolayer at 37°C, in a humidified 5% CO_2 atmosphere and in RPMI 1640 medium supplemented with 10% fetal calf serum (FCS). Before each experiment cells were plated in 48-well plate in 250 µl of medium supplemented with 10% FCS.

Primary ovarian cancer cells were isolated from tumor masses or ascites using a mechanical separation method followed by purification with Cancer Cell Isolation Kit (Panomics). Isolated cancer cells (viability >60 %) were used within 5 days after isolation. In this period, primary ovarian cancer cells were maintained at 37°C, in a humidified 5% CO_2 atmosphere and in RPMI 1640 medium (Cambrex Bio Science, Verviers, France) supplemented with 10% fetal calf serum (FCS)

FACS staining of sigma-1 receptors

Staining of sigma-1 receptors was performed in human ovarian cancer cells in the exponential phase of growth. First, the dead floating cells were removed from culture by 2x washing with PBS. Adherent cells were detached with trypsin and counted. For permeabilization (Fix and Perm kit, Invitrogen), 600 000 cells were used for each sample. After permeabilization, cancer cells were incubated (30 min, in darkness at 4°C) with a primary rabbit antibody recognizing an internal domain of human sigma-1 receptor (dilution 1:1000) and washed 3x by resuspension in cold PBS and repeated centrifugation (5 min, 900 rpm). Afterwards, cells were incubated (30 min, in darkness at 4°C) with the secondary PE-labeled goat anti-rabbit antibody (dilution 1:100) and washed as above. Two negative controls were taken along for each condition (one, unstained cells; second, cells incubated only with the secondary but not primary antibody). Mean fluorescence intensity (MFI) was quantified by FACS (Accuri C6 Flow Cytometer, BD) and corrected for background and non-specific binding.

Combination Treatment with Sigma Ligands and scFv425:sTRAIL

Combination treatment with sigma ligands and scFv425:sTRAIL was assessed in ovarian cancer cells pre-cultured in a 48-well plate at a concentration of 3×10^4 cells/well. On the next day, cells were treated as indicated and apoptosis was assessed

by DiOC6 staining measuring changes of mitochondrial membrane potential (Δψ). After 24 h treatment, cells were harvested and incubated for 20 min with DiOC6 (0.1 μM) at 37°C, centrifuged (1000 x g, 5 min), re-suspended in PBS, and assessed for staining by flow cytometry (Accuri C6 Flow Cytometer, BD). Experiment was repeated three times in OVCAR-3 and SKOV-3.

Primary ovarian cancer cells were incubated (24 h) with: 1. scFv425:sTRAIL (300 ng/ml), 2. rimcazole (23 μM) or 3. rimcazole + scFv425:sTRAIL. Two methods for measurement of cytotoxicity were used: 1. trypan blue staining followed by manual counting of the dead and viable cells in the Bürker chamber, and 2. DiOC6 staining for decrease of mitochondrial membrane potential during the onset of apoptosis assessed by FACS (Accuri C6 Flow Cytometer, BD). Experiments were approved by the local Medical Ethics Committee and patients/healthy volunteers signed for informed consent.

Synergy was assessed by calculating the cooperativity index (CI) in which the sum of apoptosis induced by single-agent treatment is divided by apoptosis induced by combination treatment. When CI was less than 1, treatment was considered synergistic; when CI equalled 1, treatment was considered additive; when CI was greater than 1, treatment was considered antagonistic.

Preliminary results

Identification of sigma-1 receptors in OC

Only limited data (immunohistochemical staining, www.proteinatlas.com) is available on the expression levels of sigma-1 receptors in OC. We performed a fluorescent staining and flow cytometry (FACS) analysis to compare sigma-1 receptor levels in four ovarian cancer cell lines (SKOV-3, OVCAR-3, A2780, A2780/CP70) and in one short culture of primary ovarian carcinoma (POC) derived from a patient. The analysis indicated that sigma-1 receptors are present at high levels in ovarian cancer cell lines and

Table 1. Sigma-1 receptor staining in ovarian cancer

	Sigma-1 receptors [MFI]
SKOV-3	0
OVCAR-3	2.70×10^6
A2780	2.34×10^6
A2780/CP70	4.13×10^6
POC	4.27×10^6

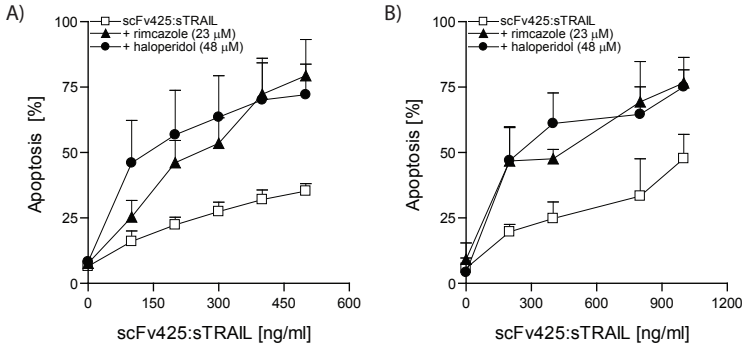

Fig.1. Synergistic enhancement of TRAIL-induced apoptosis by sigma ligands in ovarian cancer cell lines: A) OVCAR-3, and B) SKOV-3. Data are expressed as mean ± SEM. Differences between groups were examined using 1-way ANOVA. Significant differences ($P < 0.05$) were found between monotreatment and co-treatment conditions.

in primary ovarian carcinoma (Table 1). The order of the mean fluorescent intensity (MFI) for the total sigma-1 receptor pool is: POC ≈ A2780/CP70 > A2780 ≈ OVCAR-3. Sigma-1 receptors were not detected in SKOV-3. The observed difference in MFI between a drug-sensitive OC cell line (A2780) and a cisplatin-resistant variant of this cell line (A2780/CP70) may suggests that sigma-1 receptor expression is different in treatment-sensitive and -resistant OC cells.

Sigma ligands enhance TRAIL-induced apoptosis in OC cell lines and in short cultures of POC

Combined administration of a sigma-1/-2 ligand, rimcazole or haloperidol, and an EGFR-targeted TRAIL fusion protein (scFv425:sTRAIL) resulted in synergistic induction of apoptosis in OVCAR-3 and SKOV-3 cell lines (Fig. 1A-B).

In the next pilot study we evaluated the anti-cancer activity of combination treatment with the sigma ligand, rimcazole, and EGFR-targeted scFv425:sTRAIL or EpCAM-targeted scFvC54:sTRAIL, on POC cells derived from six POC patients. Patients were divided into two groups, responders and non-responders, based on the effect of combination treatment.

POC cells from four out of six patients (67%) responded synergistically to combination treatment with rimcazole and the EGFR-selective fusion protein scFv425:sTRAIL (Fig. 2A). Treatment for 24h with rimcazole, scFv425:sTRAIL or their combination resulted in induction of apoptosis in 17%, 27%, and 69% of short cultures

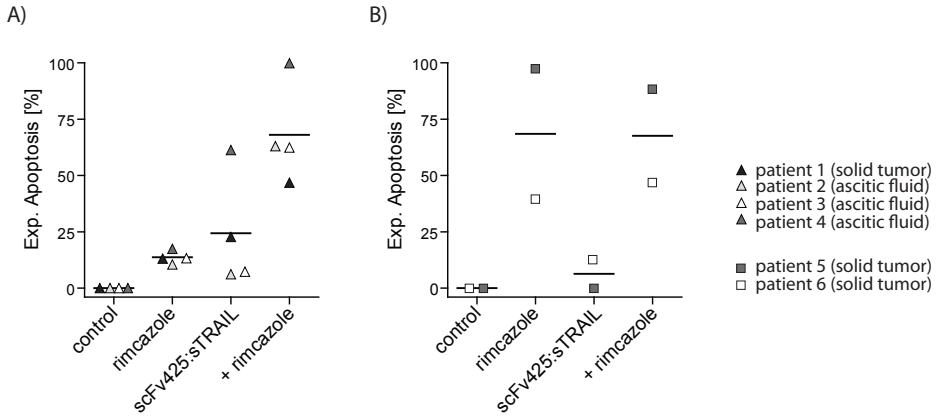

Fig.2. Synergistic enhancement of TRAIL-induced apoptosis by sigma ligands in patient-derived POC: A) samples responding to drug combination, B) samples already responding to rimcazole only.

of POC, respectively. A CI = 0.6 indicated synergism.

POC cells from two out of six patients (33%) showed no synergistic enhancement of apoptosis (Fig. 2B). However, single-agent treatment with rimcazole induced already apoptosis in ~ 68% of cancer cells derived from samples of these two patients. In these cells, scFv425:sTRAIL had a minimal effect on cell viability. Thus, cell death in combination treatment was comparable to cell death in treatment with rimcazole alone. These preliminary results indicate that both groups of patients might benefit from the rimcazole and scFv425:sTRAIL combination.

Conclusion

The data presented in this chapter are limited to two cell lines and six patient-derived POC. However, the strong apoptotic effect of the combination treatment with sigma ligand and TRAIL fusion protein in these cells encourages us to further evaluate this treatment in a greater number of OC cell lines and POC samples.

Rimcazole in combination with TRAIL preparations (particularly those currently under clinical and pre-clinical investigation) may be of potential value for the treatment of refractory ovarian carcinoma. This aspect will be explored in greater detail in the proposed project.

Perspectives

Our preliminary results indicate that it may be worthwile to perform a more detailed pre-clinical evaluation of sigma ligands for their suitability in the treatment of OC and other types of cancer. In the first part of such a project, one or two candidate sigma ligands may be identified for further evaluation regarding the treatment of refractory OC. Also, investigators could assess the phenotype(s) of OC patients that would be eligible for sigma ligand therapy. In the second part of the project, optimal treatment schemes (sequential- or co-administration or dosing of a sigma ligand with a conventional anti-cancer drug or TRAIL) can be determined, in order to overcome therapy resistance in OC.

To this end:

1. Anti-cancer activity of a small panel of selected sigma ligands should be evaluated using chemo-sensitive vs. chemo-resistant OC cell lines and patient-derived OC cells
2. Anti-cancer activity of sigma ligands should be correlated to the respective sigma receptor expression levels in an elaborate panel of chemo-sensitive and chemo-resistant OC cell lines and in patient-derived short-term cell cultures of OC. Sigma receptor expression must be determined in different phases of the cell cycle and after (pre-)treatment with various anti-cancer drugs.
3. MicroPET imaging with a suitable sigma ligand will be applied to evaluate sigma levels *in vivo* in xenograft tumor models of OC at various stages of disease.
4. Based on the outcome of the experiments described above, optimal combination treatment schemes (sequential or co-administration and dosing of sigma ligands with various conventional anti-cancer drugs) should be identified and evaluated for their efficacy and toxicity in established i.p. and s.c. xenografted mouse models of OC.

Finally, data obtained from this project will show if sigma ligands alone or in combination with various anti-cancer drugs (in particular, cisplatin and paclitaxel) can be applied to overcome drug resistance in OC. These results may significantly accelerate the testing of sigma ligands in a pilot clinical study in a small number of OC patients (e.g. undergoing peritoneal cavity wash).

References

1 Yap TA, Carden CP, Kaye SB. Beyond chemotherapy: targeted therapies in ovarian cancer. Nat Rev Cancer. 2009;9:167–81.

2 Rein BJD, Gupta S, Dada R, Safi J, Michener C, Agarwal A. Potential markers for detection and monitoring of ovarian cancer. J Oncol. 2011;2011:475983.

3 Herzog TJ. Recurrent ovarian cancer: how important is it to treat to disease progression? Clin Cancer Res. 2004;10:7439–49.

4 Vasey PA. Resistance to chemotherapy in advanced ovarian cancer: mechanisms and current strategies. Br J Cancer. 2003;89 Suppl 3:S23–8.

5 Matsuo K, Lin YG, Roman LD, Sood AK. Overcoming platinum resistance in ovarian carcinoma. Expert Opin Ivestig Drugs. 2010;19:1339–54.

6 Bowen WD, Jin B, Blann E, Vilner BJ, Lyn-Cook BD. Sigma receptor ligands modulate expression of the multidrug resistance gene in human and rodent brain tumor cell lines. Proc Am Assoc Cancer Res. 1997;38:479.

7 Kataoka Y, Ishikawa M, Miura M, Takeshita M, Fujita R, Furusawa S, et al. Reversal of vinblastine resistance in human leukemic cells by haloperidol and dihydrohaloperidol. Biol Pharm Bull. 2001;24:612–7.

8 Crawford KW, Bowen WD. Sigma-2 receptor agonists activate a novel apoptotic pathway and potentiate antineoplastic drugs in breast tumor cell lines. Cancer Res. 2002;62:313–22.

9 Crawford KW, Coop A, Bowen WD. Sigma(2) Receptors regulate changes in sphingolipid levels in breast tumor cells. Eur J Pharmacol. 2002;443:207–9.

10 Spruce BA, Campbell LA, McTavish N, Cooper MA, Appleyard MV, O'Neill M, et al. Small molecule antagonists of the sigma-1 receptor cause selective release of the death program in tumor and self-reliant cells and inhibit tumor growth in vitro and in vivo. Cancer Res. 2004;64:4875–86.

11 Colabufo NA, Berardi F, Contino M, Niso M, Abate C, Perrone R, et al. Antiproliferative and cytotoxic effects of some sigma2 agonists and sigma1 antagonists in tumour cell lines. Naunyn Schmiedebergs Arch Pharmacol. 2004;370:106–13.

12 Azzariti A, Colabufo NA, Berardi F, Porcelli L, Niso M, Simone GM, et al. Cyclohexylpiperazine derivative PB28, a sigma2 agonist and sigma1 antagonist receptor, inhibits cell growth, modulates P-glycoprotein, and synergizes with anthracyclines in breast cancer. Mol Cancer Ther. 2006;5:1807–16.

13 Dai Y, Wei Z, Sephton CF, Zhang D, Anderson DH, Mousseau DD. Haloperidol induces the nuclear translocation of phosphatidylinositol 3'-kinase to disrupt Akt phosphorylation in PC12 cells. J Psychiatry Neurosci. 2007;32:323–30.

14 Zeng C, Vangveravong S, Xu J, Chang KC, Hotchkiss RS, Wheeler KT, et al. Subcellular localization of sigma-2 receptors in breast cancer cells using two-photon and confocal microscopy. Cancer Res. 2007;67:6708–16.

15 Kashiwagi H, McDunn JE, Simon PO, Goedegebuure PS, Vangveravong S, Chang K, et al. Sigma-2 receptor ligands potentiate conventional chemotherapies and improve survival in models of pancreatic adenocarcinoma. J Transl Med. 2009;7:24.

16 Bremer E, Kuijlen J, Samplonius D, Walczak H, de Leij L, Helfrich W. Target cell-restricted and -enhanced apoptosis induction by a scFv:sTRAIL fusion protein with specificity for the pancarcinoma-associated antigen EGP2. Int J Cancer. 2004;109:281–90.

Summary

Chapter 10

The heterogeneous biology of cancer compels development of novel targeted therapeutics and suitable, personalized imaging methods (**Chapter 1**). This thesis describes the use of sigma ligands as new cancer-targeting therapeutics and cancer imaging tools.

Sigma receptors are a class of transmembrane proteins present in plasma, endoplasmic reticulum, mitochondrial and lysosomal membranes [1,2]. Initial research on sigma receptors was focused on the brain rather than on tumors [3], since several clinically used neuroleptic drugs were found to have high affinity towards sigma receptors. Overexpression of sigma receptors in tumor tissue and anti-tumor activity of sigma ligands were later reported [4-6] (**Chapter 2**).

Sigma receptors are more abundant in cancer tissue than in corresponding normal tissue [6]. Also, they have higher expression in high-grade *vs.* low-grade carcinomas [7]. This suggests that radiolabeled sigma ligands may be used for tumor detection and staging. Two studies aimed at evaluation of radiolabeled sigma ligand for cancer detection are described in the initial part of this thesis (**Chapter 3-4**).

Sigma ligands inhibit cancer cell proliferation and induce cancer cell death [8]. Furthermore, sigma ligands are capable of killing cancer cells with a drug-resistant phenotype and they enhance the oncolytic activity of chemotherapeutics [9,10]. Five studies aimed at evaluation of sigma ligands for cancer treatment are described in the second part of this thesis (**Chapter 5-9**).

Evaluation of Sigma Ligand, ^{11}C-SA4503, for Tumor Imaging

Several issues must be considered when developing and evaluating a radioligand for tumor imaging using PET. These issues will be discussed here in a context of the sigma-1 ligand, 1-(3,4-dimethoxyphenethyl)-4-(3-phenylpropyl)piperazine (SA4503), which was used in the research described in this thesis.

1. *Ligand must be amenable to labeling.*

A compound amenable to labeling with a positron emitter (^{11}C, ^{18}F) must be selected. The labeling should also be possible by a rapid synthetic procedure, because half-lives of PET radionuclides are short (see Table 1 in **Chapter 1**). Successful radiochemistry with PET isotopes ^{11}C and ^{18}F was reported for sigma ligand, SA4503 and its derivatives [11]. Whereas, ^{18}F-derivatives of SA4503 displayed similar affinity to sigma-1 and sigma-2 receptors, ^{11}C-SA4503 was selective for sigma-1 receptors. ^{11}C-SA4503 was already used in human volunteers and is the most widely employed sigma ligand for PET. Labeling of SA4503 with ^{11}C is reliable (uses our routine, automated synthesis method with ^{11}C-methyl iodide as a building block) and results in a product with sufficient yield, high specific radioactivity and radiochemical purity (Table 1A) [12,13].

2. *Small molecular size. Lipophilicity. Charge.*

The blood-brain barrier (BBB) is a complex membranous structure that protects brain and spinal cord from potentially harmful substances present in the circulating blood, whereas it allows access of the essential substances such as glucose and oxygen [14]. The BBB may create a problem in visualization and treatment of brain tumors by limiting the uptake of radiopharmaceuticals and therapeutic drugs [14,15], even though some brain tumors can disrupt the BBB and allow entry of a broader range of compounds into the brain. Problems remain because the changes in permeability of the BBB are usually local and nonhomogenous [16]. Therefore, the BBB must be considered when developing a tracer for imaging of brain tumors. Compounds that pass the BBB must be small (molecular mass smaller than 600 Da), moderately lipophilic (logP between +2 and +3, as higher lipophilicity promotes nonspecific binding of the compound) and optimally charged (pKa between 7.4 and 8.3) [17-19]. ^{11}C-SA4503, due to its small-size, favorable lipophilicity and optimal charge (Table 1B), is capable of reaching intracellular binding sites by penetrating biological membranes, and entering the brain by passive diffusion across the BBB [20](**Chapter 3-4**).

Furthermore, these features allow fast distribution of the compound throughout the body. An *in vitro* study with ^{11}C-SA4503 has shown that this tracer binds rapidly to tumor cells, whereas *in vivo* experiments indicated a rapid blood clearance and distribution to target tissues (Table 1B) [13]. Importantly, a rapid uptake in C6 tumors was followed by minimal washout, whereas no detectable washout occurred from spontaneous pituitary tumors in rats within 60 min after tracer injection (**Chapter 3-4**).

3. *High affinity for target. High density of target in tumor.*

For good visualization of the receptors by PET, the ratio of specifically bound (B) ligand and free background radioactivity (F) must be sufficient ($B/F \geq 4$). An elevated B/F ratio results from a high affinity of the ligand (low dissociation constant, Kd, of the ligand-receptor complex) and a high density of the receptor (Bmax) in target tissue [21]. ^{11}C-SA4503 shows high affinity to sigma receptors [22,23] (Table 1C). Also, sigma-1 receptors are present in tumors in sufficiently high densities for PET imaging (~ 170 fmol/mg protein in s.c. grown C6 glioma, ~ 1700 fmol/mg protein in AH109A hepatoma) [24,25]. With B/F ratio >> 10, ^{11}C-SA4503 should be potentially able to image sigma-1 receptors in cancer.

4. *Specificity for target. Overexpression of target in tumor.*

The quality of tumor imaging is dependent on the specificity of a radioligand for its target. Binding to non-target proteins should preferably occur with affinities at least 50-fold lower than the affinity of the probe for its target. Moreover, the target protein

should be more highly expressed in tumor than in non-tumor tissue in order to obtain a low background signal.

a) *off-target affinity:* ^{11}C-SA4503 showed a high affinity to sigma-1 receptors, but negligible affinity to many other neuroreceptors, transporters and enzymes (Table 1C) [22]. The compound displayed ~100-times lower affinity to sigma-2 receptors, α1-adrenergic, dopamine D_2, serotonin (5-HT)1A, 5-HT2, histamine H1, and muscarinic M1 and M2 receptors, and no affinity at all to another 29 receptors, ion channels, and second messenger systems [22]. Brain uptake of ^{11}C-SA4503 is not affected by the activity of the drug-efflux pump, P-glycoprotein (P-gp), present in BBB and in some tumors with acquired drug resistance [20]. Therefore, ^{11}C-SA4503 will not be actively removed from P-gp expressing cells.

b) *uptake in healthy, non-tumor tissues:* The highest *in vivo* uptake of ^{11}C-SA4503 was noticed in rat organs, such as liver, pancreas, kidney, bone marrow, lung, intestines, spleen and brain (Table 1C and **Chapter 3**) [13]. The absorbed dose of radiation in liver, pancreas and kidneys (the organs with highest ^{11}C-SA4503 accumulation) was low enough to allow clinical use [12]. Specific binding of ^{11}C-SA4503 to sigma receptors was observed in rat brain, intestines, kidneys and liver [13].

Other semi-quantitative indices allowing a comparison of tumor activity to "background activity" are tumor-to-muscle and tumor-to-plasma ratios. The higher these values are the better a tumor is visualized. ^{11}C-SA4503 showed better tumor-to-muscle ratios than ^{11}C-choline, ^{11}C-methionine or ^{18}F-FLT, but lower ratios than ^{18}F-FDG, whereas the tumor-to-plasma ratio of ^{11}C-SA4503 was the highest of all tested tracers (Fig. 1., Table 1D and **Chapter 3**) [13,26,27].

c) *uptake in tumor:* Sigma-1 receptors were shown to be overexpressed in tumor tissue in comparison to the tissue of its origin (see Table 3 in **Chapter 2**, for pituitary gland and pituitary tumor see **Chapter 4**) [28]. Indeed, high specific binding of ^{11}C-SA4503 was also found in subcutaneous C6 glioma xenografts [13]. However in previous studies, a higher ^{11}C-SA4503 uptake was observed in rat brain than in C6 tumors grown subcutaneously [13,27]. If the amount of ^{11}C-SA4503 binding in spontaneous brain tumors or intracranial tumors is similar to ^{11}C-SA4503 uptake in C6 glioma, tumor-to-brain ratios of radioactivity will be low (< 1) in ^{11}C-SA4503-PET. This would limit the applicability of ^{11}C-SA4503 for tumor detection in close proximity to sigma receptor-rich organs like brain. However, microPET scanning with ^{11}C-SA4503 proved capable of detecting spontaneous rat pituitary adenomas with a size smaller than 10 mm^3. Tumor-to-brain uptake ratios were approximately 5.7, whereas tumor-to-plasma uptake ratios were > 100 (**Chapter 4** and Table 1D). Accumulation of ^{11}C-SA4503 in these pituitary tumors appears partially due to increased sigma-1 receptor expression. We also noticed that the presence of a pituitary tumor affects the distribution of ^{11}C-SA4503 in many other

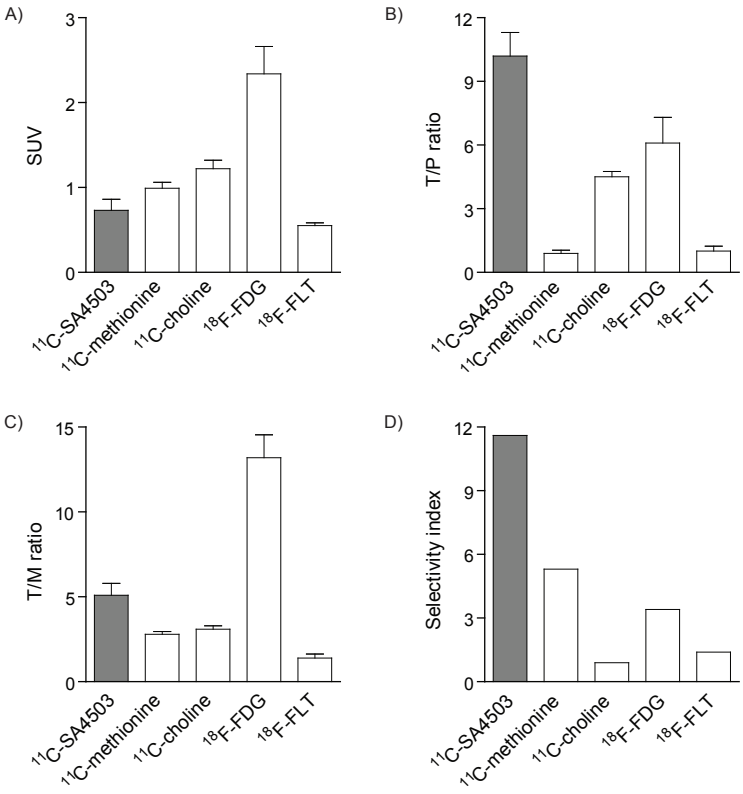

Fig.1. Comparison of ^{11}C-SA4503 to other oncologic PET tracers: A) standard uptake value (SUV); B) tumor-to-plasma ratio (T/P), C) tumor-to-muscle ratio (T/M), D) selectivity index (tumor-to-inflammation ratio corrected for the uptake in non-inflamed muscle). For graphs A-C, data are expressed as mean ± SEM. For graph D, deviation could not be given, because of indifferent uptake in inflamed and non-inflamed contralateral muscle in some animals. The original data were adapted from previous publication [27].

tissues. This may be a consequence of a decreased rate of blood flow and altered tracer distribution throughout the body. Since the distribution volume of ^{11}C-SA4503 is highly sensitive to changes of blood flow, kinetic modeling may be necessary for quantification of sigma receptors.

d) *uptake in inflammatory tissue:* Inflammatory cells may cause a false-positive diagnosis of neoplasm, especially in FDG-PET scans [27]. Moreover, chemotherapy can trigger inflammation in and around tumors. This inflammation may obscure tumor responses to chemotherapy, since these responses are evaluated by measuring decreases

of metabolic activity in the tumor region. Decreases of metabolism in tumor cells may be off-set by active metabolism in infiltrating non-tumor cells (e.g. neutrophils, macrophages, fibroblasts and lymphocytes) [29]. In the model of acute, sterile muscle inflammation ^{11}C-SA4503 demonstrated a much better selectivity for tumor over inflammatory tissue than other commonly used oncologic PET tracers, such as ^{11}C-choline, ^{18}F-FDG or ^{11}C-methionine (Table 1D) [27]. The tumor selectivity of ^{11}C-SA4503 was comparable to ^{18}F-FLT, a tracer which monitors the activity of thymidine kinase 1, an enzyme involved in cell proliferation. This shows that ^{11}C-SA4503 may be used for selective detection of tumors, although more study is needed for examining ^{11}C-SA4503 uptake in chronic inflammation (see future perspectives in **Chapter 11**).

5. *Effect of the endogenous competitor.*

Endogenous sigma (ant)agonists could compete with ^{11}C-SA4503 for binding to sigma receptors in tumors, thus changes of the levels of such compounds could affect the tumor-to-muscle and tumor-to-plasma ratios of this radioligand and affect the interpretation of PET data. Competition of an endogenous antagonist for binding to sigma-1 receptors was considered and its possible impact on ^{11}C-SA4503 PET was studied in **Chapter 3**. Steroid hormones (particularly progesterone and testosterone) were proposed to bind sigma receptors. However, identification of steroid hormones as endogenous sigma receptor ligands remained uncertain since the examined steroids showed a rather low affinity [30]. We demonstrated that *in vitro* and *in vivo* binding of ^{11}C-SA4503 to rat C6 glioma cells is sensitive to modifications in steroid hormone levels (Table 1E). We calculated that at least 16% of the sigma receptor population in C6 tumors may normally be occupied by endogenous steroids. Decreasing the endogenous steroid levels resulted in increased tumor-to-muscle and tumor-to-plasma ratios of ^{11}C-SA4503 (from 5 to 7 and from 10 to 15, respectively). An IC50 value (concentration of drug inhibiting ^{11}C-SA4503 binding by 50%) of 33 nM was measured for the strongest competitor, progesterone. This level can be exceeded in human blood during the luteal phase of the menstrual cycle. Also, chemotherapy in oncology patients is sometimes accompanied by hormonal changes, which may affect ^{11}C-SA4503 uptake. Therefore, correction of the PET data for the levels of progesterone in blood may be necessary in ^{11}C-SA4503 PET.

6. *Metabolism in plasma and in target.*

The ideal radioligand should show little metabolism during a few half-lives of the PET nuclide, i.e. the time window available for acquisition of tumor images. In case of ^{11}C-SA4503, only a small amount of metabolites was detected in rat brain 30 min after tracer injection. However in plasma,. 20% to 50% of total radioactivity at this time point

Table 1. Characteristic features of ^{11}C-SA4503

	^{11}C-SA4503		References
A) Labeling	Synthesis Time	45 min	[13]
	Yield	~ 9-11%	[13,27]
	Specific Radioactivity	~ 11-22 TBq/mmol	[13,27]
	Radiochemical Purity	> 95%	[13,27]
B) Distribution	Molecular Size	368.51 Da	
	Lipophilicity (Log*P*)	+ 2.52	[31]
	Charge (pKa)	8.2	[32]
	In vitro Equilibrium (37˚C)	~ 20 min	[13]
	In vivo Blood Clearance	> 80% at 20 min after injection	Chapter 3
	Plateau of TAC in Brain and Tumor	in 10 min after injection	Chapter 3
	Crossing Cell Membrane & BBB	yes	[20]
	Washout from C6/Pituitary Tumor	< 4.5%/no at 60 min after injection	Chapter 3-4
C) Binding	Affinity to Sigma-1 Receptors [nM]	IC50=17.4 or Ki=4.6	[22,23]
	Affinity to Sigma-2 Receptors [nM]	IC50=1784 or Ki=63.1	[22,23]
	Selectivity Sigma-1/-2 receptor	100-fold or 14-fold	[22,23]
	Off-target Affinity	low (rat brain)	[12]
	P-gp Modulation	no	[20]
	Specific Binding	brain, intestine, kidney, liver, C6 tumor	[13]
D) Selectivity	Tumor-to-Muscle Ratio	~5 (C6 glioma)	[27]
	Tumor-to-Plasma Ratio	~10 (C6 glioma), ~100 (pituitary tumor)	[27], Chapter 4
	Tumor-to-Inflammation Selectivity	~10 (C6 glioma)	[27]
	Tumor-to-Tissue of Origin Ratio	~ 3 (pituitary tumor/pituitary gland)	Chapter 4
E) Endogenous Competitor	Steroid Hormones	progesterone (IC50 = 33 nM)	Chapter 3
	In vivo Occupancy in C6 Tumor	> 16% of sigma receptors	Chapter 3
F) ^{11}C-Metabolites	Rat Plasma	20-50% (30 min)	[12,33]
	Rat Brain	< 7% (30 min)	[12,33]
G) Applications	Tumor Detection	glioma, pituitary tumor	Chapter 3-4
	Disease-Free Survival (?)	progesterone receptor and Bcl-2 status	?
	Early Cancer Responses	to doxorubicin treatment	[24,26]
	Sigma Receptor Occupancy	dose of therapeutic sigma ligand	Chapter 5

represented metabolites (Table 1F) [12,33]. Since most radioactive metabolites derived from SA34503 are hydrophilic, they do not pass the BBB and do not significantly affect brain imaging. Hydrophilic metabolites will also be taken up less easily in tumor tissue than the moderately lipophilic parent ligand. However, to the best of our knowledge, the ratio of parent compound and metabolites in implanted tumors after injection of

^{11}C-SA4503 has never been examined (see future perspectives in **Chapter 12**).

7. *Relation of target expression or affinity state to response of cancer to treatment.*

An *in vitro* study in C6 cells treated with chemotherapeutic agents showed that the uptake of ^{18}F-FLT and ^{11}C-SA4503 was more rapidly altered than uptake of other tested PET tracers (Table 1G) [26]. *In vivo* doxorubicin treatment of C6 xenografts had no inhibitory effect on tumor growth at 48h, but it reduced ^{11}C-SA4503 uptake in the tumor (as a result of downregulation of sigma-1 receptors) and ^{18}F-FDG uptake (indicating inhibition of metabolism) [24]. Changes of the tumor uptake of PET tracers (^{11}C-SA4503 and ^{18}F-FDG) preceded morphological changes. Radiolabeled sigma ligands may therefore be applied for monitoring early responses to chemotherapy.

In conclusion, the main challenge of nuclear medicine is to visualize tumors and to monitor therapeutic responses as early as possible. The data provided in this thesis indicate that radiopharmaceuticals for sigma receptors may be used for tumor detection, tumor staging, and evaluation of anti-tumor therapy. In addition, radioligands for sigma receptors can be used for monitoring the dose-dependent occupancy of sigma receptors in tumors by non-radioactive sigma ligands (see next paragraph).

Evaluation of Sigma Ligands for Cancer Treatment

Sigma ligands have shown promising anti-tumor activity in pre-clinical studies [8-10]. Antagonists at sigma-1 receptors and agonists at sigma-2 receptors induce changes in cancer cell proliferation and release an internal "brake" in cancer cells on the apoptotic machinery (see **Chapter 1-2**). The anti-tumor activity of sigma ligands is associated with a minimal toxicity towards normal cells and tissues (see **Chapter 6** for hepatocytes and **Chapter 8** for human umbilical vein epithelial cells), with epithelial lens cells as the only known exception [34]. This observation has led to several *in vitro* and *in vivo* studies in which sigma ligands were evaluated as potential anti-cancer agents, including clinical trials with rimcazole (Modern Biosciences), siramesine (H Lundbeck A/S), and SR31747A (Sanofi-Aventis).

Sigma ligands must be applied in micromolar doses to trigger cell death in cancer cells, i.e. at significantly higher concentrations than reported Kd values for their *in vitro* binding to sigma-1 receptors [35,36]. By performing competition studies with ^{11}C-SA4503 in intact cells, we showed that occupancy of the sigma-1 population is not related to the cytotoxic effect, but almost complete occupancy of the sigma-2 receptor population is required for rapid cell death (**Chapter 5**) These data suggest that determination of sigma-2 receptor levels in tumors and sigma-2 receptor occupancy by therapeutic drugs may be important for assessment of the therapeutic dose of sigma ligands.

Treatment of cancer cells with sigma ligands induces changes of cellular

metabolism. We examined early metabolic changes following sigma ligand administration in order to predict which PET tracer is most suitable for evaluation of tumor responses to therapy. Results, presented in **Chapter 5** and **Chapter 8**, suggest that the best tracers for monitoring such changes are ^{18}F-FLT and ^{18}F-FDG. Uptake of ^{18}F-FLT is mainly determined by the activity of thymidine kinase 1, which is highest in S-phase and very low in G0/G1. Treatment of glioma and melanoma cells with sigma ligands strongly decreased the uptake of ^{18}F-FLT (**Chapters 5** and **Chapter 8**). Moreover, it changed the distribution of cells through different phases of the cell cycle. The population of cells in S-phase (dividing) was decreased and the fraction of non-dividing cells (G0/G1-phase) was increased (**Chapter 8**). Uptake of ^{18}F-FDG is dependent on the activity of proteins involved in glucose transport and metabolism, such as glucose transporters (GLUTs) and hexokinases (HKs) [37]. A decreased ^{18}F-FDG uptake in tumors is normally considered to reflect a positive response to treatment, although a transient increase ("metabolic flare") may be initially observed [38,39]. Since we studied predominantly early changes right after the onset of treatment with sigma ligands, we observed a strongly increased ^{18}F-FDG uptake in tumor cells *in vitro* (**Chapter 5** and **Chapter 8**) and a moderately increased ^{18}F-FDG uptake in implanted tumors *in vivo* (**Chapter 6**). This "metabolic flare" appears to be a response to stress, i.e. increased energy consumption because the cells attempt to repair damage to cellular components induced by the treatment. Increased uptake of ^{18}F-FDG in dying cancer cells was not related to the activity of caspases but it was related to oxidation of cellular lipids (**Chapter 8**). ^{18}F-FLT and ^{18}F-FDG-PET can provide insight into the molecular events underlying successful chemotherapy (inhibition of the cell cycle, decrease in cellular ATP levels). However, synergistic effects of chemotherapeutic agents on cancer cell death should rather be assessed by a tracer measuring apoptosis, e.g. radiolabeled Annexin A5 or a caspase-3 ligand.

Cancer cell death induced by sigma ligands can be independent of the p53 protein status of tumors and also be independent of caspase activation [9](**Chapter 7**). Therefore, sigma ligands may be suitable for treatment of a wide variety of tumors, including those resistant to any treatment which depends on p53 or caspase downstream signaling. A regulatory effect of sigma receptors on ceramide levels, calcium homeostasis, reactive oxygen species, lysosomal cathepsins and/or the activity of Akt kinase is supposed to underlie the anti-cancer activity of sigma ligands (see **Chapter 2**). Activation of such a large variety of death pathways may help overcome therapy resistance in cancer.

Sigma ligands are capable of potentiating the anti-cancer effects of conventional chemotherapeutics or small inhibitory molecules in a broad spectrum of human malignancies. For instance, the sigma ligands CB64D and CD184 synergized the anti-tumor activity of doxorubicin and actinomycin D in both MCF-7 and drug-resistant MCF-7/Adr breast cancer cells. Likewise, the sigma ligand haloperidol significantly

enhanced the anti-tumor activity of a tyrosine kinase inhibitor (Gleevec, also known as imatinib) towards SK-MEL-28 melanoma cells [40]. Sigma ligands may kill both sensitive and drug-resistant tumor cells when used in a proper drug combination [41]. We showed that sigma ligands synergistically potentiate the tumor-selective pro-apoptotic activity of TRAIL (Chapter 7-9). Combination of sigma ligands and TRAIL displayed robust anti-cancer effects, both in established human melanoma cell lines (**Chapter 7** and **Chapter 8**) and in short term cultures of primary human ovarian carcinoma (**Chapter 9**). In primary samples of ovarian carcinoma patients, two groups of responses could be discriminated. In the first group, cancer cells responded very well to a combination of sigma ligand and TRAIL. In the other group, cancer cells were already strongly responsive to treatment with sigma ligand alone, and combination treatment did not result in a greater anti-cancer effect. Thus, the final outcome of combination treatment in the two groups was comparable.

We conclude that sigma ligands may be valuable chemotherapeutic agents; both when applied alone or in combination with conventional chemotherapy, TRAIL, or novel small inhibitory molecules; and can improve the treatment outcome of refractory cancers.

References

1 Zeng C, Vangveravong S, Xu J, Chang KC, Hotchkiss RS, Wheeler KT, et al. Subcellular localization of sigma-2 receptors in breast cancer cells using two-photon and confocal microscopy. Cancer Res. 2007;67:6708–16.

2 Hayashi T, Su T-P. Sigma-1 receptors (sigma(1) binding sites) form raft-like microdomains and target lipid droplets on the endoplasmic reticulum: roles in endoplasmic reticulum lipid compartmentalization and export. J Pharmacol Exp Ther. 2003;306:718–25.

3 Itzhak Y, Stein I. Sigma binding sites in the brain; an emerging concept for multiple sites and their relevance for psychiatric disorders. Life Sci. 1990;47:1073–81.

4 Largent BL, Gundlach AL, Snyder SH. Sigma receptors on NCB-20 hybrid neurotumor cells labeled with (+)[3H]SKF 10,047 and (+)[3H]3-PPP. Eur J Pharmacol. 1986;124:183–7.

5 Kushner L, Zukin SR, Zukin RS. Characterization of opioid, sigma, and phencyclidine receptors in the neuroblastoma-brain hybrid cell line NCB-20. Mol Pharmacol. 1988;34:689–94.

6 Van Waarde A, Rybczynska AA, Ramakrishnan N, Ishiwata K, Elsinga PH, Dierckx RAJO. Sigma receptors in oncology: therapeutic and diagnostic applications of sigma ligands. Curr Pharm Des. 2010;16:3519–37.

7 Roperto S, Colabufo NA, Inglese C, Urraro C, Brun R, Mezza E, et al. Sigma-2 receptor expression in bovine papillomavirus-associated urinary bladder tumours. J Comp Pathol. 2010;142:19–26.

8 Spruce BA, Campbell LA, McTavish N, Cooper MA, Appleyard MV, O'Neill M, et al. Small molecule antagonists of the sigma-1 receptor cause selective release of the death program in tumor and self-reliant cells and inhibit tumor growth in vitro and in vivo. Cancer Res. 2004;64:4875–86.

9 Crawford KW, Bowen WD. Sigma-2 receptor agonists activate a novel apoptotic pathway and potentiate antineoplastic drugs in breast tumor cell lines. Cancer Res. 2002;62:313–22.

10 Kashiwagi H, McDunn JE, Simon PO, Goedegebuure PS, Vangveravong S, Chang K, et al. Sigma-2 receptor ligands potentiate conventional chemotherapies and improve survival in models of pancreatic adenocarcinoma. J Transl Med. 2009;7:24.

11 Kawamura K, Elsinga PH, Kobayashi T, Ishii S, Wang WF, Matsuno K, et al. Synthesis and evaluation of (11)C- and (18)F-labeled 1-[2-(4-alkoxy-3-methoxyphenyl)ethyl]-4-(3-phenylpropyl)piperazines as sigma receptor ligands for positron emission tomography studies. Nuclear Medicine and Biology. 2003;30:273–84.

12 Kawamura K, Ishiwata K, Shimada Y, Kimura Y, Kobayashi T, Matsuno K, et al. Preclinical evaluation of [11C]SA4503: radiation dosimetry, in vivo selectivity and

PET imaging of sigma1 receptors in the cat brain. Ann Nucl Med. 2000;14:285–92.

13 Van Waarde A, Buursma AR, Hospers GAP, Kawamura K, Kobayashi T, Ishii K, et al. Tumor imaging with 2 sigma-receptor ligands, 18F-FE-SA5845 and 11C-SA4503: a feasibility study. J Nucl Med. 2004;45:1939–45.

14 Herholz K, Wienhard K, Heiss WD. Validity of PET studies in brain tumors. Cerebrovasc Brain Metab Rev. 1990;2:240–65.

15 Soni V, Jain A, Khare P, Gulbake A, Jain SK. Potential approaches for drug delivery to the brain: past, present, and future. Crit Rev Ther Drug Carrier Syst. 2010;27:187–236.

16 Siegal T, Zylber-Katz E. Strategies for increasing drug delivery to the brain: focus on brain lymphoma. Clin Pharmacokinet. 2002;41:171–86.

17 Eckelman WC. Sensitivity of new radiopharmaceuticals. Nucl Med Biol. 1998;25:169–73.

18 Dishino DD, Welch MJ, Kilbourn MR, Raichle ME. Relationship between lipophilicity and brain extraction of C-11-labeled radiopharmaceuticals. 1983;24:1030–8.

19 Friebe M, Suda K, Spies H, Syhre R, Berger R, Johannsen B, et al. Permeation studies in vitro and in vivo of potential radiopharmaceuticals with affinity to neuro receptors. Pharm Res. 2000;17:754–60.

20 Kawamura K, Kobayashi T, Matsuno K, Ishiwata K. Different brain kinetics of two sigma 1 receptor ligands, [3H](+)-pentazocine and [11C]SA4503, by P-glycoprotein modulation. Synapse. 2003;48:80–6.

21 Van Waarde A, Vaalburg W, Doze P, Bosker FJ, Elsinga PH. PET imaging of beta-adrenoceptors in human brain: a realistic goal or a mirage? Curr Pharm Des. 2004;10:1519–36.

22 Matsuno K, Nakazawa M, Okamoto K, Kawashima Y, Mita S. Binding properties of SA4503, a novel and selective sigma 1 receptor agonist. Eur J Pharmacol. 1996;13;306:271–9.

23 Lever JR, Gustafson JL, Xu R, Allmon RL, Lever SZ. Sigma1 and sigma2 receptor binding affinity and selectivity of SA4503 and fluoroethyl SA4503. Synapse. 2006;59:350–8.

24 Van Waarde A, Shiba K, De Jong JR, Ishiwata K, Dierckx RA, Elsinga PH. Rapid reduction of sigma1-receptor binding and 18F-FDG uptake in rat gliomas after in vivo treatment with doxorubicin. 2007;48:1320–6.

25 Kawamura K, Kubota K, Kobayashi T, Elsinga PH, Ono M, Maeda M, et al. Evaluation of [11C]SA5845 and [11C]SA4503 for imaging of sigma receptors in tumors by animal PET. Ann Nucl Med. 2005;19:701–9.

26 Van Waarde A, Been LB, Ishiwata K, Dierckx RA, Elsinga PH. Early response of

sigma-receptor ligands and metabolic PET tracers to 3 forms of chemotherapy: an in vitro study in glioma cells. J Nucl Med. 2006;47:1538–45.

27 Van Waarde A, Jager PL, Ishiwata K, Dierckx RA, Elsinga PH. Comparison of sigma-ligands and metabolic PET tracers for differentiating tumor from inflammation. J Nucl Med. 2006;47:150–4.

28 Megalizzi V, Le Mercier M, Decaestecker C. Sigma receptors and their ligands in cancer biology: overview and new perspectives for cancer therapy. Med Res Rev. 2010;[epub ahead of print].

29 Kubota R, Kubota K, Yamada S, Tada M, Ido T, Tamahashi N. Microautoradiographic study for the differentiation of intratumoral macrophages, granulation tissues and cancer cells by the dynamics of fluorine-18-fluorodeoxyglucose uptake. 1994;35:104–12.

30 Waterhouse RN, Chang RC, Atuehene N, Collier TL. In vitro and in vivo binding of neuroactive steroids to the sigma-1 receptor as measured with the positron emission tomography radioligand [18F]FPS. Synapse. 2007;61:540–6.

31 Kawamura K, Ishiwata K, Tajima H, Ishii S-I, Matsuno K, Homma Y, et al. In vivo evaluation of [11C]SA4503 as a PET ligand for mapping CNS sigma1 receptors. Nucl Med Biol. 2000;27:255–61.

32 Valade A, Cross SB, Brown C, Detrait E, Ene D, Gillard M, et al. Discovery of novel selective Sigma-1 ligands as cognitive enhancers. Med Chem Comm. 2011;2:655.

33 Elsinga PH, Kawamura K, Kobayashi T, Tsukada H, Senda M, Vaalburg W, et al. Synthesis and evaluation of [18F]fluoroethyl SA4503 as a PET ligand for the sigma receptor. Synapse. 2002;43:259–67.

34 Wang L, Prescott AR, Spruce BA, Sanderson J, Duncan G. Sigma receptor antagonists inhibit human lens cell growth and induce pigmentation. Invest Ophthalmol Vis Sci. 2005;46:1403–8.

35 Brent PJ, Pang GT. Sigma binding site ligands inhibit cell proliferation in mammary and colon carcinoma cell lines and melanoma cells in culture. Eur J Pharmacol. 1995;278:151–60.

36 Vilner BJ, de Costa BR, Bowen WD. Cytotoxic effects of sigma ligands: sigma receptor-mediated alterations in cellular morphology and viability. J Neurosci. 1995;15:117–34.

37 Haberkorn U, Ziegler SI, Oberdorfer F, Trojan H, Haag D, Peschke P, et al. FDG uptake, tumor proliferation and expression of glycolysis associated genes in animal tumor models. Nucl Med Biol. 1994;21:827–34.

38 Slosman DO, Pugin J. Lack of correlation between tritiated deoxyglucose, thallium-201 and technetium-99m-MIBI cell incorporation under various cell stresses. 1994;35:120–6.

39 Furuta M, Hasegawa M, Hayakawa K, Yamakawa M, Ishikawa H, Nonaka T, et al. Rapid rise in FDG uptake in an irradiated human tumour xenograft. 1997;24:435–8.

40 Nordenberg J, Perlmutter I, Lavie G, Beery E, Uziel O, Morgenstern C, et al. Anti-proliferative activity of haloperidol in B16 mouse and human SK-MEL-28 melanoma cell lines. Int J Oncol. 2005;27:1097–103.

41 Mégalizzi V, Mathieu V, Mijatovic T, Gailly P, Debeir O, De Neve N, et al. 4-IBP, a sigma1 receptor agonist, decreases the migration of human cancer cells, including glioblastoma cells, in vitro and sensitizes them in vitro and in vivo to cytotoxic insults of proapoptotic and proautophagic drugs. Neoplasia. 2007;9:358–69.

Chapter 11

Conclusions and perspectives

This thesis was focused on the evaluation of sigma ligands for cancer imaging and cancer treatment. In **Chapter 3**, we confirmed that steroid hormones (particularly progesterone) can bind *in vivo* to sigma-1 receptors in the brain and tumor, and may be the endogenous competitors to the sigma-1 ligand, ^{11}C-SA4503. In **Chapter 4**, we showed that spontaneous pituitary tumors can be clearly visualized with ^{11}C-SA4503, despite a high physiologic expression of sigma-1 receptors in the normal brain. In **Chapter 5**, we concluded that almost complete occupancy of sigma-2 receptors is associated with anti-cancer effects. In **Chapter 6**, we demonstrated strong antitumor action of rimcazole (sigma-1/-2 ligand) against metastatic melanoma xenografts in the absence of acute side-effects. In **Chapters 7-9**, we reported a robust synergistic killing of various cancer cell lines and patient-derived primary ovarian cancer cells by combining sigma ligands and TRAIL preparations. In the following paragraphs, we identify some areas for further study and we discuss our findings in the context of new discoveries in the sigma receptor field.

Is tumor imaging influenced by ^{11}C-SA4503 metabolites?

We observed differences in the washout kinetics of ^{11}C from brain and tumor in ^{11}C-SA4503 PET (**Chapter 3-4**). During a 60 minute scan, the decay-corrected activity in the brain showed a significant decline, whereas activity in the tumor was maintained at the initial level. A similar observation was made by other investigators, who used different tumor models and/or different radioligands [1-5].

One possible explanation for differences in washout kinetics of ^{11}C-SA4503 in the brain and tumors is that ^{11}C-SA4503 uptake may be affected by competition with endogenous sigma-1 ligands (neurosteroid hormones, N,N-dimethyltryptamine, or some other endogenous ligand) in a brain, but not in tumor (**Chapter 3**, [6]). Second possible explanation for the difference in kinetics is that sigma-1 receptors in tumors and the brain have different affinity states. Due to a higher ratio of k_{on}/k_{off}, the ligand-receptor complex may remain assembled for a longer period of time in the tumor than in the brain [7,8]. This property of tumoral receptors would be very desirable for tumor imaging. However, third possible mechanism underlying the kinetic differences is that ^{11}C-SA4503, after crossing cellular membranes, is metabolized to hydrophilic radioactive metabolites which are then trapped inside the cell. Since tumor cells have an increased metabolic activity in comparison to non-tumor cells, trapping may preclude washout from tumors but not from brain. If significant intracellular metabolism of the tracer occurs, it may be difficult to quantify sigma-1 receptors in tumors by kinetic modeling. The ratio of parent compound and metabolites in tumors after injection of ^{11}C-SA4503 has never been examined. Future experiments are required to establish or refute mechanisms 1, 2 and 3, and to prove that it is possible to quantify sigma-1 receptors in tumors

with ^{11}C-SA4503 and PET.

Can sigma ligands distinguish tumor from chronic inflammation?

Significant uptake of a PET tracer in inflammatory cells may be a cause of false-positive tumor diagnosis and may complicate the interpretation of tumor responses to treatment (**Chapter 10**). Based on their time course, inflammatory processes can be divided, into acute and chronic inflammations. Acute inflammation is mediated mainly by granulocytes, chronic inflammation by monocytes and lymphocytes.

In a model of acute, sterile muscle inflammation, ^{11}C-SA4503 demonstrated a much better selectivity for tumor over inflammatory tissue than the metabolic PET tracers, such as ^{18}F-FDG, ^{11}C-choline, or ^{11}C-methionine, and a similar selectivity as the nucleoside ^{18}F-FLT. Proliferation markers like ^{18}F-FLT show little uptake in acute inflammation, but they can accumulate in chronic inflammation, because of infiltrations of rapidly dividing lymphocytes, macrophages and/or fibroblasts [9-13]. Thus, the selectivity of ^{18}F-FLT for tumor over acute inflammation is much better than its selectivity for tumor over chronic inflammation. The uptake of ^{11}C-SA4503 in chronic inflammation has not yet been examined. Future experiments are required to determine if tumors can be distinguished from chronic inflammations by ^{11}C-SA4503-PET.

Since ligands for sigma-2 receptors have been reported to be better proliferation markers than sigma-1 receptor ligands, the tumor selectivity of such ligands should be examined in animal models of acute and chronic inflammation. Such studies have not been reported in the literature.

Are non-subtype-selective ligands better for tumor detection than sigma-1 ligands?

Sigma receptors are potential biomarkers for tumor imaging. Both sigma-1 and (particularly) sigma-2 receptors are overexpressed in tumors [14-19]. Radioligands which bind to both sigma receptor subtypes may therefore be accumulated more in tumor tissue than sigma-1-subtype-selective tracers, and higher tumor-to-background ratios may be achieved by using such compounds for PET imaging [1,19]. Imaging of breast tumors showed that better tumor visualization was achieved with a radioligand which is selective for the sigma-2 subtype than a non-selective or selective for the sigma-1 subtype [20,21]. Future studies should investigate the suitability and benefits from using non-subtype-selective (e.g. ^{18}F-FESA5845) or sigma-2 subtype-selective (e.g. ^{125}I-RHM-4) sigma ligands for tumor detection with PET and SPECT.

Which sigma receptor subtype is a better biomarker for monitoring of therapy responses?

In several studies, sigma-1 receptor expression and the binding of sigma-1 agonists (e.g. ^{11}C-SA4503) have been reported to be not closely related to cellular proliferation [22,23]. Other studies reported that sigma-1 receptors are involved in cellular proliferation. In these studies, sigma-1 antagonist treatment and silencing of sigma-1 receptor subtype reduced proliferation of cancer cells [14,24-26]. Also, alterations in cell cycle had an effect on the uptake of the radioligand (^{125}I-PAB) selective for sigma-1 subtype [27]. This last result must be interpreted with caution because melanin pigment, in addition to sigma-1 receptors, interacts with ^{125}I-PAB [28]. Furthermore, sigma-1 receptor RNA levels did not determine the susceptibility to rimcazole in NCI60 cell line panel [26]. Other study examined the prognostic value of sigma-1 receptor expression in breast cancer [22]. This study showed that sigma-1 receptor levels were related to progesterone receptor positivity, Bcl-2 expression and poorer disease-free survival, but were not related to tumor size, histological grade or the expression of the Ki-67 proliferative marker, in 95 human breast cancer patients. Based on these conflicting reports regarding relation of sigma-1 receptor expression to cellular proliferation, the expression and function of sigma-1 receptors in various types of malignancy should be re-examined and correlated to the proliferative status of cancer and prognosis.

In contrast to the conflicting findings regarding sigma-1 receptors, sigma-2 receptor expression and the binding of non-subtype-selective (e.g. ^{18}F-FE-SA5845 or ^{18}F-FE-SA4503) or sigma-2-selective ligands (e.g. fluorescently labeled SW120, PB28) was found to be related to cellular proliferation [23,24,29-31]. Therefore, sigma-2 receptor expression is proposed to be a biomarker of cellular proliferation and sigma-2 selective ligands may be useful for assessing the proliferative status of tumors and evaluating tumor responses to chemotherapy [32-36]. Furthermore, there are several reasons why sigma-2 ligands appear to be better candidates for tumor imaging than sigma-1 ligands: 1. Sigma-2 receptor is more commonly expressed in cancer and sigma-2 receptor levels in cancer are generally much higher than those of the sigma-1 subtype [18]; 2. Sigma-2 receptors densities correlate to histopathologic grade of human urinary bladder carcinomas [15]; 3. Sigma-2 receptor density is related to cellular proliferation [33]; 4. In cancer cells responsive to treatment with tamoxifen, decrease in sigma-2 densities correlates to Ki-67, IdU labeling indexes and AgNOR scores [32]; 5. In general, signaling is considered to be pro-survival downstream sigma-1 receptor and pro-apoptotic downstream sigma-2 receptor. Therefore, evaluation of the early responses to anti-cancer therapy may be more rapid and easily quantifiable while using radioactive sigma-2 ligand (and not sigma-1 ligand) for PET or SPECT. Assuming a pro-survival function of sigma-1 receptors in tumors, an early increase in the tumor uptake of sigma-1 ligands may be observed after

the onset of an effective treatment (reflecting activation of survival pathways), which is later followed by a decrease when cells start to die. In contrast, a sudden decrease in the tumor uptake of sigma-2 ligands may be expected (reflecting inhibition of cellular proliferation). In conclusion, sigma-2 ligands appear to be better candidates for imaging of tumor responses to anti-cancer therapy than sigma-1 ligands.

What would increase the importance of sigma-2 receptors as a target in oncology?

Sigma-2 ligands with high subtype selectivity have only been explored for tumor imaging by three research institutions (Washington University School of Medicine, St.Louis, USA, Wake-Forest University School of Medicine, Winston-Salem, USA, and University of Bari, Bari, Italy). These institutions developed their own sigma-2-selective radioligands. SM-21 is to date the only available non-radioactive sigma-2 antagonist. Unfortunately, SM-21 is only ~14-fold selective for sigma-2 over sigma-1 receptor subtype and binds with similar affinity also to dopamine D2 and 5-HT2 receptors [37]. Studies on the biology of sigma-2 receptors and the development of sigma-2 ligands for PET imaging would be greatly facilitated if better sigma-2 ligands than SM-21 became commercially available. Synthetic efforts should be directed towards the development of novel sigma-2 (ant)agonists with improved affinity and selectivity. Novel sigma-2 ligands could be derived from e.g. 1. benzomorphan-7-one; 2. 3-(ώ-aminoalkyl)-1H-indole; 3. tropane; or 4. piperazine [38]. These scaffolds were previously used in synthesis of ligands with high affinity and selectivity towards sigma-2 receptors.

Do PET scans of sigma-2 receptor densities allow prognosis of the therapeutic outcome?

Sigma-2 receptor levels and occupancy may determine the anti-tumor effect of sigma-2 ligands (**Chapter 5**) and/or their adjuvant action in chemotherapy. If a selective sigma-2 tracer for PET becomes available, a study correlating sigma-2 receptor levels to anti-cancer activity of sigma-2 ligands could be performed in cancer cells with drug-sensitive and -resistant phenotypes, as a continuation of the work described in **Chapter 9**. The results of such a study may enable identification of the phenotypes of cancer patients that are eligible for sigma-2 ligand-based therapy, and may provide data about the drug dose necessary for optimal cancer killing. Furthermore, sigma-2 receptor expression is probably different in different stages of cancer progression. Thus, the novel study could also indicate when the treatment with sigma-2 ligands will have the strongest effect. Sigma receptor levels and oncolytic activity of sigma ligands should be determined in patient-derived primary samples of carcinoma of different stages. A parallel study in experimental animals could assess sigma-2 expression during different

stages of carcinogenesis with microPET. Results of these studies could indicate if PET scans of sigma-2 receptor expression allow prognosis of the therapeutic outcome.

Imaging of which sigma receptor subtype is worthwhile testing in oncology patients?

a) *sigma-1 receptor*

^{11}C-SA4503 has already been successfully employed for imaging sigma-1 receptors in healthy volunteers and patients with Alzheimer's or Parkinson's disease [23,39-42]. In these human studies, high uptake was seen in the liver, followed by lung and brain. Low uptake was seen in kidneys, extremities and the abdominal region. A small pilot study with ^{11}C-SA4503 has been performed in four untreated patients with non-small cell lung cancer which were also scanned with ^{18}F-FDG. In contrast to ^{18}F-FDG, ^{11}C-SA4503 was found to be not suitable for staging of non-small cell lung cancer. ^{11}C-SA4503-PET did not detect all lesions. Several local metastases, bone or brain metastases were visible with ^{18}F-FDG but not with the sigma-1 ligand. Tumors frequently showed up as cold spots in ^{11}C-SA4503 scans, and a weak accumulation of radioactivity was observed only at the tumor rim. In a few cases, ^{11}C-SA4503 was showing complementary hot spots to those observed in the ^{18}F-FDG scan. Despite these negative results, the feasibility of ^{11}C-SA4503 PET for imaging of hormone-responsive tumors could be examined (e.g., ovarian carcinoma or breast cancer), since sigma-1 receptor levels in such tumors have been reported to be related to hormone receptor positivity [22].

b) *sigma-2 receptor*

Sigma-2 ligands or non-subtype-selective sigma ligands seem to be more promising for tumor imaging than sigma-1 ligands, because the expression of sigma-2 receptors is considered to be related to cellular proliferation. However, no human PET study with a selective sigma-2 ligand has been performed thus far. In order to make such a study possible, toxicity and mutagenicity data for a newly developed sigma-2 ligand should be collected. If no adverse toxicity or mutagenicity is observed, pilot studies in healthy volunteers and small groups of cancer patients are a logical continuation of the research of the St. Louis group.

Has the sigma-2 receptor really been identified?

The sigma-1 receptor gene of several mammalian species has been cloned and is known to be encoded in band p13 of human chromosome 9. However, the existence of the sigma-2 receptor has only been proven by pharmacological methods. This makes the sigma-2 receptor a somewhat enigmatic protein which is not easily studied. The possibility of the sigma-2 receptor being a histone binding protein was once considered [15], but evidence to confirm this hypothesis is lacking. In July 2011, the progesterone

receptor membrane component 1 (PGRMC1) protein complex was tentatively identified as the putative sigma-2 receptor [43]. Although these data seem very convincing, they need to be confirmed by other research institutions. It is important to perform functional experiments in which changes of PGRMC1 expression and sigma-2 ligand binding are monitored in parallel, e.g. after chemotherapeutic treatment. Some doubt may be raised by the fact that PGRMC1 is localized in the plasma membrane, cytoplasm and nuclear spindle, whereas confocal microscopy with fluorescent sigma-2 ligands has not shown any accumulation of these compounds in the nucleus [43,44]. With respect to the evaluation of sigma-2 intrinsic activity, Colabufo et al. suggested that sigma-2 ligands which inhibit electrically evoked contractions in guinea pig bladder and ileum might be considered sigma-2 agonists [45]. However, the use of guinea pig bladder instead of tumor cells to distinguish between sigma-2 agonistic and antagonistic ligands limits the use of this assay in oncology. Furthermore, whereas sigma-2 agonists display oncolytic activity, PGRMC1 plays an essential role in promoting the *in vitro* survival of normal and cancer cells [44]. A better definition and assay for determination of agonistic or antagonistic action at sigma-2 receptors are urgently required.

What is the precise role of sigma-2 receptors in cancer cell proliferation?

Sigma-2 ligands were shown to affect transition of cell through the phases of cell cycle. Since the majority of sigma-2 selective ligands (with exception of PB28) do not show any accumulation in the nucleus, sigma-2 receptors may influence cell cycle regulatory proteins in the cytoplasm (e.g. Akt kinase), or proteins capable of crossing the membrane between cytoplasm and nucleus (e.g. cyclin-dependent kinases and cyclins), rather than directly affecting nuclear proteins (such as p21, p27 or p53). Future studies should examine the function of sigma-2 receptors in control of the cell cycle, particularly because sigma-2 receptors were found to be biomarkers of cellular proliferation.

Conclusion

Sigma receptors are an interesting target for tumor imaging and treatment. However, based on our own data (presented in Chapter 5 and Chapter 7) and data from other institutions, sigma-2 ligands are more promising for treatment and imaging of cancer than ligands for the sigma-1 receptor. Sigma-2 receptors, in contrast to sigma-1 receptors, are thought to be markers of cellular proliferation.

References

1 Kawamura K, Kubota K, Kobayashi T, Elsinga PH, Ono M, Maeda M, et al. Evaluation of [11C]SA5845 and [11C]SA4503 for imaging of sigma receptors in tumors by animal PET. Ann Nucl Med. 2005;19:701–9.

2 Waterhouse RN, Chang RC, Zhao J, Carambot PE. In vivo evaluation in rats of [(18) F]1-(2-fluoroethyl)-4-[(4-cyanophenoxy)methyl]piperidine as a potential radiotracer for PET assessment of CNS sigma-1 receptors. Nucl Med Biol. 2006;33:211–5.

3 Waterhouse RN, Zhao J, Stabin MG, Ng H, Schindler-Horvat J, Chang RC, et al. Preclinical acute toxicity studies and dosimetry estimates of the novel sigma-1 receptor radiotracer, [18F]SFE. Mol Imaging Biol. 2006;8:284–91.

4 John CS, Lim BB, Vilner BJ, Geyer BC, Bowen WD. Substituted halogenated arylsulfonamides: a new class of sigma receptor binding tumor imaging agents. J Med Chem. 1998;41:2445–50.

5 John CS, Bowen WD, Fisher SJ, Lim BB, Geyer BC, Vilner BJ, et al. Synthesis, in vitro pharmacologic characterization, and preclinical evaluation of N-[2-(1'-piperidinyl) ethyl]-3-[125I]iodo-4-methoxybenzamide (P[125I]MBA) for imaging breast cancer. Nucl Med Biol. 1999;26:377–82.

6 Fontanilla D, Hajipour AR, Pal A, Chu UB, Arbabian M, Ruoho AE. Probing the steroid binding domain-like I (SBDLI) of the sigma-1 receptor binding site using N-substituted photoaffinity labels. Biochemistry. 2008;47:7205–17.

7 Millet P, Lemignone Y. Molecular Imaging: Computer Reconstruction and Practice. In: Lemoigne Y, Caner A, editors. Molecular Imaging: Computer Reconstruction and Practice. Dordrecht: Springer Netherlands; 2008. p. 211–28.

8 Innis RB, Cunningham VJ, Delforge J, Fujita M, Gjedde A, Gunn RN, et al. Consensus nomenclature for in vivo imaging of reversibly binding radioligands. J Cereb Blood Flow Metab. 2007;27:1533–9.

9 Reilkoff RA, Bucala R, Herzog EL. Fibrocytes: emerging effector cells in chronic inflammation. Nat Rev Immunol. 2011;11:427–35.

10 Tetley TD. Inflammatory cells and chronic obstructive pulmonary disease. Curr Drug Targets Inflamm Allergy. 2005;4:607–18.

11 Aggarwal BB, Gehlot P. Inflammation and cancer: how friendly is the relationship for cancer patients? Curr Opin Pharmacol. 2009 Aug;9(4):351–69.

12 Saga T, Kawashima H, Araki N, Takahashi JA, Nakashima Y, Higashi T, et al. Evaluation of primary brain tumors with FLT-PET: usefulness and limitations. Clin Nucl Med. 2006;31:774–80.

13 Yap CS, Czernin J, Fishbein MC, Cameron RB, Schiepers C, Phelps ME, et al. Evaluation of thoracic tumors with 18F-fluorothymidine and 18F-fluorodeoxyglucose-positron

emission tomography. Chest. 2006;129:393–401.

14 Aydar E, Onganer P, Perrett R, Djamgoz MB, Palmer CP. The expression and functional characterization of sigma (sigma) 1 receptors in breast cancer cell lines. Cancer Lett. 2006;242:245–57.

15 Colabufo NA, Berardi F, Contino M, Ferorelli S, Niso M, Perrone R, et al. Correlation between sigma2 receptor protein expression and histopathologic grade in human bladder cancer. Cancer Lett. 2006;237:83–8.

16 Thomas GE, Szucs M, Mamone JY, Bem WT, Rush MD, Johnson FE, et al. Sigma and opioid receptors in human brain tumors. Life Sci. 1990;46:1279–86.

17 Roperto S, Colabufo NA, Inglese C, Urraro C, Brun R, Mezza E, et al. Sigma-2 receptor expression in bovine papillomavirus-associated urinary bladder tumours. J Comp Pathol. 2010;142:19–26.

18 Vilner BJ, de Costa BR, Bowen WD. Cytotoxic effects of sigma ligands: sigma receptor-mediated alterations in cellular morphology and viability. J Neurosci. 1995;15:117–34.

19 Bem WT, Thomas GE, Mamone JY, Homan SM, Levy BK, Johnson FE, et al. Overexpression of sigma receptors in nonneural human tumors. Cancer Res. 1991;51:6558–62.

20 Mach RH, Huang Y, Buchheimer N, Kuhner R, Wu L, Morton TE, et al. [F-18]N-4'-fluorobenzyl-4-(3-bromophenyl)acetamide for imaging the sigma receptor status of tumors. J Label Comp Radiopharm. 1999;42 Suppl 1:S258–60.

21 Mach RH, Huang Y, Buchheimer N, Kuhner R, Wu L, Morton TE, et al. [[(18)F] N-(4'-fluorobenzyl)-4-(3-bromophenyl) acetamide for imaging the sigma receptor status of tumors: comparison with [(18)F]FDG, and [(125)I]IUDR. Nucl Med Biol. 2001;28:451–8.

22 Simony-Lafontaine J, Esslimani M, Bribes E, Gourgou S, Lequeux N, Lavail R, et al. Immunocytochemical assessment of sigma-1 receptor and human sterol isomerase in breast cancer and their relationship with a series of prognostic factors. Brit J Cancer. 2000;82:1958–66.

23 Van Waarde A, Buursma AR, Hospers GAP, Kawamura K, Kobayashi T, Ishii K, et al. Tumor imaging with 2 sigma-receptor ligands, 18F-FE-SA5845 and 11C-SA4503: a feasibility study. J Nucl Med. 2004;45:1939–45.

24 Wang L, Prescott AR, Spruce BA, Sanderson J, Duncan G. Sigma receptor antagonists inhibit human lens cell growth and induce pigmentation. Invest Ophthalmol Vis Sci. 2005;46:1403–8.

25 Brent PJ, Pang GT. Sigma binding site ligands inhibit cell proliferation in mammary and colon carcinoma cell lines and melanoma cells in culture. Eur J Pharmacol. 1995;278:151–60.

26 Spruce BA, Campbell LA, McTavish N, Cooper MA, Appleyard MV, O'Neill M, et al. Small molecule antagonists of the sigma-1 receptor cause selective release of the death program in tumor and self-reliant cells and inhibit tumor growth in vitro and in vivo. Cancer Res. 2004;64:4875–86.

27 Zamora PO, Moody TW, John CS. Increased binding to sigma sites of N-[1'(2-piperidinyl)ethyl)-4-[I- 125]-iodobenzamide (I-125-PAB) with onset of tumor cell proliferation. Life Sci. 1998;63:1611–8.

28 Michelot JM, Moreau MF, Veyre AJ, Bonafous JF, Bacin FJ, Madelmont JC, et al. Phase II scintigraphic clinical trial of malignant melanoma and metastases with iodine-123-N-(2-diethylaminoethyl 4-iodobenzamide). J.Nucl.Med. 1993;34:1260–6.

29 Elsinga PH, Kawamura K, Kobayashi T, Tsukada H, Senda M, Vaalburg W, et al. Synthesis and evaluation of [18F]fluoroethyl SA4503 as a PET ligand for the sigma receptor. Synapse. 2002;43:259–67.

30 Zeng C, Vangveravong S, Jones LA, Hyrc K, Chang KC, Xu J, et al. Characterization and Evaluation of Two Novel Fluorescent Sigma-2 Receptor Ligands as Proliferation Probes. Mol Imaging. 2011;[epub ahead of print].

31 Abate C, Hornick JR, Spitzer D, Hawkins WG, Niso M, Perrone R, et al. Fluorescent Derivatives of σ Receptor Ligand 1-Cyclohexyl-4-[3-(5-methoxy-1,2,3,4-tetrahydronaphthalen-1-yl)propyl]piperazine (PB28) as a Tool for Uptake and Cellular Localization Studies in Pancreatic Tumor Cells. J Med Chem. 2011;54:5858–67.

32 Al-Nabulsi I, Mach RH, Wang LM, Wallen CA, Keng PC, Sten K, et al. Effect of ploidy, recruitment, environmental factors, and tamoxifen treatment on the expression of sigma-2 receptors in proliferating and quiescent tumour cells. Brit J Cancer. 1999;81:925–33.

33 Mach RH, Smith CR, Al-Nabulsi I, Whirrett BR, Childers SR, Wheeler KT. Sigma 2 receptors as potential biomarkers of proliferation in breast cancer. Cancer research. 1997;57:156–61.

34 Wheeler KT, Wang LM, Wallen CA, Childers SR, Cline JM, Keng PC, et al. Sigma-2 receptors as a biomarker of proliferation in solid tumours. Brit J Cancer. 2000;82:1223–32.

35 Cobos EJ, Entrena JM, Nieto FR, Cendán CM, Del Pozo E. Pharmacology and Therapeutic Potential of Sigma1 Receptor Ligands. Current Neuropharmacology. 2008;6:344–66.

36 Mach RH, Wheeler KT. Development of molecular probes for imaging sigma-2 receptors in vitro and in vivo. Cent Nerv Syst Agents Med Chem. 2009;9:230–45.

37 Matsumoto RR, Pouw B, Mack AL, Daniels A, Coop A. Effects of UMB24 and (+/-)-SM 21, putative sigma2-preferring antagonists, on behavioral toxic and stimulant effects of cocaine in mice. Pharmacol Biochem Behav. 2007;86:86–91.

38 Mach RH, Wheeler KT. Development of molecular probes for imaging sigma-2

receptors in vitro and in vivo. Central nervous system agents in medicinal chemistry. 2009;9:230–45.

39 Sakata M, Kimura Y, Naganawa M, Oda K, Ishii K, Chihara K, et al. Mapping of human cerebral sigma1 receptors using positron emission tomography and [11C] SA4503. Neuroimage. 2007;35:1–8.

40 Jansen KL, Faull RL, Storey P, Leslie RA. Loss of sigma binding sites in the CA1 area of the anterior hippocampus in Alzheimer's disease correlates with CA1 pyramidal cell loss. Brain Res. 1993;623:299–302.

41 Mishina M, Ohyama M, Ishii K, Kitamura S, Kimura Y, Oda K-ichi, et al. Low density of sigma1 receptors in early Alzheimer's disease. Ann Nucl Med. 2008;22:151–6.

42 Toyohara J, Sakata M, Ishiwata K. Imaging of sigma1 receptors in the human brain using PET and [11C]SA4503. Centr Nerv Syst Agents Med Chem. 2009;9:190–6.

43 Xu J, Zeng C, Chu W, Pan F, Rothfuss JM, Zhang F, et al. Identification of the PGRMC1 protein complex as the putative sigma-2 receptor binding site. Nat Commun. 2011;2:380.

44 Peluso JJ, Liu X, Gawkowska A, Lodde V, Wu CA. Progesterone inhibits apoptosis in part by PGRMC1-regulated gene expression. Mol Cell Endocrinol. 2010;320:153–61.

45 Colabufo NA, Berardi F, Contino M, Perrone R, Tortorella V. A new method for evaluating sigma(2) ligand activity in the isolated guinea-pig bladder. Naunyn Schmiedebergs Arch Pharmacol. 2003;368:106–12.

Nederlandse samenvatting, Streszczenie po polsku

Chapter 12

Achtergrond

Wereldwijd sterven er ongeveer acht miljoen mensen per jaar aan kanker. Hoewel er al aanzienlijke vooruitgang is geboekt met het vaststellen en behandelen van kanker zal dit aantal nog steeds verder toenemen. Het is dan ook niet verrassend dat er intensief gezocht wordt naar nieuwe mogelijkheden om kanker sneller vast te stellen en beter te behandelen. Het vergaren van kennis over het ontstaan en groei van kankercellen speelt hierbij een belangrijke rol.

Kanker is een complexe ziekte die ontstaat als normale lichaamscellen "ontsporen". Hierbij gaat een lichaamscel zich steeds meer geïsoleerd gedragen zonder dat daarbij een gezonde interactie met de rest van het lichaam wordt gewaarborgd. Helaas is vrijwel elke lichaamscel in principe in staat om een kankercel te vormen. Hierdoor verschillen kankercellen aanzienlijk van patiënt tot patiënt en zelfs kankercellen van één enkele patiënt zijn vaak verschillend van elkaar. Als gevolg hiervan manifesteren verschillende kankers zich dikwijls met verschillende symptomen. Bij alle vormen van kanker kunnen echter vier stadia van ontwikkeling worden onderscheiden, namelijk: initiatie, promotie, progressie en conversie (zie ook Figuur 1).

Tijdens al deze stadia veranderen kankercellen steeds meer ten opzichte van het celtype waaruit ze oorspronkelijk zijn ontstaan. Deze veranderingen beschermen de kankercel tegen de afweermechanismen van het lichaam, en stellen de cel ook in staat om onbeperkt te blijven doorgroeien. Bekende voorbeelden hiervan zijn: 1. het vermogen van kankercellen om hun eigen groei te blijven stimuleren 2. de ongevoeligheid van kankercellen voor geprogrammeerde celdood (apoptose) en 3. het vermogen van een kankercel om zich ongelimiteerd te blijven delen in twee identieke dochtercellen. Vanwege deze veranderingen is een kankercel in het voordeel ten opzichte van normale cellen, maar wordt daarvan ook beter te onderscheiden.

Bijvoorbeeld: bij normale groei van cellen bindt een groeifactor aan een receptor. Door deze binding wordt de groei van de cel gestimuleerd. Om maximaal gebruik te maken van groeifactoren verhogen kankercellen dikwijls de hoeveelheid receptoren die zij bezitten (verhoogde expressie). Hierdoor wordt de groei van kankercellen gestimuleerd, maar ontstaat er ook een onderscheid met normale cellen die minder receptoren bezitten hetgeen de mogelijkheid tot mogelijke behandeling biedt. Eén van de receptoren die verhoogd tot expressie komt op kankercellen is de zogenaamde sigma receptor.

Sigma receptoren zijn eiwitten die voorkomen in de wanden van cel compartimenten zoals het endoplasmatisch reticulum, de mitochondriën, de lysosomen en tevens het plasmalemma (de buitenwand van de cel). Omdat sigma receptoren meer tot expressie komen in kankercellen dan in normale cellen, kunnen deze receptoren wellicht gebruikt worden om kanker op te sporen. Dit zou bijvoorbeeld kunnen met behulp van

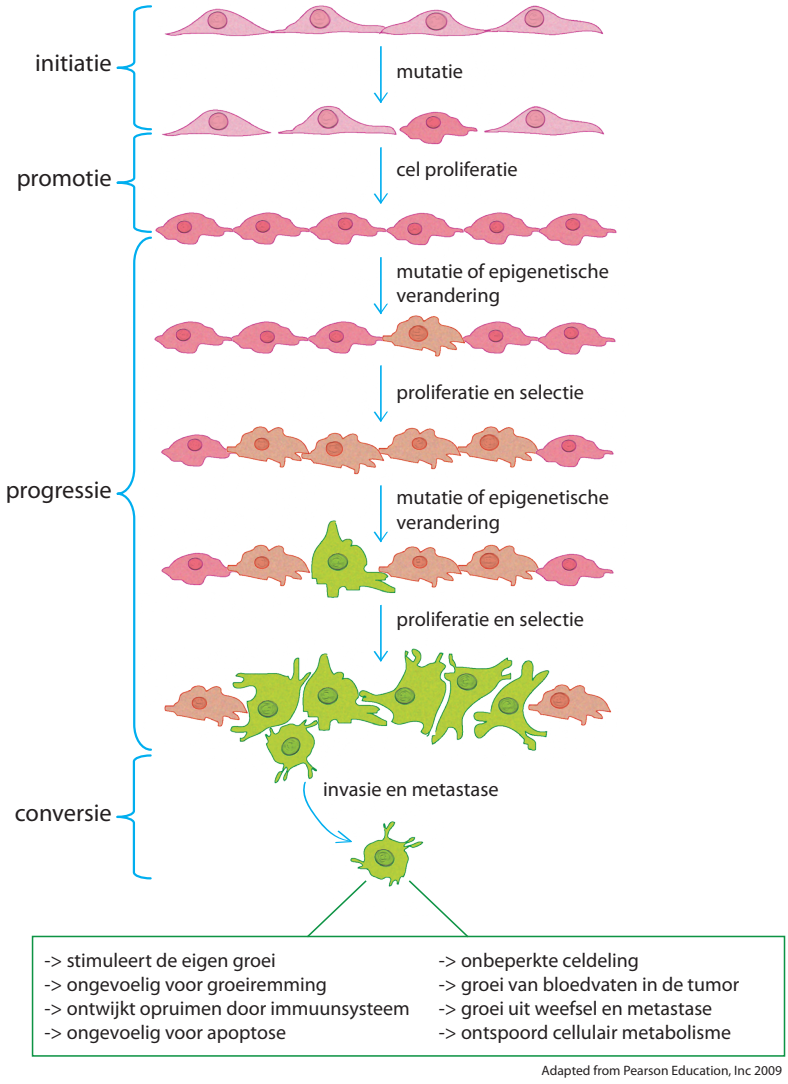

Adapted from Pearson Education, Inc 2009

Fig. 1. Verschillende fasen van de ontwikkeling van kanker. Het ontstaan van tumoren wordt geïnitieerd door verscheidene mutaties in de cel. Verdere ontwikkeling van kanker wordt bevorderd als de gemuteerde cel vervolgens ontsnapt aan de verdedigingsmechanismen van het lichaam en zich abnormaal door blijft delen. Hierdoor ontstaan verdere mutaties of zogeheten epigenetische modificaties. Tijdens de voortgang van de vorming van een tumor ondergaan kankercellen verschillende rondes van adaptatie, proliferatie en selectie. Hierdoor blijven uiteindelijk resistente en invasieve tumorcellen over die een grote overlevingskans hebben en vaak uitzaaien naar andere locaties.

chemische stoffen (liganden) die binden aan sigma receptoren. Daarnaast is gebleken dat zulke liganden kankercellen kunnen doden (zie **hoofdstuk 2** voor een overzicht van het onderzoek naar sigma liganden).

In dit proefschrift werden dan ook mogelijke toepassingen van sigma liganden getest zowel bij de diagnose als de behandeling van kanker.

Vaststellen van kanker

Helaas treedt er na de behandeling van kanker meestal geen genezing op. Dit komt onder andere doordat de effectiviteit van de behandeling afhankelijk is van een groot aantal factoren, waaronder 1. een snelle diagnose, 2. het precies vaststellen van de locatie van zowel primaire tumoren als metastasen, en 3. de effectiviteit van de gebruikte geneesmiddelen. Bij het verbeteren van de huidige therapieën voor het behandelen van kanker is een snelle diagnose dan ook van groot belang.

Diagnose van kanker kan geschieden door middel van invasieve en niet-invasieve methoden. Bij invasieve methoden kan men denken aan het nemen van een biopsie of aan lichamelijk onderzoek tijdens een exploratieve operatie. Deze methoden zijn echter beperkt tot het vaststellen van een tumor waarvan de locatie bekend is en zijn veel minder geschikt voor het opsporen van metastasen. Daarnaast is het lastig om met deze methoden de omvang en eigenschappen van de tumor vast te stellen. Onder niet-invasieve methoden vallen: 1. het afnemen van bloedmonsters om de eventueel verhoogde concentratie van circulerende eiwitten bij mensen met kanker te bepalen, 2. Anatomische beeldvorming van tumoren door middel van echografie, computed tomography (CT) en magnetic resonance imaging (MRI), 3. moleculaire beeldvorming met behulp van single photon emissie computer tomografie (SPECT) of positron emmisie tomografie (PET). PET is een aantrekkelijke methode omdat hierbij, in tegenstelling tot bloedmonsters, echografie, CT en MRI, zowel informatie over de locatie als de activiteit van de tumor wordt verkregen.

PET is een erg gevoelige nucleaire diagnostische techniek waarbij gebruik wordt gemaakt van radioactieve isotopen met positron verval (zie ook Figuur 2). Positronen zijn subatomaire deeltjes met dezelfde massa als een elektron, maar in tegenstelling tot negatief geladen elektronen hebben positronen een positieve lading. Wanneer na verval een positron en een elektron met elkaar in contact komen treedt er een proces op dat annihilatie heet. Hierbij worden er twee fotonen uitgezonden die opgevangen kunnen worden door een PET camera. Doordat de fotonen (gammastraling) altijd onder een hoek van 180 graden ten opzichte van elkaar worden uitgezonden kan hiermee de locatie van het vervallen isotoop in het lichaam bepaald worden. Door isotopen, zoals fluor-18, te koppelen aan biologische moleculen zoals suikers kan het suikerverbruik in het lichaam met behulp van PET in kaart gebracht worden. Doordat kankercellen gemiddeld meer energie

A)

Positron-emissie isotopen	Halfwaardetijd	β+ fractie	Max. energie (MeV)	Mediaan Bereik (mm)	Verval isotoop
^{18}F	109.8 min	0.97	0.63	0.3	^{18}O
^{11}C	20.4 min	0.99	0.96	0.4	^{11}B
^{13}N	9.97 min	1.00	1.20	0.7	^{13}C
^{15}O	2.04 min	1.00	1.74	1.1	^{15}N
^{68}Ga	68.3 min	0.88	1.83	1.2	^{68}Zn
^{89}Zr	78.4 h	0.23	0.90	1.1	^{89}Y

B)

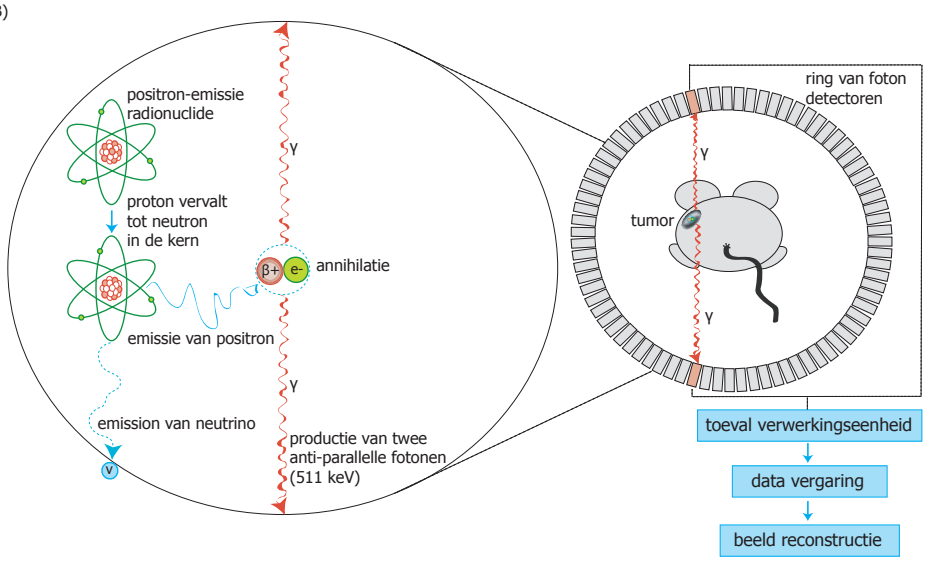

Fig. 2. Positron emission tomography: A) de positron-emmisie isotopen die het meest gebruikt worden bij PET.; B) Schematische weergave van de werking van PET.

en daarmee meer suiker verbruiken dan gezonde cellen, hoopt ^{18}F-fluorodesoxyglucose (^{18}F-FDG) zich meer op in kankercellen dan in normale cellen en kan de tumor in kaart worden gebracht. Omdat moleculen zoals ^{18}F-FDG gebruikt worden om het gedrag van de normale suiker in het lichaam te volgen worden deze tracers genoemd.

Omdat alle cellen in het lichaam suiker verbranden is het gebruik van ^{18}F-FDG niet de meest specifieke manier om tumorcellen te onderscheiden van normale cellen. Daarom is er veel aandacht voor het ontwikkelen van nieuwe moleculen die zich selectief ophopen in tumorcellen, maar niet in normale cellen. Een overzicht van zulke moleculen is weergegeven in tabel 1. Omdat sigma receptoren dikwijls hoger tot expressie komen in kankercellen dan in normale cellen is er in dit proefschrift gekeken naar het gebruik van sigma receptor liganden bij de diagnose van kanker. Voor dit doel beschikten wij

Tabel 1. Voorbeelden van PET tracers die gebruikt worden bij kankerpatiënten.

Oncologische PET tracer	Eiwit dat de tracer in kaart brengt	Geassocieerd biochemisch proces
^{18}F-fluorodesoxyglucose (FDG)	glucose transporters (GLUTs) & hexokinases (HKs)	→ cellulair energie verbruik ~ 90% scans
^{18}F-fluoro-L-thymidine (FLT)	thymidine kinase-1 (TK-1)	→ proliferatie
^{18}F-5-fluorouracil (5-FU)	thymidylate synthase	→ proliferatie
^{11}C-methionine (MET)	aminozuur transporters	→ aminozuur transport
^{18}F-fluoroethyltyrosine (FET)	aminozuur transporters	→ aminozuur transport
^{11}C/^{18}F-choline analogen	choline kinases	→ phospholipid metabolism
^{18}F-annexine A5	phosphatidylserine op het celoppervlak	→ apoptose
^{18}F-fluoroestradiol (FES)	oestrogen receptoren (ERs)	→ endocrine metabole activiteit
^{18}F-L-dihydroxyphenylalanine (DOPA)	grote aminozuur transporter (LAT), aminozuur decarboxylase (AADC), monoamine oxidase (MAO)	→ endocrine metabole activiteit
^{18}F/^{64}Ga-octreotide analogen	somatostatine receptor 2 (SST2Rs)	→ endocrine metabole activiteit
^{18}F-fluorine androgeen analogen	androgeen receptoren (ARs)	→ endocrine metabole activiteit
^{18}F-fluoromisonidazole (FMISO)	intracellulaire reductases	→ hypoxia
^{89}Zr-cetuximab	epidermale groei factor receptor (EGFR, Her1)	→ evasie & metastase
^{89}Zr-trastuzumab	humane epidermale groei factor receptor 2 (Her2/neu)	→ proliferatie, overleving, differentiatie
^{89}Zr-bevacizumab	vasculaire endotheliale groei factor A (VEGF-A)	→ angiogenese

over het sigma ligand 1-(3,4-dimethoxyphenethyl)-4-(3-phenylpropyl)piperazine dat met koolstof-11 radioactief was gemerkt (^{11}C-SA4503).

In het eerste deel van dit proefschrift werd met behulp van microPET in proefdieren onderzocht of ^{11}C-SA4503 kan worden gebruikt voor het opsporen van tumoren. Een mogelijk probleem bij het gebruik van ^{11}C-SA4503 voor tumordiagnose is competitie van lichaamseigen moleculen met de radioactieve stof voor binding aan de sigma receptoren. Uit de literatuur is bekend dat steroïdhormonen aan deze receptoren kunnen binden. Daarom hebben wij onderzocht of er *in vitro* (reageerbuis) en *in vivo* (in proefdieren) competitie optreedt tussen steroïden en ^{11}C-SA4503 voor binding aan sigma receptoren in tumorcellen (**hoofdstuk 3**). Zowel het verhogen als het verlagen van de steroïdconcentratie had een significant effect op de binding van ^{11}C-SA4503. Competitie van progesteron met ^{11}C-SA4503 voor binding aan sigma receptoren kan wellicht verklaren waarom er tijdens PET studies met sigma liganden in patiënten soms variabele uitkomsten worden verkregen. Tijdens *in vitro* experimenten bleek dat de binding niet alleen wordt beïnvloed door progesteron maar ook door het mannelijk geslachtshormoon testosteron en door afbraakproducten van deze steroïden.

Sigma receptoren komen eveneens hoog tot expressie in het centrale zenuwstelsel. Hierdoor zou er in het brein sprake kunnen zijn van een hoog achtergrondsignaal zodat hersentumoren met een radioactief sigma ligand moeilijk zichtbaar gemaakt kunnen worden. Daarom hebben wij onderzocht of ^{11}C-SA4503 gebruikt kan worden bij het opsporen van tumoren van de hypofyse. Wistar ratten (veel gebruikte proefdieren) ontwikkelen op

latere leeftijd spontaan hormoonproducerende adenomas, een bepaald type tumor van de hypofyse. Of zulke tumoren (die ook bij mensen kunnen optreden) sigma receptoren tot expressie brengen was nog nooit onderzocht. In **hoofdstuk 4** worden microPET scans van bejaarde ratten (28 tot 36 maanden) beschreven. De opname van ^{11}C-SA4503 in de gezonde hypofyse is daarbij vergeleken met de opname in hypofysetumoren. Tevens werd onderzocht of tumoren van de hypofyse invloed hebben op de opname van ^{11}C-SA4503 in het brein, de schildklier en andere organen. ^{11}C-SA4503 werd aanzienlijk meer opgenomen in tumoren van de hypofyse dan in gezond hypofyseweefsel. Met behulp van dit sigma ligand en PET konden hypofysetumoren uitstekend worden afgebeeld. Farmacokinetische analyse maakte duidelijk dat de verhoogde traceropname in de tumoren het gevolg is van een toename van het aantal sigma receptoren in de tumorcellen. In het brein van tumordragende ratten werd eveneens een geringe verhoging van de opname van ^{11}C-SA4503 waargenomen. Deze verhoging kon niet worden toegeschreven aan een verhoogd aantal sigma receptoren, maar is waarschijnlijk het gevolg van een verandering van de doorbloeding.

Behandeling van kanker

Behandeling van allerlei typen kankercellen met sigma liganden zorgt ervoor dat de kankercellen geremd worden in hun groei dan wel dood gaan. Op basis hiervan worden sigma liganden beschouwd als mogelijke nieuwe geneesmiddelen voor de behandeling van kanker. In het tweede gedeelte van dit proefschrift is de tumorremmende werking van sigma liganden onderzocht, zowel in monotherapie als tijdens gecombineerde behandeling met Tumor Necrosis Factor Related Apoptosis Inducing Ligand (TRAIL).

Sigma liganden zijn giftig voor kankercellen, maar niet voor de meeste normale cellen. Er zijn echter relatief hoge concentraties van zulke stoffen vereist om tumorcellen dood te maken (20-100 μM). Dit zou kunnen komen doordat sigma liganden barrières (membranen) moeten passeren voordat ze aan sigma receptoren kunnen binden, of doordat een relatief grote fractie van de sigma receptoren bezet moet zijn voordat het gewenste effect optreedt. In **hoofdstuk 5** hebben wij onderzocht wat de werkelijke reden is. De bezetting van sigma receptoren in tumorcellen door geneesmiddelen werd bepaald met behulp van radioaktieve technieken en gecorreleerd aan de mate van de celdood. Wij vonden dat een bijna volledige bezetting van de sigma receptoren noodzakelijk was voor het therapeutische effect. Met behulp van ^{11}C-SA4503 en PET is het wellicht mogelijk om de expressieniveaus en de bezettingsgraad van sigma receptoren in kankerpatiënten te bepalen. Zo zouden patiënten kunnen worden geselecteerd voor therapie met sigma liganden, en zou de optimale hoogte van de therapeutische dosis kunnen worden vastgesteld. Verder onderzoek is nodig om te bepalen welke tracer voor andere fysiologische processen het meest geschikt is om veranderingen van de

stofwisseling in tumorcellen na behandeling met sigma liganden zichtbaar te maken.

Tijdens onze *in vitro* experimenten namen wij waar dat de tumorcellen een verhoogd glucose metabolisme hadden dat voorafging aan de uiteindelijke celdood. Dit effect staat bekend als een "metabolic flare". Het is tijdelijk van aard en treedt ook op bij de behandeling van tumorcellen met hormonen. Omdat effecten die *in vitro* worden waargenomen niet altijd ook *in vivo* optreden hebben wij in levende proefdieren onderzocht of behandeling van tumoren met sigma liganden ook gepaard gaat met een "metabolic flare" (**hoofdstuk 6**). Hiertoe zijn muizen onderhuids ingespoten met melanoma cellen (A375M) en nadat deze cellen tumoren hadden gevormd werden de muizen behandeld met het sigma ligand rimcazol. De reactie van de tumorcellen op behandeling met rimcazol is gevolgd met behulp van ^{18}F-FDG en microPET. Behandeling van melanomen met rimcazol veroorzaakte een sterke (4-voudige) remming van de tumor groei en de opname van ^{18}F-FDG nam in eerste instantie toe. Sigma liganden hebben dus ook invloed op het glucose metabolisme van tumoren *in vivo* en ook in levende proefdieren is er sprake van een "metabolic flare".

Bij de meeste patienten met een melanoom vormen er zich door het lichaam metastasen. Gemetastaseerde melanomen zijn dikwijls ongevoelig voor de standaard geneesmiddelen die bij de behandeling van kanker worden gebruikt. Uit preklinisch onderzoek is gebleken dat behandeling met zogenaamde cytokinen (zoals interferon-gamma en TRAIL) daarentegen erg veelbelovend is. In het UMCG is een nieuw geneesmiddel ontwikkeld dat TRAIL selectief kan afleveren aan het oppervlak van melanomacellen. Dit geneesmiddel, "anti-MCSP:TRAIL", bindt selectief aan het eiwit MCSP en wordt op dat moment actief. MCSP is een eiwit dat in meer dan 95% van alle melanomen tot over-expressie komt. Helaas kunnen melanoom cellen ook resistent worden voor TRAIL. Omdat sigma liganden de werking van chemotherapie kunnen versterken (zie hoofdstuk 2) hebben we getest of het sigma ligand rimcazol de therapeutische werking van anti-MCSP:TRAIL in melanomen kan versterken (**hoofdstuk 7**). Dit bleek inderdaad het geval te zijn en uit de gegevens die in hoofdstuk 7 worden gepresenteerd blijkt dat er een aanzienlijke versterking optreedt. In het volgende hoofdstuk (**hoofdstuk 8**) is nagegaan welke veranderingen er optraden in de stofwisseling van melanomacellen (A375M) na behandeling met anti-MCSP:TRAIL en rimcazol. Hiertoe werd de opname van de PET tracers ^{18}F-FDG en ^{18}F-FLT in de tumorcellen gemeten. De opname van ^{18}F-FDG is een maat voor het suikerverbruik en die van ^{18}F-FLT voor de DNA synthese en daarmee de snelheid van celdeling. Na behandeling met anti-MCSP:TRAIL en rimcazole was er een verhoging in de opname van ^{18}F-FDG zichtbaar, in overeenstemming met de eerder genoemde "metabolic flare". Daarnaast trad er een sterke vermindering op van de opname van ^{18}F-FLT wat erop duidt dat rimcazol de celdeling remt. Wanneer melanomacellen behandeld werden met zowel rimcazole als anti-MCSP:TRAIL leken met name de cellen die zich niet

meer deelden te worden gedood door anti-MCSP:TRAIL.

De effectiviteit van deze combinatie van rimcazole en in dit geval oplosbaar TRAIL combinatie hebben wij vervolgens onderzocht in kanker van de eierstok (**hoofdstuk 9**). Kankercellen uit biopsiemateriaal van patiënten met eierstokkanker werden daartoe behandeld met rimcazol en TRAIL. Bij de ene helft van de patiënten konden de kankercellen al worden gedood door ze alleen maar met rimcazol te behandelen. Bij de andere helft van de patienten reageerden de cellen slechts matig op de behandeling met rimcazol, maar in deze gevallen kon de werking van rimcazol aanzienlijk worden versterkt door gelijktijdige toediening van TRAIL. Op basis van deze (zeer voorlopige) bevindingen concluderen wij dat sigma liganden mogelijk gebruikt kunnen worden als geneesmiddel bij de behandeling van eierstok kanker.

Conclusies

Sigma liganden zijn interessante moleculen die kunnen worden gebruikt bij het ontwikkelen van technieken om tumoren op te sporen en te behandelen.

Wstęp

Rak zabija corocznie około ośmiu milionów ludzi na całym świecie. Pomimo znacznego postępu w diagnozowaniu i leczeniu raka, w następnych latach przewiduje się wzrost liczby osób cierpiących na nowotwory złośliwe. Aby zmniejszyć liczbę ofiar, intensywnie poszukiwane są nowe metody pozwalające na szybsze wykrycie raka i bardziej efektywną terapię przeciwnowotworową. Dlatego zgromadzenie wiedzy na temat powstawania i wzrostu komórek nowotworowych ma istotne znaczenie.

Rak jest grupą chorób nowotworowych o charakterze złośliwym i powstaje, gdy normalne komórki ciała zwyradniają się. Podczas tego procesu, komórka ciała zaczyna się izolować i ogranicza swój normalny kontakt z resztą organizmu. W zasadzie każda komórka może przekształcić się w komórkę nowotworową. W związku z tym, komórki nowotworowe często różnią się znacznie u poszczególnych pacjentów, a nawet komórki nowotworowe u tego samego pacjenta mogą bardzo odbiegać od siebie. Dlatego pacjenci, którzy zapadli na raka, mogą prezentować zróżnicowane objawy. Wszystkie typy raka wykazują cztery stadia rozwoju, tzn. inicjację (zapoczątkowanie), promocję (wdrażanie), progresję (rozwój, postęp) i konwersję (przekształcanie się) (rys. 1).

Podczas tych wszystkich stadiów komórki nowotworowe zmieniają się i coraz mniej przypominają komórki, od których się wywodzą. Te zmiany chronią raka przed systemem obronnym organizmu i umożliwiają niekontrolowany wzrost komórki rakowej. Znanymi przykładami zmian są: 1. stymulacja przez komórki rakowe własnego wzrostu, 2. niewrażliwość na programowaną śmierć komórki (naturalny proces śmierci uszkodzonych i/lub bezużytecznych komórek, profesjonalnie nazywany apoptozą), 3. zdolność do wielokrotnego i nieograniczonego podziału komórki nowotworowej na dwie identyczne komórki siostrzane. Dzięki tym przeobrażeniom komórka rakowa nabywa istotną przewagę nad normalnymi komórkami, ale może być przez to również łatwiej odróżniona od normalnych komórek.

Na przykład, przy normalnym wzroście komórek, czynnik wzrostu wiąże się z białkiem receptorowym i stymuluje wzrost komórkowy. W celu zmaksymalizowania użytku czynnika wzrostu, komórki rakowe często zwiększają liczbę posiadanych receptorów dla określonego czynnika wzrostu (następuje tzw. nadekspresja tego receptora). Ta nadekspresja aktywuje wzrost komórek nowotworowych, ale również pozwala na odróżnienie ich od normalnych komórek organizmu. Jednym z receptorów, który ulega nadekspresji w nowotworach, jest receptor sigma.

Receptory sigma są rodzajem białek występujących w błonach różnych przedziałów komórkowych tj. retikulum endoplazmatycznego, mitochondriów, lizosomów i plazmolemmy (zewnętrznej błony otaczającej komórkę). Ponieważ receptory sigma są liczniejsze w komórkach nowotworowych niż w normalnych komórkach, mogą być

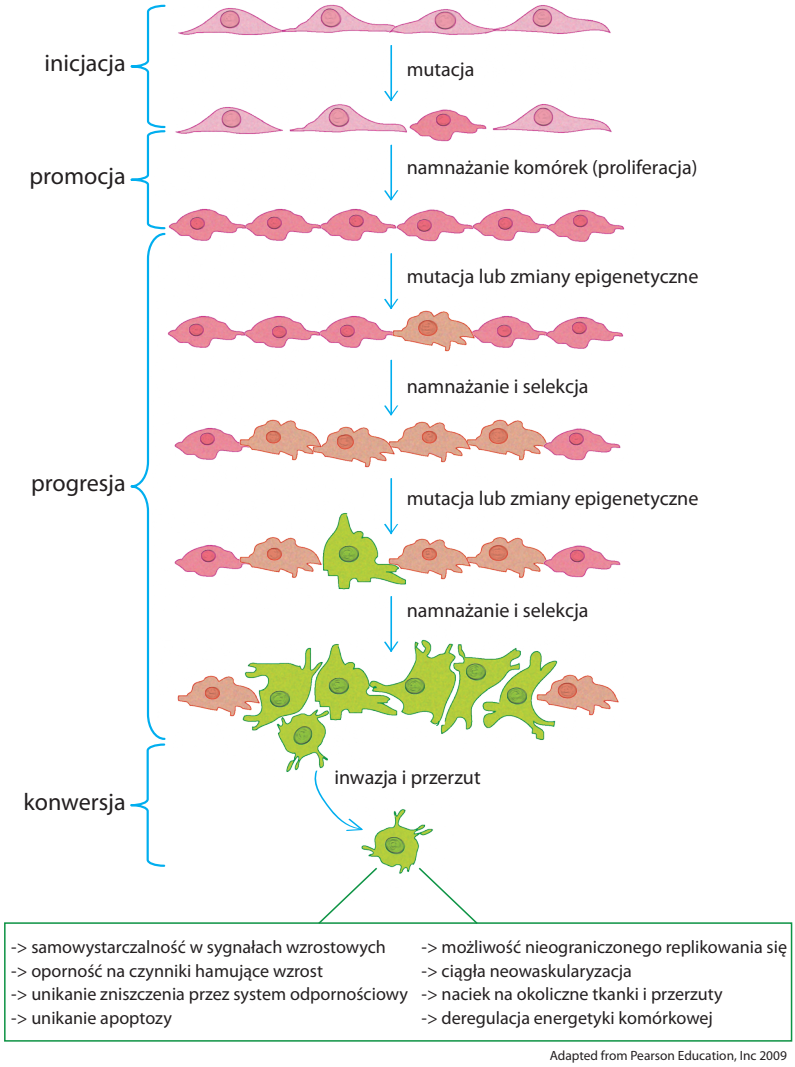

Adapted from Pearson Education, Inc 2009

Fig. 1. Stadia rozwoju nowotworu. Genezę nowotworu rozpoczynają wieloczynnikowe mutacje w komórce. Proces chorobowy jest ponaglony, gdy obciążona mutacjami komórka umyka mechanizmom obronnym ciała, rozpoczyna nietypowe namnażanie i posiada łatwość genomicznego przystosowania się, umożliwiającą dalsze mutacje i/lub zmiany epigenetyczne. Progresji guza towarzyszy kilka cykli adaptacji, namnażania i selekcji. Te procesy, w których komórki nowotworowe nabywają cech bardziej inwazyjnych i lekoopornych, zwiększają przeżycie komórek raka. Ostatecznie, tylko komórki nowotworowe o wysokiej ruchliwości przeniosą się z guza pierwotnego do odległych rejonów ciała i rozpoczną zaawansowane stadium choroby.

one użyte do wykrywania nowotworów. W celu obrazowania receptorów sigma można wykorzystać związki chemiczne (ligandy) o wysokim powinowactwie do tych receptorów. Ponadto, badania naukowe wykazały, że ligandy receptorów sigma mają właściwości przeciwnowotworowe (**rozdział 2**).

W tej pracy doktoranckiej opisane zostały zastosowania ligandów receptorów sigma zarówno w diagnozowaniu jak i w leczeniu raka.

Wykrywanie raka

Niestety, często terapia przeciwnowotworowa nie gwarantuje całkowitego wyleczenia. Jest to spowodowane m.in. tym, że wynik leczenia zależny jest od różnorodnych czynników takich jak: 1. szybka diagnoza, 2. określenie dokładnej lokalizacji guzów pierwotnych i wszystkich przerzutów (metastaz), 3. dobór odpowiedniej terapii przeciwnowotworowej. Dlatego natychmiastowa diagnoza jest niezbędna, aby polepszyć obecne terapie do walki z rakiem.

Diagnoza raka może być przeprowadzona przy użyciu inwazyjnych lub nieinwazyjnych technik. Do inwazyjnych metod diagnostycznych zalicza się np. biopsje oraz badanie podczas zabiegu chirurgicznego. Te metody ograniczają się do badania nowotworów o znanej lokalizacji, ale są mniej użyteczne w stwierdzeniu rozległości procesu nowotworowego. Ponadto, określenie rozmiaru nowotworu i jego charakteru przy użyciu tych metod jest trudne i niedokładne. Do nieinwazyjnych metod diagnostycznych zalicza się: 1. pobranie próbki krwi w celu stwierdzenia, czy w krwiobiegu obecny jest podwyższony poziom czynników związanych z chorobą nowotworową, 2. anatomiczne obrazowanie guzów nowotworowych metodą ultrasonografii (USG), tomografii komputerowej (TK), obrazowania magnetyczno-rezonansowego (MR), 3. molekularne obrazowanie za pomocą tomografii emisyjnej pojedynczych fotonów (SPECT) lub pozytonowej tomografii emisyjnej (PET). PET jest atrakcyjną metodą ponieważ, w przeciwieństwie do próbek krwi, TK i MR, dostarcza informacji o lokalizacji i funkcjonowaniu nowotworu.

PET jest bardzo czułą techniką medycyny nuklearnej, która wykorzystuje izotopy radioaktywne ulegające pozytonowemu rozpadowi (rys. 2). Pozytony są subatomowymi cząstkami elementarnymi, o tej samej masie jak elektron, ale w przeciwieństwie do elektronów o negatywnym ładunku, pozytony są pozytywnie naładowane. Po kontakcie pozytonu i elektronu następuje proces anihilacji (zamiany materii na promieniowanie elektromagnetyczne). W tym procesie następuje emisja dwóch fotonów (kwantów światła, promieniowania gamma, γ), które zarejestrowane są przez kamerę PET. Ponieważ te dwa fotony ulegają emisji zawsze pod kątem 180° w stosunku do siebie, ta właściwość może być użyta w celu zlokalizowania rozpadającego się izotopu w ludzkim ciele. Przyłączanie izotopu np. fluoru-18 (^{18}F) do związków biologicznych takich jak cukry, może być użyte do zobrazowania zużycia cukru przez organizm

A)

Izotopy emitujące pozytony	Okres półtrwania	β+ fraction	Max. energia (MeV)	Średni zasięg (mm)	Produkt rozpadu
^{18}F	109.8 min.	0.97	0.63	0.3	^{18}O
^{11}C	20.4 min.	0.99	0.96	0.4	^{11}B
^{13}N	9.97 min.	1.00	1.20	0.7	^{13}C
^{15}O	2.04 min.	1.00	1.74	1.1	^{15}N
^{68}Ga	68.3 min.	0.88	1.83	1.2	^{68}Zn
^{89}Zr	78.4 godz.	0.23	0.90	1.1	^{89}Y

B)

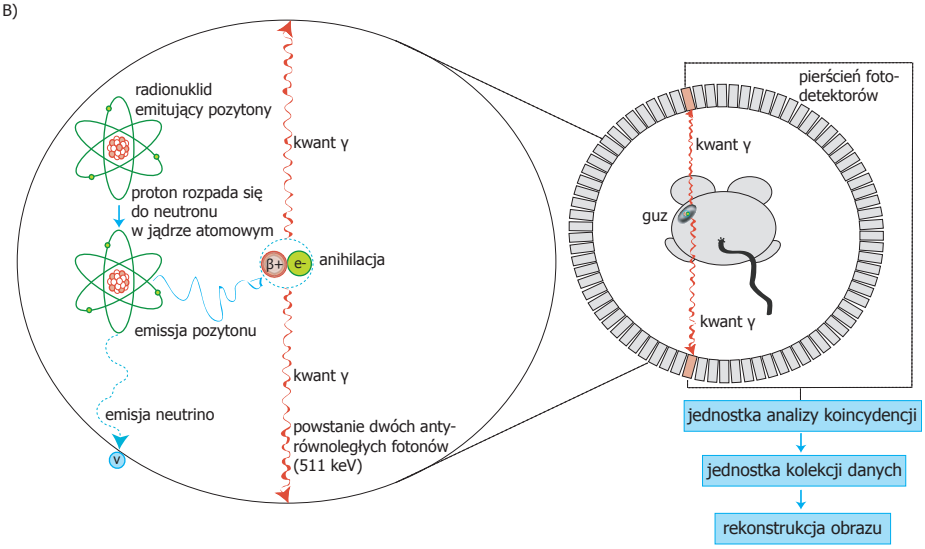

Fig. 2. Pozytonowa tomografia emisyjna: A) powszechnie używane izotopy emitujące pozytony w PET; B) schemat pokazujący zasady działania techniki PET: lewy panel ilustruje zasady fizyczne a prawy panel pokazuje metodologię praktyczną.

(metabolizm cukrów) za pomocą PET. Ponieważ komórki nowotworowe potrzebują generalnie więcej energii (np. z cukrów) niż zdrowe komórki, ^{18}F-fluorodeoksyglukoza (^{18}F-FDG) gromadzi się w nich w większej ilości niż w zdrowych komórkach. W ten sposób można dokładnie zlokalizować pierwotny guz i wszystkie przerzuty. Związki takie jak ^{18}F-FDG mogą być użyte do monitorowania zachowania normalnego cukru w organizmie, dlatego nazywa się je znacznikami.

Wszystkie komórki ciała przyswajają cukry, dlatego ^{18}F-FDG nie jest specyficznym znacznikiem do odróżnienia komórek nowotworowych od normalnych komórek. Dlatego nauka skupia się na rozwijaniu nowych związków, które wybiórczo gromadzą się w nowotworach. Przegląd takich znaczników przedstawiony jest w tabeli 1. Receptory sigma często ulegają nadekspresji w nowotworach, dlatego ta praca poświęcona jest

Tabela 1. Przykłady znaczników PET wykorzystywanych w onkologii

Znaczniki PET w onkologii	Białka docelowe	Proces biochemiczny
^{18}F-fluorodeoksyglukoza (FDG)	transportery glukozy (GLUTs) i heksokinazy (HKs)	→ energetyka komórkowa ~ 90% skanów
^{18}F-fluoro-L-tymidyna (FLT)	kinaza tymidyny typu 1 (TK-1)	→ namnażanie komórek
^{18}F-5-fluorouracyl (5-FU)	syntaza tymidylanowa	→ namnażanie komórek
^{11}C-metionina (MET)	transportery aminokwasów	→ transport aminokwasów
^{18}F-fluoroetylotyrozyna (FET)	transportery aminokwasów	→ transport aminokwasów
^{11}C/^{18}F-analogi choliny	kinaza choliny	→ metabolizm fosfolipidów
^{18}F-aneksyna A5	eksponowanie fosfatydyloseryny na powierzchni błony komórkowej	→ apoptoza
^{18}F-fluoroestradiol (FES)	receptory estrogenowe (ERs)	→ funkcja endokrynna
^{18}F-L-dihydroksyfenyloalanina (DOPA)	wielki transporter aminokwasów (LAT), dekarboksylaza aromatycznych L-aminokwasów (AADC), oksydaza monoaminowa (MAO)	→ funkcja endokrynna
^{18}F/^{64}Ga-analogi oktreotydu	receptory somatostatynowe typu 2 (SST2Rs)	→ funkcja endokrynna
^{18}F-fluoryzowane analogi androgenu	receptory androgenowe (ARs)	→ funkcja endokrynna
^{18}F-fluoromisonidazol (FMISO)	reduktazy wewnątrzkomórkowe	→ hipoksja (niedotlenienie)
^{89}Zr-cetuksymab	receptor naskórkowego czynnika wzrostu typu 1 (EGFR, Her1)	→ naciek nowotworowy i przerzuty
^{89}Zr-trastuzumab	receptor naskórkowego czynnika wzrostu typu 2 (Her2/neu)	→ namnażanie, przeżywanie, różnicowanie
^{89}Zr-bewacizumab	czynnik wzrostu śródbłonka naczyniowego A (VEGF-A)	→ neowaskularyzacja

badaniom wykorzystującym ligandy receptorów sigma w diagnozowaniu guzów. Do naszej dyspozycji mieliśmy ligand receptorów sigma: 1-(3,4-dimetoksyfenetyl)-4-(3-fenylopropylo)piperazynę oznakowaną izotopem węgla-11 (^{11}C-SA4503) o aktywności promieniotwórczej.

W pierwszej części pracy doktoranckiej opisana jest weryfikacja ^{11}C-SA4503 w wykrywaniu i obrazowaniu guzów u zwierząt eksperymentalnych za pomocą mikroPET (skanera PET przystosowanego do małych zwierząt). Możliwym problemem ^{11}C-SA4503 w diagnozowaniu nowotworów może być współzawodnictwo naturalnego fizjologicznego liganda ze związkiem promieniotwórczym o miejsce wiążące w receptorach sigma. Z literatury wiadomo, że hormony steroidowe mają powinowactwo do receptorów sigma i wiążą się z nimi. Aby wykazać możliwe wiązanie się tychże hormonów do receptorów sigma w komórkach nowotworowych hodowanych *in vitro* (w probówce) oraz w guzach nowotworowych *in vivo* (u zwierząt eksperymentalnych), przeprowadziliśmy badania nad współzawodnictwem pomiędzy hormonami steroidowymi a ^{11}C-SA4503 (**rozdział 3**). Zauważyliśmy, że zarówno podwyższenie poziomu hormonów steroidowych, jak i ich obniżenie, miało znaczny wpływ na swoiste gromadzenie się ^{11}C-SA4503 w komórkach nowotworowych. Współzawodnictwo progesteronu z ^{11}C-SA4503 o miejsce wiążące w receptorach sigma może wyjaśnić, dlaczego badania PET przy użyciu ligandów receptorów sigma dają czasami różniące się rezultaty. Eksperymenty *in vitro* wykazały, że nie tylko progesteron miał wpływ na swoiste wiązanie ^{11}C-SA4503, ale także męski hormon płciowy testosteron oraz produkty przemiany tych hormonów steroidowych.

Wysoka ekspresja receptorów sigma obecna jest również w ośrodkowym układzie nerwowym. Dlatego w przypadku mózgu mówi się o wysokim sygnale tła, który może utrudnić obrazowanie nowotworów mózgu za pomocą radioaktywnie oznakowanych ligandów receptorów sigma. W dalszej części niniejszej pracy doktoranckiej opisane są badania nad obrazowaniem gruczolaków przysadki mózgowej (guzów o czynności hormonalnej) za pomocą ^{11}C-SA4503. Albinotyczny szczep szczurów Wistar (powszechnie stosowany model do badań naukowych nad anatomią i fizjologią ssaka) predysponowany jest w późniejszej fazie życia do spontanicznego rozwoju gruczorlaków przysadki. Warto nadmienić, że ten typ nowotworu występuje także w ludzkiej przysadce. Niniejsza praca opisuje pierwsze badania nad ekspresją receptorów sigma w gruczolaku przysadki. **Rodzdzial 4** zawiera skany przeprowadzone za pomocą metody mikroPET na podstarzalych szczurach (w przedziale wiekowym od 28 do 36 miesięcy). Porównany jest tu pobór ^{11}C-SA4503 przez zdrową przysadkę z poborem ^{11}C-SA4503 przez gruczolaka przysadki. Ponadto testowaliśmy, czy gruczolaki przysadki mają wpływ na wchłanianie ^{11}C-SA4503 w mózgu, w tarczycy i w innych organach. Zastosowanie ligandów receptorów sigma i techniki PET z wysoką dokładnością rozpoznało wszystkie gruczolaki przysadki, gdyż ^{11}C-SA4503 gromadził się w większej ilości w guzach przysadki niż w zdrowej przysadce. Analiza farmakokinetyczna wykazała, że przyczyną podwyższonego wchłaniania znacznika przez guzy był zwiększony poziom receptorów sigma w komórkach guza. Zauważone zostało również, że mózg szczurów posiadających guzy wykazywał umiarkowany wzrost wchłaniania ^{11}C-SA4503. Ten wzrost w mózgu nie był spowodowany wzrostem ilości receptorów sigma, lecz prawdopodobnie rezultatem zmian w przepływie krwi.

Leczenie raka

Leczenie różnych typów raka ligandami receptorów sigma wstrzymuje namnażanie się komórek nowotworowych i prowadzi następnie do ich śmierci. Dlatego doszukuje się zastosowania ligandów receptorów sigma jako nowych terapeutyków do walki z rakiem w medycynie klinicznej. W drugiej części pracy doktoranckiej opisane są przedkliniczne badania nad aktywnością przeciwnowotworową tychże ligandów, stosowanych zarówno w monoterapii (przy użyciu jednego preparatu) jak i politerapii (przy łączeniu kilku leków) z ligandem wywołującym apoptozę i spokrewnionym z czynnikiem martwicy nowotworu TNF, nazywanym TRAIL (od skórtu angielskiej nazwy Tumor necrosis factor (TNF)-Related Apoptosis Inducing Ligand).

Ligandy receptorów sigma są toksyczne dla komórek nowotworowych, ale nie dla większości normalnych komórek. Jednakże stosunkowo wysokie stężenie (20-100 μM) ligandów receptorów sigma jest niezbędne aby zabić komórki nowotworowe. Może być to spowodowane przez fakt, że ligandy receptorów sigma muszą przekroczyć bariery (błony komórkowe), zanim będą one mogły związać się z receptorami sigma. Innym

wytłumaczeniem może być, że relatywnie wysoki ułamek receptorów sigma powinien być związany z ligandem, aby wywołać pożądany efekt terapeutyczny. **Rozdział 5** wyjaśnia, który z tych spekulowanych powodów zgadza się z prawdą. Zapełnienie miejsc wiążących receptorów sigma w komórkach nowotworowych przez terapeutyki zostało wyznaczone techniką wykorzystującą związki promieniotwórcze, a następnie zostało porównane z poziomem śmierci komórkowej. Eksperymenty wykazały, że związanie prawie wszystkich receptorów sigma przez ligand jest konieczne w celu wywołania efektu terapeutycznego. Przypuszczamy, że wykorzystanie ^{11}C-SA4503 i techniki PET umożliwi określenie poziomu ekspresji i stopnia zapełnienia receptorów sigma u pacjentów z chorobą nowotworową. W ten sposób pacjenci kwalifikujący się do terapii z ligandami receptorów sigma mogliby być wyselekcjonowani i optymalna dawka terapeutyczna takiego liganda mogłaby być wyznaczona. Przyszłe badania są konieczne aby określić, który znacznik jest najbardziej stosowny do zobrazowania zmian metabolizmu komórek nowotworowych po podaniu ligandów receptorów sigma.

Podczas eksperymentów *in vitro* zaobserwowaliśmy, że komórki nowotworowe prezentowały wzmożony metabolizm glukozy, który poprzedzał śmierć komórkową. Ten efekt, opisany jako „wybuch metaboliczny" („metabolic flare"), ma tymczasową naturę i pojawia się także, gdy komórki noworowe leczone są hormonalnie. Niestety, badania *in vitro* nie zawsze odzwierciedlają te przeprowadzone *in vivo*. Dlatego użyliśmy zwierząt doświadczalnych do sprawdzenia, czy podawanie ligandów receptorów sigma poprzedzone jest również „wybuchem metabolicznym" (**rozdział 6**). Najpierw komórki nowotworowe czerniaka złośliwego (linii komórkowej A375M) wstrzyknięte zostały podskórnie myszom laboratoryjnym, a po uformowaniu się guzów nowotworowych, myszom podawany był ligand receptorów sigma o nazwie rimcazol. Reakcja komórek nowotworowych na leczenie rimcazolem była monitorowana przy użyciu ^{18}F-FDG i skanera mikroPET. Rimcazol spowodował silne zahamowanie (czterokrotne) wzrostu czerniaka i początkowe wzmożenie poboru ^{18}F-FDG przez guza. Ligandy receptorów sigma mają przez to wpływ na metabolizm glukozy i wywołują efekt „wybuchu metabolicznego" także u zwierząt doświadczalnych.

Większość pacjentów z czerniakiem złośliwym posiada przerzuty oddalone (rozsiane po całym ciele). Przerzuty czerniaka są często oporne na standardowe metody leczenia nowotworów. Badania przedkliniczne wykazały, że dobre rezultaty terapii przeciwnowotworowej osiągane są za sprawą tzw. cytokin (np. interferonu-gamma i białka TRAIL). W Uniwersyteckim Centrum Medycznym w Groningen (UMCG) opracowany został nowy terapeutyk, który wybiórczo dostarcza TRAIL na powierzchnię komórek czerniaka złośliwego. Ten eksperymentalny terapeutyk, „anty-MCSP:TRAIL", wybiórczo wiąże się z białkiem MCSP (proteoglikanem siarczanu chondroityny czerniaka złośliwego) i zostaje zaktywowany. MCSP to białko, które jest nadekspresjonowane w przynajmniej

95-ciu procentach czerniaków złośliwych. Niestety, po pewnym czasie komórki czerniaka złośliwego stają się oporne na działanie cytokiny TRAIL. Natomiast ligandy receptorów sigma potrafią wzmocnić działanie chemoterapii (rozdział 2). Dlatego przeprowadziliśmy badania nad rimcazolem i jego możliwością zwiększenia efektu terapeutycznego białka fuzyjnego anty-MCSP:TRAIL w czerniaku złośliwym hodowanym *in vitro* (**rozdział 7**). Rezultaty tych eksperymentów wykazały znaczne wzmocnienie efektu przeciwnowotworowego. W następnym rozdziale (**rozdział 8**) podajemy, jakie zmiany metaboliczne występują w czerniaku złośliwym (A375M) po jednoczesnym podaniu rimcazolu i białka anty-MCSP:TRAIL. Następnie przeprowadziliśmy pomiary wchłaniania znaczników PET, ^{18}F-FDG i ^{18}F-FLT, przez komórki nowotworowe, które zostały lub nie zostały poddane opisanej powyżej terapii. Wchłanianie ^{18}F-FDG odzwierciedla konsumpcję glukozy, a wchłanianie ^{18}F-FLT odzwierciedla syntezę DNA i intensywność podziałów komórkowych. Komórki leczone rimcazolem i białkiem anty-MCSP:TRAIL zwiększyły pobór ^{18}F-FDG, zgodnie z wcześniej opisanym efektem „wybuchu metabolicznego". Ponadto, zauważony został znaczny spadek poboru ^{18}F-FLT sugerujący hamowanie podziału komórkowego przez rimcazol. Podawanie komórkom czerniaka zarówno rimcazolu jak i białka anty-MCSP:TRAIL spotęgowało śmierć tych komórek, których podział został zahamowany przez rimcazol.

Kombinacja rimcazolu i białka TRAIL była następnie testowana na komórkach guza jajnika (**rozdział 9**). Komórki nowotworowe wyizolowane z pacjenta metodą biopsji inkubowane były z rimcazolem i białkiem TRAIL. Komórki nowotworowe pochodzące od połowy pacjentów mogły być zabite przez sam rimcazol. Komórki nowotworowe od drugiej połowy pacjentów były jedynie umiarkowanie wrażliwe na rimcazol. W tym jednak przypadku działanie przeciwnowotworowe było znacznie wzmocnione przez równoczesne podanie rimcazolu i białka TRAIL. Na podstawie tych wstępnych badań wywnioskowaliśmy, że ligandy receptorów sigma mogą być obiecującymi terapeutykami w leczeniu raka jajnika.

Podsumowanie

Ligandy receptorów sigma są obiecującymi związkami, które mogą dać początek nowym metodom rozpoznawania i leczenia nowotworów.

Acknowledgements

And every time it rains
You're here in my head
Like the sun coming out.
(...) Ooh, I just know that something
good is gonna happen.
(...) I'm Cloudbusting

[Kate Bush]

I found these four years of my PhD study exhilarating, never boring, and oh so educational. Besides the mountain of knowledge about nuclear medicine, cancer biology, sigma receptors and scientific writing styles, I learned independence in thinking and designing my experiments

Still, no work performed or success achieved is a one person-effort, but is shared by an individual and all groups of people supporting her on the way. Without the great support from my supervisors, friends and family, I would not be standing in this place today.

Therefore, I would like to start of by thanking Prof. Dr. Rudi Dierckx, my first promoter and the head of the Department on Nuclear Medicine and Molecular Imaging, for accepting me as a PhD candidate and giving me the opportunity to work in such a fast developing department. Rudi, thank you for your example on how one should make goals, and how one should achieve them. Thank you for being a good boss and always supplying our brains with supreme quality glucose in the form of Belgian chocolate. Furthermore, on the eve of completing my PhD, I would like to thank you for giving me the opportunity to further develop my interests as a post-doc in the department.

I would also like to thank Prof. Dr. Philip Elsinga, my second promoter, and Dr. Aren van Waarde, my supervisor. Philip and Aren, this research definitely would not be possible without you. Thank you for your valuable suggestions, for reading and correcting my manuscripts, for feeding my crazy ideas, or starving them (if necessary), and for all the interesting conversations. Philip, special thanks to you for producing "our" tracer used in my first cell and animal studies (I hope that your hands were not glowing in the dark afterwards). Aren, thank you for teaching me everything that I know today about nuclear medicine, for sending me all news in the field of sigma receptors, for all advise, for your support and criticism, for giving me the immense freedom in my research, and for you and Maria being good friends.

I am really grateful to the reading committee, Prof. Dr. Kiichi Ishiwata, Prof. Dr. Ate van der Zee and Prof. Dr. Christophe van de Wiele for critically reviewing my dissertation.

I would further like to thank Dr. Erik de Vries, Dr. Jan Pruim, Prof. Dr. Frank Kruyt, Dr. Hetty Timmer-Bosscha and Dr. Coby Meijer. Thank you for the interesting

discussions and that I could always knock on your doors and get almost instant help with solving my problems. I would also like to extend my thanks to Dr. Wijnand Helfrich and Dr. Edwin Bremer for the support with the work in chapters 7-9. Furthermore, I want to express my sincere gratitude to Dr. Simon Daenen and Dr. Gert Luurtsema. Thank you for your great interest in my research and for our collaborations.

I would not be here doing my PhD study if not the support from Prof. Dr. Paul Luiten, Dr. Ulrich Eisel, Dr. Ingrid Nijholdt and Prof. Dr. Maria Malicka-Blaszkiewicz. It was you that permanently infected me with the love to explore the unknown.

I am grateful to Henk Moes and Geert Mesander for all their friendly assistance with FACSing. Thanks to Gert Jan Meersma and many other friendly people from the Department of Medical Oncology for all kinds of help with my research. Thanks to Jacco Zwaagstra and Janneke Wiersema-Buist from the Department of Surgery for their kind assistance with my first IHC stainings. Thanks to all friendly people from the Central Animal Laboratory for support, advise and help with my animal studies. Special thanks go out to Ari Nijmeijer, Wiebe Hofstra, Silvia Kiewiet, Ar Jansen and Hester Geleynse.

I would like to also acknowledge the great contribution of Jurgen Sijbesma to the *in vivo* studies included in this thesis. I want to thank Klaas Willem Sietsma, Chantal Kwizera, Bram Maas, Joost Bruns, Remko Koning, Hans Pol, Hilde Dekens, Bertha Tamming, Jitze Medema, Hugo Nijnuis and Hans ter Veen for their invaluable technical assistance and nice chats. Thanks to our brave crew of physicists: Johan de Jong, Sergiy Lazarenko, Roel Wierts and Marcel Segberts for their patience and help with "safely" acquiring and processing my data.

My dear cheerful roommates, Sheida, Vale, Mehrsima, Ines and Daniele, I honestly cannot imagine my time here without you. For over four years we shared our joys and miseries, our research puzzles and solutions, our headaches, our pastries, "100% Arab" coffees and chocolates, our allergies and a falling wall… Peppe, Andrea, Nisha, Anniek, Nathalie, Zilin, Reza, Hans, Janine, Ewelina, Ate, Urszula and Małgosia, I want to thank you for your friendship, in our basement and outside. Thanks to the rest of PhD students who made these 4 years pleasantly unforgettable.

Steven, Rory, Lisanne, Martijn, Paul and Kriszti, thanks for your friendship, all the great Fridays, the moments of relaxation that you and your Zombie movies gave me, thanks for your interest in my work, and for accepting my sleeping mode on your couches or in the cinema during James Bond movies.

My dear Magda, Ada, Daan, Gaba, Ewa, Klaudia, Ola and Robert: *Jesteście kochanymi i nadzwyczajnymi ludźmi. Wiedza, że mogę na Was zawsze polegać zawsze dodaje mi siły, motywacji i pewności siebie... a z tym ostatnim, to wiecie, ze jest u mnie czasem ciężko... Jestem Wam tym bardziej wdzięczna, że tolerujecie mój brak czasu dla Was i mój barański upór.*

I want to thank my dear brother: *Dawidku, słowa nie wyrażą, ile Ci zawdzięczam. Zawsze postrzegałam Cię jako starszego brata, który ochraniał mnie przed przytłoczeniem przez ciężar życia. Nie mogę sobie wyobrazić, że mógłbyś nie być dziś przy moim boku jako mój „paranimf".*

I want to thank my parents-in-law, Henk and Meta. Henkie and Metie, probably you have no idea how much you have not only influenced my life, but also my scientific carrier. You were always interested in my results and the topic of my thesis - you asked so many fundamental questions... In the beginning, these were really nasty, more so than the detailed scientific questions (since scientist usually have the tendency to sink in their topic), but finally these questions helped me to get an objective view and write my thesis.

From the bottom of my heart I would like to thank my parents: *Mamusiu, Tato, chciałabym z całego serca podziękować Wam za wszczepienie we mnie ciekawości. Wiem, ze czasem wydaje sie Wam wręcz kosmicznym to, czym się zajmuje, ale mam nadzieje, ze ta praca przybliży Wam temat tej dużej i ważnej części mojego życia. Mamusiu, dziękuję Ci za umożliwienie mi studiowania w Holandii, za Twoją miłość i wsparcie. Dziękuję Wam, że pomimo dystansu i innych trudności mogliście być dziś ze mną.*

My PhD project started on 17th September 2007, but almost at the same time another "project" began since me and my, "presently" ;-), husband started to live together. Thank you, Marco, for giving me your strength and support. You have been persistently inculcating self-confidence in me, repeating continuously that I should believe more in myself despite my stubbornness and wild, polish temper. You are the one that knows the best how difficult it was for me to move from Poland to the Netherlands, far, far away from everything that I was living with before, far from my friends and my family. You have helped me with starting my life over again; in a more relaxed dutchy way than a crazy polish running. Thank you for helping me with cell counting under the microscope in the very late "after work" evenings, thank you for your valuable suggestions and interesting professional discussions. Thank you for getting up in the night to call me before I fell asleep in New Orleans to wish me good luck with my presentations at the SNM meeting. Thank you for making breakfasts every day on the working days for us to have more time together. Finally, thank you for your "THE"s and "A"s in all of my publications.

In addition, my thanks go out to all the people that were involved in the creation of this thesis, but were not mentioned by name.

I want to finish with the quotation: "I love it when a plan comes together" (from TV Series "The A-Team").

Ania

List of Abbreviations

2TCM	two-tissue compartment model
Akt	a serine-threonine protein kinase, also called protein kinase B
ATCC	American Type Culture Collection
ATP	adenosine 5'-triphosphate
BBB	blood-brain barrier
Bcl-2	B-cell lymphoma-2 family of proteins
BP_{ND}	nondisplaceable binding potential
CI	cooperativity index
CT	computed tomography
DHEA-S	dehydroepiandrosterone-3-sulphate
DMEM	Dulbecco's minimum essential medium
DMT	N,N-dimethyltryptamine
DNA	deoxyribonucleic acid
DTG	1,3 di-ortho-tolylguanidine
EC50	half maximal effective concentration
FCS	fetal calf serum
FDA	Food and Drug Administration
FDG	2-deoxy-2-fluoro-D-glucose
FLT	3'-fluoro-3'-deoxy-L-thymidine
GLUT	glucose transporter
HIF1α	hypoxia-inducible factor
HK	hexokinase
H&E	hematoxylin and eosin staining
HPLC	high-performance liquid chromatography
IHC	immunohistochemistry
IC50	half maximal inhibitory concentration
i.p.	intraperitoneal administration
IVC	individually ventilated cage
K_1/k_2	partition coefficient
K_d	dissociation constant
Bq	Becquerel (MBq: megabecquerel; TBq: terabecquerel)
MCSP	melanoma chondroitin sulfate proteoglycan
MDR	multi-drug resistance
MRI	magnetic resonance imaging
OC	ovarian carcinoma
PET	positron emission tomography
PBS	phosphate-buffered saline

P-gp	P-glycoprotein
PGRMC1	progesterone receptor membrane component 1
PI	propidium iodide
PI3K	phosphoinositide 3-kinase
RBC	red blood cells
ROI	region of interest
SA4503	1-[2-(3,4-dimethoxyphenyl)ethyl]-4-(3-phenylpropyl)piperazine
s.c.	subcutaneous administration
SD	standard deviation
SEM	standard error of the mean
SPECT	single-photon emission computed tomography
SUV	standardized uptake value
TAC	time-activity curve
TRAIL	tumor necrosis factor (TNF)-related apoptosis-inducing ligand (rhTRAIL: recombinant human TRAIL; sTRAIL: soluble TRAIL)
TK1	thymidine kinase 1
V_T	total distribution volume
zVAD-fmk	N-benzyloxycarbonyl-valyl-alanyl-aspartyl-(O-methyl)-fluoromethyl-ketone